Technical Report

TR-09-35

Mechanisms and models for bentonite erosion

Ivars Neretnieks, Longcheng Liu, Luis Moreno

Department of Chemical Engineering and Technology
Royal Institute of Technology, KTH

December 2009

Svensk Kärnbränslehantering AB
Swedish Nuclear Fuel
and Waste Management Co

Box 250, SE-101 24 Stockholm
Phone +46 8 459 84 00

Mechanisms and models for bentonite erosion

Ivars Neretnieks, Longcheng Liu, Luis Moreno

Department of Chemical Engineering and Technology
Royal Institute of Technology, KTH

December 2009

Abstract

The erosion project started late 2006 and run during 2007 and 2008. It engaged a considerable number of researchers: A list of reports generated during this time is given at the end of the present report. The aim of the project was to devise ways of assessing the possible rate of erosion of the compacted bentonite buffer surrounding copper canisters with spent nuclear fuel as in the KBS-3 design. The concern was that should large amounts of non-saline groundwater seep past the canisters during a long time, smectite particles in the bentonite buffer could solubilise to form colloids, which could be carried away by the water. Should a large fraction of the buffer be lost this would impede its function to hinder corrosive agents to reach the canister. Should the canister be breached the degraded buffer would be less effective to delay any leaching nuclides.

Professor Ivars Neretnieks was asked to scientifically coordinate a research project to investigate the processes that could cause bentonite loss and to attempt to quantify the loss under conditions that reasonably could be expected to occur. A number of experimental as well as theoretical studies were undertaken to gain sufficient understanding of the underlying chemical and physical conditions to be able to make quantitative assessment of bentonite erosion. There has been only a very limited time available for this project and there are still several important areas that must be further explored. The main remaining questions are behaviour of calcium dominated systems and filtering and straining by detritus particles.

Sammanfattning

Erosionsprojektet startade sent 2006 och pågick under 2007 och 2008. Ett stort antal forskare deltog i arbetet. En sammanställning av publikationer och rapporter som producerades finns i slutet av denna rapport. Projektet hade som mål att finna metoder att uppskatta den tänkbara erosionshastigheten för bentonitbufferten som omger kopparkapslar med använt kärnbränsle i ett slutförvar av KBS-3 typ. Målet var att utreda om man kan befara att bentonitbufferten som omger kapseln skulle kunna eroderas av stora flöden färskvatten om detta får strömmar förbi bufferten under lång tid eftersom bentoniten består av i huvudsak kolloidalt små smektitpartiklar vilka kan svepas iväg av vattnet. Om en stor andel av bufferten förloras skulle mer korrosiva ämnen kunna nå kapseln. Skulle brott uppstå på kapselväggen skulle en försvagad buffert vara en mindre effektiv barriär för att fördröja eventuellt läckande nuklider.

Professor Ivars Neretnieks ombads att vetenskapligt koordinera ett forskningsprojekt med syfte att undersöka de processer som skulle kunna leda till förlust av bentonit och att söka kvantifiera förlusten under förhållanden som rimligen skulle kunna förväntas uppstå. Ett antal experimentella och teoretiska studier genomfördes för att få tillräcklig förståelse för de kemiska och fysikaliska förhållandena som krävs för att kunna kvantifiera bentoniterosion. Tiden för att genomföra detta projekt har varit knapp och det finns fortfarande flera viktiga områden som borde studeras ytterligare. De huvudsakliga frågorna rör kalciumbentonitens uppförande och filtrering av ytterligare smektitpartiklar i den mycket fina sand som blir kvar av bentoniten när en del smektit försvinner.

Summary

The present report relies heavily on the work of a large number of researchers who worked on various aspect of bentonite erosion in the erosion project.

There are concerns that the bentonite buffer surrounding the canisters with spent nuclear fuel may erode when non-saline groundwaters seep past the buffer during long periods of time. The non-saline waters may solubilise the smectite particles in the bentonite and carry them away as colloidal particles. This is known to happen if the water content of ions is below the critical coagulation concentration CCC. Above the CCC the smectite forms a coherent gel, which does not release particles. It was also found in the present investigation that the gel thus formed will not be sheared off by the shear forces of the seeping water.

One main effort in this study has been directed to assess under which conditions the pore water composition of the gel at the gel/water interface could be lower than the CCC. Another main effort has been directed to understanding the behaviour of expansive gel when the pore water is below the CCC. In the latter case most work has been made on the behaviour of *sodium dominated smectite* because if most of the counterions in the smectite are calcium such smectites do not readily release colloidal particles. The reason is that the smectite particles in a calcium dominated gel hold together in larger and less mobile particles consisting of many individual smectite sheets. Such particles are too heavy to be much influenced by Brownian motion. The particles are also bulkier and are much easier strained in narrow pores and passages. Strongly dominated calcium gels are therefore not expected to cause erosion problems.

Sodium dominated gels in waters below the CCC are therefore the main concern because such gels will expand “forever” and release colloidal smectite particles to the seeping water. In addition, as the gel grows increasingly dilute, it becomes less viscous and can *flow* downstream.

We have developed a Dynamic model for sodium gel expansion in fractures where the gel soaks up non-saline water as it expands. The model is based on a force balance between and on smectite particles, which move in the water. Attractive van der Waals forces, vdW, repulsive electric diffuse layer forces, DDL, gravity and buoyancy forces and forces caused by the gradient of chemical potential of the particles act to move the particle in the water. Friction between particles and water restrain the movement. The DDL forces strongly depend on the type of ion and concentration in the water surrounding the particles. The Dynamic model of gel expansion showing the evolution in time and space of a gel was successfully tested against expansion experiments in test tubes. The expansion was measured with high resolution and in great detail over many months by Magnetic Resonance Imaging, MRI. The model also predicted the gel expansion through filters with very narrow pores well. In addition the model predicts the CCC fairly well, order to orders of magnitude better than the conventional DLVO theory.

A gel viscosity model of dilute gels was derived, which accounts for ion concentration influence as well as the volume fraction of smectite in the gel. The model accounts for the presence of the DDL, which seemingly makes the particles larger so that they interact at lower particle densities. The viscosity model uses experimental data to obtain the necessary fitting parameters but is otherwise based on established theories of suspension viscosity.

These models form the core of the erosion model. Both show a strong dependence on the ionic strength of the pore water. Simulations were performed for a case where the gel expands outward into the fracture that intersects the deposition hole. Fresh groundwater approaches and passes the gel/water interface. Smectite colloids move out into the water due to the repulsive forces between the particle and by Brownian motion (effect included in the Dynamic model). The dilute gel/sol is mobilised and flows downstream in a thin region where the viscosity is low enough to permit flow. Sodium diffuses from the compacted bentonite into and through the expanding gel towards the gel/water interface and further out into the seeping water. Mass transfer resistance for ions as well as smectite particles in the seeping water is accounted for in the simulations. The sodium concentration profile in the gel influences the repulsive forces between the particles as well as the viscosity of the

expanding gel. Under the most unfavourable circumstances, i.e. at high flowrates and large fracture apertures, considerable loss of smectite can be expected for a buffer that consists of *only smectite.*

Other calculations have been done to assess under which conditions of flowrate, water compositions and initial bentonite chemical compositions the water composition at the gel/water interface could become larger than the CCC. At the same time the proportion of calcium and sodium as counter ions in the smectite at the gel/water interface was studied. This was done because should the calcium make up more than about 90% of the counterions, the smectite behaves very differently from than smectite with less calcium. There are indications that such gel will not release colloids readily. In a number of studied cases such stabilizing conditions could not be achieved. In these calculations we have accounted for ion exchange in the expanding gel, for diffusion of ions in the gel, for transport to and from the seeping groundwater, and of the dissolution of soluble minerals that may supply the gel with ions.

We conclude that with our present understanding of the processes it is not possible to affirmatively state that erosion of *pure* smectite gels cannot occur to a considerable extent.

In experiments in downward facing slits (fractures) it has been found that bentonite releases gel agglomerates much faster than our model predicts. These are released and sediment also under conditions where it is expected that the smectite particles should have separated into individual smectite sheets, which would not noticeably be influenced by gravity. The reasons for this behaviour are not understood.

However, the commercial bentonites that have been extensively investigated in earlier and present SKB investigations contain tens of percent of non-smectic accessory minerals. These materials do not exhibit the strong repulsive forces as the smectites do because the surface charge density is essentially negligible at the circum neutral pH expected. Furthermore the particle size of these materials is one to two orders of magnitude larger than those of the smectite particles, so they are much less mobile and they could not be lost as colloids in the water. It is highly likely that such particles will penetrate some distance into the fracture and form a porous network through which the smectite particles must pass. We have investigated the idea that the accessory particles left behind could form a porous bed with small enough pores to slow down smectite loss after a short initial period when some smectite is lost leaving the accessory mineral particles behind to form the filter bed. A few cm long region of detritus material in the fracture has a strong restraining effect on the rate of smectite loss by colloidal diffusion through the pores.

A set of experiments where highly compacted beds of smectite between metal filters flushed by water on the outside show that sodium smectite readily penetrates filters with 2 μm pore size or larger but are stopped by 0.5 μm filters. The smectite particles are one to a few μm large.

Furthermore, theoretical deliberations and modelling suggest that the particle size distributions are favourable for smectite *straining* in already a thin bed of accessory minerals. The porous bed can have so small pores that the smectite particles are prevented from passing so narrow pores. A set of experiments where mm thick beds have been used to filter a suspension of smectite particles show very promising results.

Our overall conclusions are that a buffer with practically only smectite cannot be proved not to erode significantly with the flowrates and water compositions expected. On the other hand, we strongly believe that the accessory minerals will effectively hinder major loss of buffer. There is also the possibility to add material with optimally chosen particle sizes to further strengthen the filtering and straining of smectite colloids. There is a need for more experimental data to prove this.

Contents

1 Background and introduction

1.1 The Swedish repository for spent nuclear fuel based on the KBS-3 concept

The Swedish repository for spent nuclear fuel is planned to be located at about 500 m depth in granitic rock.

The fuel rods containing spent fuel are emplaced in canisters made of an inner steel structure and an outer copper shell. The copper corrodes only if corrosive agents such as sulphide or oxygen can be transported to the copper surface. The canisters, which are about 5 m long and 1.05 m in diameter are placed in about 8 m deep, 1.75 m diameter vertical boreholes from the floor in tunnels. The canisters are surrounded by highly compacted bentonite, which swells as water from the rock intrudes and saturates it. The hydraulic conductivity of the saturated bentonite is so low that it is effectively stagnant and dissolved constituents, including the corrosive agents, migrate very slowly through the buffer by molecular diffusion.

The integrity of the canister is one of the important features of the repository design. A main function for the buffer is to ensure that the intrusion of corrosive agents is kept low. Then the corrosion rate will be acceptably low and the canister will not be breached for more than hundreds of thousands of years.

Should the buffer be lost this function would be impaired.

In the present report we discuss one potentially possible process by which the buffer material could be lost, namely that the colloidally small smectite particles that make up most of the buffer could be carried away by high flowrates of intruding waters with low salt content. Such waters can be meteoric or glacial melt waters that have not had time to dissolve enough minerals on their way down to the repository.

1.2 Aim and scope

The aim of this report is to summarize and give an overview of the most important processes and mechanisms that will influence the swelling and expansion of compacted bentonite and the release of the smectite particles to groundwater seeping past a deposition hole containing a canister with nuclear waste. Analyses are also made to quantify the rate of release as influenced by different factors.

This report is an overview report and will give guidance to more detailed investigations and reports. For this, basic ideas underlying the models used are outlined and numerical examples are used to illustrate forces acting in the system studied and to assess when some processes may become important for gel/sol transition and release of colloids.

It is known that when the buffer swells into water with high concentration of especially divalent ions such as calcium the bentonite does not release colloids. In this report we therefore concentrate the effort on situations where the pore water composition is near or lower than the Critical Coagulation Concentration, CCC. We also study how and when the smectite and pore water compositions at the gel/ water interface could lead to conditions that favour erosion.

1.3 Overview of report

Chapter 2 describes some important properties of bentonite clays and how these can influence erosion.

In chapter 3 a conceptual model for bentonite erosion and experiments that illustrate some important processes are presented.

Chapter 4 describes our concept of bentonite sheets and how they can form stacks or larger particles under certain conditions.

Chapter 5 presents models and concepts of gel viscosity and how this is influenced by particle size, volume fraction and ionic strength.

Chapter 6 is the central chapter of the report. Here the dynamic model for smectite gel/sol behaviour is presented. The basis for the model is the balance forces between and on the particles.

Chapter 7 introduces the notion of diffusion of smectite particles on a gel/sol system ranging from very dense to very dilute systems. This is used in the dynamic model to predict gel expansion and to compare with experiments.

Chapter 8 discusses and describes experiments on filtering and straining of smectite particles in beds of inert particles somewhat larger than the smectite particles themselves.

Chapter 9 discusses various aspects of quantifying erosion rates and relates this to the material in the previous chapters. In this chapter several modes of erosion are described and some quantitative results are presented. Section 9.4 presents the models we have developed. In section 9.5 the impact of gravity is discussed and in 9.6 uncertainties and conservatisms are discussed.

Chapter 10 gives a summary discussion and conclusions.

Chapter 11 gives notation used.

An appendix clarifies our view on a mechanism of gel expansion in a fracture that led to considerable discussions and comments from several reviewers and other interested researchers.

2 Bentonite clays and some important properties influencing erosion

This chapter gives an overview of bentonite properties that may influence erosion. Several of the properties are later described in more detail both qualitatively and quantitatively. It serves primarily to outline the processes that will be used in subsequent modelling and to give the reader a feeling for how they interact and influence the gel/sol properties. Some rough quantitative measures are also given to concretise the descriptions.

2.1 Explanation of some terms used

There is not a universally established set of terms and definitions for some entities used to describe clays and clay properties. Below is an explanation of terms used in this report.

Sheet: The smallest building of clay, typically a very thin irregular coin-like sheet, sometimes called lamella, platelet or flake.

Stack: A number of sheets held together mostly face to full face, although the sheets may be irregularly stacked sticking out somewhat at different locations, sometimes called tactoids or quasi-crystals.

Particle: Stacks but also other irregular forms of sheets held together in irregular configurations e.g. by a smaller overlap of face to face attachments. It may also be individual sheets when there is no need to distinguish them from stacks or other particles.

Aggregate: An agglomeration of stacks or particles held more loosely together than the sheets in stacks and particles. The number of particles in an aggregate can range from a few to many particles. When there are sufficiently many particles in an aggregate the term gel is more appropriate.

Gel: A dispersion in which the particles cannot move independently of each other. Two main reasons for this are common.

Particles are held together by attractive forces. This is the case when they have coagulated in ionic strengths above the critical coagulation concentration. This is called *cohesive* gel.

A *repulsive* or *expansive* gel expands until it either fills up all the volume available if there are no body forces e.g. gravity that hinders this. The fact that a gel expands up to a certain height (against gravity) in a test tube and has a fairly narrow region where the particle concentration drops to very low values is not a sufficient indication that it is cohesive.

Sol: A dispersion in which the particles are so far apart that they can move independently. In a *stable* sol the repulsive forces are so strong that should particles come near each other by diffusion or due to effects of gravity they do not combine to form a new particle.

2.2 Bentonite mineral properties

Bentonite is a volcanic ash weathering product. It is a generally impure aluminium phyllosilicate clay consisting mostly of montmorillonite and typically contain tens of percent of accessory minerals. Common accessory minerals are quartz, feldspar, calcite and gypsum. The main constituent i.e. montmorillonite is a member of the smectite family. It is a 2:1 clay built up of a central octahedral layer sandwiched by two tetrahedral layers, as illustrated schematically in Figure 2-1. The octahedral layer consists mostly of aluminium oxide and the tetrahedral layer of mostly silicon oxide /van Olphen 1977, Bergaya et al. 2006/. The particles are thin irregular plate-shaped sheets with diameters ranging from a few tens of nm to several hundred nm. In the octahedral layer the trivalent aluminium in some locations is substituted for magnesium, iron or some other divalent metal. In the tetrahedral layer the silica is occasionally substituted for aluminium as is seen in Figure 2-1. This causes a negative surplus

charge on the order of one charge equivalent per kg, which is compensated by cations residing at the outer surfaces of the smectite sheets. When the clay takes up water, the charge compensating cations will stay near the surface of the sheets, forming a thin diffuse layer with a high concentration of cations nearest the surface and a decreasing cation concentration with increasing distance from the surface. The diffuse layers of nearby sheets repel each other. This is a very important property for the discussions in this report.

The most common charge compensating cations are sodium and calcium, although potassium and magnesium are also found in some clays. When the dominating cation is sodium or calcium the clay is often called sodium bentonite and calcium bentonite respectively. Sodium and calcium bentonites have somewhat different swelling properties when wetted, and also have different tendencies to disperse in water. The charge compensating cations are only bound to the surface of the sheets by electrostatic forces. They can readily be exchanged for other cations by ion exchange. This can be expressed as the cation exchange capacity, CEC. The CEC can be considerably different in bentonites from different locations. Values ranging from 0.27 to 0.87 equivalents per kg are reported /Karnland et al. 2006/.

An originally sodium rich bentonite will exchange the sodium for calcium when exposed to a calcium rich water and vice versa. This can impact the evolution of the swelling and other properties of the clay.

The accessory mineral particles are on average much larger than the smectite particles and have much smaller, if any, surplus charge. They influence the swelling properties of the clay and cannot move far into the smallest rock fractures into which swelling clay will expand because the apertures of these fractures are smaller than the mean particle size of the detritus. This potential clogging of the rock fractures is another important mechanism we explore in this report.

2.3 Bentonite gel/sol properties

Compacted bentonite used as buffer around the copper canisters has a very high swelling pressure when wetted. Several tens of MPa are typically found for a dry density of 1,700 kg/m^3. A buffer with this density has porosity around 37%. If the bentonite is allowed to swell the density and the swelling pressures will decrease. Further swelling decreases the volume fraction of bentonite and the swelling pressure becomes increasingly lower. A sodium exchanged Wyoming bentonite at 80% porosity (20% volume fraction of bentonite) still has a swelling pressure in the range 0.03 to 0.3 MPa depending on the water ionic strength. The higher the ionic strength, the lower is the swelling pressure. Swelling can stop entirely, at a given volume fraction, when the ionic strength in the pore water is above a critical value, the critical coagulation concentration, CCC. This will be discussed in detail later. At present it should be noted that below the CCC sodium dominated clays will expand "forever" eventually filling up all available water volume unless held back by gravity. Horizontal swelling will not be influenced by gravity and downward expansion will be aided by gravity. The gel turns into a sol in which the repulsion forces between particles hinder them from

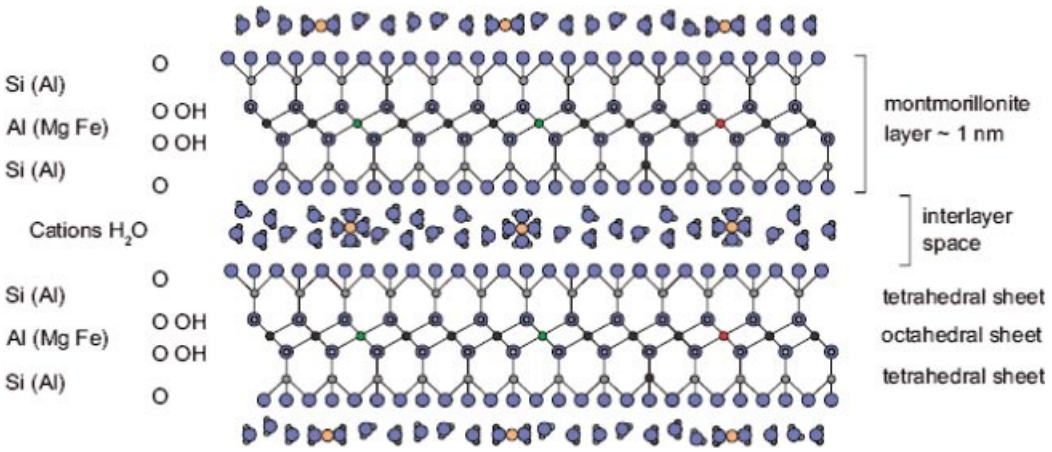

Figure 2-1. *Structure of montmorillonite.*

recombining. During these conditions colloids are formed and the sol can be transported away by the water seeping in the fractures. This will cause erosion of the buffer. The behaviour of the gel/sol system is very complex and in this section only the most important properties are mentioned. A more detailed discussion is given in Chapters 4 and 5.

Bentonite gels have many uses where their special and rather unique properties are utilised. Bentonites are used as drilling mud in the drilling for oil and gas. In the geotechnical engineering industry also their special rheological properties are essential. Relatively small quantities of bentonite in water generate a viscous, shear thinning material. Bentonite suspensions are also often thixotropic, which means that their viscosity increases with time after stirring and decreases during stirring. For this reason, bentonite is used as an additive to many paints causing the paint to be easily applied as it has a low viscosity when stirred and then becoming much more viscous hindering dripping of the applied paint. At high enough concentrations, approximately 50 grams of bentonite per litre, (around 2% by volume) the suspension begins to take on the characteristics of a pseudoplastic gel. This implies that a minimum yield strength is needed to make it move. Information on properties and uses of bentonite can be found in a recently published book /Bergaya et al. 2006/. Another overview paper that covers many aspects of bentonite behaviour is that by /Luckham and Rossi 1999/. Van Olphen's book on clay colloid chemistry from 1977 is still a very valuable source of information on bentonite uses and properties.

However, there are several difficulties in measuring such properties as minimum shear stress and viscous properties of bentonite gels. Some of them are discussed by /Möller et al. 2006/. They find that fluids that appear solid for stresses below a critical limit, called yield stress fluids, are often modelled as yield stress fluid models such as the Herschel–Bulkley model. The authors point out some fundamental conflicts between experiments on the one hand and the predictions of such models on the other hand. Indeed problems arise even with the definition and concept of a yield stress as the stress where the fluid just starts/stops flowing. Thixotropy is another prominent feature of many complex fluids and it appears to be present whenever a yield stress is present. Both phenomena are believed to be caused by the same underlying physics, but have traditionally been modelled as separate phenomena. /Möller et al. 2006/ summarize a number of recent experimental findings and present the results of some developments within a group of models designed to describe the interplay between yield stress and thixotropy. They use very simple models to explain both thixotropy and yield stress and conclude that the two effects have the same cause, namely the interplay between flow and structure of a fluid. Some of these aspects will be discussed in more detail in later sections.

Already at moderately high volume fractions the expanding gel has a very high viscosity. It will not readily be sheared away by the seeping water. In a gel volume with fractions less than on the order of 0.1% the sol viscosity is not very much larger than water. However, electroviscous effects play a role especially at low ionic strengths where the electrical diffuse layers extend far from the particle surface. Then the diffuse layers of the particles interact and influence each other /Adachi et al. 1998/. It is expected that the gel/sol viscous properties can play an important role for the erosion of the bentonite because as the gel expands into the seeping water in the fracture its viscosity will decrease and it will flow with the water, albeit with lower velocity than water without sol. Thus the influence of both particle concentration and ionic strength of the water must be understood.

2.4 The Critical Coagulation Concentration, CCC

One of the important properties of bentonite systems is their ability to form cohesive gels under some conditions and stable sols at other conditions. At low ionic strength in sodium dominated bentonite the repulsive forces caused by the cations in the diffuse layer dominate over the attractive forces at all distances between particles of interest in this report. At higher ionic strength the diffuse layer shrinks and the attractive van der Waals force can become stronger than the repulsive force at some distance. Then the individual particles will coagulate forming a stable, cohesive gel that will not spontaneously release particles. Particle volume fractions in such gels vary from a few % to more than 20% depending on the clays and on the charge of the dominating cation. Divalent ions such as calcium tend to form denser gels than monovalent ions such as sodium. In strongly calcium dominated gels the sheets tend to combine into dense stacks. Such stacks will not readily be released even into very non-saline waters. The DLVO theory /Derjaguin, Landau, Verwey, Overbeek) describes

how attraction and repulsion forces between particles can turn from purely repulsive to attractive forces when the ionic strength in the water increases. It has not been possible to use this model to quantitatively assess the Critical Coagulation Concentration, CCC, in the smectite systems of interest here. Reliance has been put on the large number of experimental investigations to assess the CCC for monovalent and divalent ions.

We wish to point out that the CCC as commonly used in many publications is based on the *"Initial"* ion concentration in the water to determine when the particles coagulate to form a cohesive gel. Although it is well known and described in books and publications that the smectites have considerable ion exchange capacity, the impact of ion exchange is seldom discussed. Different CCC's are obtained when different solid/liquid ratios are used in the experiments because the final water composition and the composition in the smectite will be considerably influenced by the solid/liquid ratio in addition to the initial water and smectite compositions. It is the composition in the diffuse layer of the smectites that sets the CCC and this composition is determined by the equilibrium concentration in the water.

This seems to be one of the reasons that different investigations can present considerably different CCC's for very similar smectites. There are however also other reasons why CCC's differ. /See e.g. section 5.1 in Jansson 2009/.

2.5 Views on gel/sol structure

In dry bentonite the smectite sheets are packed close together with distances between the faces of the sheets of about one nm and less. When wetted with low ionic strength water the sheets separate into stacks of 5–20 sheets for calcium dominated clays but mostly individual sheets for sodium dominated clays /Push and Yong 2006, Bergaya et al. 2006/. The sheets are typically hundreds of times larger than they are thick. Because of the size of the thin sheets they must arrange themselves essentially in parallel formation when the volume fraction is above a few percent for purely geometrical reasons if most sheets are separated into individual particles. When conditions are such that they form stacks with tens of sheets or more the stacks can move and rotate freely at higher volume fractions.

On the other hand, it has been experimentally demonstrated recently in the case of monodisperse or slightly polydisperse platelets (sheets) that the suspension exhibited two clear phase transitions. The system evolves from a dense columnar phase over a semiordered nematic phase to a fully isotropic phase with decreasing volume fraction. These phases can be in equilibrium with each other /Brown et al. 1998, 1999, van der Kooij and Lekkerkerker 1998, van der Kooij et al. 2000, Michot et al. 2004/.

Although not discussed in these publications the authors of the present report argue that such phases can only form in the presence of body forces such as gravity. This is important for the discussion of erosion because if gravity does not act on particles, which it will not in horizontal expansion, no phase separation should be expected. In a thin horizontal slit the particles should expand until they fill out the entire water volume and attain equal concentration everywhere. In this case, gravitational forces will be overcome by the thermal energy forces so that the Brownian motion evens out the vertical concentration. We wish to point this out already here to prepare the reader for subsequent modelling of these processes.

2.6 Particle size distributions

/Cadene et al. 2005/ studied size, morphology, and apparent charge of individual Na-montmorillonite particles of natural MX-80 sodium montmorillonites as well as synthetic montmorillonite clays. The particles were investigated by the use of three methods; atomic force microscopy (AFM), photocorrelation spectroscopy (PCS) and microscopic analysis. Two clay populations with a high dispersion of the length distribution were identified. The clay particles could be reasonably approximated at low concentrations to be ellipsoidal tactoids (sheets) about 1.2 nm thick. For the first population average dimensions were typically 320–400 nm long/250 nm wide and 200–250 nm long/120 nm wide for

natural and synthetic clays, respectively. The second population exhibits smaller sizes: 65 and 50 nm long and 35 and 25 nm wide for natural and synthetic clays, respectively. The statistics obtained for natural clay were then verified by PCS experiments on sodium montmorillonite suspensions.

/Plashke et al. 2001/ studied the size and shape of colloids released from a natural bentonite into a low-mineralized groundwater by different colloid characterization methods. They found that different colloid characterization methods are needed to get complementary information about colloid size and shape, which is essential for the understanding of natural colloidal systems. The different methods gave different results with mean sizes obtained by the different methods ranging from about 70 to 200 nm.

The studied clay is called FEBEX bentonite, which has been extensively investigated in the Swiss repository program. The atomic force micrograph showed cylindrical shape of the colloids with a major part of particles having diameters in the range of 30–100 nm and thickness of 5–15 nm. The mean particle diameter was 70 nm. The thickness of the particles suggests that the particles are formed of 3 to 6 sheets.

2.7 Natural analogues

A literature survey was compiled by /Puura and Kirismäe 2008/ with the specific objective to find information for smectite mobilization and/or retention in natural clay formations caused by contact with water with low ionic concentrations such as can be expected during and after an ice age. Evidence was sought if smectite particles are lost from the clay to the water and if accessory minerals that remain could form a growing filter slowing down or stopping further loss of smectite.

Bentonites are present in geological layers for hundreds of millions of years. There is limited exchange with surrounding layers, e.g. K transported into the bentonite layer from surrounding shale layers leading to the increased illite fraction in smectite-illite of the bentonite. Another process is silicification of surrounding layers leading to lowered permeability of surrounding rocks.

Geological literature data on historical bentonites do not consider colloid formation in low ionic strength water as relevant mechanism for smectite mobilization. However, there are no studied cases where this could be a relevant mechanism (as proposed by colloid release scenario).

Soil researchers have studied the mechanism of colloid release in laboratory experiments and have found that there has to be an abrupt change in infiltrating water quality leading to ‘osmotic explosion’. Clogging the pores in the lower part of the soil column has followed, leading to total decrease of hydraulic conductivity in vertical direction and increased surface runoff. Thus, although limited, there is evidence in the literature of clay colloids release from bentonites/smectites caused by low-ionic circumneutral water.

The geological settings to look for natural analogue studies included:

1) Bentonite/smectite similar to what is used in repository.
2) Water similar to the composition of glacial meltwater.
3) Scenario similar to what is proposed in the bentonite erosion project.

The problem related to the study of historical bentonite profiles is the geological changes that have occurred in bentonites over geological time scales. The bentonite erosion project has to provide the scenarios for approximately 100,000 years, but the geological deposits have been changed and subjected to various conditions, many of those are uncertain, during tens and hundreds of millions of years. The field studies of weathering of the historical K-bentonite deposits could provide interesting and new information, but the relevance related to the bentonite erosion project is questionable.

3 Conceptual model for bentonite erosion and supporting experiments

3.1 Previous erosion modelling

Several studies have been made on erosion of bentonites. /Pusch 1983, 1999, 2007/ discussed stability of bentonite gels in crystalline rock. /Boisson 1989/ addressed the possible erosion of bentonite by flowing water. /Kanno and Wakamatsu 1991/ and /Kanno et al. 1999/ performed experiments on bentonite erosion. /Sjöblom et al. 1999/ studied erosion in connection with possible retrieval of canisters. /Grindrod et al. 1999/ considered mechanical erosion and colloid formation by flowing groundwater. /Kurosawa et al. 1999/ studied erosion properties and dispersion-flocculation behaviour of bentonite particles. /Verbeke et al. 1997/ addressed the long-term behaviour of buffer materials in geologic repositories for high-level wastes. /Tanai and Matsumoto 2007/: studied the extrusion behaviour of buffer material into fractures using an X-ray CT method. These studies mostly discuss physical erosion mechanisms. None of them address the details of chemical and surface chemical process in depth. /Liu and Neretnieks 2006/ seem to be the first to quantitatively address the role of chemistry that may influence the rate of colloid generation and the resulting erosion.

3.2 Overview of the conceptual model

The bentonite clay buffer and backfill in the KBS-3 type repository consists mostly of microscopically small smectite particles. In the highly compacted state in the buffer, when wetted by groundwater, the particles exert very large repulsive forces. This causes the buffer to swell and fill out the available space in the deposition hole. The buffer can also swell out into fractures that intersect the deposition hole. Water flowing in the fractures could conceivably shear off the outermost particles of the clay exposing new particles to the flowing water.

When the pore water in the clay contains dissolved salts in a concentration above the CCC the clay particles swell to a certain volume fraction but not more. At this point the gel is cohesive and will not release particles spontaneously. Swollen clay that has penetrated some distance into the fracture mouth can be sheared and release gel particles if shear forces are higher than the cohesive forces in the gel. This is one of the release mechanisms discussed in the present report. As will be shown later it is not likely that the cohesive gel will be sheared off by the flowing water at the possible water velocities.

However, should very fresh water flow in the fractures, the salt initially in the pore water in the gel will diffuse out into the water and be carried away. The ion concentration will drop below the CCC. Then the particles will no longer be attracted to each other, on the contrary, repulsive forces will dominate and force the gel to expand. This expansion strives to force the particles as far as possible from each other. The outermost particles move into the flowing water, which carries them away. The process can be compared to the expansion of a gas into a large empty volume.

Should fresh water flow over long periods of time, considerable amounts of clay could be washed away, at least in the fractures with high flowrates. The particles could form a stable colloidal suspension in the non-saline waters and could conceivably be carried very long distances without being filtered or clog the fracture network. As the particles have an inherent negative charge and the minerals in the fractured rock also are mostly neutral and negatively charged the particles will not be attracted to them. The little fraction of the surface that can have a positive charge may bind some particles but when these sites are filled no more particles will stick to the surfaces. Thus filtering of the colloids in the fractures is not expected to slow down erosion markedly unless the fractures contain much small particles that form a physical filter.

In the gel the main forces acting on the particles are gravitation, buoyancy, diffusion, electrical double layer repulsive forces (DDL) and van der Waals (vdW) attractive forces. All these forces are balanced by friction forces if the particles are induced to move. Only the DDL forces are influenced by the water composition to a degree we need to consider. In waters with ionic strength below

the CCC, the DDL forces dominate over the vdW forces and the particles repel each other at all distances to be considered here. At high particle concentrations, as in compacted clay, the forces are very large. The clay expands and the rate of expansion is set by the balance of repulsion forces and the friction forces of the particles against the water. Friction of the gel, containing only montmorillonite particles, against the fracture walls seems not to play a role. This has been found in experiments with filters with very small pores where it is found that a 2 mm thick filter with pore sizes of 2 μm allows smectite particles to penetrate nearly as rapidly as through 10 μm filters /Birgersson et al. 2009/. Should wall friction between the gel/sol and pore walls, as for a fluid flowing through a porous medium have played a role, the finer filter should have slowed down the flow by a factor 25. This is because the flowrate in each pore is proportional to the pore diameter to the 4^{th} power and the total number of pores is inversely proportional to the diameter to the 2^{nd} power. This gives the flowrate per cross section area of the filter proportional to the diameter to the 2^{nd} power. This can be seen in Equation 6-14 and 6-12.

Gravity and diffusion have a negligible impact at high particle concentrations. At lower particle concentrations the gel expands more slowly as the repulsive forces decrease. Below the CCC the gel continues to expand by the DDL forces until these are so weak that thermal (Brownian) motion of the particles becomes more important to further dilute the system, which now has turned from a gel into a sol. Gravity now also starts to play a role. In upward expansion, gravity pulls back the particles and in a downward expansion it helps to dilute the sol. Horizontal expansion where gravity has no impact would allow the sol to expand isotropically in all available water volume.

The gel is thixotropic and behaves as a pseudoplastic fluid. In a range of particle concentrations around a few percent by weight the gel is more viscous when at rest and less viscous when subjected to shear. A rested gel will need a larger shear force to set it in motion and to shear off particles at the gel/water interface. However, once the gel has been sheared and set in motion it will flow more easily.

The gel does not flow like a Newtonian fluid such as water but deforms slowly when subjected to a shear force. Sometimes it needs a minimum shear force to start deforming it. This is called the yield stress. The gel then behaves like a Bingham body or fluid. At shear stresses larger than the yield stress it flows nearly like a Newtonian fluid. Often in practice there is not so clear minimum shear stress but more gradual decrease in viscosity with increasing shear rate. As the viscosity is the ratio between shear stress and shear rate, the viscosity seems to decrease as more force is applied. The higher the particle concentration is the more nonlinear these effects are.

This has an important impact on the erosion. At high particle concentrations, for illustration purposes, thinking in terms of 5 volume percent or more, the viscosity of the gel at low shear forces is several orders of magnitude higher than that of water. The lower the particle concentration is the relatively speaking high viscosity decreases and approaches that of water. The water flowing in the fracture which has taken up only some particles from the expanding gel flows more slowly than the water, but it flows. The whole gel, if above the yield stress, is set in motion and slowly moves downstream. It is gradually replaced by more swelling gel from the deposition hole. This is another mechanism that influences the erosion.

Above the CCC the gel expands to a point where the vdW attractive forces become equal to the DDL forces, which have decreased and act at shorter distances by the increase in ionic concentration. When this point is reached, the gel expansion stops and particles that try to escape by thermal motion and possibly gravity are pulled back. Particles are not spontaneously released anymore and the gel is what is called a cohesive gel. A very sharp boundary between gel and water develops. It should be noted, however, that in most experiments using visual observations to determine the CCC, gravity probably has played an important role to restrain colloid dispersion to a dilute sol.

Figure 3-1 shows a fracture intersecting the canister deposition hole which is filled with compacted bentonite. The bentonite, when wetted, swells out into the fracture. It has a very high swelling pressure when highly compacted but the swelling pressure decreases with decreasing bentonite density. The smectite particles are pulled and pushed into the water that seeps in the fracture by the different forces acting on the particles. If the pore water is below the CCC the particles at the bentonite/water interface can diffuse into the moving water and be carried away. There is also a region where the gel/sol has so low a particle concentration that it is little more viscous than water and can flow away.

The loss of particles is thus influenced both by particle diffusion and by advective flow of the dilute gel/sol. For both mechanisms, the flowrate of water and gel in the fracture will set the total rate of loss. This has been modelled and is reported in chapter 9.

The pore water composition strongly influences the DDL forces but has a very weak influence on the other forces. The viscosity of the dilute gel increases with decreasing ionic strength when the electrolyte concentration is smaller than CCC. See Chapter 9 for details. The CCC determines when the smectite particles can be released to the water in the form of colloids or when they still will be held together by the attractive vdW forces and will not diffuse out into the passing water and be carried away. It can, therefore, be used to set up the borderline between a cohesive and an expansive gel. If the gel at the gel/water interface is cohesive, it behaves like a pseudoplastic body and may not start to flow or allow shearing off of gel at the gel/water interface by the small shear forces the seeping water in the fractures can generate.

The water composition in the deep groundwaters at repository depth is normally above the CCC and no release of colloids is then expected. It is also not expected that the cohesive gel can be sheared away at any of the expected water velocities. This is argued in more detail in section 9.4. However, if fresh water were to intrude, the pore water composition at the gel/water interface could decrease and become lower than the CCC that would allow particles to be released causing bentonite loss. The rate of leaching of the ions in porewater will, therefore, influence or limit the possible erosion rate.

When the pore water composition in the buffer is below the CCC and when the water seeping in the fractures also is below the CCC the gel is expansive and its rate of expansion will not be limited by the rate of leaching of CCC determining ions. The rate of expansion will then only be limited by

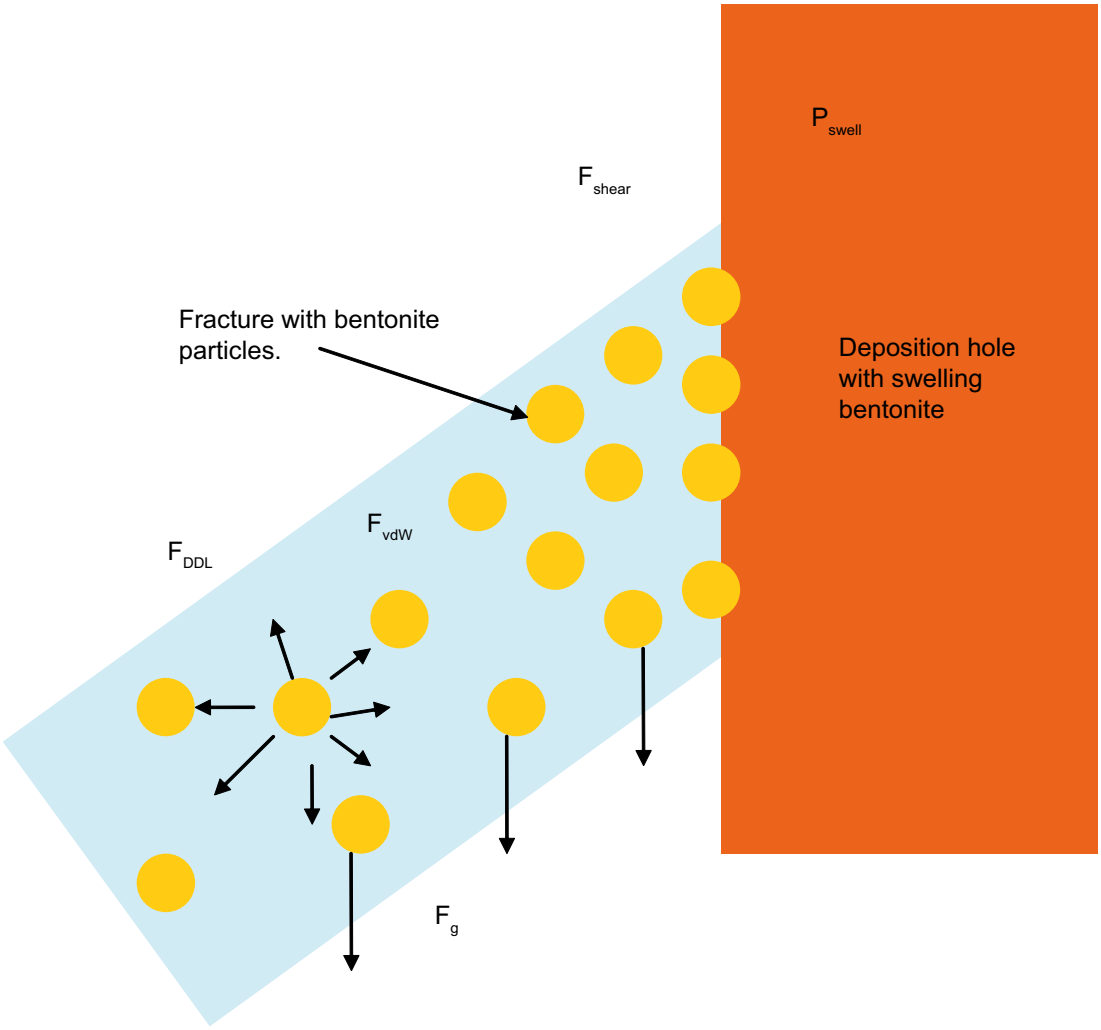

Figure 3-1. *Schematic of forces acting on the bentonite in a deposition hole and fracture.*

the friction forces between the water and the particles in the gel/sol. In clays that contain sand-like, non-smectite particles, friction against the fracture walls may also slow down expansion. The rate of expansion would gradually slow down for two reasons. The expansion rate slows down inversely proportional to the square root of time because the water that intrudes into the gel has further and further to travel as the gel has expanded further into the fracture. Another reason is that should there be a noticeable loss of swelling pressure in the buffer due to loss of clay, the rate also slows down.

A further factor comes into play in practice. The commercial bentonites contain accessory minerals in addition to the smectite particles. This is sometimes called detritus material. This material can be thought of as very fine sand. These particles are much less influenced by the DDL forces than the smectite particles because of their different electrical charge properties and because they in general consists of much larger particles. It is envisaged that as the clay gel expands out into the fracture it will carry with it the small sand particles. Where the gel has expanded so much that it forms a sol, i.e. where the individual smectite particles no longer have strong repulsion forces between them and move essentially randomly and independently of each other propelled by thermal forces (Brownian diffusion), they no more carry the sand particles with them. These are left behind and gradually build up a porous sand bed with essentially stagnant water. The smectite particles now have to move through the sand bed to reach the mobile water. As more smectite is lost, the sand bed keeps increasing in size. The transport of the smectite particles will gradually slow down and may even totally stop when the sand bed is compressed and forms pores smaller than the smectite particles. This is called straining. The particle size distribution of the detritus material should be such that it overlaps with that of the smectite particles for the straining to be effective. Filtering and straining are discussed in chapter 9.

Even if the sand bed does not fully strain the smectite particles, it will slow down particle movement as well as the exchange of solutes between the seeping groundwater and the pore water in the bentonite inside the sand bed. The longer the sand region is the longer distance ions and smectite have to diffuse, which limits the rate of mass transfer. The loss of CCC determining ions will slow down and may eventually become the rate determining step for the colloid formation.

Figure 3-2 illustrates the expansion of the gel in a fracture, the formation of the sand bed and the transport of solutes and colloids through it. At present, we only discuss the case when the pore water is below the CCC in the region around the gel/water interface although it may be above the CCC further into the buffer. DDL forces expand the bentonite into the fracture. The fracture is slanting and gravity will therefore pull back upward expanding particles but pull them downwards into the water at the lower end of the intersection with the deposition hole. The sand particles are left behind when the gel turns to a sol and form a porous bed through which the smectite particles have to pass. This slows down the flux of the smectite particles. In addition, the sand and the gel will slow down the diffusion of ions from the pore water in the gel as the particles form a diffusion barrier with their stagnant water. The sand will be pushed outward in the fracture by the swelling gel but will be restrained by friction against the walls of the fracture. Larger particles will also be physically hindered (strained) from entering and moving far in narrow fractures. This will in turn help to strain smaller particles that get stuck and so on. The particle size distribution in relation to the fracture aperture distribution will determine how far the particles can migrate before clogging the fracture. The particle size distribution of the detritus material overlaps that of fracture apertures and straining and clogging is expected to be potentially important mechanisms that can decrease or even stop erosion.

The thicker the sand bed becomes the more difficult it will be for it to move further out into the fracture. It is also expected that a sand bed will form in the deposition hole at the mouth of the fracture because the expansion into the fracture is increasingly slowed down by friction and straining. This sand bed will be compressed and compacted by the swelling clay. The sand bed at the mouth of the fracture as well as in the fracture itself will grow with time but the rate of growth will decrease as less and less smectite particles can negotiate paths through the narrow pores of the bed.

In fractures with downward facing component, the sand particles can be pulled downward by gravity contributing to the loss of such particles, as shown in Figure 3-3. Hypothetically the whole downward facing fracture could be filled with such sedimenting sand particles if straining has not set a limit beforehand. The water flowrate will slow down in the fracture now filled with particles and its carrying capacity of smectite particle will decrease.

The solubilised smectite particles that reach the outer rim of the sand bed will diffuse into the boundary layer of the seeping water. The diffusivity of smectite particles is orders of magnitude lower than that of ionic species. During a given time they move a short distance into the seeping water. When the water has passed the deposition hole it has picked up a limited amount of colloids. This can be thought of as a resistance to colloid transfer to the seeping water. However, at the downward sloping part of the fracture, gravitation helps to pull the sol particles down into the water. At the lower end of the fracture, the rate of loss of smectite is therefore faster than at the upper parts.

One may speculate on the fate of the sand. At least the sand particles that are larger than the smectite particles will tend to sediment to the bottom of the fracture eventually filling a section below the deposition hole with sand. Water flowrate will decrease there and slow down the rate of transport of the smectite particles.

3.3 Overview of some experiments

In the previous section, a conceptual picture of buffer erosion was presented. It is based on general observations described in books and papers as well as deliberations of how the different processes and mechanisms governing gel/sol behaviour might influence the erosion processes. We are convinced by numerous investigations that when the ion concentration in the pore water in the gel at the gel/water interface is above CCC, colloidal particles will not be released from the gel to the water seeping in the fractures.

In the erosion project, therefore most effort is spent on situations where the ion concentration is below CCC and where sol formation is favoured. Some experiments were performed above CCC to further confirm the non-erosion in such circumstances. It is thus important to be able to assess

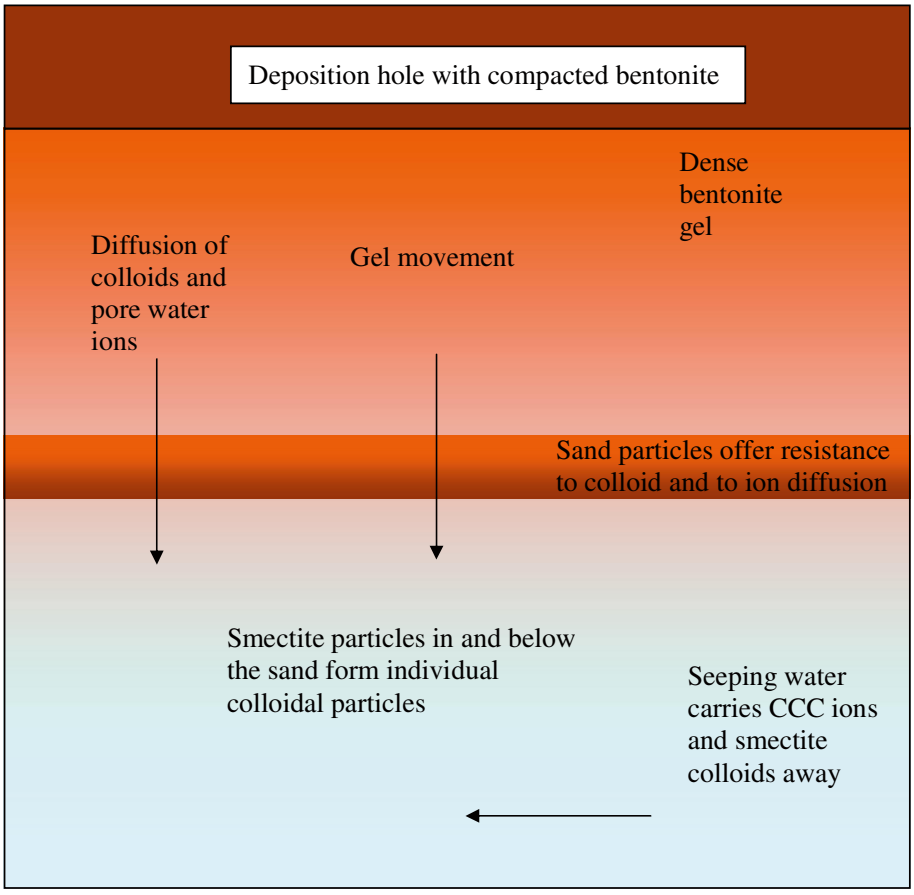

Figure 3-2. *Bentonite gel expands downwards from the deposition hole into and in a fracture. Smectite colloids are released from the gel, move through the sand bed and are carried away by the seeping water.*

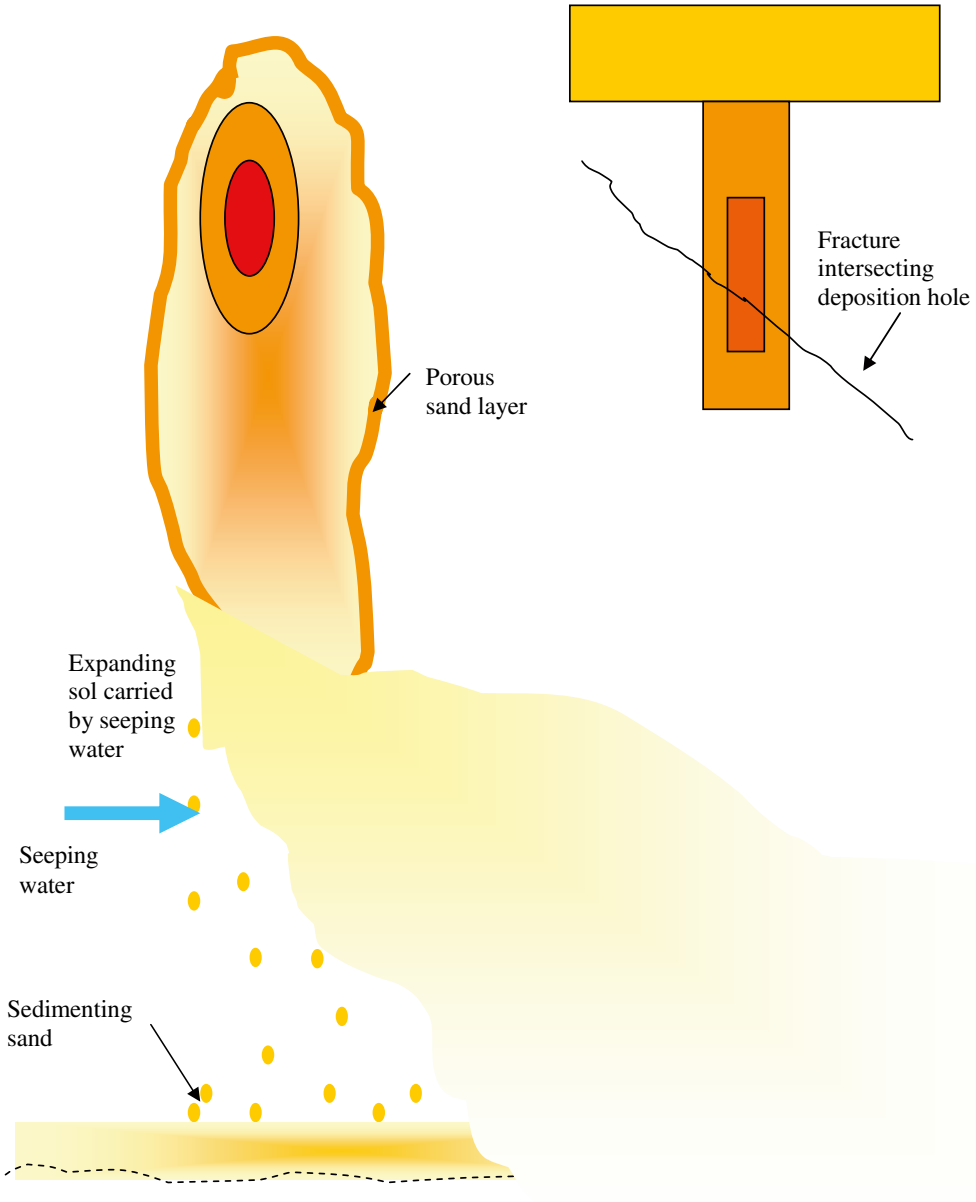

Figure 3-3. *Cartoon of how a sand region could develop in the fracture around a deposition hole and that it may be breached and sediment away in the lower parts of the fracture.*

the range of CCC values and if and when the pore water concentration at the gel/water interface can become less than this. Sodium and calcium are expected to be the most important cations that influence the CCC and the investigations focus on these.

Two groups of experiments are presented. In the first group expansion of gels and sol formation into waters with different concentrations of sodium and/or calcium are described. The clays used were both natural commercial clays with detritus materials and clays separated from detritus and cation exchanged to form homoionic pure Na- or Ca- smectites.

In the second group of experiments, filtering and straining of smectite particles in small filter beds of detritus materials and in metal filters with well defined pore sizes were studied and are described.

Smectites very rich in calcium as charge compensating ions are theoretically supposed not to expand more than marginally, and therefore special attention was paid to this potential no-swelling effect. The full set of experiments is reported in the references from which highlights are extracted in the sections below. The highlights were selected because they illustrate many of the most important aspects of mechanisms we study and because several of the experiments have compiled data that can be and have been quantitatively tested by our models.

3.3.1 Swelling ability of bentonite

Highlights from: /Birgersson et al. 2009/

Figure 3-4 shows how different homoionic smectites swell in deionised water. It is seen that with the monovalent ions Na and K the smectite swells considerably, whereas with the divalent ions swelling is considerably less. Figure 3-5 shows how the height of the gel evolved over time. The two clays with monovalent ions have still not stopped swelling after 60 days. They have expanded from 2.5 mm dry clay originally deposited in the vessels to more than 60 mm. The clays with divalent ions stop swelling at about 9 and 15 mm. Of special interest is that smectite with 80% calcium and 20% sodium swells nearly as well as the pure Na smectite.

Clearly in deionised water the monovalent smectites form repulsive gels that continue to expand. The smectites with divalent ions swell much less and seem to have a narrower diffuse region at the gel/water interface. From these observations alone, however, it is not possible to know if these gels are repulsive or cohesive. They may be just denser sediments of particles consisting of many smectite sheets that are too heavy to be mobilized upward against gravity by Brownian motion.

Note, however, that a relatively small content of monovalent ions (Na^+) in a calcium dominated system may still lead to general colloid formation at low ion concentrations. This may further be illustrated by the performed series of simple swelling experiment with 0.5 grams of homoionic smectites, called WyNa and WyCa, to give calcium-sodium ratios of 80/20, 60/40. The pure Na-smectite was, in addition, mixed with relatively large amounts of calcite and gypsum to show the effects of typical equilibrium concentrations of Ca^{2+}, for these minerals. This is shown in Figures 3-6 and 3-7.

In particular, these experiments show that, when the water contains calcium in a concentration given by the solubility of gypsum, the original Na smectite swells similarly to calcium smectite. As will be discussed later, calcium has a solubility of about 15 mM, which is well above the CCC. However, it may be noted that ion exchange in this case also may have played a major role, as the charge compensating sodium ions originally in the smectite have to a considerable extent been ion exchanged for calcium, forming very calcium rich smectite.

The experiment with calcite mixed with sodium smectite on the other hand has not generated a calcium dominated smectite or a water composition above the CCC.

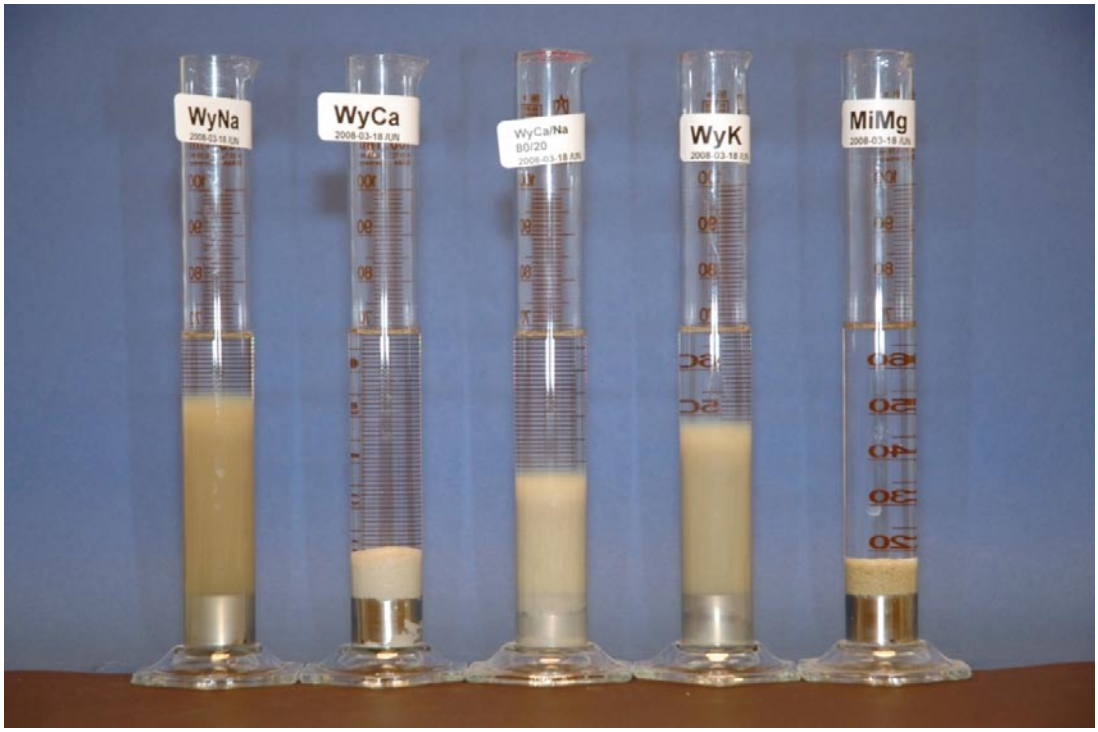

Figure 3-4. *Free swelling tests with pure montmorillonites with only Na^+ as counter ion (left), only Ca^{2+} as counter ion (second from left), Ca^{2+}/Na^+ ratio of 80/20 (middle), only K^+ as counter ion (second from right), and only Mg^{2+} as counter ion (right).*

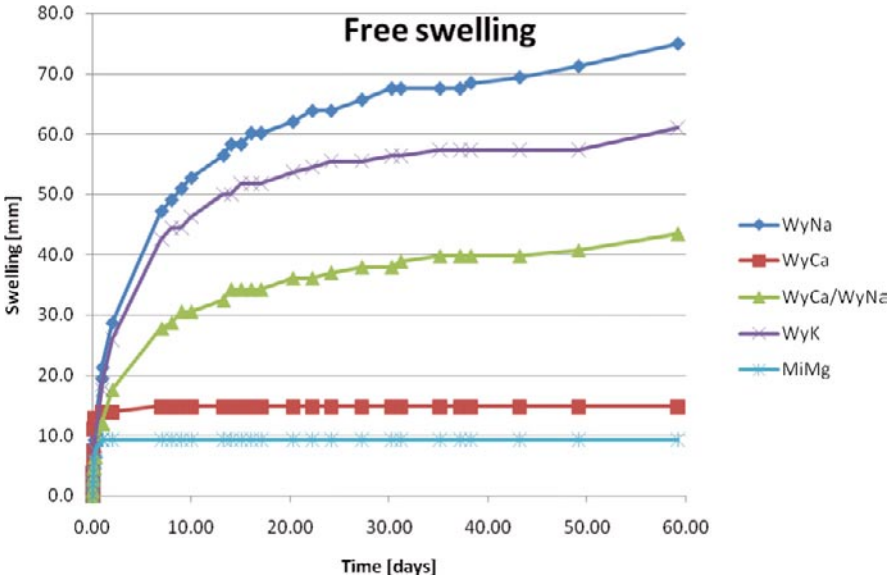

Figure 3-5. *Height of test samples versus time measured for free swelling in deionised water. The initial height of the water-saturated samples was of 2.5 mm. The final conditions of the samples are shown in Figure 3-4.*

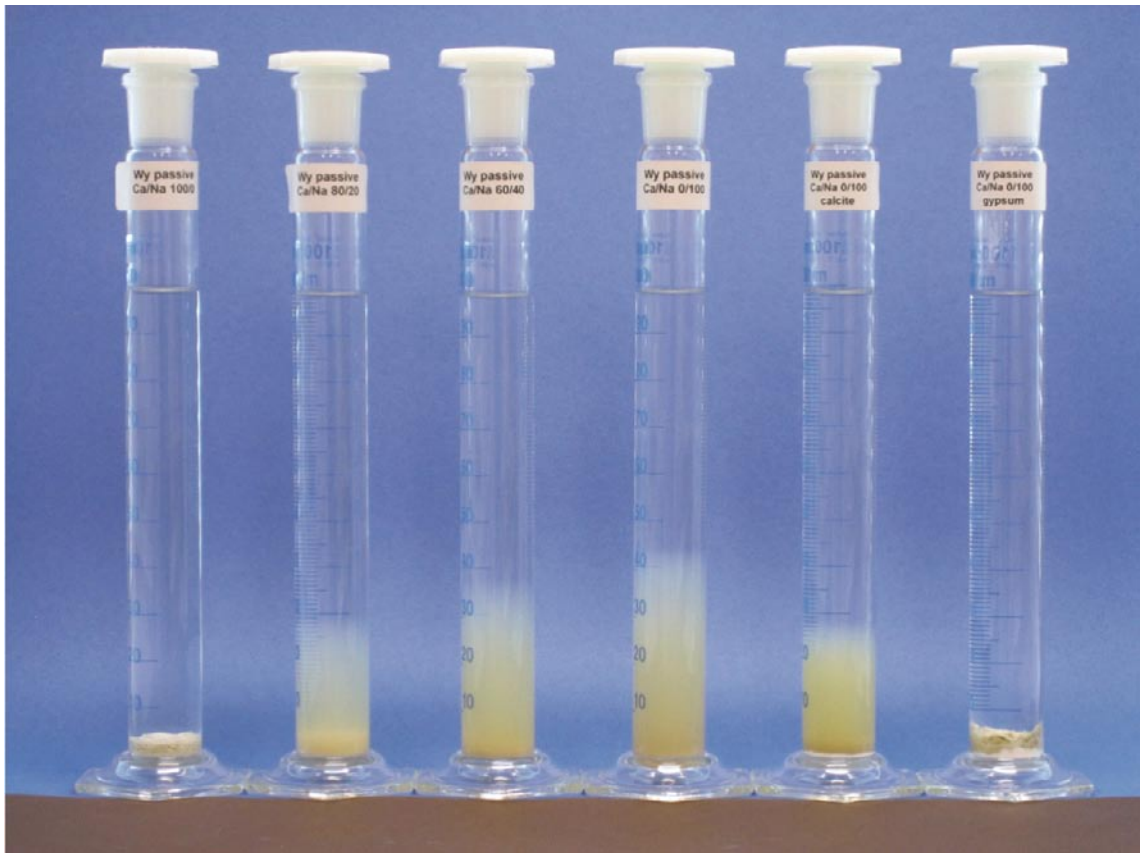

Figure 3-6. *Free swelling tests after 165 days with 0.5 grams of homoionic smectite prepared to contain the following Ca^{2+}/Na^{+} ratios: 100/0 (left), 80/20 (second from left), 60/40 (third from left), 0/100 (third from right), 0/100 mixed with calcite (second from right), 0/100 mixed with gypsum (right).*

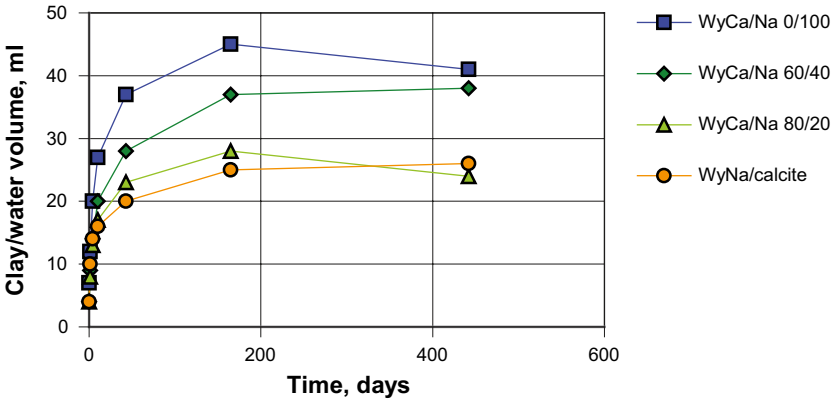

Figure 3-7. *Volume change of the clay/water system versus time in free swelling experiments with 0.5 grams of montmorillonite. Figures indicate the calcium/sodium ratios. The final conditions are illustrated in Figure 3-6.*

3.3.2 Expansion in slits and influence of gravity

Highlights from: /Jansson 2009/.

Some simple tests were made where a small amount of clay (0.2 g) was put into the bottom of test tubes. 10 ml deionised water was poured onto the clay which was allowed to swell and expand in the water giving a volume fraction of smectite of 0.7%. A thin very fine filter with nominal hole size of 10 µm was fastened in the tube at the top of the gel/sol. The tubes were then filled to the rim with water with different compositions. After one day the tube was turned upside-down. The response was easy to observe visually within 5 minutes. Either the clay dispersed and started to fall through the net or else it stayed above the net. Some tubes where the clay stayed above the net were left for 1 month (for instance untreated MX-80 in deionised water) without anything happening.

Untreated MX-80 bentonite did not disperse in limited volumes of deionised water. However, when accessory minerals were removed from MX-80 bentonite by washing twice, centrifuging and collecting the top fraction, the treated clay fell through the net when deionised water was used. At least two reasons for this difference were identified. The detritus material could have formed a mechanical filter and/or the gypsum in the detritus material dissolved to raise the calcium concentration above the CCC.

The tests with the ion exchanged and purified materials were used to determine the lowest calcium concentration needed to keep homoionic sodium smectite from dispersing. According to the tests performed, a calcium concentration of about 1 mM is needed to stop the particles from penetrating the filter. This is in agreement with observations of CCC of Ca as the dominating cation in water. It should be noted that the notion of a CCC is not well defined. For Na exchanged clay contacted with calcium containing water, ion exchange will play a role, as sodium in the smectite will exchange for calcium in the solution and then sodium would be CCC-determining ion, at least partly.

Figure 3-8 shows how the clay particles (rapidly) penetrate through the filter and sediment downwards in the tube. This phenomenon was observed for Na-exchanged smectite in waters below the CCC. In these experiments, the amount expressed as charge equivalent of ion exchange sites were about the same as the total amount of calcium in the added water with 2 mM. This implies that even if most of the calcium enters the exchange sites there still is about half the calcium concentration remaining in the water.

Tests with 0.02 g of smectite were also performed. Then the smectite will have more than 90% calcium in the exchange sites. (See chapter 7 where ion exchange equilibria are discussed). The CCC, meaning when the smectite no longer could pass the net was again about 2 mM.

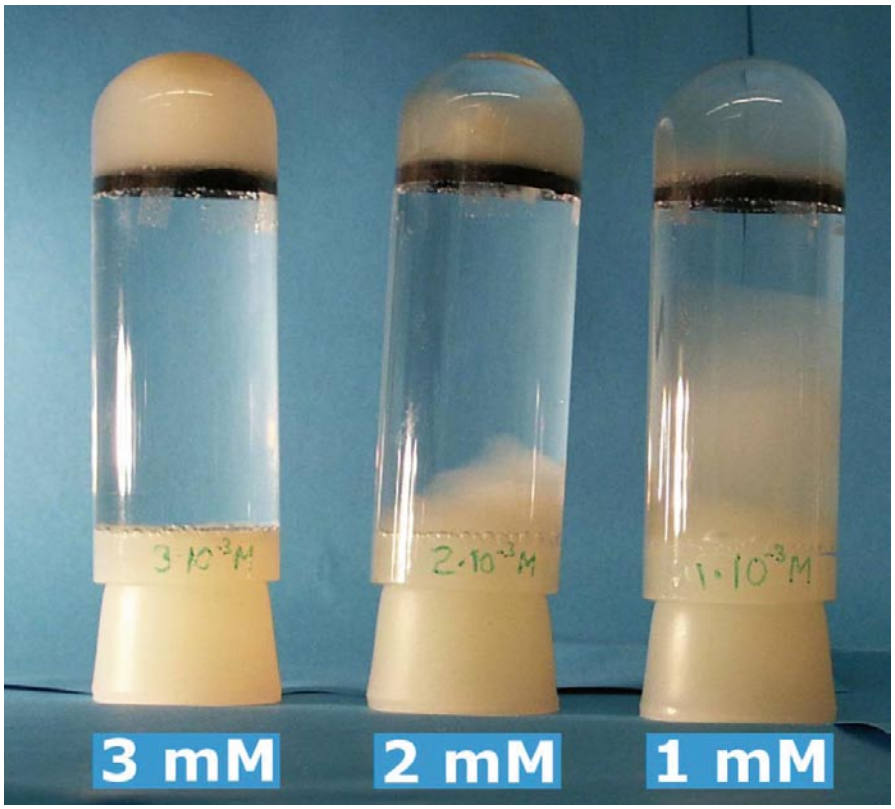

Figure 3-8. *Determination of lowest calcium concentration needed to keep homoionic sodium smectite from dispersing.*

When starting with fully Ca exchanged clay, no particles were released even in very low ionic strength waters. This partly supports theories stating that calcium rich smectite particles will tend to stick strongly and closely together. The experimental conditions thus influence the gel properties and it must expected that calcium dominated clay will behave differently if it is expanding or if it is sedimenting. Some possible reasons for such behaviour will be discussed in chapter 7.

It should be noted that the gel particles sediment much faster than individual smectite sheets can, see section 6.3. Similar observations are reported by /Birgersson et al. 2009/. This indicates that even at ionic strengths below the CCC the smectite particles can agglomerate to form flocs that sediment much more rapidly than individual smectite sheets can do. At the same time such flocs can easily break up to pass very fine holes and recombine after passage. The underlying mechanisms are not understood.

Another set of experiments were conducted in an artificial fracture to study the scenario where bentonite swells into a fracture and comes in contact with low salinity water that slowly seeps past the expanding gel/sol. To simulate a fracture, a 50·50 cm Plexiglas plate was placed on top of another Plexiglas plate, as shown in Figure 3-9. The plates were separated by 1 mm thick small plastic cylinders. At one end of the plates, a 1 cm thick and deep bentonite container was placed in direct contact with the fracture while the opposite end was blocked. Perpendicular to the bentonite container a distributor was located, supposed to distribute water evenly over the whole side. Opposite to the distributor the flow is collected into 5 slots.

A first experiment using this set-up started in the beginning of June 2006. Purified MX-80 bentonite free from readily soluble minerals and other accessory minerals was used. The bentonite was placed in the bentonite container. The dry density of the bentonite was 1,000 kg/m^3. After assembling all parts, deionised water was added via a channel at the bottom of the container for four weeks, to ensure full water saturation. The channel was then closed and deionised water was pumped into the fracture via the distributor. The effluent was collected in five slots. The flow rate was about 5 ml day^{-1}. After five weeks of pumping the bottles collecting the outlet were weighed and analyzed for

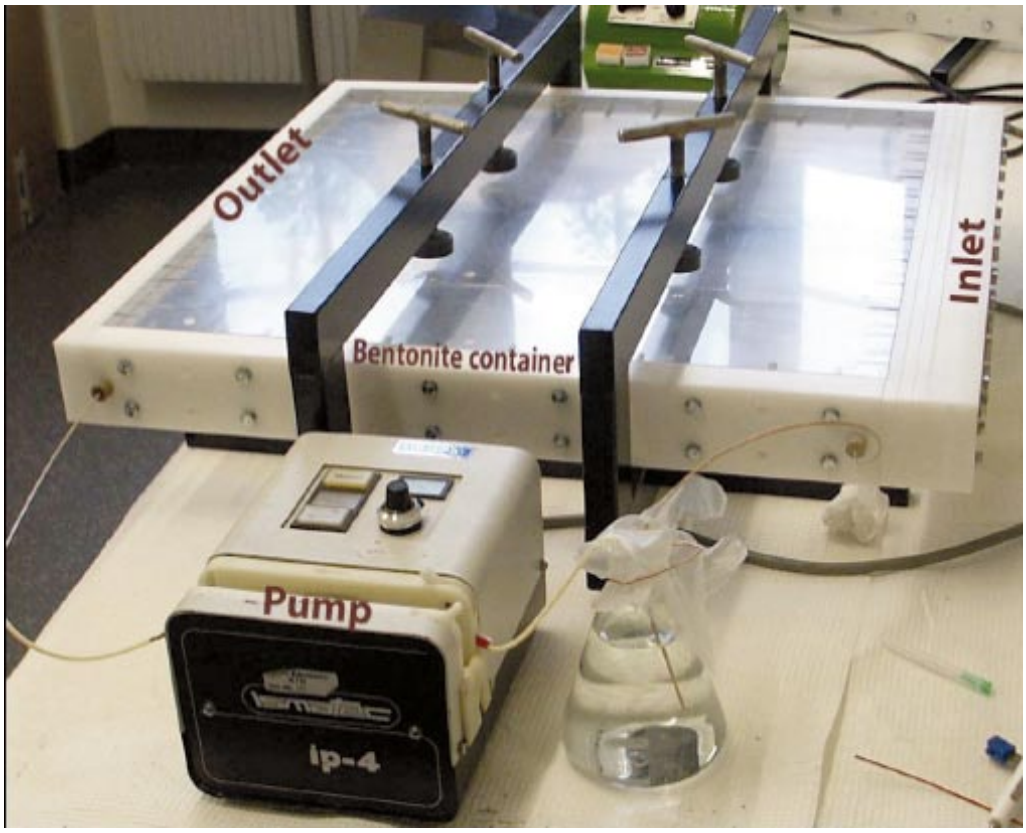

Figure 3-9. *The setup with the artificial 0.5·0.5 m fracture showing the bentonite container and the in- and outlet sections.*

colloid concentration. The water flowrate was unevenly distributed between the channels. The colloid concentration nearest the bentonite container was much higher than in the waters from the other sampling points, as expected. The smectite concentration varied between 0.02 and 0.16 g/l.

Figure 3-10 shows how a part of the fracture looked after the water saturation. Figures 3-11 and 3-12 show the gel expansion after 4 and 28 weeks after start of water seeping, respectively.

It is seen clearly that there is a faint darker, greyish, irregular stripe extending from top to bottom of the picture in Figure 3-12 just to the left of the white coin-like distance holder. We believe that this is the little amount of detritus material that could not be separated from the smectite particles. These are pushed along by the expanding gel but left behind when the gel turns to a dilute sol, which cannot push the small detritus particles any further but they can pass through the bed of particles that were left behind. We believe that we see the embryo of formation of a "sand" containing porous region as was described in the conceptual model in Figures 3-2 and 3-3.

In the second fracture experiment, bentonite that had been washed twice in order to remove readily soluble minerals (i.e. gypsum) was used. The other detritus particles were left in the bentonite. The behaviour of the bentonite was similar but the dark band was more prominent.

As can be seen in Figure 3-13, the clay disperses into the fracture. A clay concentration gradient can clearly be observed from right to left. Another interesting thing is the black rim between what seems to be denser and a more dilute gel/sol. This rim was seen also in the first experiment, Figure 3-12, but is even more pronounced in the second experiment, Figure 3-13, where the bentonite was only washed of soluble calcium minerals and not purified in any other way. The rim was subsequently found to be considerably enriched in the fine grained accessory mineral. The fraction of montmorillonite decreased from 76 to 45%. Thus in the rim more than half the mass consists of detritus material.

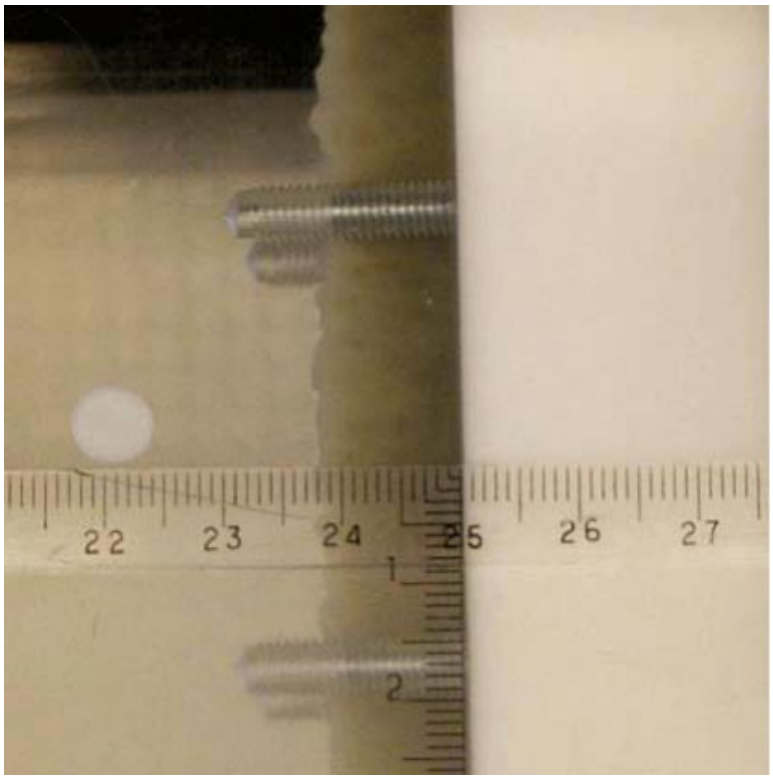

Figure 3-10. *After four weeks of water saturation the bentonite from the back side had swollen 12–14 mm into the fracture. During this time there is no water in fracture.*

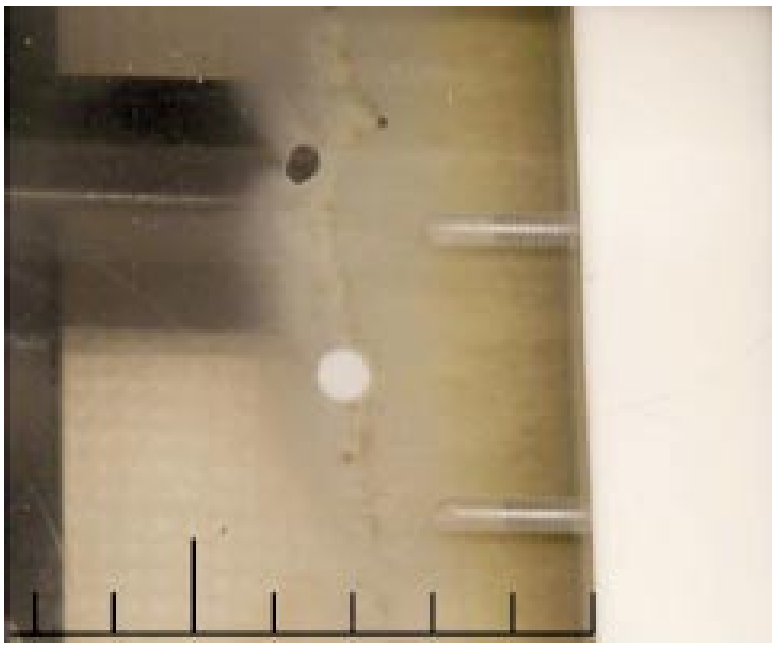

Figure 3-11. *Bentonite in the fracture after pumping water for 4 weeks.*

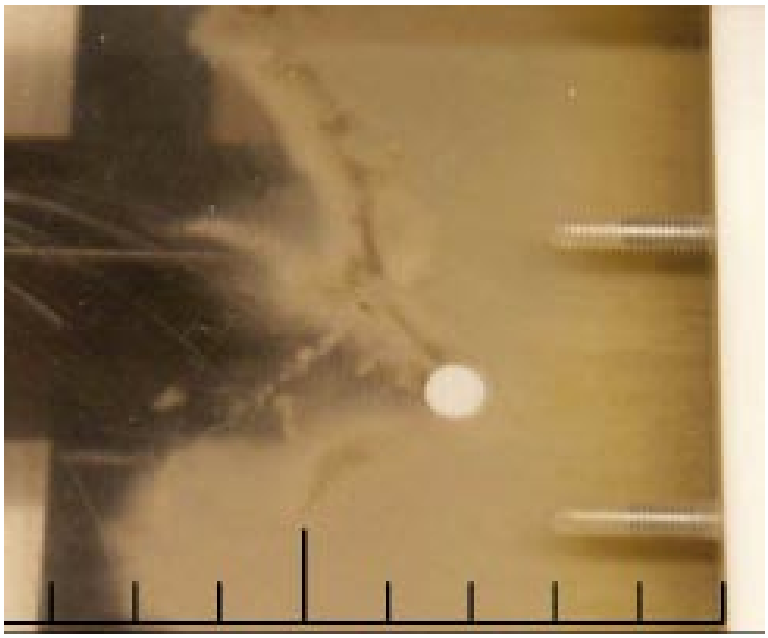

Figure 3-12. *Bentonite in the fracture after pumping water for 28 weeks.*

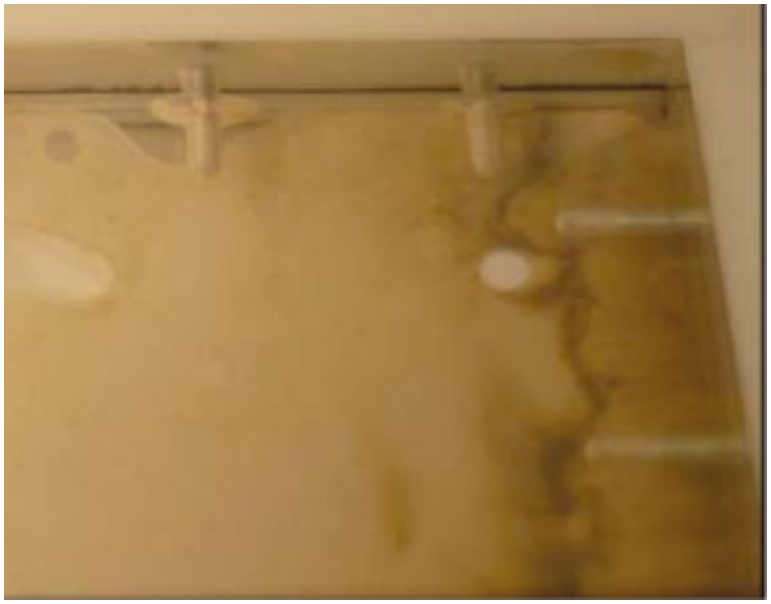

Figure 3-13. *In the second experiment the fracture inclined a few degrees which caused the dispersed clay to sediment close to the water inlet side, which is at the upper side of the picture.*

In the second experiment the fracture contained air bubbles that were hard to get rid of. Therefore, the fracture was tilted some 2–3 degrees so the bubbles could move towards the water exit side (downward in the picture). Surprisingly a relatively thick gel accumulated at the water inlet side of the fracture, i.e. not following the flow but sedimenting at the lowest point of the fracture, see upper right hand corner in Figure 3-13. This shows that the gel has a viscosity low enough to allow it to flow driven by gravity.

The water exiting from the five slots was collected in bottles. Spot tests of the bottles were taken and analyzed on a Single Particle Counter (SPC). The results can be seen in Figure 3-14.

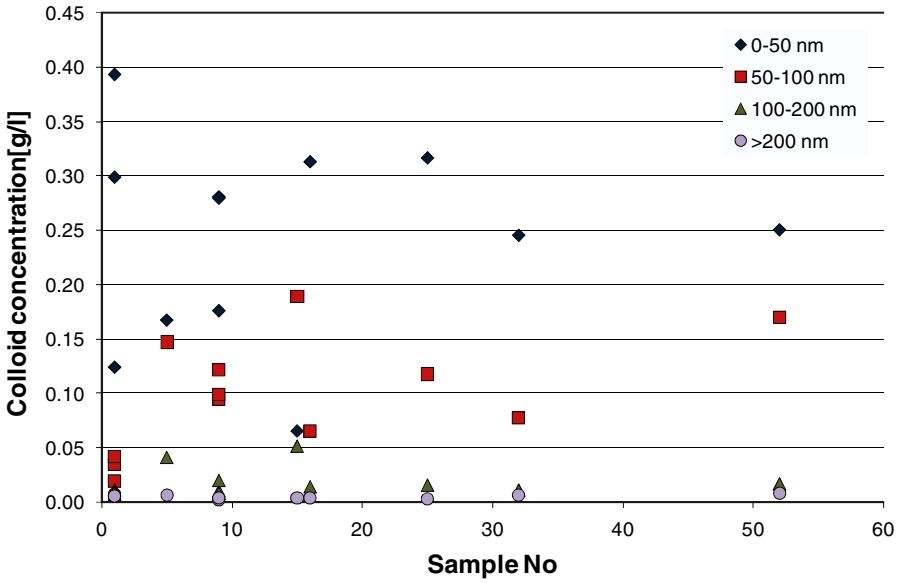

Figure 3-14. *Results from SPC (Single particle counter) analysis of randomly taken samples of the outlet solutions. The sample numbers correspond to increasing sampling time.*

The concentrations in the samples are relatively uniform, independent of time after the start of the experiment and independent of which slot in the outlet the sample was taken. The particle concentration is less than 0.4 mg/l. It is clearly seen that the clay particles are polydisperse and that the smaller particles move more readily out into the seeping water.

Dye was added at one instance during the experiment to visualize the flow pattern. Flow channelling was clearly observed and location and pattern of channels varied over time. The presence of smectite in the water in the fracture thus considerably influences the local flowrates and where the flow moves. We assign this to differences in gel/sol viscosity.

We conclude from these experiments that the smaller smectite particles will be more readily solubilised and more prone to be carried away by the seeping water.

Another important observation is that the gel/sol can flow.

3.3.3 Gel expansion and Nuclear Magnetic Resonance imaging, MRI

Highlights from: /Dvinskikh and Furó 2009/

Disk-shaped compacted bentonite pellets of diameter 8.0 mm and height 3.0 mm and density 1.8 g/cm^3 (22–25% water) were formed using pneumatic press, as shown in Figure 3-15. This corresponds to a dry density of 1.35 to 1.40 g/cm^3. At this compactness, the air volume in sample was estimated to be ~7 volume%. Pellets were tightly inserted from the bottom in the quartz tube of 8.0 mm inner diameter and 200 mm length. The tubes were sealed from the bottom with a plastic cap which reaches the bottom of the pellet, Figure 3-16.

For each sample, first magnetic resonance imaging, MRI, measurement was performed on the sample in “dry” state. Then, water was added from the top of the vertically standing tube (water height is about 18 cm in the tube).

Nuclear magnetic resonance, NMR, data were processed to calculate the vertical distribution profile of the clay volume fraction in the sample during the swelling process. In this analysis, possible effect of air volume was neglected. Analyzed data are presented as clay volume fraction depending on the vertical distance from the upper edge of the plastic cap (which is also the bottom of the dry tablet).

Results of the swelling experiments with different clays are presented in Figures 3-17 to 3-20.

Figure 3-15. *Disc shaped pellet used in expansion experiment.*

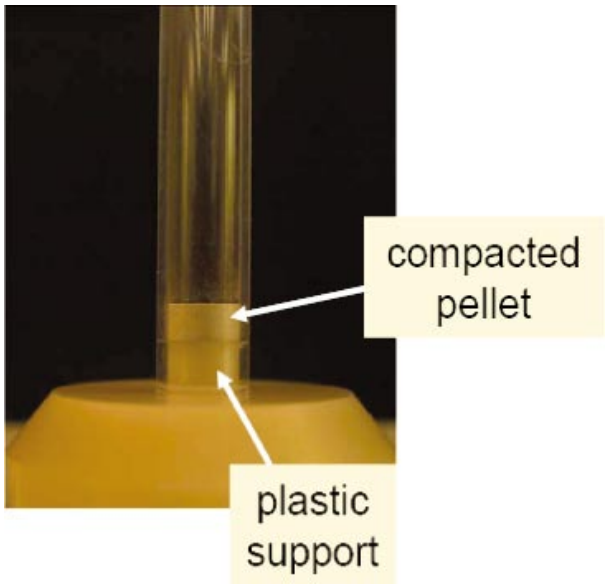

Figure 3-16. *Tube with pellet used in expansion experiment.*

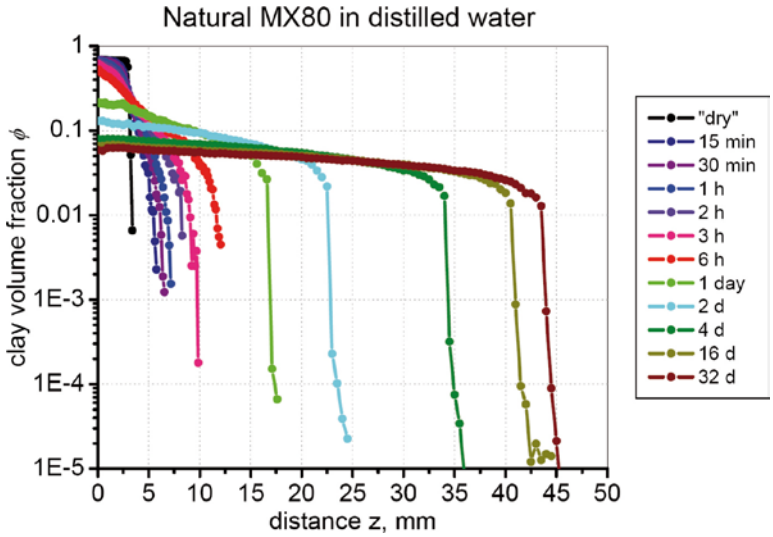

Figure 3-17. *Natural MX-80 bentonite swelling upward in the vertical tube in deionised water. Note the logarithmic scale. z denotes the distance from the bottom of the tablet.*

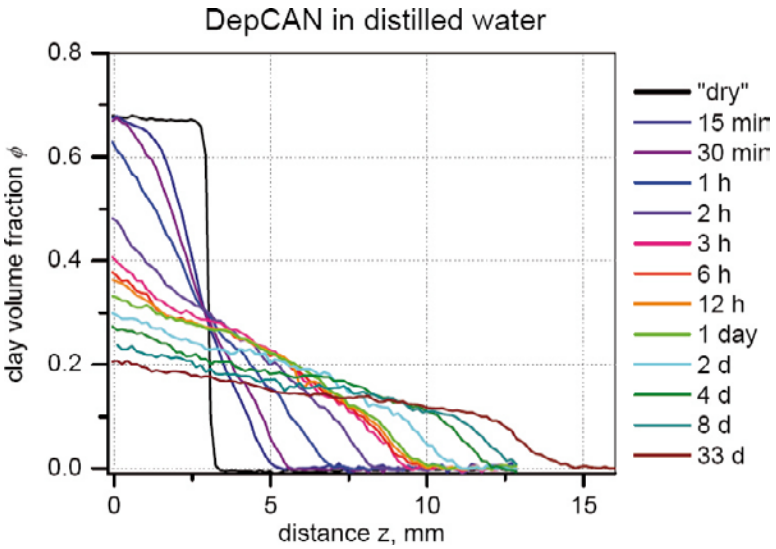

Figure 3-18. *Natural Deponit-CAN (a calcium rich bentonite) bentonite swelling upward in the vertical tube in deionised water. Note the linear scale.*

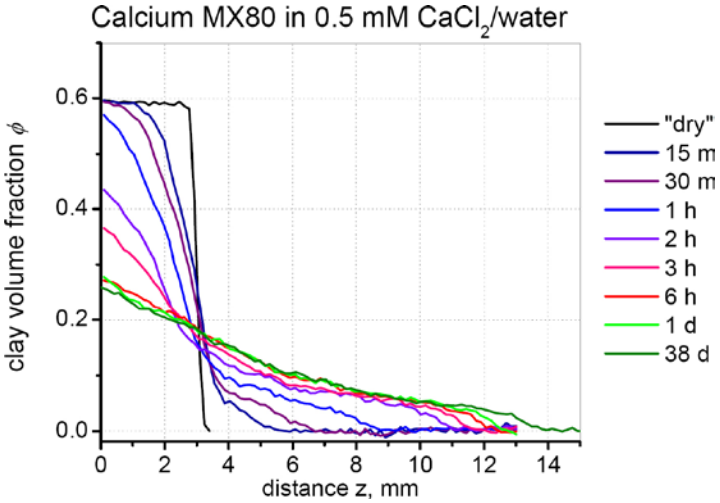

Figure 3-19. *Homoionic calcium exchanged and detritus free MX-80 bentonite swelling upward in the vertical tube in 0.5 mM $CaCl_2$ solution. Note the linear scale.*

These results show that sodium as well as calcium rich bentonites swell rapidly and that compacted calcium rich bentonites swell to at least four times their original volume. The most swollen parts have a volume fraction of about 5% smectite. In the purified and sodium exchanged bentonite, the MRI technique gave extremely good resolution of volume fractions spanning nearly five orders of magnitude.

Figure 3-20 shows the expansion of the very sharp gel front against the water intruding into the gel and against gravity. The impact of gravity is clearly shown in the three rightmost curves taken after 81 to 301 days. The less sharp front shows the typical effect of gravity when particle diffusion will force the particles upward but gravity pulls them back. For the earlier time curves, the rate of expansion is such that the gel front overtakes particle diffusion compressing the sharp front propagation.

Figure 3-19 shows that fully calcium exchanged bentonite swells to about 5 volume% at the dilute end and then drops to very low values over a few mm. Nearly identical results were obtained with 2 mM calcium concentration. As will be discussed later, it has been suggested that fully calcium exchanged clays should not swell beyond 50% void fraction and that they should be cohesive. The above results show that this is not the case. Furthermore, the concentration profile of smectite at the

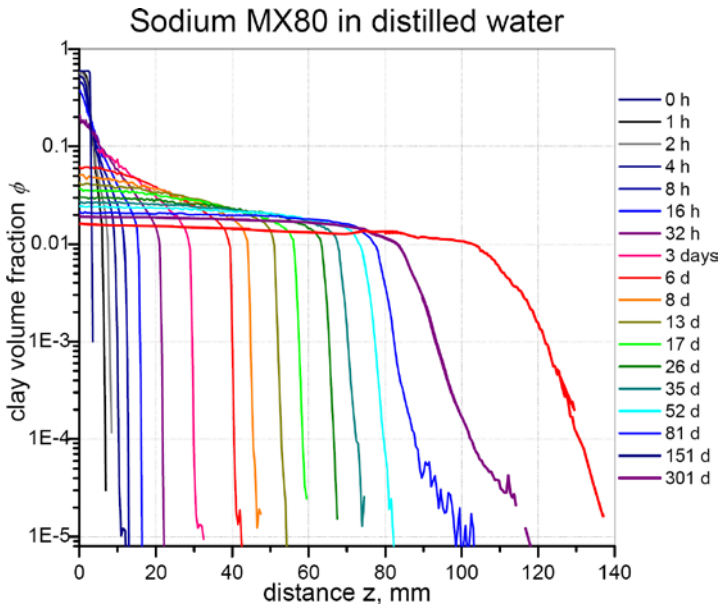

Figure 3-20. *Sodium exchanged and detritus free MX-80 bentonite swelling upward in the vertical tube in deionised water. Note the logarithmic scale.*

upper part of the gels suggests that colloidal particles can be released against gravity. Should the gel be cohesive, an extremely sharp drop in smectite should be observed. As this may be an important issue we bring it to the attention of the reader already here.

These data are used to test and verify our dynamic model for gel expansion. See section 6.11.

Note also that there are considerable differences between the sodium dominated bentonites and the calcium dominated bentonite. The latter swells more rapidly than the sodium dominated bentonites from the 3 mm high pellet to 13 mm as seen in Figures 3-19 and 3-21. It expands to an average distance between sheets starting at about 1 nm and stopping at about 7 to 8 nm average distance between sheets, had all sheets separated fully. By contrast, the purified and sodium ion exchanged bentonite continues to swell still after 8 months.

The influence of calcium concentration in the water is seen in Figure 3-22.

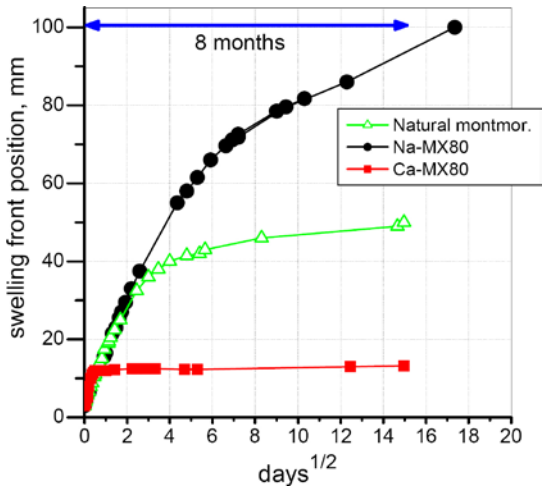

Figure 3-21. *The propagation of the swelling front (the gel/water interface) for different bentonites in deionised water. Note the horizontal scale of square root of time. Na-MX-80 stands for homoionic smectite from MX-80.*

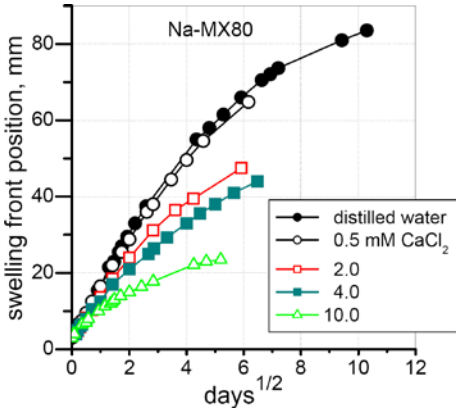

Figure 3-22. *Propagation of the swelling front for sodium exchanged bentonite and different calcium concentrations. Note the horizontal scale of square root of time.*

In addition, a number of other experiments were performed using different combinations of calcium and sodium bentonites with different proportions of sodium and calcium in the added water. The reader is referred to /Dvinskikh and Furó 2009/.

The sodium smectites exhibit the expected swelling behaviour in low ionic strength waters. The gel is expansive, as can be seen in Figure 3-20, where the smectite continues to expand against gravity even after 300 days. For long times it is also seen that the smectite concentration drops by 3 orders of magnitude over a distance of about 30–40 mm. As shown later (Equation 6-49), the atmospheric equation predicts approximately such a fall off shape and distance for 300 nm diameter, 1 nm thick smectite sheets.

The very different behaviour of the homoionic calcium smectite will be discussed later but it is mentioned already here that we think that this is caused by calcium dominated smectites forming larger particles of many individual sheets. For such systems the observed behaviour is expected.

The uniquely high resolution swelling experiments described above have been used to validate our dynamic swelling model. This is described in Chapter 6.

3.3.4 Gel/sol behaviour by turbidity measurements of smectite suspensions

Highlights from: /Birgersson et al. 2009/

A series of swelling and sedimentation experiments were performed with observations of the turbidity in the dilute dispersion. Some observations and deductions can be made.

The experiments are performed using cylindrical glass vials, with outer dimensions: height 35 mm and diameter 23 mm. In swelling experiments, a given amount of montmorillonite is dried-in at the bottom of the vials and 10 ml of either purified water or NaCl solution is added. The swelling and colloidal release vertically, i.e. against gravity, is monitored by measuring the change in turbidity with time at approximately 12–13 mm above the bottom. At low particle concentrations, the turbidity is directly proportional to the concentration. Similarly, for sedimentation the same equipment is used. In order to ensure complete delamination, the montmorillonite is dispersed in 5 ml purified water and later 5 ml NaCl solution (of double strength) is added.

Sedimentation experiments of the clay–electrolyte mixture show two major patterns. Below the CCC, the sol sediments as aggregates and above the CCC there is a rapid formation of a percolation gel that slowly consolidates under gravity. In Figure 3-23, one notices how sedimentation patterns for homoionic WyNa (Wyoming MX-80 purified and ion exchanged) in 0, 5 and 10 mM NaCl are similar, showing a steady decrease in mid-point turbidity. This experiment is done at a concentration of 5 g WyNa/litre, which is a very dilute suspension and the assumption that the sedimentation could be explained by non-interacting 1 nm thick clay disks by numerically solving the diffusion equation in a gravitational field was tested. Such assumption leads to a too slow sedimentation. In other words,

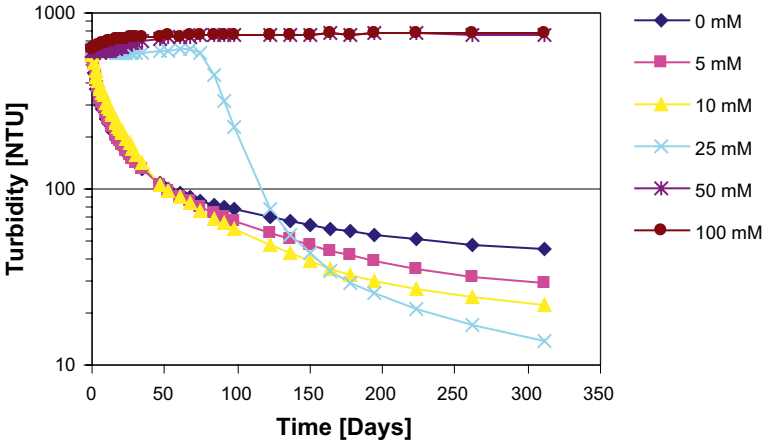

Figure 3-23. *Turbidity vs. sedimentation time for WyNa 5 g/l at different NaCl concentrations.*

individual clay particles are too light to be substantially influenced by gravity and it would take several weeks to get a lowering of the mid-height turbidity, whereas in reality the drop in turbidity is registered within a few hours even in de-ionized water. The faster than expected sedimentation was also observed in Jansson's experiments described above.

The sedimentation experiments reported here show that even at low ionic strength (de-ionized water) there exist attractive forces among the clay particles that come into play at high water ratios. It is speculated that the clay particles form aggregates that grow in size and eventually reach a point where gravity dominates over Brownian motion. /Birgersson et al. 2009/ suggest that the most likely force of attraction is electrostatic, between positive edge charges and negative faces also at somewhat elevated pH, probably leading to overlapping coin configurations rather than house of cards.

Above the CCC, there is no drop in the mid-point turbidity at the initial stages. From Figure 3-23, one sees that there is a gradual increase in turbidity especially with 50 and 100 mM NaCl but also with 25 mM. The suspension has become a gel (sediment) that slowly consolidates giving a two-phase system, a gel at the bottom with a clear almost clay-free electrolyte above. When the upper border of the gel phase has arrived at the detection height in the vial, there is a rapid lowering of the turbidity as can be seen for the 25 mM curve, but not yet for 50 and 100 mM.

With a modified turbidimeter, which could be moved vertically, it was possible to follow the sedimentation profile at a 1.5 mm resolution in the vial and the result for WyNa in 25 mM NaCl is shown in Figure 3-24. During the first week there is almost no change in the turbidity at any height, and only after two weeks there is a tendency of consolidation, seen as an increase in turbidity at the lower section of the vial. Above the gel phase, the turbidity is essentially zero as is very clear from the profile at 83 days. The limit of the turbidimeter is 1,000 NTU so one cannot expect to monitor the conservation of particles by integrating the curves. Furthermore, the turbidity is not measured at the top and the very bottom where the meniscus and the glass curvature, respectively, would give a distortion, which already affects the turbidity at relative depth 0 and 18 mm (curves bend initially upwards at both ends).

The particle volume fraction ϕ is proportional to turbidity up to about 1,000 NTU where ϕ is 0.32%. The concentration profile at long times shows that the diffuse layer extends over about 10 mm. A cohesive gel is expected to have a much sharper boundary between gel and water, so the CCC may not have been reached at the 25 mM NaCl concentration. Alternatively the sedimentation time has not been long enough.

The authors of the present report have not been able to use the numerous turbidity measurements with a fixed measurement point to determine whether the gels are expansive or cohesive. To determine whether a gel is cohesive with these type of observations, one would need to make very detailed measurements at the gel/sol interface, to find a sharp interface and to find that there are no or negligible amounts of particles at the interface. Probably, also rheologic measurements would be needed to determine if the gel is cohesive or is just a sediment of particles that do not cling together.

We stress this point because if the gel is not cohesive gravity and shear forces may dislodge colloidal particle from the gel.

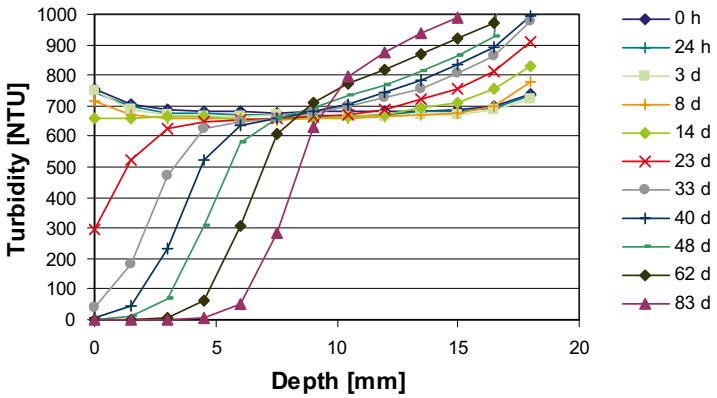

Figure 3-24. *Sedimentation profiles of 5g/l WyNa in 25 mM NaCl.*

3.3.5 Particle size distribution of detritus material and pressure drop

/Liu and Neretnieks 2006/ explored the idea that the detritus material in the natural bentonite potentially could form a filter cake of small accessory mineral particles, should some smectite be lost by erosion leaving the accessory minerals behind.

Sizes of the detritus particles from Wyoming MX-80 bentonite were measured using an optical microscope, /Liu and Neretnieks 2006 (unpublished results)/. The sizes of a total number of 2,787 particles were measured using a picture-handling program. As the software program used counts only particles larger than about 6–7 µm, the number of particles less than this size has to be estimated subjectively. The rough estimate is that there is about 15% of all the particles smaller than 6–7 µm. The number of particles smaller than 6–7 µm is thus about 400.

Among the 2,787 particles counted, 12 of them have sizes larger than 100 µm. In the left histogram in Figure 3-25 those 12 particles are not included.

The number of particles per "bin" in the two figures above are not identical because different bin-sizes were used for the linear and logarithmic distributions.

Figure 3-25 shows the particle size distribution. The distribution resembles a log normal distribution, although truncated at small particle sizes. The truncation is caused by cut off of the measurement technique using visible light, which does not permit the detection of particles smaller than about 6–7µm.

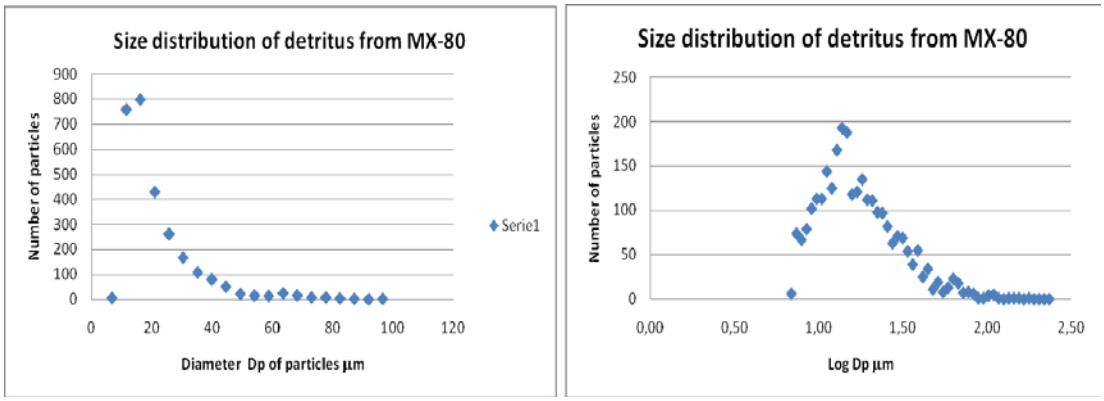

Figure 3-25. *Particle size distribution. Linear scale for particle sizes in left hand figure and logarithmic in right hand figure.*

This particle size distribution suggests that the larger particles may have difficulties penetrating far into fractures with apertures around 0.1 mm. The results also suggest that the smectite particles, which typically have particle sizes between 0.05 and 0.3 µm, might be filtered or even strained in a bed formed by the detritus particles.

To test this possibility, experiments were made to assess the pore sizes in a bed of detritus material. For this, the water flowrate through a 10 mm long bed of the detritus material was measured for a given pressure drop over the bed. Using the Kozeny-Carman equation (see section 6.4) the mean particle size was calculated to be 0.44 and 0.98 µm in two different experiments. Between particles narrow pores will form. The equivalent circular tube diameter giving the measured pressure drop is about 30% of the mean particle size, i.e. 0.13 to 0.3 µm. For a tetrahedral packing of like sized particles, the pore throat size are 0.07 and 0.15 µm for the mean particle size given above, See chapter 8. This suggests that the typical smectite particles with sizes 0.05 to 0.3 µm can be expected to be efficiently filtered or even strained in a short bed of detritus particles.

Inspired by these results, a series of filtration/straining experiments were started. The results of these experiments are described below.

3.3.6 Filtration and straining of bentonite suspensions

Highlights from: /Richards 2009/

/Richards 2009/ determined particle size distributions of detritus material as well as of a number of materials, which potentially could be used as additives to the bentonite to form a filter cake with small pores. These are shown in Figures 3-26 and 3-27.

The distribution in Figure 3-25 is for the number of particles whereas that in Figure 3-26 is the volume fraction, so they are not directly comparable. Furthermore, there are differences in the preparation methods as well as in measurement methods. However, both distributions reveal that there is a considerable amount of particles smaller than a few µm.

In the filtration experiments, filter cakes of 1.5–10 mm high of detritus material were formed in cylindrical tubes. Suspensions of purified and homoionic sodium exchanged bentonite with 1% by weight smectite in deionised water were pressed through the filters. The filtration resistance in the filter support was negligible compared to that in the detritus filter cake. Filtration was maintained for more than 80 days showing a typical fall off of filtration rate. The water that passed was analysed for its smectite content. Figure 3-28 shows some typical filtration curves.

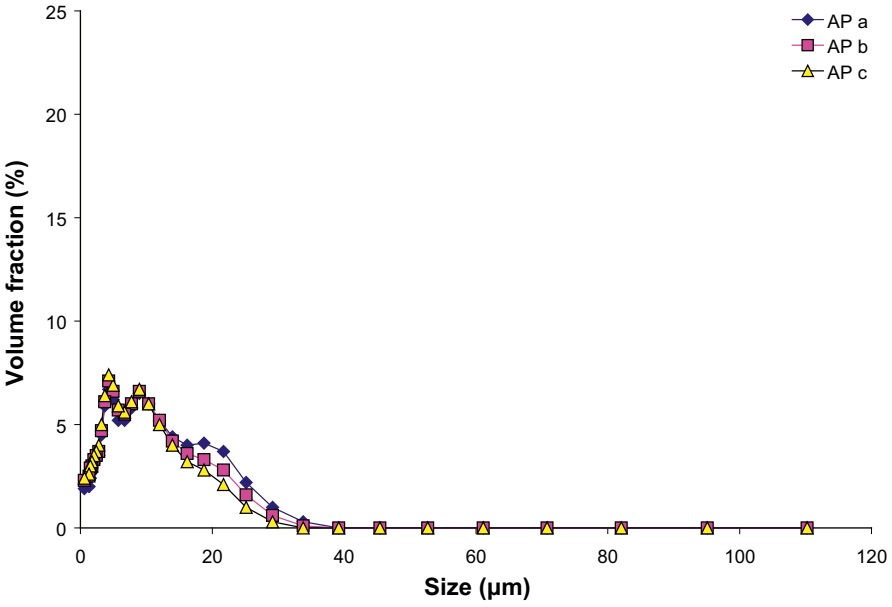

Figure 3-26. *Particle size distribution for accessory mineral particles measured on three different batches.*

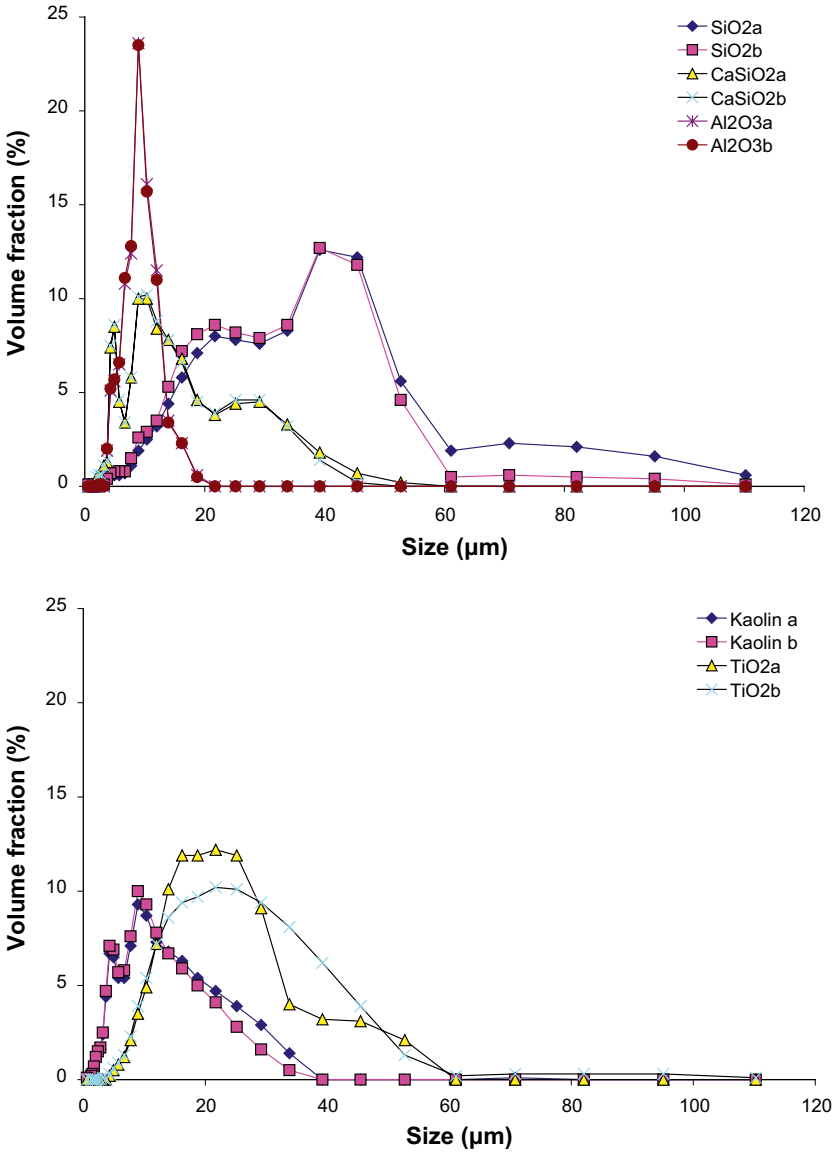

Figure 3-27. *Particle size distributions for some added materials.*

The general form of the curves is expected and shows that, as the filter cake of smectite particles builds up, the flowrate decreases because of the increasing filtration resistance in the increasingly thick cake.

The filtrate was collected and analyzed on dry substance by evaporation. Due to the low amount of solid material in the initial solution (1%), it was necessary to have at least 25 ml of filtrate to have low measurement errors. The result, as given in Table 3-1, showed a clear decrease of the initial solid concentration (1%) in all cases. In two cases, the solid concentration was higher the first day (could also be seen as a higher flow rate), indicating that the structure of the filter cake was not homogeneous and material could therefore pass.

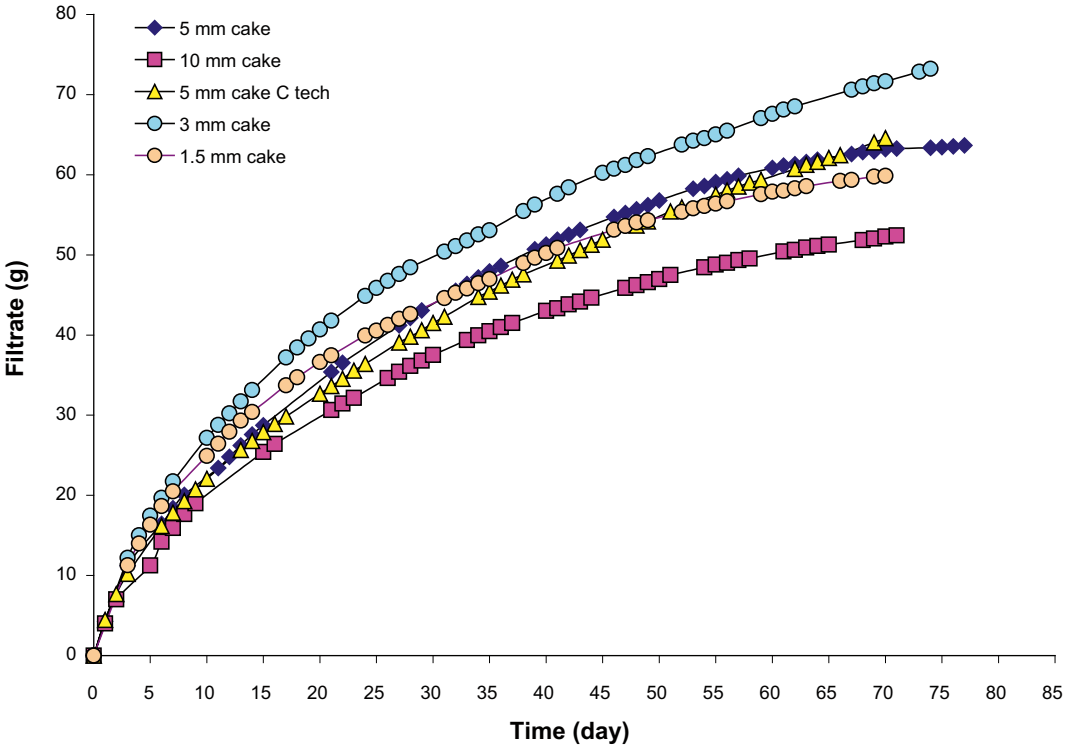

Figure 3-28. *Amount of filtrate versus time for different cake heights.*

Table 3-1. Solid material in filtrate.

Filter cake	Sampling days	Amount of filtrate (g)	Solid concentration in filtrate (%)
1.5 g	1–4	28.86	0.06
1.5 g	4–49	44.47	0.02
3 g	1–9	29.59	0.008
1.5 g clay tech	1	30.75	0.7
1.5 g clay tech	2–21	32.68	0.017
1.5 g pH 7	1–12	36.52	0.05
1.5 g pH 5	1–13	38.62	0.058
1 g	1	43.39	0.84
1 g	2–14	31.73	0.02
0.5 g	1–6	26.98	0.082
0.5 g	7–	30.65	0.02
3 g upwards	1–10	36.67	0.05
3 g upwards	11–		0.0021

Some filter cakes were sectioned and analyzed. They were divided in several parts, including both the original filter bed material (accessory minerals) and the formed filter cake of montmorillonite. The material was analyzed in two ways, in one the solid content was measured through evaporation and in another the amount of particles was measured in a solution consisting of cake material and deionised water. The particle concentration was measured with a turbidity meter at Clay Technology AB. The dry content in the filter cake increased with increasing depth. A sharp transition was found between the formed montmorillonite cake and the original accessory minerals, as shown in Figure 3-29. The original cake contained a low amount of montmorillonite, even though there is an initial penetration.

The results show that even a thin filter cake of detritus material acts as an effective filter for smectite particles.

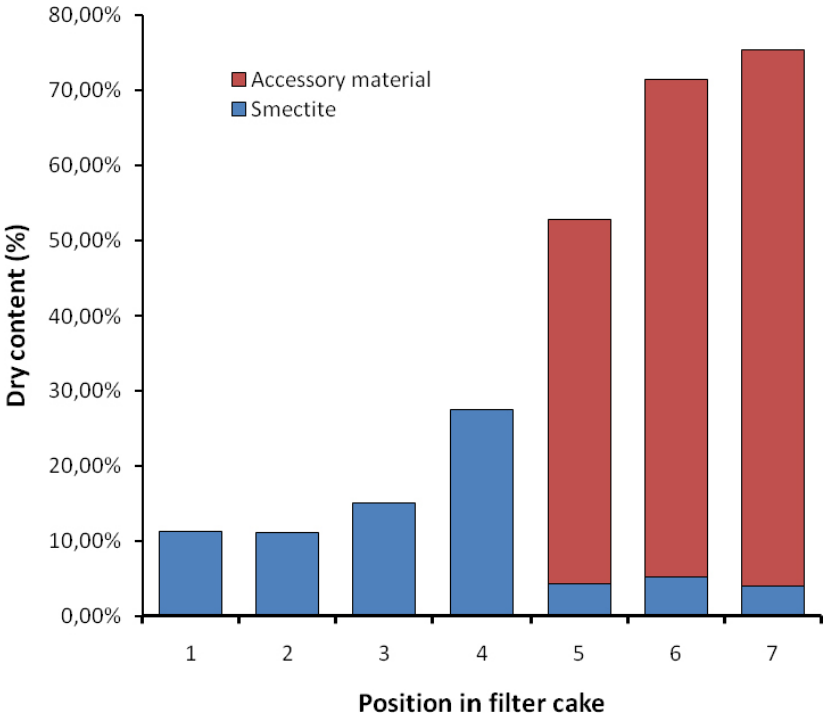

Figure 3-29. *Dry content (mass fraction) in different places in a filter cake (a higher number represent further down in the cake). Number 4 represent the boundary between the original filter cake and the formed cake of montmorillonite.*

A series of filtration experiments were also performed with filter beds consisting of 0.5 g material totally but with different proportions of detritus accessory material and added material. The material added consisted of fine grained titanium oxide, calcium silicate, silicon oxide, aluminium oxide and kaolinite clay. The particle size distributions are shown in Figure 3-27. The amount of accessory material particles varied from 0.4 down to 0.2 g: The filter cake height was about 1.5 mm. The result can be found in Table 3-2 (AP stands for accessory material particles). An X indicates that the separation succeeded, i.e. that practically no smectite passed the bed. A double X means that the result was similar in both duplicates. Two distinct cases were observed. Either the smectite dispersion penetrated rapidly yielding no separation or filtration was slow and separation was virtually 100% with respect to the smectite particles.

From this, it is still difficult to draw any conclusions regarding if addition of material really improve the separation beyond what the detritus material achieves by itself. However, as can be seen in Table 3-2, practically complete separation does occur when other material is added which indicates that there is an effect.

Table 3-2. Filtration of smectite dispersion through filter cakes of different composition.

	AP 0	AP 0.2	AP 0.3	AP 0.4
Only detritus			X X	X
TiO2			X X	
CaSiO2				X
SiO2			X	
Al2O3		X		
Kaolin		X	X	X

3.3.7 Smectite penetration through fine filters

Highlights from: /Birgersson et al. 2009/

To test if colloids could penetrate a filter with a given pore size, clay samples were placed in a test cell between two filters. The samples were saturated with water circulated over the filter. The swelling pressure and amount of particles in the water were measured.

The test cell used is a 35 mm diameter cell with filter on both sides. Normal sample height is 5 mm. Materials in the test cell are titanium in the ring and PEEK in the bottom and the piston, both highly inert materials that has been tested previously. On the backside of the filters there is a channel where water can be circulated by use of a peristaltic pump. The test cell is shown in Figure 3-30.

The swelling pressure was measured with load cells. Turbidity in the circulation water was measured with a turbidimeter, which gives a clear indication whether colloids are present or not. The turbidity values can also be translated to a mass clay/volume number. The filters were sintered titanium or stainless steel filters. The thickness of the filter was 2 mm with a pore size ranging from 0.2µm to 100 µm.

The clay used in these tests was untreated MX-80, as well as purified and ion exchanged to two homoionic forms, sodium and calcium, called WyNa and WyCa. The clay fraction of MX-80 was extracted and all exchangeable ions were changed to either Na or Ca ions. The purified sodium clay is named WyNa and the calcium clay is named WyCa. A detailed description of materials and treatment can be found in /Karnland et al. 2006/. All samples were made to buffer density, $\rho_{saturated}$ = 2,000 kg/m^3 (ρ_{dry} = 1,570 kg/m^3).

Figures 3-31 and 3-32 show that the homoionic calcium smectite did not pass the filters during the 20 day observation time, whereas untreated MX-80 and homoionic sodium smectite was rapidly lost to the circulation deionised water, which was exchanged for fresh water every day.

Mixtures of calcium and sodium bentonites in different proportions show that a mixture of as much as 80% Ca and 20% sodium exchanged bentonite does not prevent loss of swelling pressure and erosion of smectite through 2 µm pore size filters. This is shown in Figure 3-34. A 90/10 mixture, however, shows no loss of swelling pressure.

The figures show that when the swelling pressure decreases, which is a direct indication that mass is lost. The swelling pressure drops show that tens of % and more of the original buffer mass was lost in three weeks. Figures 3-33 to 3-34 show that in filters with pore sizes larger than 2 µm the WyNa smectite particles and those from MX-80 readily pass the filters in days to weeks. They are, however, totally retained in filters with 0.5 and smaller pore sizes. Here straining is effective. WyCa did not pass 40 and 100 µm filters even to deionised water.

The results suggest that even if a thin filter cake of extraneous material could be formed between the buffer and the mouth of the fracture or in the fracture itself, having a pore size smaller than 0.5 µm, loss of smectite could be considerably decreased or even effectively stopped.

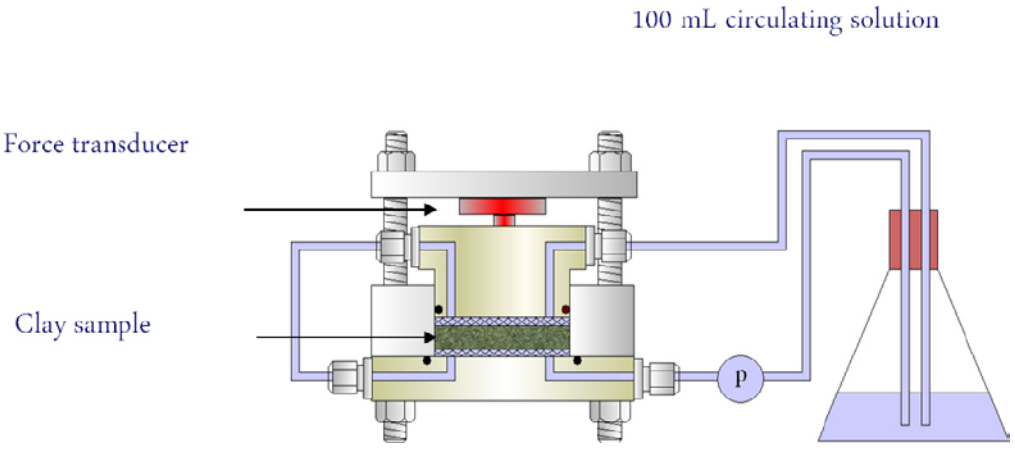

Figure 3-30. *Schematic illustration of the test cell used.*

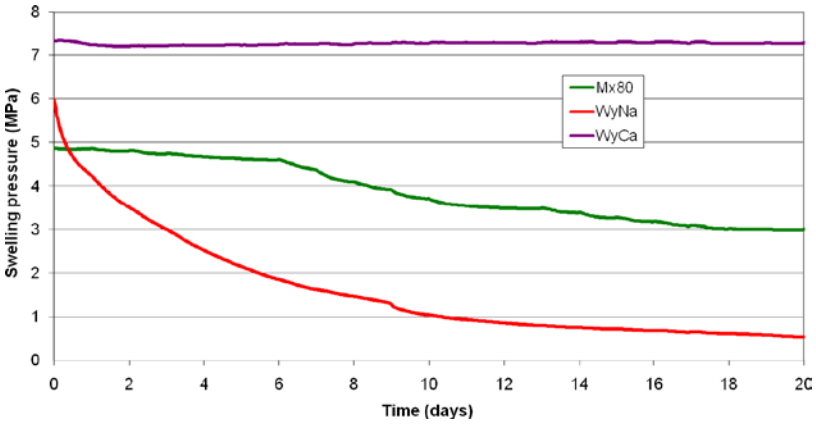

Figure 3-31. *Swelling pressure as a function of time with the 10 µm filter.*

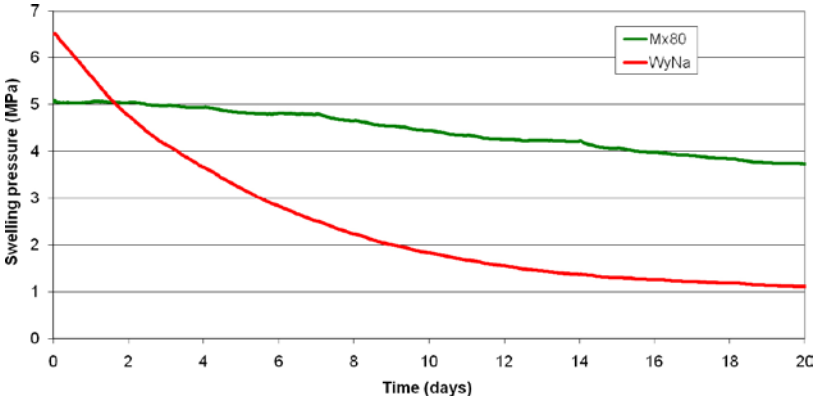

Figure 3-32. *Swelling pressure as a function of time with the 2 mm thick, 2 µm pore size filter.*

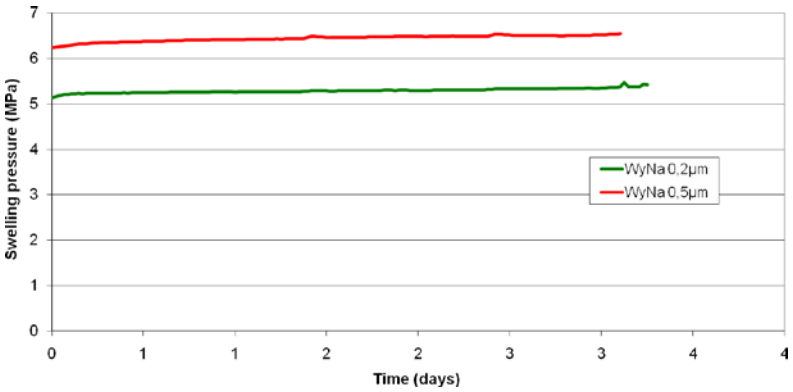

Figure 3-33 . *Swelling pressure as a function of time with filters 0.2 and 0.5 µm pore size filters.*

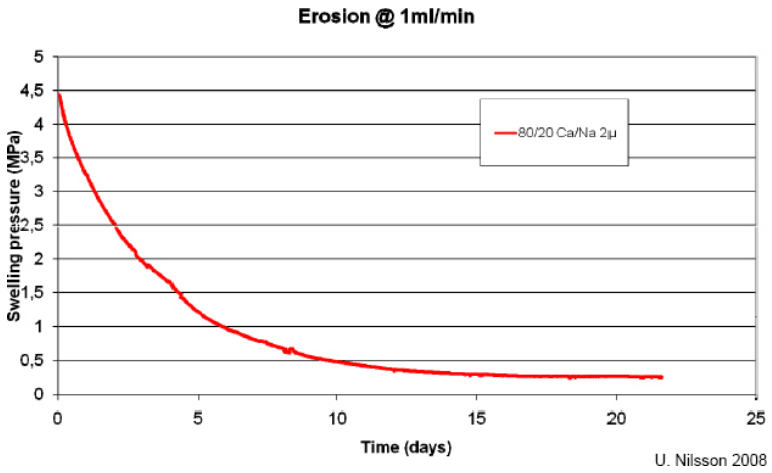

Figure 3-34. *Swelling pressure as a function of time for 80/20 mixture of WyCa/WyNa and a 2 µm pore size filter.*

3.3.8 Tests with addition of detritus and other materials

Knowing that colloids could be stopped by a filter with a pore size less than 0.5µm, tests were conducted with natural filler materials (kaolinite, diatomite and MX80 accessory minerals) between the clay sample and the steel filter in the test cell.

The first test was a 2 mm thick layer of compacted kaolinite between the WyNa bentonite and the filter. To make sure the kaolinite did not affect the bentonite, circulation on one side with two stacked standard filters was made. After an initial drop, the swelling pressure stabilised and no outflow of colloids could be detected, as seen in Figure 3-35.

In other tests mixtures of WyNa and kaolinite in different proportions were then used. The results for a 50/50 by weight mix are shown in Figure 3-36. It is seen that, initially there was a drop in swelling pressure when the water was changed, but later it stopped. In the long run a small leakage and subsequent drop in pressure can be seen. Results from the 50/50 (WyNa/kaolinite) test were initially encouraging enough to test 80/20 and 90/10 mixes, as shown in Figure 3-37. The 90/10 mix continued to lose swelling pressure but the 80/20 mix reached equilibrium at 1 MPa.

The second test was with diatomite, (diatomaceous earth or kieselguhr). Again a 2 mm thick compacted layer was used as a filter. Results are presented in Figure 3-38, where small variations in swelling pressure are seen but no apparent loss. Very small amounts or particles were detected in the circulating water.

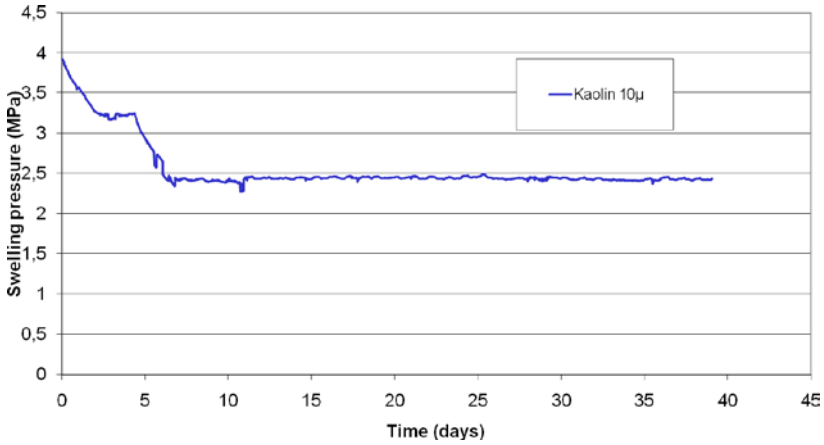

Figure 3-35. *Swelling pressure as a function of time for a WyNa sample with a 2 mm thick layer of kaolinite on one side and an extra steel filter on the other. After day 5, circulation of water was only made on the kaolinite side.*

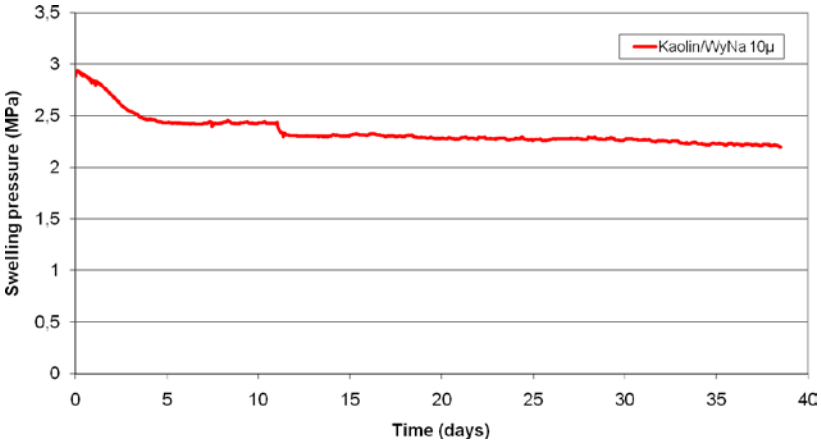

Figure 3-36. *Swelling pressure as a function of time for 50/50 mixture of WyNa and kaolinite. The circulating water was exchanged at 11 days.*

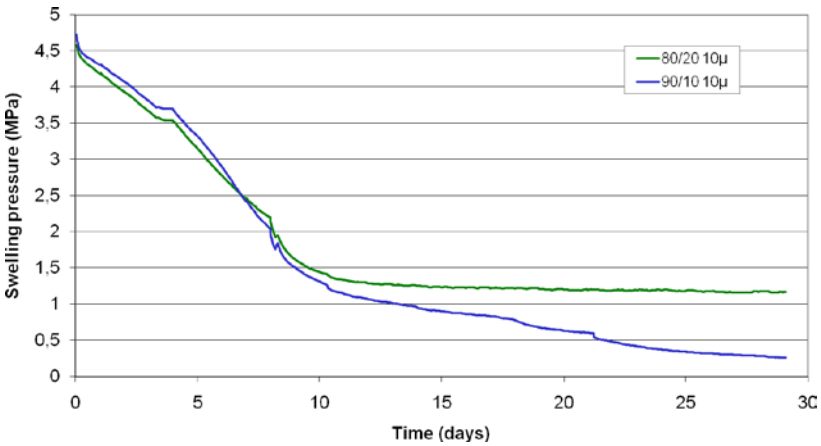

Figure 3-37. *Swelling pressure as a function of time for 80/20 and 90/10 mixtures of WyNa and kaolinite.*

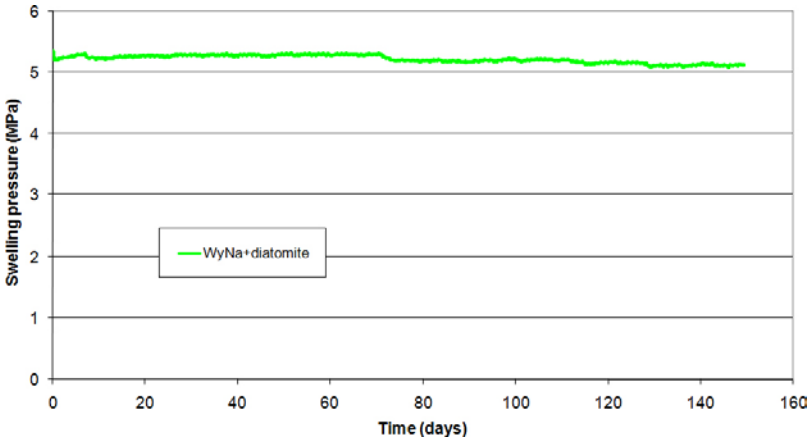

Figure 3-38. *Swelling pressure as a function of time for a WyNa sample with a 2 mm thick layer of diatomite.*

Also the accessory minerals in MX-80 were tested in two experiments, see Figure 3-39. The first sample is a standard 5 mm thick WyNa at wet density 2,000 kg/m^3 with an extra 2 mm thick cake of accessory minerals. The second test is with a 10 mm MX-80 sample and only circulation on one side to see if the normal accessory minerals could form a filter cake. The slow pressure drop is not in agreement with the behaviour in Figure 3-31, where the swelling pressure drops significantly

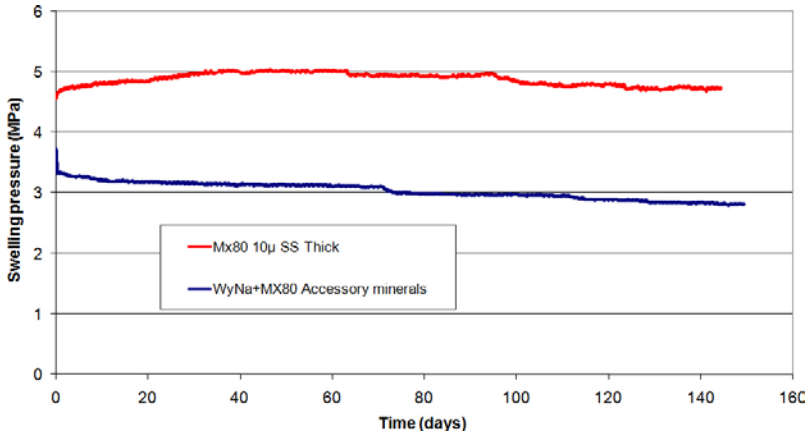

Figure 3-39. *Swelling pressure as function of time for a 10 mm thick untreated MX-80 sample and a WyNa sample with a 2 mm thick layer of accessory minerals.*

within 20 days. The difference between the two experiments is the difference in proportions of the sample and the ratio between the water reservoir and clay mass. The larger amount of clay has more soluble calcium minerals that take longer time to dissolve. Later measurements of electric conductivity show values that are consistent with the values that stopped erosion in the earlier experiments. The apparent stop for colloid release is perhaps due to chemical processes.

These experiments show that sodium smectite particles from an expansive gel below CCC readily can pass through pores down to 2 µm but are stopped in 0.5 µm pores. Calcium dominated particles do not pass 100 µm pores, even when the pore water is well below the CCC. We tentatively conclude that this is because in strongly calcium dominated systems the smectite sheets form large cohesive particles that are not readily broken up.

Thin layers of detritus material or other material with small particles can considerably slow down or even stop smectite migration through the layer. The presence of detritus material in the bentonite or materials admixed to it slow down smectite loss. The rate of penetration of homoionic sodium smectite through 2 and 10 µm filters is used to test and validate our model for smectite expansion and solubilisation. See section 8.5.4.

3.3.9 Experiments on expansion in slits – Formation of enriched detritus region

Highlights from: /Neretnieks 2009/

Some scoping experiments in thin slits between two glass plates with the aim of visually observing the behaviour and structure of expanding clays were performed. Experiments were made with untreated MX-80, detritus free homoionic Na and Ca smectite and MX-80 washed of gypsum (a soluble calcium mineral). The clays were allowed to swell into deionised water vertically upward in 1.2 mm aperture slits until no more swelling could be observed. The sealed slits were then turned upside down and the release and sedimentation of particles was observed. These scoping experiments were not well controlled but the slits were sealed so no influence of atmospheric CO_2 can have influenced the results.

In one of the experiments, MX-80 was washed in a large volume of deionised water to dissolve mainly gypsum but to retain the detritus material in the subsequently collected clay. In the washing, some tens of percent of the smectite stayed in the water so the clay had a larger fraction of detritus than MX-80.

A sample of the washed and dried bentonite, after considerable grinding in a hand mortar, was emplaced in the bottom of the slit, as shown in Figure 3-40, and the slit was then filled with deionised water. After about two days the clay had ceased swelling. This is shown in Figure 3-41. The slit was then turned upside down. Small clay blobs immediately were released and started to slowly fall, see Figure 3-42.

In Figure 3-43 the wormlike piece of gel released by turning the slit upside down consists of a light dilute gel to the right and a much darker region which contains small particles. In the locations where the blobs were released, the gel that remained was denser but seemed to be more homogeneous and have fewer particles.

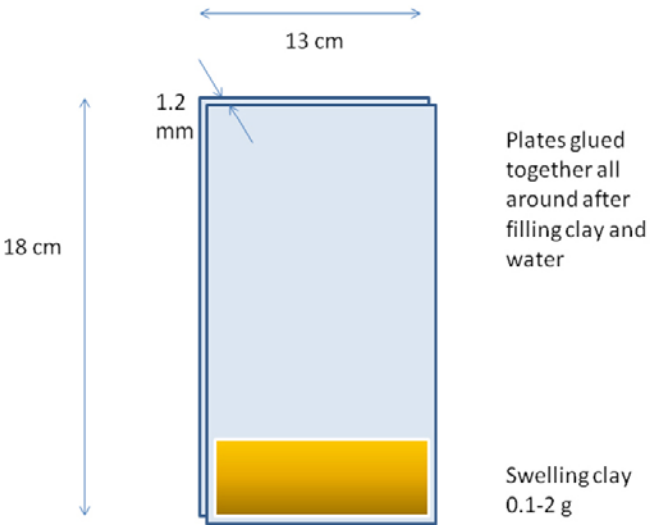

Figure 3-40. *A slit formed between two glass plates.*

Figure 3-41. *The swollen clay after two days. Width of slit is 13 cm.*

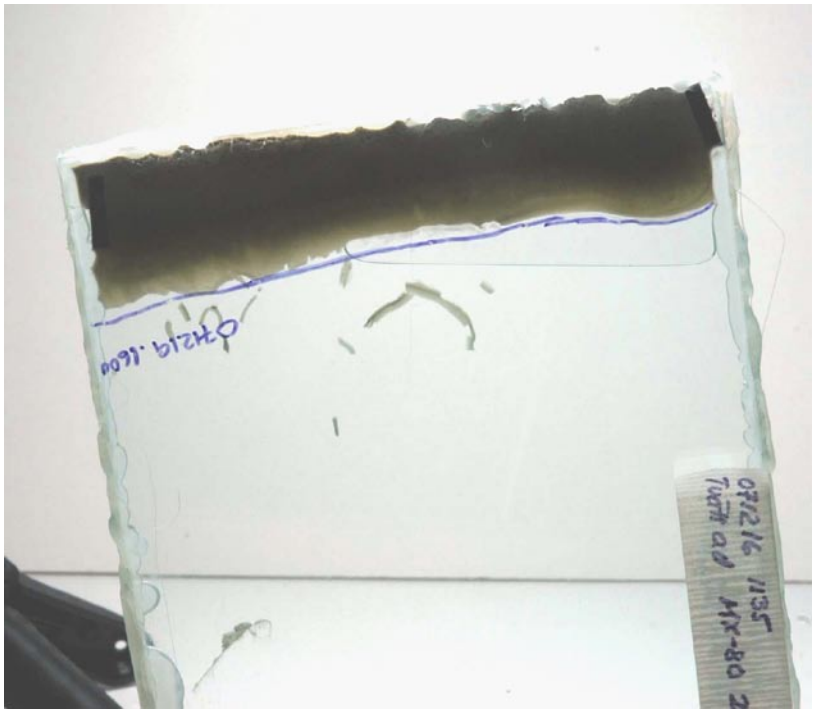

Figure 3-42. *Falling worm like blobs hours after turning the slit upside down.*

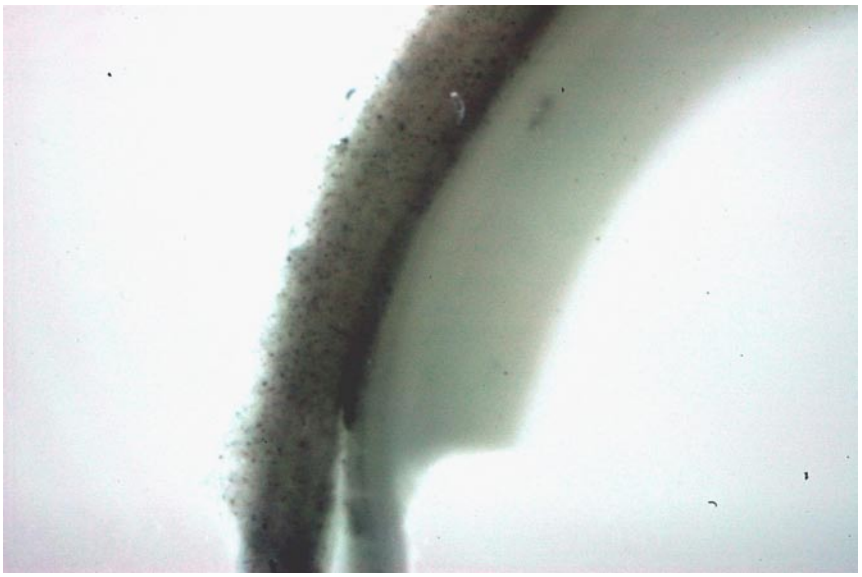

Figure 3-43. *Enlargement of worm like blob. The picture shows a 4 mm high section.*

A tentative interpretation is that as the gel expanded upwards the detritus material expands with it, but near the edge where the gel density had decreased the smectite particles could move independently of the detritus leaving it behind. In this case, half a mm thick region of more concentrated detritus remained forming a potential filter cake.

Measurements of the water compositions, three months after start of the experiments, revealed that the purified and ion exchanged smectite dissolved, releasing silica to about 1 mM. This is about the solubility of amorphous silica. One mM concentration of calcium was found from the dissolution of calcium exchanged bentonite and more than 7 mM sodium resulted from the sodium exchanged bentonite. This suggests that smectite dissolution may have occurred.

3.4 Other Laboratory experiments

There are few recent laboratory experiments that have addressed the erosion of a swelling bentonite into passing water.

/Kanno et al. 1999/ performed two kinds of experiments, namely extrusion and erosion tests in Plexiglas cells simulating near field rock mass. The bentonite used was Kunigel(VI) which is a Japanese natural Na bentonite and has a montmorillonite content of 47.5%. Tests were also made with a mixture of bentonite and 30% sand. The cell with compacted bentonite is in contact with a single, smooth, parallel-walled slot simulating a rock fracture. The "dry" density was 1.8 g/cm^3 which includes a water content of 10%. The bentonite specimen was 50 mm in diameter and height for the extrusion test and 10 mm in diameter and height for the erosion test. The slot apertures varied as 0.5 and 1.5 mm for the extrusion test and 0.3, 0.5, 1.0 and 1.5 mm for the erosion tests.

The extrusion rate was measured in the extrusion test and the occurrence of the bentonite erosion at different water flow rates was evaluated in the erosion test. The critical flow rate of the bentonite erosion experimentally determined is $2 \cdot 10^{-5}$m/s. The extrusion reached 40 mm radially in 1,000 hours in the 1.5 mm slit and 15 mm in 2,500 hours in the 0.5 mm slit. In the erosion tests in the narrowest aperture, 0.3 mm, the gel expanded to 50 mm in the downstream direction and to 15 to 20 mm in other directions after more than 1,000 days. For larger apertures no difference could be seen with directions. No measurements of the colloid content in the effluent water were made in the erosion tests.

A model of solid particle diffusion was developed for the extrusion. The expansion is treated as a combination of the free swelling of compacted bentonite and viscous flow of bentonite gel in a narrow fracture. The solid diffusivity as a function of the volume fraction of solid is derived from

the hydraulic conductivity, swelling pressure and viscosity of the bentonite and the aperture of the fracture. The calculated results of the extrusion rate were in good agreement with the experimental results. The model could reproduce the aperture dependence of the extrusion rate.

/Missana et al. 2003/ in one experiment studied the release of colloids from compacted clay (dry density 1.65 g/cm^3) to the water passing between the clay and a granite surface. The granite was unusually porous, 5%. So it cannot be ruled out that much of the flow passed through the granite. This is not discussed in the paper nor is data available to test this hypothesis. Small solid particles (> 1 μm) as well as colloids <1 μm were found in the effluent water. Very low water flowrates were used in the experiments, less than 1 ml/day. Solid particles were released into water from the clay to concentrations ranging from 10 to 20 mg/l of which about 10% were bentonite colloids. Particle and colloid release increased with water flowrate.

In another experiment the particles were allowed to diffuse from the compacted bentonite into a porous geotextile. In this experiment no flow was applied during the experiment. After one month the water in the 5 mm thick porous geotextile was collected and particle and colloid concentrations were measured. The total amount of particles was 200 mg/l of which colloids were 4–8 mg/l.

/Baik et al. 2007/ studied erosion of bentonite particles caused by a groundwater flow at the interface of a compacted bentonite and a fracture in a granite core under various geochemical conditions. Water flows around a bentonite cylinder in the slit between two granite cylindrical halves in which the bentonite is fixed. The bentonite contains 30% detritus material and the exchangeable ions are dominated by calcium. Ionic strengths of 1, 10 and 100 mM $NaClO_4$ waters were used and the pH 7, 8.5 and 10 were used. Water velocities in the about 0.5 mm aperture fracture were $1.5 \cdot 10^{-7}$, $1.5 \cdot 10^{-6}$ and $1.5 \cdot 10^{-5}$ m/s. The swelling bentonite had intruded about 3 mm into fracture after 60 days.

The bentonite particles could be eroded from a compacted bentonite buffer by a flowing groundwater depending upon the contact time, the flow rate of the groundwater, and the geochemical parameters of the groundwater such as the pH and ionic strength of the approaching water.

The particle concentration in the effluent decreased noticeably with time, from many tens to several hundreds of mg/l to low values at long times. No explanation was offered for such a decrease. For the highest and the middle velocity the effluent concentration dropped to about 1–10 mg/l after two months. For the lowest velocity the effluent concentration was consistently higher than for the middle velocity. Consistently the bentonite concentration in the effluent after a long time was between a few and 20 mg/l irrespective of flow velocity, pH and ionic strength. The eroded bentonite particles were expected to be stable at the given groundwater condition.

One could speculate that the sharp initial drop in effluent concentration and subsequent increasingly slower erosion could be due to build up of a layer of detritus material. The used bentonite contained 30% such matter, 29% feldspar and 1% quartz.

None of these experiments are in contradiction to our conceptual picture of bentonite erosion.

3.5 Field experiments on colloid transport related to release of colloids

Some experiments have been performed in the field and in fractures in large blocks. They have mostly been aimed at studying colloid generation and stability and are less easy to use to quantify erosion under well characterised conditions.

/Kosakowski 2004/ reported migration studies and bentonite colloid breakthrough curves in a dipole experiment in Grimsel.

/Kurosawa et al. 2006/ described the colloid and radionuclide retardation experiments performed at NAGRA's Grimsel Test Site in Switzerland designed to collect in situ data on the impact of colloids on radionuclide transport. In this work modelling of colloid-facilitated solute transport in discretely-fractured, porous media and fits to the experimental results are described.

Detailed information on the Grimsel experiments including laboratory supporting experiments and modelling is published in the reports by /Missana and Geckeis 2008/ and /Möri 2004/. /Smith et al. 2008/ summarize conclusion from the above experiments.

Sodium dominated bentonites will readily release smectite particles to waters with ion concentrations below CCC. The colloidal smectite particles will readily migrate through pores as narrow as 2 μm but will be strained by pores smaller than 0.5 μm. The presence of detritus material with small particle sizes can slow down the migration of the smectite particles when the detritus is left behind forming an increasingly thick porous bed through which the smectite particles must move.

Strongly calcium dominated bentonites and smectites will not readily release colloidal particles to water above or even below the CCC. However, already about somewhat more than 10% sodium in ion exchange positions make the smectite behave much like a sodium bentonite.

Gravity aids in releasing colloids as well as agglomerates from a downward facing gel/sol interface.

The smectite particles in sodium dominated gel with little or no detritus material and below CCC are not noticeably hindered by friction against the walls of the pores. The forces between the colloidal particles rapidly propagate them through pores not much larger than the particles themselves. To totally hinder smectite movement through a porous medium, the pore throats in the pore network must essentially cause straining of the particles.

4 Structure of bentonite stacks and impact on bentonite gel behaviour

In this section, the structure of clay made up mainly of smectite sheets and how the structure could influence the swelling pressure and particle separation is discussed. The impact of particle size variations and charge of counterions on the swelling process is also described. One specific issue addressed is that calcium smectites are observed to swell with nearly as high pressures as sodium smectites at moderate to high compactions. They also maintain swelling pressures at even considerably lower densities. This contradicts the idealised theoretical models, which suggest that the highly charged smectite particle should not swell beyond about 50% porosity corresponding to 1 nm distance between sheets, when the counterions are mainly divalent. We explore possible reasons for this important difference between idealized theories and observations. For the subsequent discussion, our conceptual picture of the smectite system is described.

Should swelling beyond 1 nm not be possible and cementing of the clay occurs this would seriously impede the possible use of calcium dominated bentonite as buffers.

4.1 Conceptual picture of smectite clays

The individual smectite stacks are shaped as irregular cards or coins and their size varies. The individual smectite sheets are about 1 nm thick and range in size from some tens of nm to several hundred nm. They are sometimes described as ellipsoidal sheets or platelets. /Cadene et al. 2005/ investigated size, morphology, and apparent charge of individual Na-montmorillonite particles of natural MX-80 sodium montmorillonite with atomic force microscopy (AFM) and photo-correlation spectroscopy (PCS). They found two clay populations with a large variation of length distribution. It may be noted that the AFM measured particle thickness finds a small fraction of particles less than 1 nm thick, even down to 0.6 to 0.8 nm in thickness. Montmorillonite sheets seem to be slightly crumpled. This suggests that there are broken fragments of the sheets present. This may have an impact on the stack properties. Some of the smaller particles were found superimposed onto sheets of the larger, mainly on their borders, presumably indicating a difference in the density of charge. They also found that thickness of tactoids (stacks), increased by sheet-stacking, but still remains negligible in comparison to their major length. At higher particle concentration the stacks form aggregates.

At high solid volume fractions the sheets need to be arranged in stacks (tactoids, aggregates, quasi-crystals and also other names are found in the literature) with many sheets parallel. Figure 4-1 shows an example of an arrangement that could lead to volume fraction of 50% or more.

The individual sheets in the stack are about 1 nm thick. They are somewhat flexible. At a void fraction of 50% they have approximately the same average distance between the sheets as the sheets are thick. The sheets vary in size and the stacks could be arranged as shown in the left part of Figure 4-1. There will be voids between the stacks that add to voids of the system, decreasing the volume fraction of solids further. At higher compactions the distance between the sheets must be less than 1 nm. Charge compensating ions are located between the sheets, which have charge dislocations because of isomorphic substitution of aluminium atoms for magnesium or ferrous iron atoms in the middle octahedral layer formed by an aluminium oxide lattice. This lattice is sandwiched between the two tetrahedral layers of silicon oxide lattice. Typical charge compensating ions are monovalent sodium and divalent calcium ions but also potassium and magnesium ions are found.

When the clay is exposed to water vapour or liquid water the water molecules intrude between the sheets, sorb water on their surface and hydrate the charge compensating ions. This leads to very strong swelling of the clay. Highly compacted bentonite clay with a solid volume fraction $\phi = 0.7$ (dry density 1,810 kg/m^3) can exert swelling pressures of ten MPa or more when fully water saturated /Karnland et al. 2003, 2006, Pusch and Yong 2006/. In low ionic strength waters the repulsion forces between the sheets can dominate over attractive forces and the particles can disengage from the

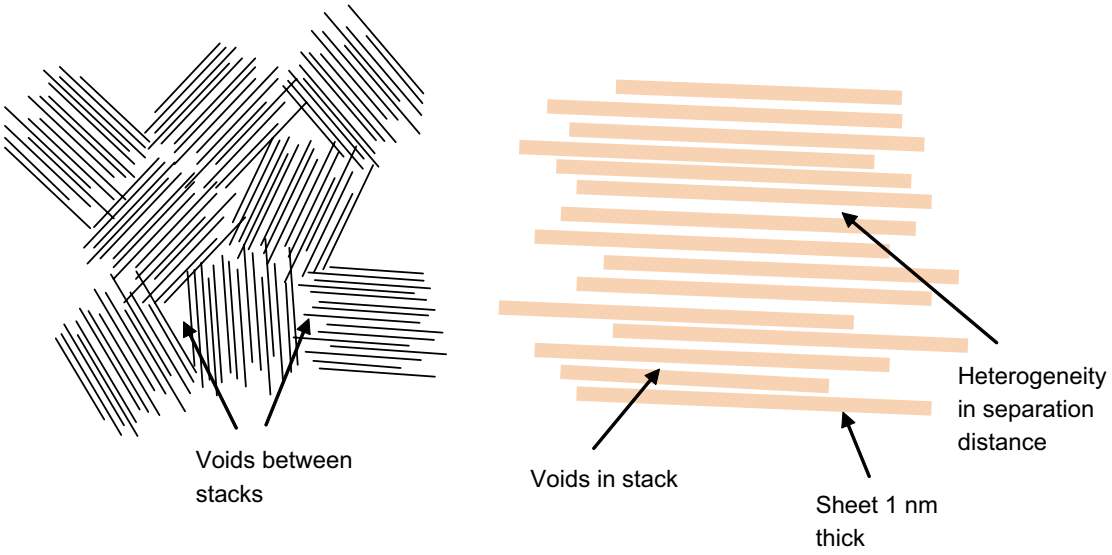

Figure 4-1. *The figure shows how the individual sheets can be arranged in stacks, right hand figure, and how such stacks can be arranged in a compacted system, left figure.*

stacks in the gel and form a stable colloidal sol if given enough water. When sodium is the dominating counterion the particles consist of one or a few sheets /Cadene et al. 2005/. When divalent calcium or magnesium dominates the particles or stacks consist of typically 5 to 15 sheets or more /van Olphen 1977, Push and Yong 2006, Bergaya et al. 2006/.

/Bergaya et al. 2006, Fig. 5.5/ show that sodium clay particles with up to 30 to 40% calcium consist of one to 1.5 sheets on average. With 100% calcium, stacks with on the average 7 sheets are formed.

There can be several reasons for such behaviour. One is indicated in Figure 4-1, suggesting that there may for some reason be differences in separation distance between the sheets in the stacks due perhaps to different surface charge densities between different sheets so that attractive and repulsive forces differ between different sheets. This could give rise to separation between parts of the stack during swelling but still retain stacks of several sheets at close distance, potentially caused by the attractive ion-ion correlation effects in the presence of divalent ions on highly charged particles.

/Jönsson et al. 2009/ predict that smectites with calcium as counterions, even at fairly low calcium fractions, should stop swelling and actually develop strongly cohesive forces between the smectite sheets when the distance between sheets is about 1 nm. This corresponds to a porosity of about 50% as the sheet thickness is about 1 nm. They were not able to explain the reasons why such behaviour is not observed in reality.

Simulations show that these attractive forces are very strong at distances shorter than one nm and can dominate over the repulsive double layer forces. At larger sheet distances the repulsive forces dominate even for divalent counterions /Kjellander et al. 1988, Evans and Wennerström, 1999, Jönsson et al. 2009/. The net force as a function of distance for a calcium smectite is illustrated in Figure 4-2 /Jönsson et al. 2009/. A negative osmotic pressure P_{osm}/RT of nearly –1 corresponds to a cohesion pressure of more than 2 MPa. This is a very strong cohesion pressure. These results suggest that the sheets should collapse into an essentially solid body with sheet distances near 1 nm. Such a body would have a porosity of about 50%. The body would have a tensile strength comparable to or larger than concrete. This is not observed although stacks with such sheet distances are observed, /Pusch and Yong 2006, Bergaya et al. 2006, Birgersson et al. 2009, Jönsson et al. 2009/.

In a configuration of stacks and sheets as shown in Figure 4-1, the initial strong swelling pressure is due to repulsion between stacks as well as between the sheets in the stacks at the location where repulsion dominates. A fully Ca exchanged Milos bentonite still has measurable swelling pressure in fresh water at a dry density of 522 kg/m^3, at which density the average distance between the sheets is 4.2 nm and a volume fraction of 0.19 /Karnland et al. 2006, Table 4-5/. Similarly, a fully Ca exchanged Wyoming bentonite still has measurable swelling pressures in fresh water as well as $CaCl_2$ concentrations up to 3M with a dry density of 502 kg/m^3. At this density the average distance

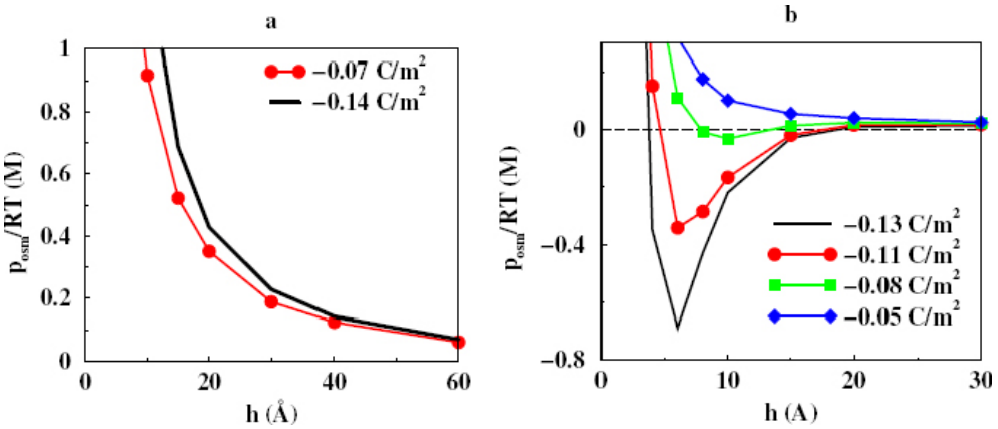

Figure 4-2. *Ion-ion correlation gives rise to repulsive forces at short distances when counterions are monovalent (left figure) but attractive forces when the ions are divalent, right figure /From Jönsson et al. 2009/.*

between the sheets is 4.4 nm and the volume fraction is 0.18 /Karnland et al. 2006, Table 4-7/. It also agrees with the observations that calcium bentonite initially swell faster than sodium bentonite starting at the same compaction /Dvinskikh and Furó 2009/. The reason for this is that the hydraulic conductivity of the calcium bentonite is higher than that of the sodium bentonite, because at the same porosity the calcium bentonite consists of larger particles than those in the sodium bentonite where the sheets tend to separate in stacks with fewer sheets or even into individual sheets.

This discrepancy between idealised theory and real systems was already found by /Kjellander et al. 1988/ who also sought reasons for the disagreement. For idealised infinitely large surfaces with even charge distributions /Kjellander et al. 1992/ have studied the forces between sheets of Ca, Mg and Ba smectites using the anisotropic Hypernetted Chain Approximation, HNC. They show that for typical surface charge densities and with divalent counterions very strong attractive forces can develop between the sheets. Several MPa attractive forces are predicted. The maximum attractive force is found at distances around 1 nm. /Kjellander et al. 1988/ show that this compares well with the observed distances between sheets obtained by X-Ray diffraction. /Jönsson et al. 2009/ report similar results. /Kjellander et al. 1988/ discuss mechanisms not included in the HNC model such as hydration effects of the counterions, the impact of the size of water molecules and specific binding of calcium to the surface of the sheets but conclude that although such effects can be expected they would only affect the results in a minor way.

It should be noted that such attraction forces do not develop for monovalent ions according to the HNC model. For divalent ions and sheet distances larger than a few nm (about 3 nm in the examples) the force between the particles is predicted to become repulsive although with much lower values than what the non-linear Poisson-Boltzmann approximation predicts.

/Bergaya et al. 2006 pp 186 ff/ summarize and discuss a number of causes discussed in the literature for the deviations of the observed behaviour of different clay systems and what the DLVO theory predicts. It includes Stern layer adsorption, hydration shell effects, formation of band type aggregation and more. /Kjellander et al. 1988/ also discuss the arrangement of the individual sheets forming larger particles. They suggest that the individual sheets “condensate” to quasi-crystals. These are not like the floccu-lated particles that can form because in the latter the sheets are loosely attached to each other and can be readily broken up again. By contrast, the quasi-crystals form large essentially flat sheets with up to 5,000 nm lateral size and 5 nm thickness. This compound particle (quasi-crystal) is strongly held together by the ion-ion correlation forces. The forces between the larger particles are, however, repulsive because they cannot approach each other sufficiently close for the attractive forces to dominate. This configuration is suggested in Figure 4-3. Such configuration would also have the properties observed in expansion and filtering experiments where calcium exchanged bentonite has difficulties passing 100–200 µm pore size filters. Sodium exchanged bentonite on the other hand readily passes down to 2 µm filters and are only stopped by 0.5 µm filters /Birgersson et al. 2009/. In addition this configuration may decrease the CCC to a significant extent, according to the findings about the particle size influence on the CCC /Liu et al. 2009b/.

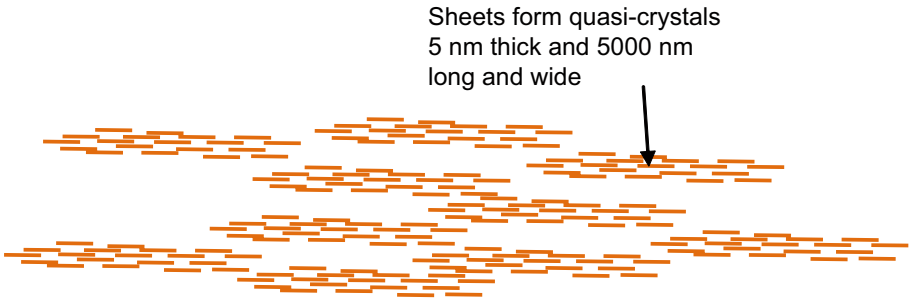

Figure 4-3. *Conceptualisation of "quasi-crystals" of individual Ca smectite sheets arranged in a configuration that makes it possible to have a high solid volume fraction when compacted but may allow swelling between the quasi-crystals. Based on /Kjellander et al. 1988/ description.*

Figure 4-4 shows a conceptual picture of how calcium clay could be arranged in compacted and swollen conditions. During swelling the quasi-crystals distance themselves from each other and may also partly break up at weak points. Re-arrangement of sheets within stacks and quasi-crystals can also take place.

In the sodium form, smectites disintegrate in water or low-concentrated electrolyte solutions into the individual sheets. Complete separation of the sheets requires the absence of divalent and trivalent cations /Frey and Lagaly 1979/. /Frey and Lagaly 1979/ by selective coagulation investigated particle charge density differences of montmorillonite and beidellite. The interlayer cation density is not constant throughout the individual crystals. It varies between –0.161 and –0.245 C/m^2 for montmorillonite and between –0.201 and 0.347/C/m^2 for beidellite. The average charge density in montmorillonite is –0.192 C/m^2 and –0.257 and –0.192 C/m^2 in beidellite. The cited charge densities are given per one side of the particle in this case. The surface charge densities will be half as large when the charge is distributed over both sides of the particles.

The solid volume fraction ϕ that will result when 1 nm thick sheets are arranged in stacks with 1 nm distance between sheets and the stacks have a distance h_{stack} is obtained from Equation (4-1) in a columnar arrangement.

$$\phi = \frac{n\,\delta_s}{h_{stack} + (2n-1)\delta_s} \tag{4-1}$$

where n is the number of sheets in a stack, and δ_s is the thickness of a sheet and the distance between the sheets. Figure 4-5 shows the solid volume fraction as a function of the distance between the stacks. The curves from bottom and up are for 1, 2, 5 and 10 sheets in each stack.

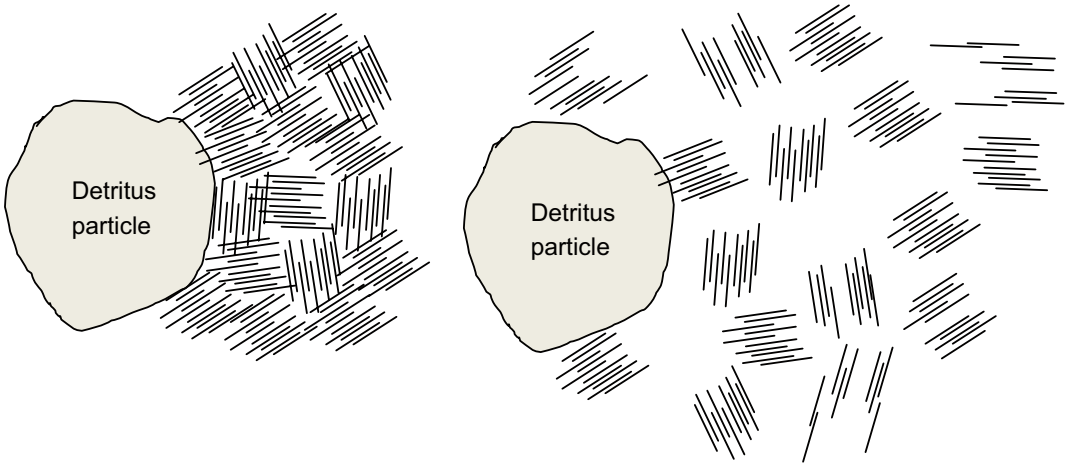

Figure 4-4. *Speculative concept of swelling untreated Ca smectite clay. Left figure shows highly compacted clay with stacks of sheets or quasi-crystals arranged for low porosity. Right figure shows expanding clay where quasi-crystals distance themselves from each other and partly break apart and rearrange themselves at the weak spots in the stacks.*

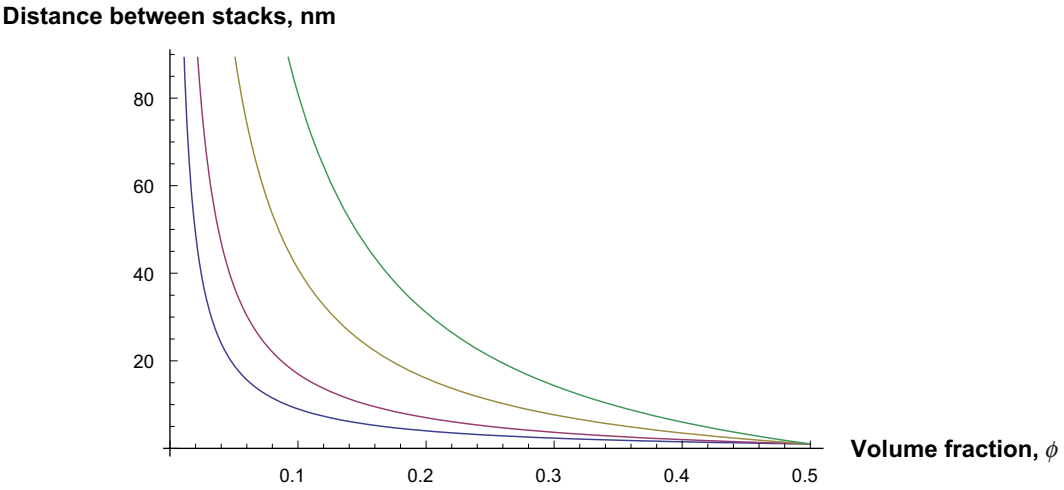

Figure 4-5. *Volume fraction as a function of the distance between outer surfaces of stacks. The curves from bottom and up are for 1, 2, 5 and 10 sheets in each stack.*

The figure is used to illustrate that if sheets are stacked to form larger particles the volume fraction of solids changes for a given particle distance. If the swelling pressure is determined by the DDL forces between stacks in a gel as with sheets at the same distance they would have the same swelling pressure. For single sheets, as can be expected for sodium dominated systems, the volume fraction will be 0.048 in the case of 20 nm separations and for ten stack particles it would be 0.27. For the same volume fraction, on the other hand, the distance between 1 and 5 sheet stacks is very different, resulting in larger hydraulic conductivity for the 5 sheet stack.

Reasons for the heterogeneities that cause stacking but not full collapse in calcium bentonites can only be speculated on at present. Some possible reasons are differences in surface charge densities between different sheets and variation of surface charge densities on the sheets.

/Pettersson et al. 2008/ made atomic force microscopy, AFM, studies of smectite sheets and found that the sheets can have uneven surfaces with height variations of 0.5 nm, which is about half the thickness of an individual smectite sheet. It is conceivable that such variations can have a noticeable impact on how sheets can align themselves to form dense stacks with average distances of 1 nm. In this study it was not possible to determine whether there were heterogeneities in the surface charge density between and on individual sheets.

Differences in sheet sizes in the stacks cause attractive forces in parts of the sheets but repulsive forces at places where the intermediate sheet is short and thus having more than double distance between the outer sheets, see Figure 4-6. Presence of broken fragments of sheets or other detritus material between sheets in some locations can also disrupt the structure.

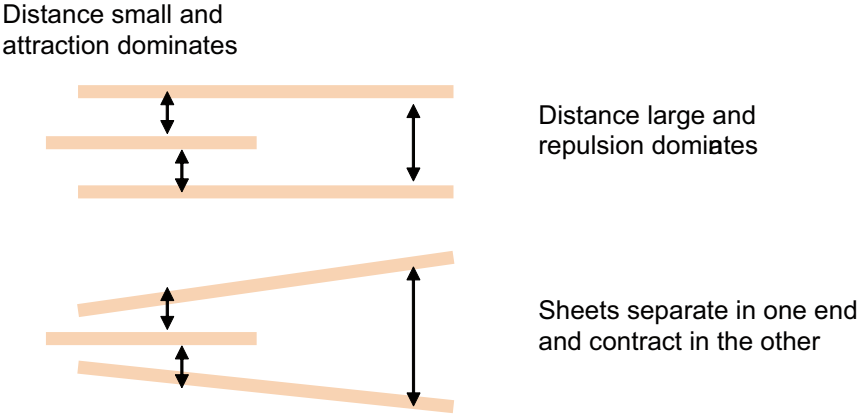

Figure 4-6. *Attractive and repulsive forces dominate in different parts of the stack.*

/Frey and Lagaly 1979/ also investigated the coagulation of smectite particles with different surface charge densities. They found that low-charged plates aggregate predominantly with low-charged plates and high-charged plates with high-charged plates.

/Christidis and Eberl 2003/ and /Christidis et al. 2006/ investigated the influence of layer charge and charge distribution of dioctahedral smectites on the rheological and swelling properties of bentonites. Using X-ray diffraction on potassium exchanged smectite and ethylene glycol saturated samples the layer charge distributions were grouped in terms of proportion of low charge and high charge layers proportions. The proportions of non-swelling particles were determined. Twenty-four bentonite samples were examined. The materials come from bentonite deposits on Milos, and on the Kimolos Islands, Greece and from Turkey respectively, and from the CMS repository. The proportions of low swelling, high swelling and non-swelling material ranged from 0.05 to 1.0, 0 to 0.5 and 0 to 0.6 respectively. The low layer charges defined as > –0.425 ranged around –0.4 charges per half formula unit. The high layer charges were in the range –0.62 to –0.425. In the various rheological measurements the pH ranged from 7.7 to 8.5. Na_2CO_3 concentrations varied between 6 and 30 mM in the tests.

Although this method does not allow the determination of a detailed surface charge distribution function, it clearly reveals that there is a wide distribution of surface charge densities on different sheets.

4.2 Conclusions

In highly compacted bentonites, the smectite clay minerals are arranged in larger particles or stacks of sheets. The thin smectite particles lie in essentially parallel arrangement. When allowed to swell the stacks can disintegrate in stacks with fewer sheets. Sodium dominated clays below the CCC disperse and form sols and can separate into nearly individual sheets. Compacted calcium dominated clays swell in a similar way as sodium dominated clays even in very saline waters but stop swelling at lower porosities than the sodium dominated clays.

Calcium dominated clays retain sheets in stacks with 5 to 15 sheets. This may be the result of ion-ion correlations. However, calcium dominated clays have swelling pressures only slightly lower that sodium dominated clays and can swell to more than 80%, which would correspond to about more than 4 nm *average* distance between sheets, should the sheets separate.

Sodium dominated clays below CCC can wriggle through very fine pores <2 μm, whereas particles from calcium dominated clays cannot pass even much larger pores.

There must be some mechanism(s) that hinder the stacks to combine to a rigid body and permit the gel from exhibiting a considerable swelling pressure at about 50% porosity and allow them to swell to distances of 4 nm and more between sheets.

5 Viscosity of dilute gels/sols and concept of co-volume of flat particles

5.1 Introduction

In this section, the gel/sol behaviour in ionic strengths below the critical coagulation concentration is addressed. We are interested in the possible release of colloidal particles from a gel/sol interface into water. In low ionic strength waters, smectite particles in montmorillonite clays repel each other also over large distances, when the counterions are mostly sodium. By contrast, in calcium rich clays many individual sheets are strongly held together in stacks. However the stacks repel each other. The reasons for this are not fully understood but may be due to heterogeneities in charge distribution between sheets, size distribution or other effects. See chapter 4.

Starting with a dense gel, e.g. when compacted bentonite soaks up water, sodium gels initially expand freely due to the repulsive forces and later by Brownian diffusion to infinite dilution if there were no gravity. Gravity will hold back such expansion against upward movement but will aid expansion in the downward direction. We are interested in gel/sol expansion in fractures in rock. The fracture can have any direction in relation to the smectite source, horizontal, vertical upward and downward or any angle in between. Water may seep or slowly flow in the fractures and sweep away colloidal particles that reach the flowing water. The water movement at the gel/sol/water interface may be influenced by the presence of the colloids because they may increase the viscosity of the suspension and slow down the water seepage.

The understanding of the colloidal particle mobility and of rheological behaviour of the gel/sol system at low solid volume fractions, ϕ, is needed in order to quantify how an expanded gel/sol could release particles to water flowing past the gel or even itself flow downstream.

The water will exert a shear force on the gel and could shear off gel aggregates or individual colloid particles from the gel at high shear rates. In an expanding gel, where the particles repel each other when close together due to electric diffuse layer forces, the individual particles can also be expelled into the water by the repulsive forces. Even when these no longer act in sufficiently dilute sols the individual particles can diffuse out into the water. In this section we address some mechanisms that influence these phenomena.

It is generally accepted that protonation of smectite edge sites can give rise to positively charged edges at pH below 6.5 to 7. This can lead to particles forming edge to face bonds between the positive edges and the negative faces. /Abend and Lagaly 2000, Tombacz and Szekeres 2004, Tombacz et al. 2004, Bergaya et al. 2006/. The pH of the waters in the granitic rocks of interest is not expected to drop below pH 7. We therefore mainly limit the discussion to conditions where there are only negative charges on the particle faces as well as edges, which is the case when pH lies above 6.5 to 7. Then it is expected that no positive charges develop on the edges by protonation of edge sites. However, /Birgersson et al. 2009/ propose that some of the phenomena observed in their experiments may have been caused by the presence of positive edge charges. Until there is clear evidence of the presence of positive edge charges at higher pH we limit the discussion to conditions where edge charges have a negligible influence.

However, there are still many different views of how sheets form larger particles. A good overview and discussion can be found in the paper by /Luckham and Rossi 1999/.

5.2 Literature on rheologic properties of bentonite suspensions

Broad overviews of rheological behaviour of bentonite/smectite suspensions can be found in /Luckham and Rossi 1999, Bergaya et al. 2006/, and references therein. /Barnes 1997/ gives an overview of Thixotropy. Measurements of shear stress-shear rate relations of purified and homoionic bentonite suspensions are reported in /Chen et al. 1990, Penner and Lagaly 2001, Adachi et al. 1998, Brandenburg and Lagaly 1988, Benna et al. 1999, Bekkour et al. 2005, Galindo-Rosales and Rubio-Hernández

2006, Duran et al. 2000, Malfoy et al. 2007/. Rheological properties of natural clays containing other mineral particles are reported in /Christidis 1998, Christidis et al. 2006, Kelessidis et al. 2007/. Methods used to determine layer charge and layer charge distributions are found in /Frey and Lagaly 1979, Christidis 2008/. Electroviscous effects are discussed by /van de Ven 2001, Rubio-Hernandez et al. 2004/.

These papers describe forces involved, shapes, sizes and structures of individual smectite sheets, cause of fixed and variable electric charges on the particle surfaces, influence of pH and ionic strength of the solution, association of individual particles in agglomerates of different sizes and shapes, impact of inorganic counterions in ion exchange positions of sorption and influence of non-ionic surfactants and polymers etc. Pseudoplastic effects and Bingham behaviour are described and analysed as well as causes for thixotropy and other nonlinear effects. The rheological behaviour of such suspensions is very complex and not understood in all details. Nevertheless, there are some effects that are generally agreed on qualitatively and sometimes also quantitatively.

Due to its direct influence on the electroviscous effect and the thickness of stacks, layer charge and charge heterogeneity is expected to strongly affect the rheological properties of smectite suspensions. This includes aspects of charge magnitude and charge localization (i.e. octahedral vs. tetrahedral) as well as the possibility of order or disorder in e.g. Mg-distribution, which influences octahedral charge /Christidis et al. 2006/.

5.3 Notion of co-volume

The smectite particles are made up of very small card- or coin-like thin sheets with irregular edges. The sheets are about 1 nm thick and typically between 50 and 300 nm in the other directions. At high compaction they must be aligned essentially parallel in stacks or quasi-crystals with very little space between the sheets. The distance between sheets in the stacks can be as low as 0.3 to 0.5 nm in “dry” clay when exposed to air with normal humidity /Push and Young 2006, Bergaya et al. 2006/. When compacted, the number of sheets in a stack is expected to be several hundred so that the stacks have approximately the same size in all directions at high compactions so that they can arrange themselves in a dense formation, avoiding large voids between the stacks. This is necessary in order to be able to compress the clay to porosities down to 0.3 to 0.4 without breaking or deforming the sheets too much. Such low porosities are readily obtained in the highly compacted bentonite blocks to be used as backfill in the repository. In water, the clay swells and the stacks distance themselves from each other and expand the distance between the sheets. The stacks also break up in thinner stacks and can break up into individual sheets, given space and favourable chemical conditions. The latter is observed for clays rich in sodium in the ion exchange positions and when the water has low salinity and not much divalent ions such as calcium and magnesium. In calcium rich clays and in waters with higher ionic strengths the sheets do not separate as readily and stacks or quasi-crystals of 5 to 15 or more sheets remain as coherent particles even when the clay has stopped swelling. Sodium rich clays behave very differently from calcium rich clays at lower solid volume fractions.

At high compaction the smectite sheets in a stack (particle) are arranged in parallel. As gel density deceases the movement of the individual particles is affected by the presence of neighbours as long as they do not have space enough to rotate freely. Rotation is a rather rapid process compared to other processes to be considered for the gel/sol behaviour /McBride and Baveye 2002/. /Onsager 1949/ introduced the concept of co-volume where the basic idea is that the particles need a volume in which the particle can rotate freely without touching neighbouring spheres. At higher volume fractions the rotation is hindered and this strongly influences the behaviour of the gel/sol.

Below we present some relations between the ratio of volume fraction ϕ and the co-volume fraction ϕ_s based on this concept. The volume fraction of solid in the dilute gel/sol is

$$\phi = \frac{V_s}{V_w + V_s} \cong \frac{V_s}{V_w} \tag{5-1}$$

as the solid volume of the thin sheet in the dilute sol can be neglected when the co-volume concept is of interest and is applicable.

The number n_s of flat cylindrical sheets with diameter l_s in a total solid volume V_s is

$$n_s = \frac{V_s}{V_{sheet}} = \frac{4V_s}{\pi l_s^2 \delta_s} \tag{5-2}$$

If the sheets form stacks with n sheets in each stack the number of stacks or particles is

$$n_{part} = \frac{4V_s}{\pi l_s^2 \delta_s n} \tag{5-3}$$

In writing the above two expressions, it has been assumed that the sheets are all of the same size and form a thin cylinder with total thickness less than the sheet diameter, forming a stack with the same diameter as the single sheet. Should the sheets arrange themselves into more complex particles; the co-volume can become larger than for a single sheet. Should the sheets arrange themselves in particles consisting of four sheets in the same plane, forming a square, the sum of co-volumes would double. Such particles could readily interfere with each other hindering the movement in narrow channels and pores although they still could retain swelling pressure.

Each particle with one or many sheets, but still thin, needs a co-volume V_{cov} of

$$V_{\mathrm{cov}} = \frac{\pi l_s^3}{6} \tag{5-4}$$

The sum of all co-volumes of the particles per water volume, the co-volume fraction ϕ_{cov} is

$$\phi_{cov} = \frac{1}{V_w}\frac{\pi l_s^3}{6}\frac{4V_s}{\pi l_s^2 \delta_s n} = \frac{2}{3}\frac{V_s}{V_w}\frac{l_s}{\delta_s n} \equiv \frac{2}{3}\phi\frac{l_s}{\delta_s n} \tag{5-5}$$

A simple example shows that for a sheet 300 times larger than its thickness, fairly representative for the smectite particles, a gel/sol with ϕ= 0.005 and the sheets separated so that n =1, the co-volume fraction ϕ_{cov} =1. The co-volumes of this dilute suspension of particles fill all the volume available. We introduce the concept of a non-interference solid volume fraction $\phi_{\mathrm{n.i.}}$ for illustrative more than quantitative purposes. It is defined as the ϕ for which ϕ_{cov}=1.

This suggests that at larger volume fraction of solids than $\phi_{\mathrm{n.i.}}$ particles can be expected to interact considerably. This is seen in viscosity experiments with sodium exchanged smectite particles /Birgersson et al. 2009, Bergaya et al. 2006, p 202–219/. Also thixotropy becomes more evident with higher solid concentrations. At such conditions the particles tend to arrange themselves in a low energy configuration. This implies that there will have sub-volumes where the sheets are in parallel arrangement. When such a gel is sheared, a certain shear stress is needed to start particles in the pseudoplastic gel to move in relation to each other. In the limit the gel behaves as a Bingham fluid needing a minimum yield stress to start to flow.

The formation of coherent stacks in calcium rich clays will decrease the number of particles and larger solid volume fractions ϕ will be needed for interaction of the co-volumes. The above described effects have been observed and are described in more detail in /Bergaya et al. 2006, p 202–219/. For calcium rich smectites it is therefore expected that the $\phi_{\mathrm{n.i.}}$ is much larger than for sodium clays. With n =20 sheets in each stack, $\phi_{\mathrm{n.i.}}$=0.1 This suggests that the properties of a calcium gel/sol would be much less influenced than sodium gel/sol for the same ϕ. However, it should be noted that the co-volume concept may be considerably less valid, in practice, for more massive particles because their larger mass will make them rotate more slowly due to thermal energy effects and gravity may influence the particles more, relative to the thermal movements. Also the sheets may not arrange themselves in ideal stacks but in irregular larger size quasi-crystals.

Figure 5-1 illustrates co-volumes for single sheets and stacks with and without influence of the diffuse electric layer. At high ionic strength the diffuse layer is thin compared to the size of the particles. In the left configuration the co-volumes of the particles are not in contact with each other and they can move independently. Electroviscous and thixotropic effects and Bingham yield stress can be expected to be small or negligible. No repulsion between particles due to diffuse layer repulsion acts between particles and they move only influenced by thermal movement (diffusion) and by gravity. The particles form a sol if the volume fraction of particles is low.

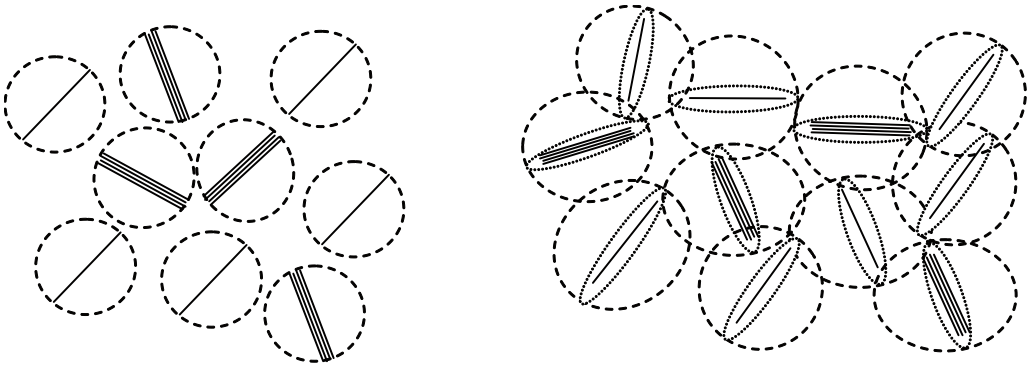

Figure 5-1. *Illustration of co-volume with and without impact of diffuse layer for a given ϕ. The extent of the diffuse layer is shown as dotted oval in the right figure.*

In the right configuration the diffuse layer is large because of very low ionic strength and the co-volume becomes larger. The particles influence each other and electroviscous and thixotropic effects as well as Bingham yield stress can be expected to be noticeable. Repulsion between particles due to diffuse layer repulsion will tend to expand the gel and it will be more viscous due the electroviscous effect. This was demonstrated by /Adachi et al. 1998/.

We have only considered the behaviour of systems where the particles do not combine to form larger aggregates. It may be noted that there is so far no generally accepted nomenclature for what is here called sheets, stacks, flocs. When flocs form at ionic strengths above the critical coagulation concentration the behaviour of the gel becomes increasingly more complicated because of the complex configurations and forces between the particles in the flocs. This is not further discussed in this section.

The notion of co-volume can be extended to include the influence of the diffuse layer in the following way. Define the co-volume by extending the size of the particle by adding a number m of the diffuse layer thicknesses κ^{-1} (m will be determined by fitting to experiments).

$$V_{cov} = \frac{\pi(l_s + 2m\kappa^{-1})^3}{6} \tag{5-6}$$

where

$$\kappa^{-1} = \sqrt{\frac{\varepsilon_0 \varepsilon RT}{2IF^2}} \tag{5-7}$$

The co-volume fraction accounting for the influence of the diffuse layer then becomes

$$\phi_{cov}^{\kappa} = \frac{V_{cov}}{V_p}\phi = \frac{2}{3}\frac{(l_s + 2m\kappa^{-1})^3}{l_s^2 \delta_s n}\phi \tag{5-8}$$

This will be used in section 5.5.1 to derive an expression for gel viscosity as influenced by ionic strength and volume fraction for the non-Newtonian smectite gels.

5.4 Non-Newtonian fluids

Suspensions of smectite particles exhibit non-Newtonian properties. The viscosity of such fluids is not constant but depends on the shear rate and can also be time dependent so that a rested fluid behaves differently from a recently stirred fluid. Bentonite gels are pseudoplastic. At low shear rates higher relative shear stress is induced than at higher shear rates. In the limit the fluid can behave like a solid body for a shear stress up to a yield stress when the seemingly solid body starts to flow. This is called a Bingham body or fluid. Figure 5-2 illustrates these properties. In addition, this behaviour can be time dependent. After some time of rest the gel can be very viscous but when subjected to shear for a short time it becomes considerably less viscous. This is utilized in "drip-free" paints.

The effect is caused by the particles arranging themselves so as to minimise the energy between them. For the flat smectite particles this can be understood by the following conceptual picture. In a dilute suspension (sol) they are far enough from each other not to feel the presence of other particles. In a more concentrated suspension the coin-like particles cannot rotate freely without their edges coming near to the edges or the faces of other particles. As the force between the particles increases exponentially with decreasing distance they tend to align themselves parallel to other particles although they still jitter due to Brownian motion. They lose a degree of freedom of movement. The denser the gel is the more pronounced this effect is. When the average distance between the particles is considerably less than the size of the particle diameter they must be arranged essentially in packages where the sheets are parallel. In such an arrangement the energy of the system will be less than if the particles are not quite parallel. Thus energy must be supplied to the gel, e.g. by stirring, to de-align the particles from the parallel arrangement. Then the particles will jitter more and may even be dislocated. The gel becomes less viscous. When stirring stops the particles again align themselves in parallel and the surplus energy dissipates as heat. In commercial applications the particle concentrations are around some percent by weight of smectite. Among other things these properties are influenced by the particle size distribution, their surface charge density distribution and the presence and type of impurities.

We anticipate that the smectite loss due to shear will be small for a gel with more than a few volume percent because of the described non-Newtonian effects. However, at lower particle concentrations, the viscosity of the gel/sol can approach that of water without particles and it could flow away. We therefore explore how the viscosity of the gel/sol is influenced by particle concentration and by the concentration of different ions. /Birgersson et al. 2009/ performed a large number of rheology measurements on different smectite gels at different volume fractions and water compositions. Different shear rates were used as well as different resting periods between tests. They also discuss the complexities of such measurements. They found that for smectite volume fractions larger than about 1% the gels become increasingly non-Newtonian but can reasonably well be fitted to a power law function.

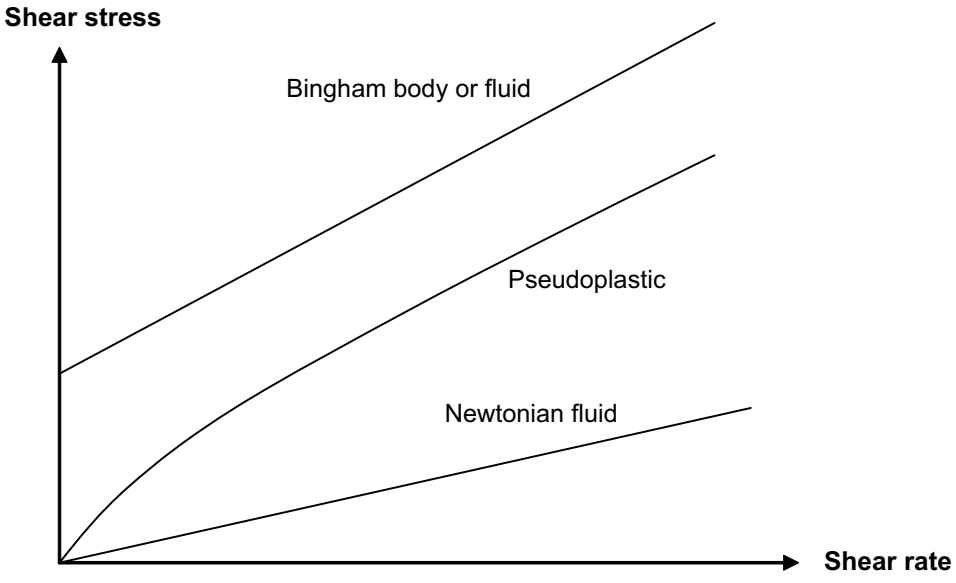

Figure 5-2. *Different behaviours of non-Newtonian fluids.*

5.5 Viscosity of smectite gels

Suspensions and sols with small particles have higher viscosities than that of the fluid due to the presence of the solid particles. For spherical particles at low volume fractions the theoretical Einstein relation has been found to give good agreement with experimental data /Hiemenz 1986, Bird et al. 2002/.

$$\eta = \eta_w(1 + 2.5\phi_{spheres}) \tag{5-9}$$

Three different mechanisms that give rise to electroviscous effects have been described by /Adachi et al. 1998/. One is caused by the resistance of the ionic atmosphere against fluid distortion by shear. Another is due to the interaction of the electric diffuse layers and a third is due to the swelling of the distances between stacks or changes in size of the particles making the particles larger at low ionic strengths. Adachi measured electroviscous effects at volume fractions below 0.5% and found an increment of viscosity with an increase of double layer thickness caused by the first two effects. He found no influence of the third effect.

Here we wish to explore whether the volume fraction of solid spheres in that model can be substituted for ϕ_{cov}. This does not have the theoretical foundation as the Einstein relation has. Here, however, a qualitative discussion is presented in the hope that it will give some insights into the gel/sol behaviour.

/Rubio-Hernandez et al. 2004/ suggest a simple extension to the Einstein equation to account or what is called primary electroviscous effect

$$\eta = \eta_w(1 + \frac{5}{2}\phi(1 + p)) \tag{5-10}$$

where p is the primary electroviscous coefficient. It is a complex function of the zeta potential, and the relative size of the particle radius with respect to the electrical diffuse layer.

/Adachi et al. 1998/ propose the following expression which also accounts directly for the electrical diffuse layer effects and the secondary electrodiffusive effect where the particle layers interact.

$$\eta = \eta_w(1 + \eta_i\phi + K_H\eta_i^2\phi^2 + higher\ order\ terms) \tag{5-11}$$

η_i is the intrinsic viscosity. See also /Evans and Wennerström 1999/. It is 5/2 for solid spheres. K_H is called the Huggins coefficient. This also has been determined on theoretical grounds for particles of simple shapes. Both these factors are influenced by the presence of the electric diffuse layer which causes the viscosity to increase.

The onset of non-interacting colloids can be expected to be strongly influenced by the number of sheets that form the stacks as well as the arrangement of the sheets in the stacks. As suggested in Figure 5-3, the particles may not have the sheets ideally arranged in regular stacks but they may form irregular particles with the sheets only partly aligned. This complicates the simple picture of co-volume arrangement.

However, it suggests that calcium rich clays would have a smaller influence on viscosity than sodium clays at a given ϕ. The calcium gel/sol would be more readily sheared off than a sodium gel/sol by flowing water. On the other hand the calcium stacks will diffuse much slower and will also be much more affected by gravity because of their larger mass.

A good overview and summary of the rheological behaviour of smectite gel/sols can be found in /Abend and Lagaly 2000/ and /Bergaya et al. 2006/. Experiments at higher temperatures are also presented in /Brandenburg and Lagaly 1988/. They show how the flow behaviour of sodium montmorillonite dispersions at concentrations below the CCC depends on the electrical diffuse layers. In higher ionic strengths or at lower pH values where the particles start to agglomerate the rheological properties become highly non-Newtonian, but below the CCC and at pH above 6.5 the shear stress

Figure 5-3. *Sheets arranged irregularly in a particle forming an irregular stack.*

is more moderately influenced by the shear rate. No distinct minimum shear stress is observed for the gel to start flowing although the apparent viscosity is higher at low shear rates than at higher. We here use the term apparent viscosity to indicate this property although no strict definition is proposed for this. With lower particle concentrations Newtonian fluid properties are approached.

It is found that at solid contents above about 2% by weight (ϕ=0.007) the dispersions start to become gel-like with the appearance of a yield value and pseudoplastic properties. Higher salt concentrations reduce the diffuse layer, which shrinks and the particles move more freely. When the critical coagulation concentration is approached apparent viscosity increases again. It is also found that natural clays can behave very differently than purified clays. The latter are commonly used in investigations aiming to gain detailed understanding of the interaction phenomena. Untreated clays disperse less than purified clays.

Rheological data presented in /Bergaya et al. 2006, p 202/ for sodium montmorillonite dispersions with 4% by weight (ϕ= 0.015) of solids at pH 6.5 give an apparent viscosity of the suspension that is about 6 times larger than pure water at room temperature. At pH 12 the apparent viscosity is nearly the same as that for water. In contrast, at pH 4.5 when the edge charges are positive the gel distinctly shows Bingham fluid properties with a minimum yield stress. Similar results are obtained by /Duran et al. 2000/ in rheological experiments with 5% (w/w) homoionic bentonite suspension in 0.01 M NaCl. At pH below 8 not very nonlinear relations between shear stress and shear rate were observed, whereas at pH 7 and below distinct Bingham effects were seen. The apparent viscosity of the gel/sol for pH 8 and above was on the order of 10 times that of water. /Tombacz et al. 2004/ present similar result under similar conditions. The experiments of /Tombacz and Szekeres 2004/ also show a significant increase in thixotropy and yield values. Also the formation of pseudoplastic gels only below pH around 6.5 verify that attractive interaction exists between positively charged edges and negatively charged surfaces of the particles. At low pH and at solid concentrations of 4% (w/w) montmorillonite suspensions in the presence of 10 mM NaCl at 25°C this is noticeable. However, their experiments show tendencies of pseudoplastic effects at low shear rates also at pH between 7.6 and 9.3. This was not so evident in the results of /Duran et al. 2000/ because of the double logarithmic plotting. At higher shear rates all experiments show a linear relation between shear rate and shear stress indicating viscosities up to 10 times larger than that of pure water at low shear rates and decreasing at higher shear rates.

At these relatively high clay concentrations all except one of the clays had minimum shear stresses to induce flow ranging from 2 to 38 Pa. The exception exhibited Newtonian flow characteristics. Apparent viscosities were between 2 and $45 \cdot 10^{-3}$ Pa s. This is 2–45 times higher than water.

/Abend and Lagaly 2000/ investigated sol–gel transitions of sodium montmorillonite dispersions. /Penner and Lagaly 2001/ investigated rheological properties of sodium montmorillonite dispersions in the presence of different anions. Clay concentrations between 0.025 and 2% (w/w) were used. It was also reported that the sodium montmorillonite formed stiff gels at solid contents above 3.5% (w/w). The viscosity decreased with increasing salt or acid concentration, decreased to a minimum, then increased sharply when the critical coagulation concentration, CCC, was approached. In 2% (w/w) sodium montmorillonite dispersions the critical coagulation concentration for sodium chloride and sulphate was higher than in dilute dispersions 0.025% dispersions. In low montmorillonite concentrations, <0.1%, the CCC was determined by test-tube tests with visual inspection or photometrical measurement of the turbidity of the dispersions at increasing salt concentration. At higher solid contents, it was derived from rheological measurements. A strong increase of the viscosity of the dispersions then indicated the critical salt concentration. For example for NaCl, Na_2SO_4 and NaNO3 the apparent viscosity for a 2% suspension at a shear rate of 120 s^{-1} decreased from $5 \cdot 10^{-3}$ to about $3.5 \cdot 10^{-3}$ Pa s in salt concentrations increasing from 10^{-3} mM to around 0.1 mM where a sharp minimum appeared. Experiments were also performed with additions of acids. Here only the results for pH> about 7 are referred to. Various phosphates showed a stabilizing effect, especially the neutral and basic Na-phosphates. The critical coagulation concentration for 0.025% montmorillonite was similar to that for the 2% suspensions. No viscosity data were reported for the dilute suspensions.

/Bekkour et al. 2005/ investigated rheological behaviour of bentonite suspensions with mass concentrations equal to 6, 8, and 10% (w/w). They found minimum yield stresses increasing with the solids concentration between 4 and 14 Pa and apparent viscosities increasing from 5 to 30 Pa·s at the highest shear rates of nearly 1,000 s^{-1}. Strong thixotropic effects were observed.

The investigations of rheological properties referred above show that the rheology is very complex and has not been summarized in a simple model that can be used quantitatively. Nevertheless, the evidence suggests that the shear strength at low shear rates is higher than 1 Pa for gels above the CCC. Such gels have a volume fraction of 1% and more. Dilute sodium dominated gels below the CCC exhibit a pseudoplastic behaviour and approach water viscosity at very low volume fractions. Such gels are specifically treated in the next section.

5.5.1 A new expression for viscosity of dilute smectite gels

We are especially interested in the viscosity of dilute gels that will form at the gel/water interface. Figure 5-4 shows the relative viscosity for a number of experiments with different volume fractions and different ionic strengths /Liu and Liu 2009/. There has not yet been time to fully utilise the large amount of rheology data in /Birgersson et al. 2009/ in the present analysis.

Experimental data in Figure 5-4 are fitted to the following expression for the relative viscosity, given that l_s varies in the range of 100 and 300 nm, and m in the range of 0.5 and 2,

$$\frac{\eta}{\eta_w} = 1 + a\phi_{cov}^{\kappa} + b(\phi_{cov}^{\kappa})^2 + c(\phi_{cov}^{\kappa})^3 \qquad (5\text{-}12)$$

Using the coefficient of multiple determination, R^2, as a measure of how well the regression line approximates the measured data points, it was found that a maximum of R^2 was obtained when l_s = 220 nm and m = 1. Then, about 99.8% of the experimental results can be well represented by the expression,

$$\frac{\eta}{\eta_w} = 1 + 1.022\phi_{cov}^{\kappa} + 1.358(\phi_{cov}^{\kappa})^3 \qquad (5\text{-}13)$$

Note that the second order term could be omitted as it contributed marginally to the fit. The coefficient for the first order term has a good foundation in theory as explained in /Liu and Liu 2009/.The value a = 1.022 in Equation (5-13) is actually derived from the theoretical value for the intrinsic viscosity for thin coinlike sheets /Batchelor 1970/. The value b was found to very close to 0 so only c was actually needed for the fitting.

Figure 5-5 shows the same data plotted as a function of the co-volume fraction. It is seen that the introduction of the co-volume concept including the diffuse layer gives a simple relation for the gel viscosity in this range of volume fractions and ionic strengths. These results form an important part of the modelling of flow of dilute bentonite gels.

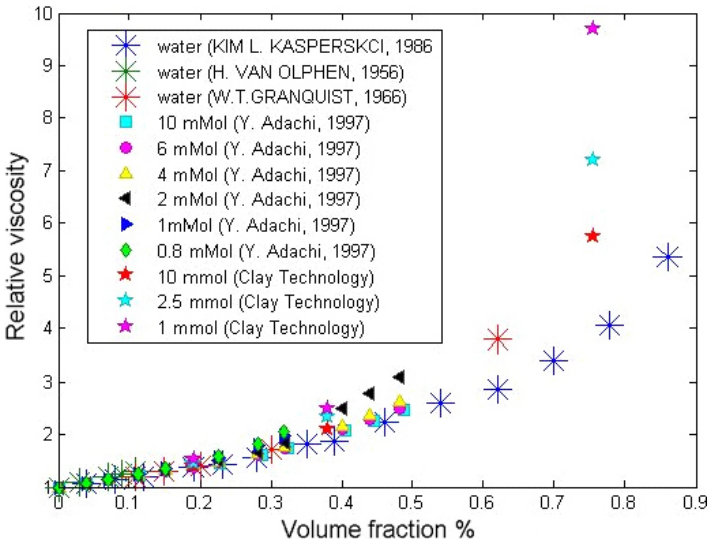

Figure 5-4. *Relative viscosity as a function of volume fraction from different sources. The Clay technology data are from /Börgesson and Nilsson 2008/.*

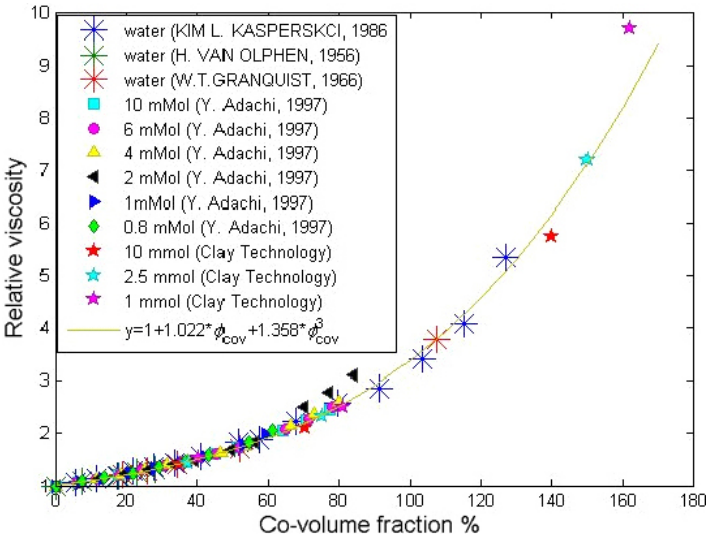

Figure 5-5. *Relative viscosity as a function of co-volume fraction from different sources.*

5.6 Discussion and conclusions

In waters with ion concentrations below the critical coagulation concentration, the colloidal particles repel each other when they come near. At close distances they may also interfere with each other by rotation when they "bump into each other". To avoid this they need a volume in which they can rotate freely, the co-volume, without touching the neighbours. For the coin like smectite particles which have length to thickness ratio typically ranging from 100 to 300 for the individual sheets the solid volume fraction ϕ for which the particles just do not touch is in the range of 0.005 to 0.015. This is equivalent to a mass fraction of 0.013 to 0.04. When sheets stick to each other in stacks or other configurations of multiple sheets, the co-volume needed for independent movement decreases approximately inversely proportional to the number of particles in the stacks. In lower concentrations the suspension behaves as a sol.

For solid concentrations higher than the volume needed for free movement, the particles interfere with each other and the suspension behaves like a gel. The viscosity of the gel increases markedly due to physical interference between the particles and thixotropic and Bingham fluid properties become apparent. Low ionic strengths lead to an increase in the thickness of electrical diffuse layer around the particles. When this is not negligible compared to the size of the particle the particle will seem larger and will need a larger co-volume. Therefore in very low ionic strength waters, the interference between particles will be noted already at lower solids concentrations.

It may also be noted that below non-interference co-volume $\phi_{n.i.}$ particles can move independently of each other. The sol will not expand due to physical or electrical interference effects between the particles but may disperse due to thermal movement (Brownian diffusion) which may be counteracted by gravity, if present in the direction of movement.

The viscosity of the sol will approach that of the water with decreasing solid concentration.

The above semi-quantitative description is in agreement with numerous experimental results. Purified homoionic clays with sodium disperse more than non-purified natural montmorillonites and clays with a high proportion of calcium or magnesium as counterions in the electrical diffuses layer. This is partly due the stacking of sheets and partly due to the presence of impurities in the natural clays.

The statements below are aimed at giving an qualitative and semi-quantitative idea of the behaviour of Na-bentonite suspensions in neutral to moderately basic waters with ionic strengths varying from essentially distilled water to somewhat above the critical coagulation concentration. Only sodium and calcium counterions are considered because they are the ions of primary interest for the problem at hand.

The rheological behaviour of Na-bentonite suspensions has the general trait that the individual smectite sheets separate into individual sheets or into particles containing two or three sheets.

For solid concentrations larger than a few % (w/w) the gels are highly non-Newtonian, exhibiting a pseudoplastic behaviour with thixotropic effects and even a Bingham fluid behaviour. The yield stress for the Bingham fluid is (considerably) larger than 1 Pa.

For clay concentrations around 2% (w/w) there are only mild nonlinear effects of shear rate on shear stress. Relative viscosities of the suspension are less than 10 times that of pure water. The viscosity at low shear rates drops from 10 times to just a few times larger than pure water when Na concentrations are below the critical coagulation concentrations. With increasing Na concentrations from 0.001 to 0.1 mM the relative viscosity is not much influenced by the Na concentration but drops to a minimum at around 1 mM and rising again when the critical coagulation concentration is approached.

Little information is available in the literature on the rheological behaviour at lower clay concentrations but it is probable that the viscosity drops and becomes more Newtonian and rapidly approaches the viscosity of water.

Clays very rich in calcium do not separate in individual sheets but form particles with up to tens of sheets. Such clays do not expand as readily as sodium clays. No rheological data have been found in the literature for such clays. However, as the particles are larger it is expected that there will be less influence on the apparent viscosity for the same clay concentrations.

6 Forces on and between smectite particles – Development of a dynamic model for gel expansion

6.1 Introduction and overview

To be able to understand and simulate the behaviour of a compacted bentonite in a deposition hole, swelling under water uptake, expanding out in the fracture as it becomes looser and possibly released colloidal particle to the seeping water we need to account for the forces that govern this process.

The underlying conceptual model is that the gel consists of thin smectite sheets aligned in parallel until the gel is so dilute that they can rotate freely. Gravity and buoyancy forces on the particles and attractive van der Waals forces as well as repulsive double layer forces between particles act to move the particles when these forces do not balance. The movement is restrained by friction against the water in which they move.

This force balance is used to set up the equation of continuity to define the change in space and time of the expanding gel. The double layer repulsive forces are based on a solution of the Poisson-Boltzmann equation. A new analytical solution was devised, which is valid over the whole range of solid volume fraction in the gel of interest here, namely from $0 < \phi < 0.7$. The particle friction is based on the Stokes-Einstein relation for individual particles in the dilute gel and on a modified Kozeny-Carman relation for the dense gel. Recently, also a correlation for the friction as related directly to the force balance model was devised, which is an alternative to the Kozeny-Carman relation.

A special bonus with the dynamic force balance model is that was successfully used to predict the range of CCC for sodium as well as calcium bentonites, much better than the conventional DLVO theory does.

The dynamic model has been successfully tested against accurate measurements of sodium smectite tablet expansion, starting from a dry density of 1,800 kg/m^3 expanding upwards in test tubes. It has also been attempted to use the model to simulate calcium bentonite expansion but although modelling results qualitatively and semi-quantitatively agree reasonably well with the experiments there are differences that makes the prediction of calcium bentonite swelling less reliable.

The dynamic force balance model makes up a central part of our larger model used for bentonite erosion simulations.

6.2 Overview of forces considered

The particles in a gel or sol will be acted on by a number of different forces. The action of these forces on the particles determines the expansion and contraction of the gel and the formation of sols. The understanding and modelling of these forces will form the basis for our modelling. We consider the following forces in this report:

- F_g Gravity and buoyant force.
- F_μ Forces due to changes in chemical potential in a concentration gradient (Diffusional forces).
- F_{vdW} van der Waals attractive forces.
- F_{DDL} Repulsive forces due to the presence of electrical charges in and on the smectite particles, so called diffuse double layer forces.
- F_η Friction forces on the particles if they move due to imbalance of the previous forces.

The sum of these forces shall be zero as we neglect acceleration of the particles. This is permissible because the changes in particle velocity are very slow.

$$F_\eta = -(F_\mu + F_g + F_{DDL} + F_{vdW}) \tag{6.1}$$

Below we describe the forces and the equations that will be used to quantify them and exemplify their effects by some numerical examples. This is done to illustrate their strengths and relative impact in different situations.

The expressions will also be used to study how compacted clay gels may swell, expand and eventually solubilise, given the proper chemical conditions for sol formation. For this the concept of CCC plays an important role. Above the CCC the clay may form a gel that expands to a given clay density but does not spontaneously release individual particles to form a sol. Below the CCC the clay may release particles and generate a dilute sol. Somewhat simplified the CCC can be seen as the ionic concentration where the attractive and repulsive forces balance.

6.3 Gravity and friction acting on single particles

We first describe the influence of gravity and friction forces. Later the other forces are also considered. Gravity acts on a particle, pulling it downward. The force on the particle is proportional to its buoyant mass and can be expressed as

$$F_g = V_p(\rho_p - \rho_w)g_c \tag{6-2}$$

This force will tend to move the particle. In dilute systems friction against the fluid, in this case the water, will oppose the movement and the particle will attain a steady state velocity as these forces balance.

The friction force on a spherical particle can for laminar flow conditions be expressed by /Bird et al. 2002/.

$$F_\eta = u_p f_{fr} = 3\pi\eta_w d_p u_p \tag{6-3}$$

η_w is the viscosity of water and d_p is the particle diameter.

The terminal velocity u_p for a falling (or rising) particle is obtained by equating the two forces in Equations (6-3) and (6-2).

$$u_p = \frac{V_p(\rho_p - \rho_w)g_c}{3\pi\eta_w d_p} = \frac{d_p^2(\rho_p - \rho_w)g_c}{18\eta_w} \tag{6-4}$$

Figure 6-1 shows the settling velocity of a spherical particle with density 2,700 kg/m^3 in water. Particles larger than 0.1 mm will attain Reynolds numbers larger than 1 and the above formula is not valid.

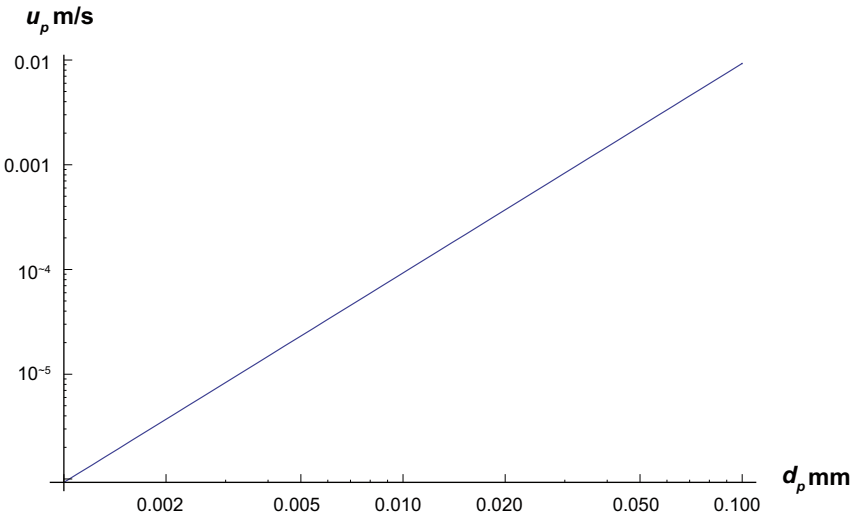

Figure 6-1. *Settling velocity of a spherical particle with density 2,700 kg/m^3 in water.*

Figure 6-2 shows the time for a particle to settle 10 cm. It is seen that smectite particles which are about 0.3 µm will move and settle very slowly, whereas the larger accessory mineral particles which span the size range 1–100 µm can settle much faster.

Note, however, that the Stokes law, as given in Equation (6-3), applies strictly only for rigid spherical particles, for which the friction coefficient reads

$$f_{fr} = 3\pi d_p \eta_w \tag{6-5}$$

For particles with other shapes, we generally have,

$$f_{fr} = 6\pi\eta_w r_{eqv} \tag{6-6}$$

where r_{eqv} is the equivalent radius of the particles and it is particle geometry dependent. Thus, for spherical particles, Equation (6-5) gives,

$$r_{eqv} = \frac{d_p}{2} \tag{6-7}$$

For coin-like particles, we have /Hubbard and Douglas 1993, Cadene et al. 2005/.

$$r_{eqv} = \frac{\frac{\delta_p}{2}\sqrt{\frac{4S_p}{\pi\delta_p^2} - 1}}{\tan^{-1}\left(\sqrt{\frac{4S_p}{\pi\delta_p^2} - 1}\right)} \tag{6-8}$$

where S_p is the surface area of the particle and δ_p the thickness.

As $\delta_p/S_p \rightarrow 0$, it reduces to

$$r_{eqv} = \frac{2}{\pi}\sqrt{\frac{S_p}{\pi}} \tag{6-9}$$

For large thin coin-like particles with diameter d_{coin} it is

$$r_{eqv} = \frac{d_{coin}}{\pi} \tag{6-10}$$

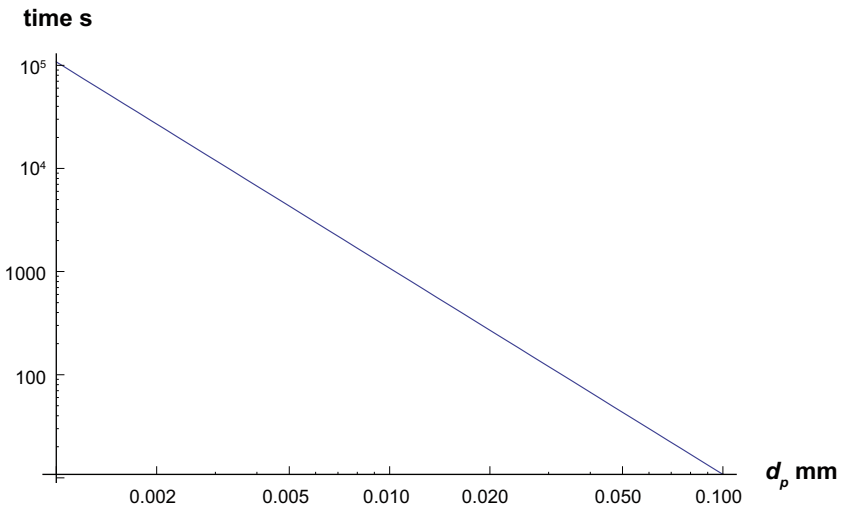

Figure 6-2. *Time for a spherical particle to settle 10 cm.*

6.4 Friction forces in porous beds and gels

Here we describe relations governing fluid flow and pressure drop in porous beds and friction forces on particles in dilute suspensions and in dense beds. We have two uses for this information.

The pressure drop properties in porous beds of particles can be used to assess the mean sizes of the pores between the particles. This information can be useful when estimating whether a porous bed of small particles, e.g. the detritus material left behind when smectite is eroded, might strain further smectite particle movement through such a bed. The information is also useful for selecting particle sizes for material to add to the buffer to facilitate formation of such filter beds.

The second use is to obtain relations for friction forces on individual particles in an expanding gel and in a dilute sol. This relation is used in our model for dynamic expansion of a gel/sol system where a number of different forces act to move the particles and the friction forces act to slow down such movement. We wish to develop a relation for the friction forces that is valid over the whole range of volume fractions that will be encountered, i.e. from around 70% for the most highly compacted bentonites (dry density 1,890 kg/m^3) down to near zero where the particles move independently of each other, under laminar flow conditions. We here develop a number of relations for later use.

6.4.1 Permeability of a porous bed

The friction force in a porous medium such as a bed of small particles can be estimated from a relation attributed to Kozeny and Carman called the Kozeny-Carman or the Blake-Kozeny relation, when the flow is laminar which is valid for Reynolds number Re<1. /Bird et al. 2002, p 191/.

The idea behind this relation is that the space between the particles forms conduits in which the fluid flows and the pressure drop in the conduits can be described in the same way as in a tube. The latter is described by the Hagen-Poiseuille equation which was derived from basic principles of viscosity. For a circular tube it is

$$u = \frac{dP}{dz}\frac{d_{tube}^2}{32}\frac{1}{\eta_w} \tag{6-11}$$

where u is the mean velocity, $\frac{dP}{dz}$ is the pressure gradient, d_{tube} the diameter of the tube and η_w the viscosity of the fluid.

The specific surface of the tube, which causes the friction, per volume of water in the tube is given by,

$$a_v = \frac{4}{d_{tube}} \tag{6-12}$$

With this the Hagen-Poiseuille equation can be written as

$$u = \frac{dP}{dz}\frac{1}{2a_v^2}\frac{1}{\eta_w} \tag{6-13}$$

Similarly for the flux u_o (m^3/m^2/s) through a porous bed although now it is more practical to relate the specific surface a_R.

$$u_o = \frac{dP}{dz}\frac{6}{25}\frac{1}{a_R^2}\frac{\varepsilon^3}{(1-\varepsilon)^2}\frac{1}{\eta_w} \tag{6-14}$$

although now it is more practical to relate the specific surface a_R of the particles forming the bed, m^2 surface/m^3 of solid, with,

$$a_R = \frac{6}{d_p} \quad \text{and} \quad a_R = \frac{2}{\delta_p} \tag{6-15}$$

for spheres and large thin sheets, respectively, where δ_p is the sheet thickness. The former is applicable to a bed of spherical particles and the latter to a bed (gel) formed of flat sheets such as smectite particles.

The mean velocity in the pores in the bed, *u,* thus reads, with the help of Equation (6-16),

$$u = u_o/\varepsilon = \frac{dP}{dz}\frac{1}{\eta_w}\frac{6}{25}\frac{1}{a_R^2}\frac{\varepsilon^2}{(1-\varepsilon)^2} \tag{6-16}$$

It may be noted that the so called cubic law, which describes flow in a slit between two parallel plates, also gives Equation (6-16) but with a constant 1/3 instead of 6/25 if a number of such slits are arranged in a stack. The constant 6/25 in Equation (6-16) accounts for the tortuosity effect in the randomly arranged particles that is the basis of this equation. Also constrictivity and orientation effects due to e.g. uneven alignment and varying orientation are included in this constant.

On the other hand, the flux in a porous bed is sometimes written as the product of the hydraulic conductivity K_h and the hydraulic gradient i, the so-called Darcy's law

$$u_o = K_h i = K_h \frac{dP}{dz}\frac{1}{\rho g} \tag{6-17}$$

This gives, by combining with Equation 6-16, the Kozeny-Carman relation for K_h

$$K_h = \frac{1}{a_R^2}\frac{6}{25\eta_w}\frac{\rho g\varepsilon^3}{(1-\varepsilon)^2} = d_p^2\frac{1}{150\eta_w}\frac{\rho g\varepsilon^3}{(1-\varepsilon)^2} = \delta_p{}^2\frac{3}{50\eta_w}\frac{\rho g\varepsilon^3}{(1-\varepsilon)^2} \tag{6-18}$$

Correspondingly, the permeability of the porous bed reads,

$$k = \frac{1}{k_0 a_R^2}\frac{\varepsilon^3}{(1-\varepsilon)^2} \tag{6-19}$$

where k_0, accounting for the pore shape and the tortuosity of the flow channels, is often called the Kozeny's constant and it is 25/6 in this case.

In the equations above we have used porosity ε to denote the volume fraction of fluid because this is the conventional way in most textbooks. In many of our other models we prefer to use the volume fraction of solids ϕ instead because most data on clay experiments are reported based on how much solid material was used in the experiments. The relation between ε and ϕ is

$$\varepsilon = 1 - \phi \tag{6-20}$$

Thus, Equation (6-19) becomes,

$$k = \frac{1}{k_0 a_R^2}\frac{(1-\phi)^3}{\phi^2} \tag{6-21}$$

Although the Kozeny-Carman equation, as given in Equation (6-18) or (6-19), has long been developed, there exists a large consensus that this equation is valid only for porous media, such as sands and nonplastic soils, where particles are approximately equidimensional, uniform and larger than 1 μm, but not valid for clays. More recently, however, a systematic investigation suggests that, as a general rule, the Kozeny-Carman equation predicts fairly well the saturated permeability of most soils, including clays in particular /Chapuis and Aubertin 2003/. The reason of observed differences between predicted and measured k values has been attributed to inaccurate estimates of specific surface area, a_R, unreliable testing procedures and theoretical limitations of the equation (e.g. it is inadequate to apply this model into cases where the medium is anisotropic).

To demonstrate how well the Kozeny-Carman equation predicts, in Figure 6-3 we show an example of measured hydraulic conductivities of the commercial bentonite MX-80, and Na and Ca exchanged bentonites. The latter are also devoid of the about 20% accessory minerals in the MX-80 /Karnland et al. 2006/.

It is seen that the hydraulic conductivity of the gel is over estimated, especially for the high densities. Several reasons for this can be conceived. Tortuosity of the flowpaths can be expected to be higher in beds of thin flat particles than in beds of essentially spherical particles. Another effect that has been proposed is that electroviscous effects play a role making the water adjacent to the surfaces

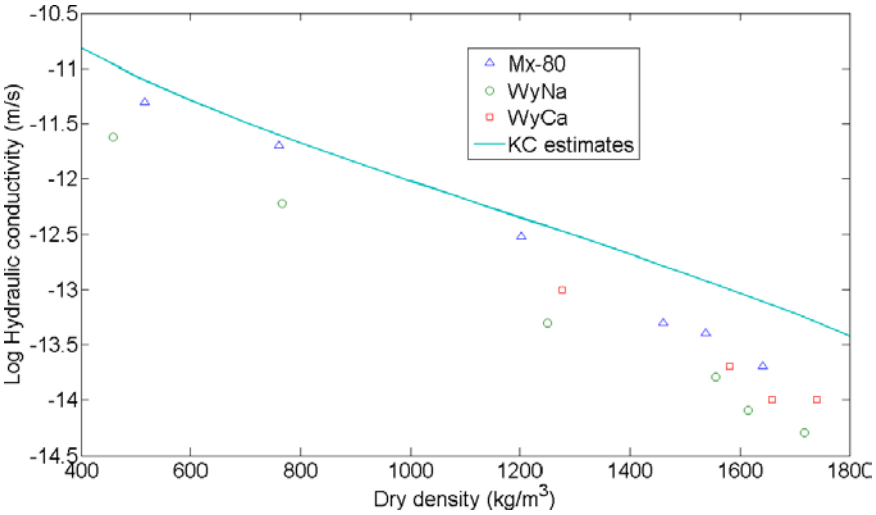

Figure 6-3. *Hydraulic conductivity of some bentonites and Kozeny-Carman equation.*

of the particles more viscous. In a dense gel there are only 3–4 water molecules between the sheets. This has been modelled by /Ichikawa et al. 1999/. They made molecular dynamic simulations and found that the viscosity of the water nearest the surface is considerably larger than far away water. They also solved the Navier-Stokes equations with the variable viscosity and did calculations on the permeability of dense gels. Some order of magnitude higher viscosity was obtained for 1–8 nm distances between sheets.

All these facts suggest that, in modelling of a specific clay, it is better to use data obtained on that clay and obtain best fits using e.g. a modification of the Kozeny-Carman equation. Indeed, for sodium exchanged bentonite it was found /Liu 2009/ that the permeability at low ionic strength is independent of the ionic concentrations, and it can be well approximated by a modified Kozeny-Carman model with ϕ^3 instead of ϕ^2 and k_0=182. The permeability is then given by /Liu 2010/,

$$k = \frac{1}{k_0 a_R^2} \frac{(1-\phi)^3}{\phi^3} \tag{6-22}$$

The comparison of the permeability by this expression with experimental results is shown in Figure 6-4. These results are obtained by fitting experimental data on different sodium exchanged bentonites at different ionic strengths (up to 300 mM NaCl solutions).

Permeability data for MX-80 and similar bentonites /Karnland et al. 2006/ were used to obtain the dependence of k on ϕ. It was found, with the method detailed in /Liu 2010/, that the permeability of natural MX-80 is very different from that of sodium exchanged bentonite. It can be well described over a wide range of solution concentrations by,

$$k = \frac{1}{k_0 a_R^2} \frac{(1-\phi)^6}{\phi^2} \tag{6-23}$$

where k_0 is about 0.6, provided that the particle thickness is on average 1 nm.

For calcium exchanged bentonite, however, no reliable expressions similar to Equations (6-22 and (6-23) could be found, because of lack of the permeability data, which covers in all cases only the range of $\phi > 20\%$.

On the other hand, it should be point out that, although Equations (6-22) and (6-23) give better descriptions of the permeability of specific clay than the Kozeny-Carman equation does, Equation (6-18) or (6-19) is still valuable in rough estimates. The reason for this is that not only it is simple and well known, but it may also be used to asses in a simple way if a porous bed might strain particles of a certain size.

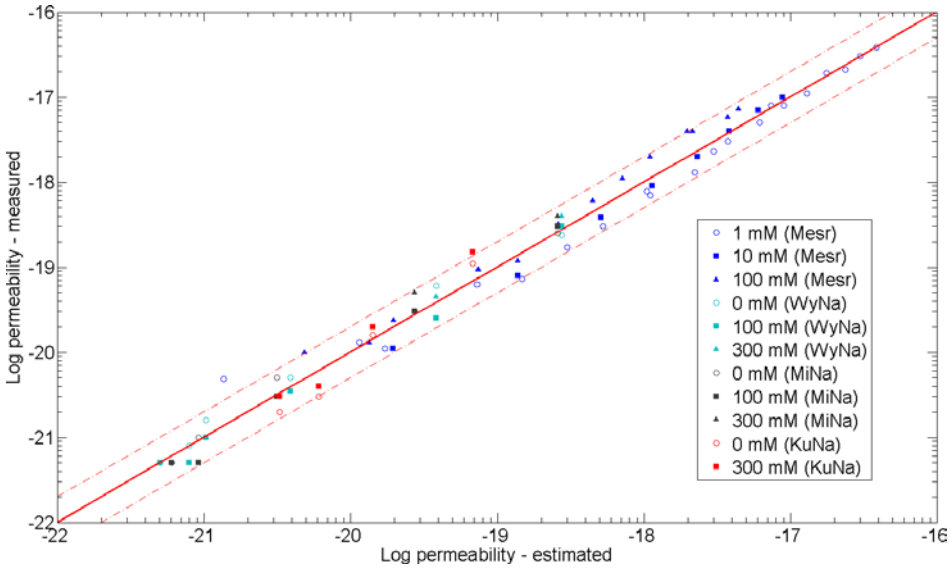

Figure 6-4. *Permeability of sodium exchanged bentonite estimated by Equation (6-22) and experimental results.*

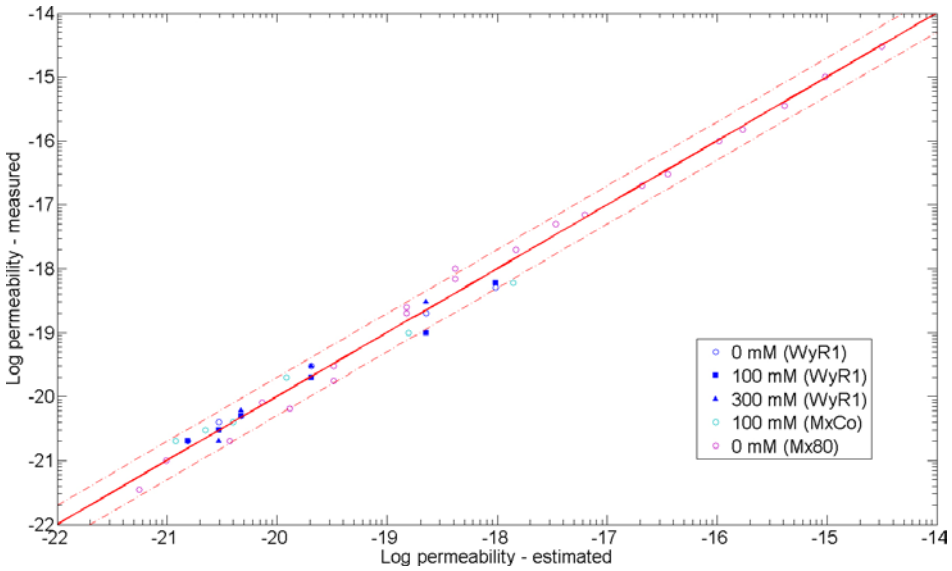

Figure 6-5. *Comparison of the permeability of natural MX-80 between estimated values by Equation (6-23) and experimental results.*

6.4.2 Pore sizes in a bed of spheres

Pressure drop measurements in porous beds can be used to estimate the mean particle diameter and the mean pore diameter of an equivalent circular tube.

As an example consider a case where spherical particles form a bed. If a given pressure gradient leads to the same mean velocity in a bed and a tube, the Kozeny-Carman equation and the Hagen-Poiseuille equation together gives the following relation between the tube diameter d_{tube} and the particle diameter d_p

$$d_{tube} = \sqrt{\frac{16}{75}} \frac{\varepsilon}{1-\varepsilon} d_p \cong 0.462 \frac{\varepsilon}{1-\varepsilon} d_p \qquad (6\text{-}24)$$

For a typical porosity of 0.4 the tube diameter is 31% of the diameter of the sphere.

However, the mean pore size is larger than the constrictions between the particles forming the bed. In a tetrahedral packing of spheres, the largest diameter of small spheres that could enter the void between the spheres forming the bed is 15.5% of the bed forming spheres. This is illustrated in Figure 6-6. An infinitely thin sheet with a smallest size $d_p(\sqrt{3}–1)/2 \cong 0.37d_p$ could also just wriggle through such a bed. With this information, we can asses if a porous bed might strain particles efficiently.

6.4.3 Friction coefficient for an individual particle in a porous bed

The average friction force acting on a particle in a porous bed, F_η, is equal to the force on the bed, F_{bed}, divided by the number of particles n_{part} in the bed,

$$F_\eta = \frac{F_{bed}}{n_{part}} = uf_{fr} \tag{6-25}$$

with

$$F_{bed} = \frac{dP}{dz} A_{bed} \Delta z = \frac{dP}{dz} V_{bed} \tag{6-26}$$

The number of particles in the bed is

$$n_{part} = V_{bed}(1-\varepsilon)/V_p \tag{6-27}$$

For spheres

$$V_p = \frac{\pi d_p^3}{6} \tag{6-28}$$

and for coins

$$V_p = \frac{\pi d_{coin}^2 \delta_p}{4} \tag{6-29}$$

Combining these equations with the Darcy's law, Equation (6-17), gives for the friction factor of a particle in a bed,

$$f_{fr} = \frac{\varepsilon}{1-\varepsilon} \frac{\eta_w}{k} V_p \tag{6-30}$$

where the permeability k is used instead of the hydraulic conductivity K_h.

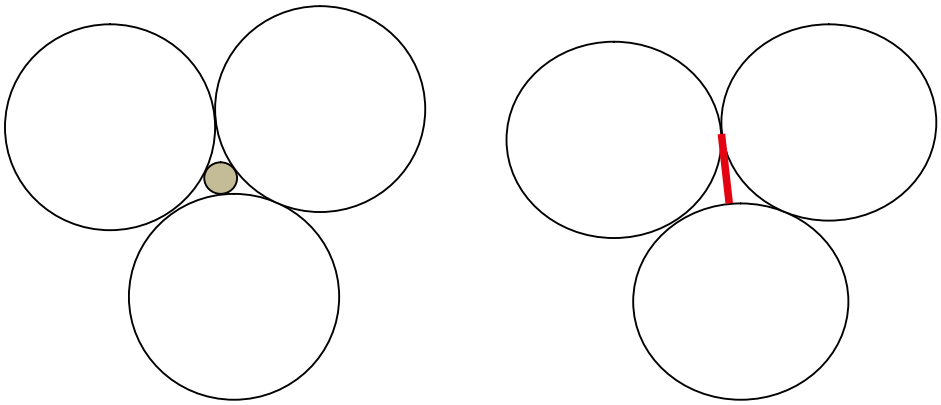

Figure 6-6. *In a bed formed of spheres arranged in a tetrahedral pattern the largest sphere that could move through the bed is 0.155 of the diameter of the bed forming sphere, left figure. A thin sheet with a size of 0.37 of the diameter of the bed forming sphere could also wriggle through, right figure.*

If we use the Kozeny-Carman relation or similar ones to describe the permeability, the friction factor as given in Equation (6-30) would not reduce to Equation (6-6) but go to zero when ε approaches 1. At present, however, we have found no theoretical model describing the transition and have chosen to add the friction factors for a single particle to that obtained for the bed. This gives a smooth transition in the intermediate range. /Petsev et al. 1993/ also tested the Kozeny-Carman equation over a wide range of volume fractions and arrived at similar conclusion. We deem this to be sufficient for our purposes.

$$f_{fr} = f_{fr,particle} + f_{fr,bed} \tag{6-31}$$

Figure 6-7 shows a plot of the friction factor for particles with d_p= 50 and 300 nm in water at room temperature derived by Equation (6-31), if we use the Kozeny-Carman relation i.e. Equation (6-19) to describe the permeability of the porous bed. It is seen that the friction factor strongly increases with the volume fraction of solids.

6.5 Chemical potential and diffusion

The chemical potential of the smectite particles in a suspension can be written as

$$\mu = \mu_0 + k_B T \ln(\phi) \tag{6-32}$$

In a concentration gradient a force F_μ will act on the particles which can be obtained by differentiation of (6-28)

$$F_\mu = -\frac{d\mu}{dz} = -k_B T \frac{d\phi}{dz}\frac{1}{\phi} \tag{6-33}$$

Nature tends to minimize the energy of a system, in this case μ. If this is the only energy we were to account for, it acts to spread the particles further and further apart. The spreading velocity will be determined by the friction. This can be derived by balancing Equations (6-3) and (6-33) for a dilute suspension,

$$F_\mu = -k_B T \frac{d\phi}{dz}\frac{1}{\phi} = F_\eta = 3\pi\eta_w d_p u_p \tag{6-34}$$

from which the particle velocity relative to that of the water is obtained

$$u_p = -\frac{k_B T}{3\pi\eta_w d_p}\frac{d\phi}{dz}\frac{1}{\phi} \tag{6-35}$$

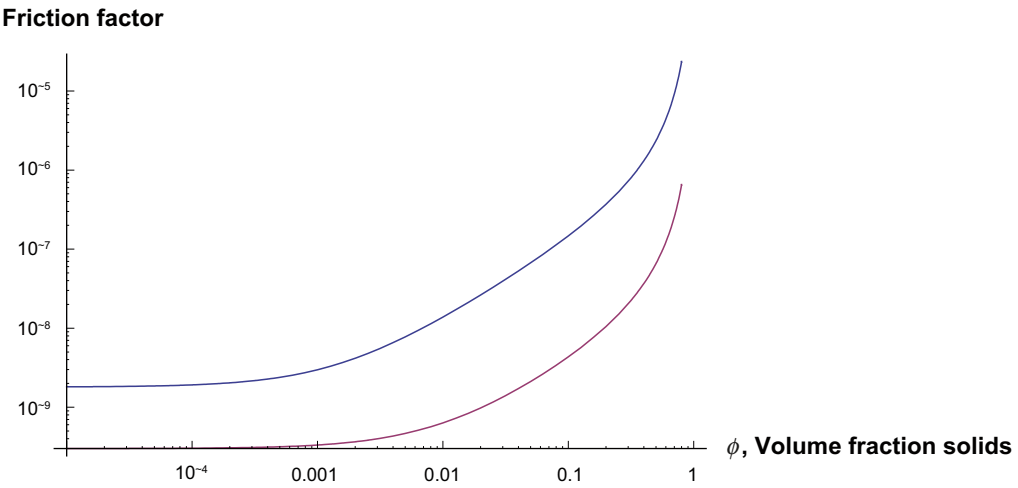

Figure 6-7. *Friction factor for coin-like particles as function of volume fraction of solids for 50 nm, upper curve, and 300 nm diameter particles, lower curve. Note the double logarithmic scale.*

The flux, J, of particles, expressed as volume of particles, is the product of the velocity u_p and the concentration (volume fraction) ϕ.

$$J = \phi u_p = -\frac{k_B T}{3\pi\eta_w d_p}\frac{d\phi}{dz} = -D_p\frac{d\phi}{dz} \tag{6-36}$$

This is the well-known diffusion equation, Fick's first law when $\phi \to 0$.

The diffusivity is then given by,

$$D_p = \frac{k_B T}{3\pi\eta_w d_p} \tag{6-37}$$

This is the Stokes-Einstein equation which is valid for large spherical particles (or molecules) in low molecular weight solvents /Bird et al. 2002, p 529/.

For a smectite particle, d_p=0.3 µm in water at room temperature D_p=5·10^{-13}m^2/s. This is 3–4 orders of magnitude less than that for small molecules.

6.6 Van der Waal's forces, vdW

In the previous sections forces acting on particles have been described. These were due to chemical potential, gravity and friction. In the present and the next section pressure forces between flat particles are described. For particles of a known size the force is the product of the surface area of the particle and the pressure acting on this surface. In the following we use the term "force" for pressure meaning that the pressure acts on a particle with given size.

We conceive the smectite particles to be thin sheets that are aligned parallel to each other, at least at higher particle densities. This seems reasonable because they are about 300 times larger in two dimensions than in the third (thickness) dimension and must essentially be aligned parallel to each other to attain volume fractions larger than about a third of a percent, ϕ=0.003. This will be discussed further in a later section.

Van der Waals forces between two parallel particles are described by Equation (6-38) **(**Evans and Wennerström 1999**).** The vdW force is always attractive. We give the absolute value here. Expressed as pressure (force per area) we have

$$P_{vdW} = \frac{A_H}{6\pi}\left[\frac{1}{h^3} - \frac{2}{(h+\delta_p)^3} + \frac{1}{(h+2\delta_p)^3}\right] \tag{6-38}$$

where A_H is the Hamaker constant, and h the separation between the particles.

6.7 Diffuse Double layer forces, DDL

The smectite particles have a negative charge mainly due to isomorphic substitution in the crystal lattice of silicon (Si) for aluminium (Al) and aluminium for divalent atoms such as iron (Fe) and magnesium (Mg). This leads to a negative charge on the order of one meq/g. One can also view this as an equivalent mass of 1,000 g/eq. This means that the smectite has a considerable permanent charge which must be compensated by attachment of charge compensating ions. These are commonly sodium (Na), potassium (K), calcium (Ca) and magnesium (Mg) ions. In addition to the fixed charges, the surface of the smectite particle, which is made up of silica, can hydrolyze and attach water to form S=OH groups on the surface. S= stands for surface here. These groups can detach protons (H^+) when pH of the water is high to form negatively charged surface groups S=O$^-$ or attach protons in low pH waters to form positive groups S=OH$_2^+$. At the edges the alumina layer sandwiched between the two silica layers also can be hydrolyzed and protonated or de-protonated. In circum neutral water most of these surface groups are neutral in low ionic strength waters with negligible amounts of specifically sorbing ions and do not add or detract much to the surface charge.

When such smectite particles are wetted, the ions dissolve in the water but stay very near to the surface in what is called a diffuse double layer. This is illustrated in Figure 6-8.

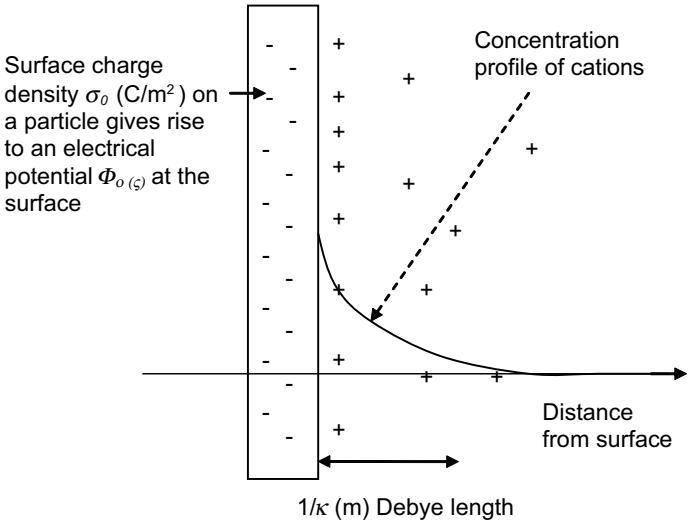

Figure 6-8. *Negative charges in a smectite particle generate a diffuse layer of counter ions in the water.*

At large distances between the particles (what is large distance will be explained presently) the diffuse layers have little overlap and the repulsion forces are small. Diffusion and gravity will mainly influence the movement of the particles.

A measure of the distance can be assessed from the Debye length $1/\kappa$. For a symmetrical electrolyte, the inverse of the length κ is given by,

$$\kappa = Fz\sqrt{\frac{2c}{\varepsilon_r \varepsilon_o RT}} \tag{6-39}$$

Figure 6-9 shows $1/\kappa$, for mono- and divalent ions as a function of ion concentration. In very non-saline water the Debye length can reach 1,000 nm for monovalent ions and 500 nm for divalent ions. At high ion concentration c in the bulk water the diffuse layer will be compressed. In the concentration range 0.01 to 0.1 mM the Debye length is of the same magnitude as the size (side length) of the smectite particles. This is of some interest because at higher ion concentration, diffuse layer forces between particles will have a small, or negligible, influence and the particles can orient themselves more freely. It will be discussed later in the context of when a gel-sol transition takes place and when diffuse layer forces become small compared to diffusion movement.

If smectite particles come so near that the diffuse layers overlap considerably, repulsive forces develop. This is the reason for the strong swelling pressures exerted by wet compact bentonite.

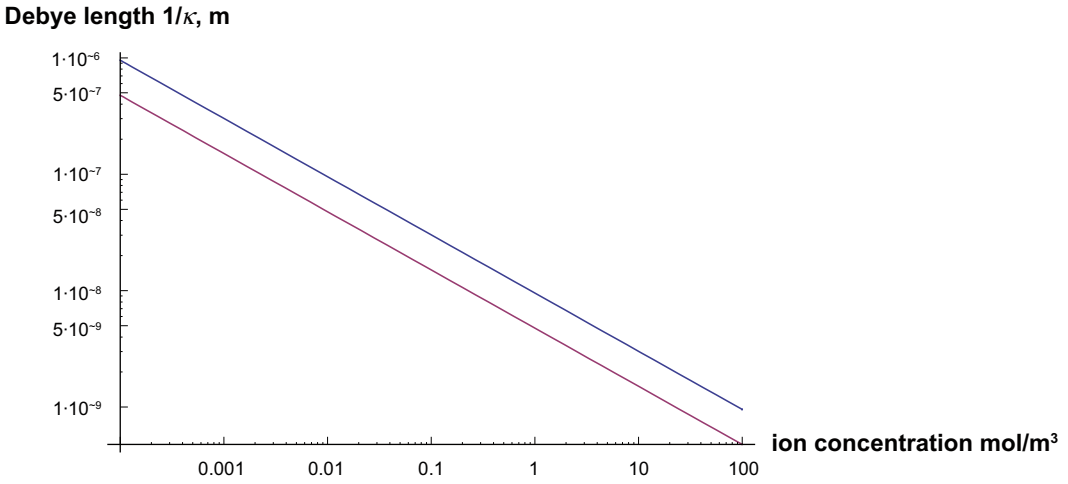

Figure 6-9. *Debye length as function of ion concentration for z=1, upper curve and z=2 lower curve.*

The osmotic pressure repelling the particles can be assessed by a number of approximate expressions, which are useful for different situations. We refer to /Evans and Wennerström 1999/ or /Lyklema 2005/ for full discussions on the different approximate expressions. The main differences between the different models are that they apply for constant potential or constant charge assumptions and that they are valid in either high or low particle distances. /Liu and Neretnieks 2008/ devised a somewhat more complicated model for the constant charge case which is applicable to the present study. It compares well with the exact solution of the Poisson-Boltzmann equations for the range of concentrations and particle distances of interest for this study. It has the advantage over the exact solution that it is readily twice differentiable and is considerable faster to evaluate in the computer programs we use to study the expansion/compression of the gel/sol systems. The solution of our parabolic/hyperbolic partial differential equations requires many millions of evaluations of the equations.

The reader is referred to the paper by /Liu and Neretnieks 2008/ for the equations. Here one simple equation is shown, which is a good approximation for the DDL forces for low surface charge or low surface potential and for not very small particle distances. Equation (6-40) shows the pressure between two flat particles as a function of the Debye length, surface potential and distance between particles.

$$P_{DDL} = 64cRT \cdot Tanh^2\left(\frac{yd \cdot z}{4}\right) e^{-h\kappa} \tag{6-40}$$

and

$$yd = \frac{\Phi_0 F}{RT} \tag{6-41}$$

yd is the dimensionless surface potential.

Thus, the repulsive pressure decreases exponentially with distance between particles. This is a fairly good approximation for $yd<1$ and $h\kappa>2$ /Evans and Wennerström 1999/. Equation (6-41) cannot be used for small $h\kappa$ because when the particles approach, the assumption of constant potential is no longer valid for the constant charge particles of interest here. Equation (6-40) will be used to illustrate the concept of the Critical Coagulation Concentration, CCC.

Figure 6-10 is based on the solution of the Poisson-Boltzmann equation by /Liu and Neretnieks 2008/ and it shows the pressure between the particles as function of distance for z=1 and σ_0=–0.131 C/m^2 for c=0.1 to 50 mol/m^3. It is seen that for low ionic strengths the disjoining pressure can extend to distances larger than the sheet diameter. At small distances very large repulsion forces are predicted. Note, in addition, that the straight portions of the curves agree with what Equation (6-40) predicts.

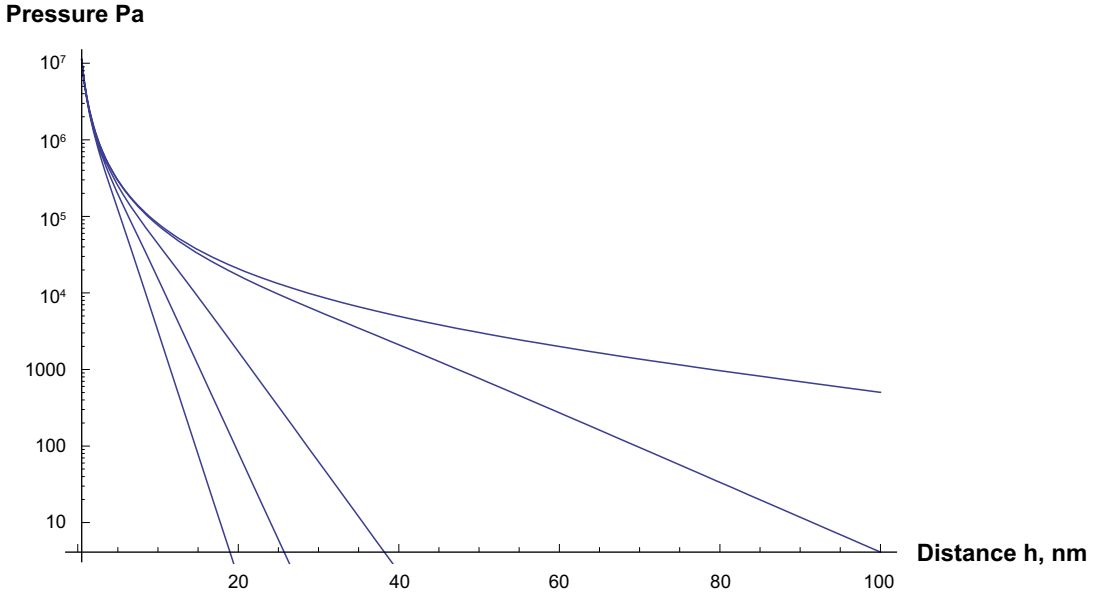

Figure 6-10. *Disjoining pressure as a function of distance between particles for monovalent ions. Curves from left to right c=50, 25, 10, 1 and 0.1 mol/m^3.*

6.8 Comparison of DDL and vdW forces

The DDL force is repulsive and the vdW force is always attractive. The DDL force decays exponentially with distance between particles, at least for larger distances. The vdW force decays approximately inversely proportional to the distance cubed. Figure 6-11 shows both the DDL and the vdW force for c=0.1 to 50 mol/m^3 and a particle thickness δ_p of 1 nm.

Figure 6-11 indicates that the vdW force would dominate over the DDL force at large distances but then the forces can become very weak, so weak in fact that the thermal energy can dominate over the pressure energies. This is discussed in section 6.11 where a new view of the CCC is presented.

For thicker particles the distance at which DDL and vdW forces balance decreases. This is illustrated in Figure 6-12. For a particle thickness δ_p=20 nm, attractive and repulsive forces will be equal at distance, h, around 20 nm for c=50 mol/m^3 at a pressure of some tens of Pa, whereas the balancing pressure for δ_p =1 nm was less than 1 Pa. This will influence the CCC as discussed in section 6.11.

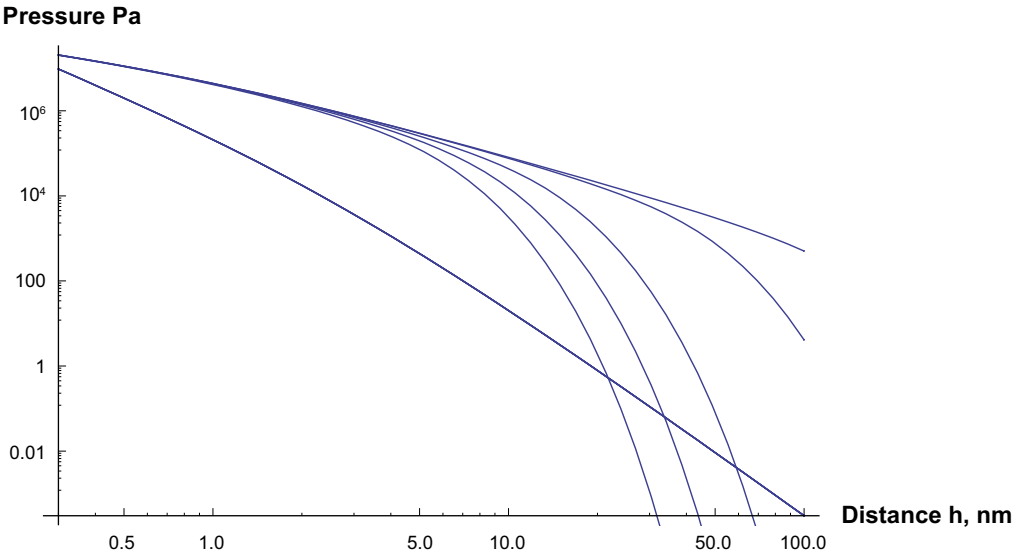

Figure 6-11. *Disjoining pressure as function of distance between particles. Particle thickness δ_p=1 nm. Curves from left to right c=50, 25, 10, 1 and 0.1 mol/m^3, z=1. Attractive vdW force is shown by the nearly straight mostly lower line.*

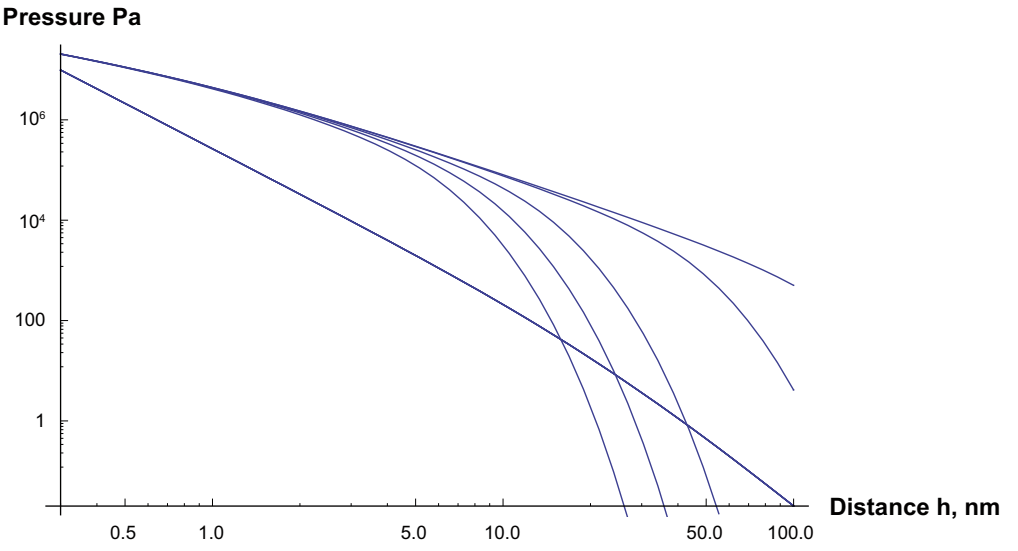

Figure 6-12. *Disjoining pressure as function of distance between particles. Particle thickness δ_p =20 nm. Curves from left to right c=50, 25, 10, 1 and 0.1 mol/m^3. z=1. Attractive vdW force is shown by the nearly straight line.*

6.9 Calcium bentonite behaviour

It has been found that one important assumption underlying the Poisson-Boltzmann equation is not valid when the particles have a high surface charge density and when the counterions are mainly divalent, namely the mean-field assumption, which implies that there are no ion-ion correlations over the mid-plane between the two particles /Jönsson et al. 2009/. For divalent ions this assumption can give grossly inaccurate results for the swelling pressure. This has long been known. It has been shown that smectite particles with calcium as counterions should have strongly attractive forces between the particles and such smectites should not swell beyond 1 nm distance, if the particles were ideal infinite plane surfaces with homogeneous charge distribution and could be aligned in parallel. This suggests that such clays should form a solid with a porosity of about 50% or volume fraction /Kjellander et al. 1988, Evans and Wennerström 1999, Jönsson et al. 2009/. Experiment show, however, that calcium smectites swell nearly as strongly as sodium smectites at high compaction densities but stop swelling at about 10–20% volume fraction, little influenced by the pore water salinity. By contrast, sodium smectites can swell indefinitely in non-saline waters when under the CCC and swell to about 5% volume fraction in waters above CCC.

The reason for the calcium smectite behaviour is not understood yet /Jönsson et al. 2009/. However, the Poisson-Boltzmann Equation is known not to be able to describe the behaviour of smectite when the charge compensating ions are divalent and at high surface charge densities because ion-ion correlation effects generate attractive forces at distances closer than about 3 nm between sheets. At larger distances the repulsive forces dominate. See section 4.1. In Figure 6-13 we show the prediction of the Poisson-Boltzmann simulated results for divalent ions and a particle thickness of 20 nm, which corresponds to a stack with about ten sheets. The figure only shows the region larger than 3 nm distance between particles where the attractive forces caused by ion-ion correlations not necessarily dominate over repulsive DDL forces. The Poisson-Boltzmann based DLVO equations would predict swelling to about 60 nm between stacks in 1 mM calcium solution for 20 nm thick (ten closely packed sheets) particles. This gives a volume fraction ϕ of 1/8=0.13. One mM is about the CCC found for divalent ions. Ten sheets in a stack is also a reasonable figure as is the volume fraction mentioned. See chapters 3 and 4. The use of the Poisson-Boltzmann equation to estimate the DDL forces in these concentration and volume fraction range does not seem to contradict observations, although the reasons are not understood.

Another important observation is that calcium smectites do not seem to release colloids even to very non-saline water, at least in tests with upward expansion where gravity restrains particle release.

Calcium smectites swell essentially as sodium smectites but only up to an average of about 10–20% solid volume fraction, and it was found to have diffuse region about 2 mm thick at the gel/water

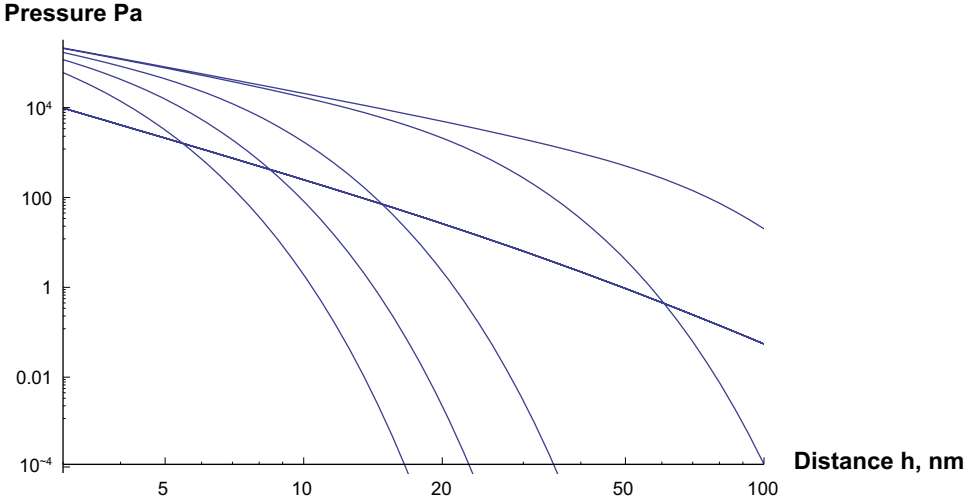

Figure 6-13. *Disjoining pressure as function of distance between sheets for divalent ions Particle thickness δ_p=20 nm. Curves from left to right c=50, 25, 10, 1 and 0.1 mol/m³. Attractive vdW force is shown by the nearly straight line.*

interface where the volume fraction drops from about 5% to very low values. According to ion correlation effects it should stop at 50% and form a strongly coherent solid body. There is evidence that the smectite particles vary in size and that they have different and varying surface charge densities. In addition they are not always ideally plane sheets. It is also known that calcium smectites aggregate in stacks with typically 5–15 sheets arranged at close distances. We therefore test the hypothesis that such stacks have different i.e. much lower surface charge densities on their outer surfaces and thus do not attain the strong attractive forces to make the stacks collapse. Should this be the case then even calcium clays could release particles, not as readily by Brownian diffusion as individual sheets, but possibly in a pulling gravitation field in a downward facing fracture. To this purpose we use the Poisson-Boltzmann equations and assume the particle thickness i.e. the number of sheets in a stack to test if there is any agreement with experiments. This was met by some success when we tested our new approach to determine CCC /Liu et al. 2009b/. The CCC for pure calcium gels in calcium pore water was predicted to lie in the range of observed values. This actually supports the idea that calcium gels may not be cohesive but only have larger particles than sodium gels that do not form so high a diffuse region at the gel/water interface as sodium smectites do.

There seems to be strong but not conclusive evidence that calcium dominated gels will not readily release colloids to the water. However, we are not convinced by the experimental evidence that calcium smectite gels are *cohesive* in very low ionic strength waters. Although they do not seem to spontaneously release colloidal particles against gravity at the gel water interface, this could be because gravity compresses a potential sol layer with particles being mobilized by Brownian motion. This is difficult to observe by the naked eye as the height of such a sol layer can be expected to be at least 10 to 20 times narrower than for sodium clay with the particle being individual sheets. This will be discussed in chapter 6, Equation (6-54). With particles consisting of 15 sheets in the sol phase, the particle concentration will drop by a factor of e=2.718 every 0.23 mm. Over 1 mm the concentration would drop by 77 times. Such a sharp drop in sol concentration is not readily seen unless specially looked for. In a situation where gravity pulls downward, such particles could be released and sediment away rapidly, orders of magnitude more rapidly than individual smectite sheets. See section 6.3.

It may need some ionic strength to compress the diffuse electric layer enough to let van der Waal's forces dominate over the repulsive forces between the stacks.

Although the above clearly is a speculative idea, we feel that it is necessary to state it because if correct it influences how erosion can take place. We have therefore tried to approach the behaviour of calcium smectite behaviour from several directions to ensure that calcium gel stability can be assured under all reasonable conditions. Considerable effort has therefore also been invested into assessing when such conditions can be assured. See chapter 7.

6.10 Forces acting in a gel/sol with a particle concentration gradient and impact on gel expansion

A force is described by its magnitude and direction. In the description of forces acting on the particles the gravity force acts on every individual particle in the direction of the gravity. The friction force is in the direction opposite to the direction in which the particle moves. The net force due to the chemical potential is in the direction of the negative concentration gradient of particles (downhill slope). If there is no gradient there will be no net force on the particle.

The vdW and DDL forces described previously were forces between particles, not net force on them. If a particle has the same but opposing force on both sides it will have no net force acting on it. However a net force will exist if the force on one side of the particle is different from that on the other side. This will occur in the system at hand when there is a particle density gradient in the same way as for the force due to the chemical potential. The derivation of the total force balance for a particle is given in /Liu and Neretnieks 2008, Liu et al. 2009a, b/**.** It is summarised here.

The model will be used to quantify the expansion and release of colloids from an expanding buffer and makes up the core of our model. The model is based on an idealized situation, as shown in Figure 6-14 (a) where the particles are very thin compared to their other dimensions. At high particle densities, i.e. when the distance between them is less than their length or width, they must be arranged essentially

parallel, so called columnar arrangement. It is assumed that the particles are all plate-like with identical dimensions and properties, and they confront each other in a strict manner as in the columnar phase as the gel expands. This implies that only the face-face distance, h, would change over time and space, whereas the edge-edge distance would keep constant all the time during the process of expansion. This is not a severe limitation and other assumptions about the edge to edge distance can also be used.

The conceptual picture does not imply that all particles must be aligned parallel in the whole gel. We conceive the system to consist of stacks of many particles at high volume fractions. The stacks can be aligned in any orientation but the swelling of parallel particle in the stack could be conceived as in Figure 6-14. See also chapter 4 and section 5.3.

The body force F_g and friction force F_η are not affected by the particle concentration gradient but the DDL and vdW forces are. For them the net force will depend on the difference in distance on one side and on the other side of the particles. The particle density (distance) gradient determines these forces. When no gradient exists, i.e. the concentration of particles does not vary, these forces are zero. In a gradient the net force on the particle caused by these two forces is obtained by

$$F_{net} = \frac{d}{dx}(F_{DDL} - F_{vdW})\Delta x \tag{6-42}$$

We deem this to be a reasonable approximation for distances between the particles roughly up to the diameter of the plate-like particles because at lower distances they will not be able to rotate freely and the preferential arrangement is for particles to be in parallel. This implies that we expect our model to be valid down to volume fractions of less than one possibly down to a few tenths of a percent in low ionic strength waters when DDL forces extend to large distances. At lower volume fractions particle diffusion (Brownian motion) will govern the movement.

The friction force balances the sum of the other forces.

$$F_\eta = F_g + F_\mu + \frac{d}{dx}(F_{DDL} - F_{vdW})\Delta x = F_g + F_\mu + \frac{d}{dh}(F_{DDL} - F_{vdW})\frac{dh}{d\phi}\frac{d\phi}{dx}(h + \delta_p) \tag{6-43}$$

where F_{DDL} and F_{vdW} are obtained by multiplying the pressures P_{DDL} and P_{vdW} by the flat particle area S_p,

the combined gravity and buoyant force is

$$F_g = V_p(\rho_p - \rho_w)g_c\cos(\theta) \tag{6-44}$$

where θ is the angle of gravity from the positive x direction, i.e. the direction of the volume fraction gradient.

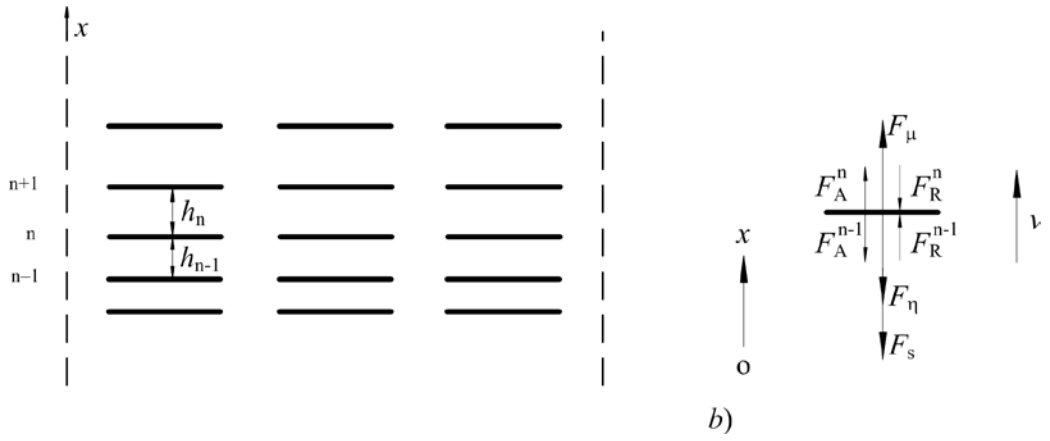

Figure 6-14. *Sketch of a) the conceptual model and b) the forces acting on an arbitrary particle in a suspension.*

The friction between particles and water in laminar flow is proportional to the relative velocity between water and particle. The particle velocity then becomes,

$$u_p = \frac{1}{f_{fr}}\left[F_g - k_B T \frac{d\phi}{dx}\frac{1}{\phi} + \frac{d}{dh}(F_{DDL} - F_{vdW})\frac{dh}{d\phi}\frac{d\phi}{dx}(h+\delta_p)\right] \tag{6-45}$$

The particle flux, J, passing (or relative to) the water is

$$J = u_p\phi = \frac{\phi}{f_{fr}}\left[F_g - k_B T \frac{d\phi}{dx}\frac{1}{\phi} - \frac{d}{dh}(F_{vdW} - F_{DDL})\frac{dh}{d\phi}\frac{d\phi}{dx}(h+\delta_p)\right] \tag{6-46}$$

The relation between particle distance and particle volume fraction in the system with large thin sheets we assume to be as follows

$$\phi = \frac{\delta_p \phi_{\max}}{h+\delta_p} \quad \text{or the inverse} \quad h = \delta_p\left(\frac{\phi_{\max}}{\phi} - 1\right) \tag{6-47a, b}$$

It describes a system where most sheets are parallel. This is a simplification that seems reasonable for large volume fraction of particles where they will have to be aligned parallel to each other or at least within the large clusters of a multitude of particles. We imagine at present that the clusters will contain particles on the order of hundred or more particles. They can be oriented randomly and still allow very small voids to exist on average between the sheets. Random arrangement of clusters would not permit the volume fraction to approach 1 and a maximum value of ϕ_{max} is assumed to exist. Clustering is known to exist and is documented in the literature. See e.g. /Pusch and Young 2006/.

From Equation (6-47), we obtain,

$$\frac{dh}{d\phi} = \frac{h+\delta_p}{\phi} \tag{6-48}$$

Thus the flux in Equation (6-46) can be written as,

$$J = \frac{F_g\phi}{f_{fr}} - \frac{k_B T}{f_{fr}}\frac{d\phi}{dx} + \frac{d}{dh}(F_{vdW} - F_{DDL})\frac{(h+\delta_p)^2}{f_{fr}}\frac{d\phi}{dx} \tag{6-49}$$

or in a more compact form

$$J = \frac{F_g\phi}{f_{fr}} - \frac{\chi}{f_{fr}}\frac{d\phi}{dx} \tag{6-50}$$

with

$$\chi = k_B T + \frac{d}{dh}(F_{vdW} - F_{DDL})(h+\delta_p)^2 = k_B T + \frac{d}{dh}(F_{vdW} - F_{DDL})\left(\frac{\delta_p\phi_{\max}}{\phi}\right)^2 \tag{6-51}$$

The expression for $\frac{d}{dh}F_{DDL}$ has an analytical solution covering the whole range of volume fraction. It is quite lengthy and is not shown here although it is readily obtained by differentiation /Liu et al. 2009a, b/.

The entity $\frac{\chi}{f_{fr}}$ may be thought of as a diffusion coefficient which very strongly depends on the particle concentration ϕ. Thus, we may call this entity the diffusivity function,

$$D_F = \frac{\chi}{f_{fr}} \tag{6-52}$$

For very low particle concentrations where neither vdW nor DDL forces are important and where gravity plays no role Equation (6-50) simplifies to the expression for Fick's first law.

A comparison of the Fickian diffusion coefficient and the effects of vdW and DDL forces is shown in Figure 6-15 where D_F is plotted over a wide range of particle concentration ϕ for different monovalent ion concentrations.

Figure 6-15 shows the diffusivity function for different ion concentrations. To the left the diffusivity is that of individual particles due to Brownian motion and is about 10^{-13} m^2/s. For 0.01 mM this applies up to ϕ=0.0006. At higher particle concentrations the DDL forces start to become noticeable and D_F increases rapidly. It levels off at about 10^{-9} m^2/s for all ion concentrations. At an ion concentration just above 50 mM the DDL forces become weaker than the vdW forces and D_F becomes negative at ϕ around 0.05. This means that the particles will move closer to each other instead of diffusing away from each other and will stabilize at a distance where the sum of the interaction energies is minimum. The ion concentration at which this happens we interpret as the CCC. This is another way of understanding the CCC phenomenon and predicts the CCC much better than the DLVO theory does for sodium as well as for calcium /Liu et al. 2009b/. They found that the CCC depends not only on the surface charge density and the charge of the counterion but also on the thickness of the particles and of the surface area of the particles. For monovalent ions the CCC is predicted to lie between 40 and 100 mM for thin (1.2 nm thick) particles larger than 10,000 (nm)^2. The CCC increases with decreasing particle size. For twice as thick particles the CCC decrease by about half.

With divalent counterions the CCC is predicted to lie between 0.7 and 2 mM for 15 nm thick particles larger than 10,000 (nm)^2 and half that for twice as thick particles. This agrees well with observed values. The traditional DLVO theory predicts about two orders of magnitude larger CCC for flat particles.

This concept is perhaps better understood if one avoids the influence of the friction factor, considering that friction is involved only when there is particle motion, which is not present in the static situation when the system forms a stable coagulated gel. The CCC can be derived directly from the force function for the ion concentration at which χ=0, /Liu et al. 2009b/. Also for other static conditions such as e.g. equilibrium concentration profiles for expansion and for sedimentation only the force function χ is needed. This is illustrated below.

We call the normalised force function $\frac{\chi}{k_B T}$ the thermal deviation factor ξ. This entity is 1 in dilute systems when the particles are only subject to the thermal forces causing Brownian motion. It increases by 6 orders of magnitude when ϕ goes up to 0.7 as shown in Figure 6-16.

On the other hand, the equilibrium particle concentration profile can be derived by setting J=0 in Equation (6-50),

which now simplifies to,

$$F_g \phi = \chi \frac{d\phi}{dx} \tag{6-53}$$

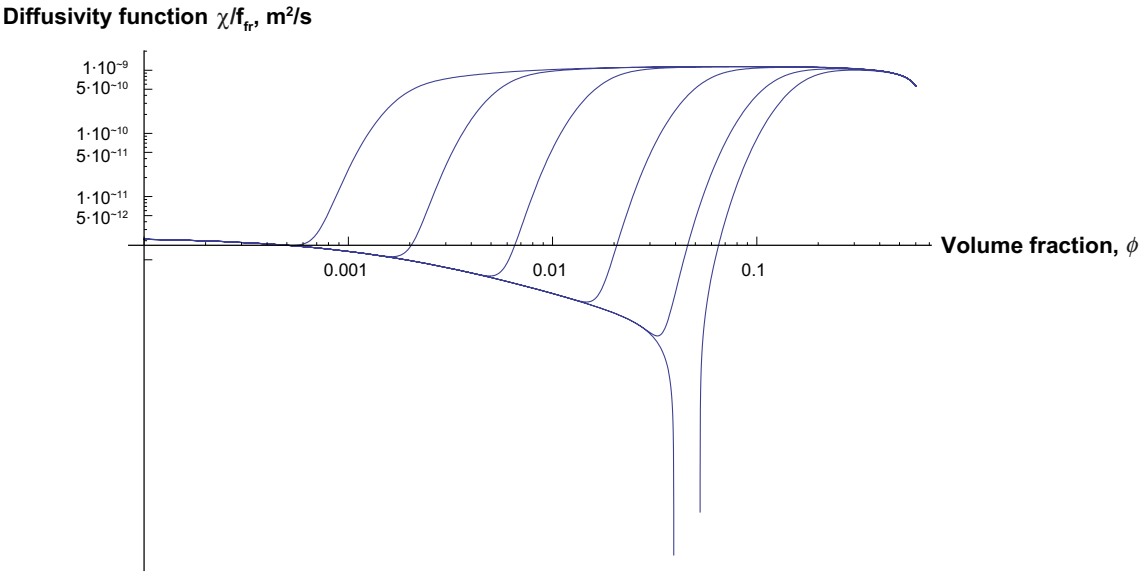

Figure 6-15. *Diffusivity function for smectite 300 nm diameter sheets for monovalent ions. The curves from left to right are for 0.01, 0.1, 1, 10, 50 and 100 mM ion for z=1, δ_p=10^{-9} m and σ_0=–0.131 C/m^2.*

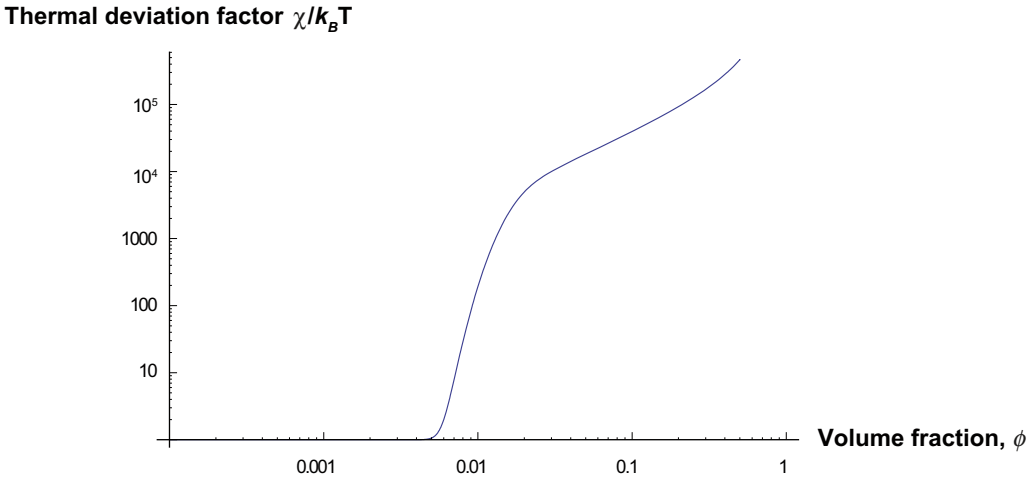

Figure 6-16. *Thermal deviation factor $\xi=\chi/k_BT$ as a function of ϕ for c=1 mol/m³, z=1, $\delta_p=10^{-9}$ m and $\sigma_0=-0.131$ C/m².*

Consider a long water filled vertical tube containing a given amount of solids. The original conditions can be either that the solids are homogeneously distributed in the tube and are allowed to sediment or by starting with all the solids at the bottom of the tube. Eventually an equilibrium concentration profile will be established. In Figure 6-17 some concentration profiles are shown for the same values of the parameters that were used to derive Figure 6-16.

As expected, for ϕ less than about 0.007 as seen in Figure 6-17, practically only the thermal energy k_BT is driving the particles apart. At ϕ= 0.01 the repulsion force has increased by a factor of about 100. The curve for ϕ= 0.005 is practically identical the exponential atmospheric curve

$$\phi = \phi_o e^{-\varsigma x} \tag{6-54}$$

with

$$\varsigma = \frac{V_p(\rho_p - \rho_w)}{k_B T} g_c \tag{6-55}$$

where V_p is the particle volume, ρ_p and ρ_w the density of particle and water respectively, g_c the gravitation constant, k_B the Boltzmann constant, T the absolute temperature, and ζ = 291 m^{-1} for the values in the example and for 300 nm diameter, 1 nm thick sheets.

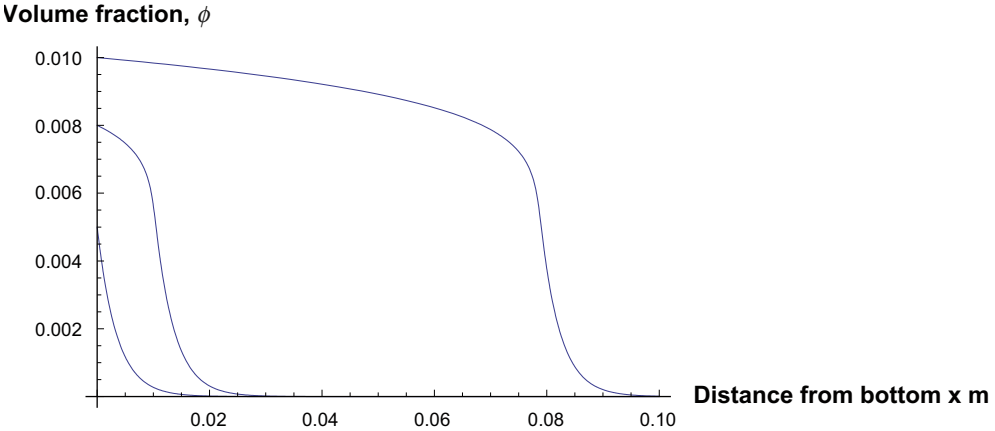

Figure 6-17. *Steady-state volume fraction of solids, ϕ, as a function of height, x above the bottom of the test tube for c=1 mol/m³, z=1, $\delta_p=10^{-9}$ m and $\sigma_0=-0.131$ C/m² in a gravity field. ϕ at the bottom of the tube is 0.005, 0.008 and 0.01 for the curves from left to right.*

Equation (6-54) gives practically an identical curve as the lowest curve in Figure 6-17. It is seen that the DDL and vdW forces can have a very strong effect on the behaviour of the gel above a certain minimum concentration of solids. Below this concentration the particles are in practice only influenced by gravity and thermal motion. At low total volume fraction (integral of the curves) the profile would not reach the top of a 10 cm high test tube. Gravity holds it back and a diffuse upper region about 10 mm high is visible. At higher particle concentrations the particles will fill all the tube in a roughly even concentration.

Figure 6-18 shows a case with divalent ions, c=2 mol/m^3, δ_p =5·10^{-9} m and σ_0=–0.131 C/m^2. This is slightly higher than the CCC. The solids concentration can be much higher at the bottom of the tube and in this example it is also shown that if the solids concentration increases so that the bottom concentration goes from 15 to 17% the tube would have a nearly even concentration. We also see that the fronts are considerably sharper. This is because the ion concentration is marginally above the CCC and the vdW forces just balance the DDL forces and the Brownian motion is held back. The particles can hardly be released from the cohesive gel. At higher ionic concentration the front is even sharper and becomes practically vertical when it meets the x-axis. It may also be noted that this is also found in the swelling experiments described in sections 3.3.3 and 3.3.4.

The χ/k_BT vs. ϕ curve for this case is shown in Figure 6-19 below. It can be seen that the thermal deviation factor dips down below 1. This implies that vdW are stronger than DDL forces and hold back diffusion, which will make the front sharper. This will occur already at ion concentrations below CCC. Above the CCC no particles can be released and there is a concentration jump at the front.

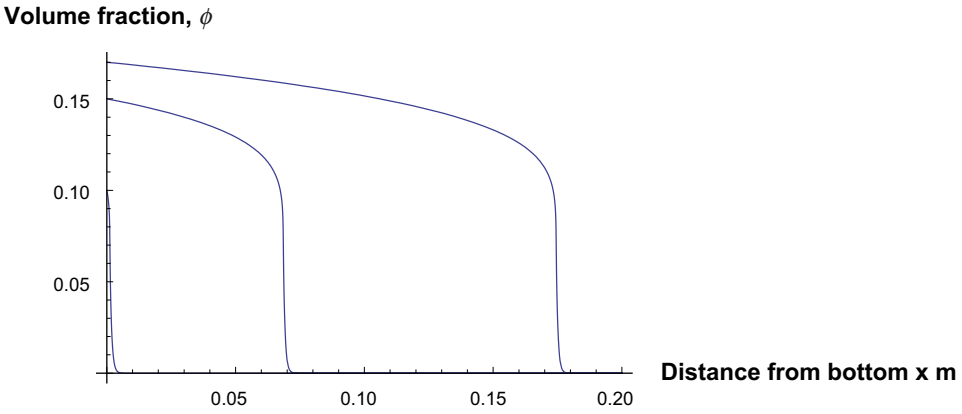

Figure 6-18. *Steady-state volume fraction of solids, ϕ, as function of height for c=2 mol/m^3, z=2, δ_p=5·10^{-9} m and σ_0=–0.131 C/m^2 in a gravity field. ϕ, at bottom of tube is 0.10, 0.15 and 0.17 for the curves from left to right.*

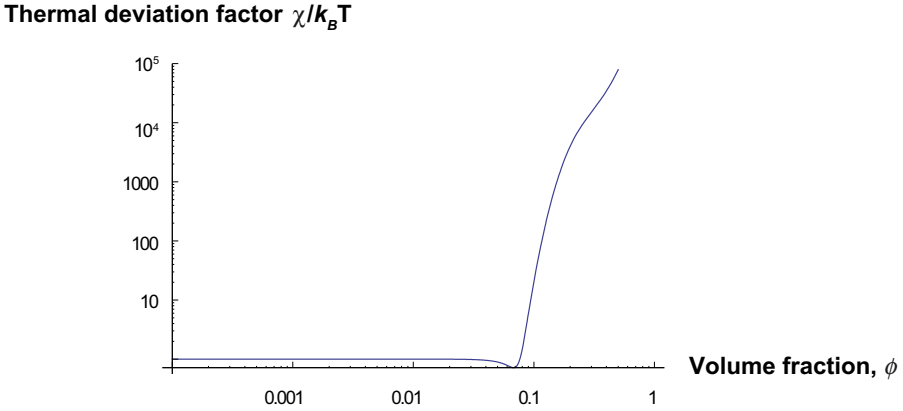

Figure 6-19. *Thermal deviation factor $\xi=\chi/k_BT$ as function of ϕ for c=2 mol/m^3, z=2, δ=5·10^{-9} m and σ_0=–0.131 C/m^2.*

Note that in these applications the DDL forces are obtained by solving the Poisson-Boltzmann equations. It is known that this is not valid for divalent ions and high surface charge densities for ideal flat surfaces at close distances because ion-ion correlation effects /Kjellander et al. 1988, Jönsson et al. 2009/. The sheets should be strongly held together and not expand beyond about ϕ=0.5. This does not agree with observations of calcium gel behaviour although narrow stacking of sheets is observed. Because of the fair qualitative agreement between experiments and the above model and because we have found no other model that reproduces the experimental results for divalent ions and high surface charge we will use our model until better models are developed.

6.11 Dynamic model for the rate of swelling and compaction of bentonite

To describe the evolution in time and space of a smectite gel the equation of continuity is defined. It states that what is transported in minus what is transport out of a control volume will accumulate in the volume or be depleted from the volume if more goes out than in. In the limit when the volume is made infinitely small the continuity equation can be written as

$$\frac{\partial \phi}{\partial t} = -\frac{\partial J}{\partial x} \tag{6-56}$$

With the flux J inserted, and setting $f = f_{fr}/(1-\phi)$, it becomes

$$\frac{\partial \phi}{\partial t} = -F_g \frac{\partial}{\partial x}\left(\frac{\phi}{f}\right) + \frac{\partial}{\partial x}\left(\frac{\chi}{f}\frac{\partial \phi}{\partial x}\right) \tag{6-57}$$

The first term shows the accumulation per time unit, the second is drift due to body forces. The third term accounts for in- and out-flux due to diffusion and forces between the particles. The equation describes the time evolution of the volume fraction of colloidal particles under the effect of drift and diffusion. The model is also applicable for other one-dimensional problems, such as colloidal sedimentation in a gravity field.

In addition, this equation can be readily extended to three dimensions but that is not shown here. A similar idea has been proposed by /Petsev et al. 1993/ for expansion of a bed consisting of spherical particles.

Equation (6-57) can be used to describe the dynamic evolution of the colloidal system in time and space. It is the central result of this report. A number of examples using the model are presented in /Liu et al. 2009a, b/.

The model has been used to simulate the expansion of a pellet in a test tube and the release of particles from the upper surface of the expanding gel. The initial and boundary conditions used are given below.

For the case of the upward expansion of a pellet in a test tube, $\theta = \pi$, and Equation (6-57) holds on an interval $0 \le x \le L_T$ for time $t \ge 0$. Particularly, at $t = 0$, the solution satisfies the initial condition,

$$\phi(x,0) = \begin{cases} \phi_0 & \text{for } x \le L_0 \\ 0 & \text{otherwise} \end{cases} \tag{6-58}$$

while the boundary conditions are given by,

$$J(0,t) = 0 \tag{6-59}$$

and

$$J(L_T,t) = 0 \tag{6-60}$$

Supplemented with the above three equations, Equation (6-57) can be solved numerically. The results regarding the ϕ profile along the test tube would demonstrate how colloidal expansion develops over time and space, and what factors may have great influences on the movement of colloidal particles.

Below are some comparisons with experimental swelling results for different ion concentrations for sodium smectites and for natural MX-80 bentonite. The experiments are described in detail in /Dvinskikh and Furó 2009/. Compacted pellets of bentonite, 3 mm thick, with a density of 1.8g/cm^3 were allowed to swell vertically upward in a tube of the same diameter. Nuclear magnetic resonance measurements were used to follow the expansion of the gel. Figures 6-20 to 6-25 show the experimental results and the simulated results using the model described previously in this chapter.

Swelling of sodium exchanged MX-80 in 0.5 mM $CaCl_2$/water

The smectite in the pellets swelling into calcium water is expected to rapidly equilibrate with the water by ion exchange. The ion exchange equilibrium is such that the calcium is nearly quantitatively exchanged for sodium so the water will have nearly 1 mM sodium in the case where 0.5 mM $CaCl_2$ was present initially in the system. In the model we thus take the water to contain 1 mM monovalent ions. The smectite still has sodium as the dominating ion in ion exchange positions.

We wish to test the capability of our model to predict the expansion using only some data that would be available without having access to specific measurement of smectite gels. This will then be the basis of improving various parts of our model by introducing various detailed observations of the smectite properties and behaviour. This we do because the large number of papers and investigations we have studied do not give a clear cut picture of the smectite properties and behaviour. We will use the first a-priory simulation as a stepping stone for improving the model and for investigation of sensitivity of the model to various parameters.

Sodium dominated smectites are known to be able to delaminate and separate into individual sheets in contrast to calcium dominated smectites, which retain several sheets in stacks. The thickness of the particles is thus expected to be 1 nm if all are separated into individual sheets. Sheet thickness influences the hydraulic conductivity of the gel as well as the swelling pressure of the gel. The only adjustable parameters in our base model are the sheet thickness and the Kozeny's constant in the Kozeny-Carman equation which determines the pressure drop of water flowing into the expanding gel bed. The Kozeny's constant k_o is expected to be around 13 for sodium exchanged bentonite, as can be seen from the following figure /Liu 2010/. The length and width of the sheets have a negligible influence except in very dilute sol and was chosen to be 250×360 nm.

Using 1 nm particle thickness and k_o=13 gives the results shown in Figure 6-21. We have thus not made any adjustments in any other parameters in our model. It is seen that the general behaviour of the swelling pellet is fairly well predicted already with this approach.

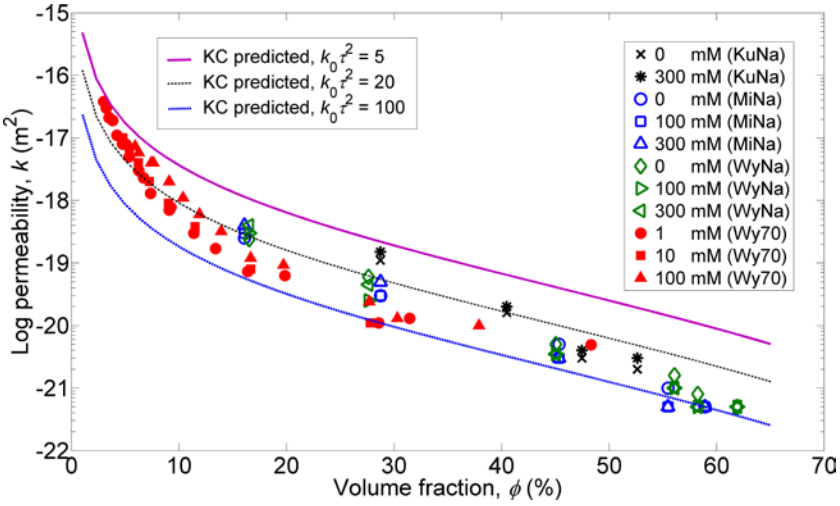

Figure 6-20. *Measured permeability for sodium exchanged bentonites in equilibrium with different NaCl solutions, together with the permeability predicted using the Kozeny-Carman equation with different Kozeny's constant for particle thickness of 1 nm.*

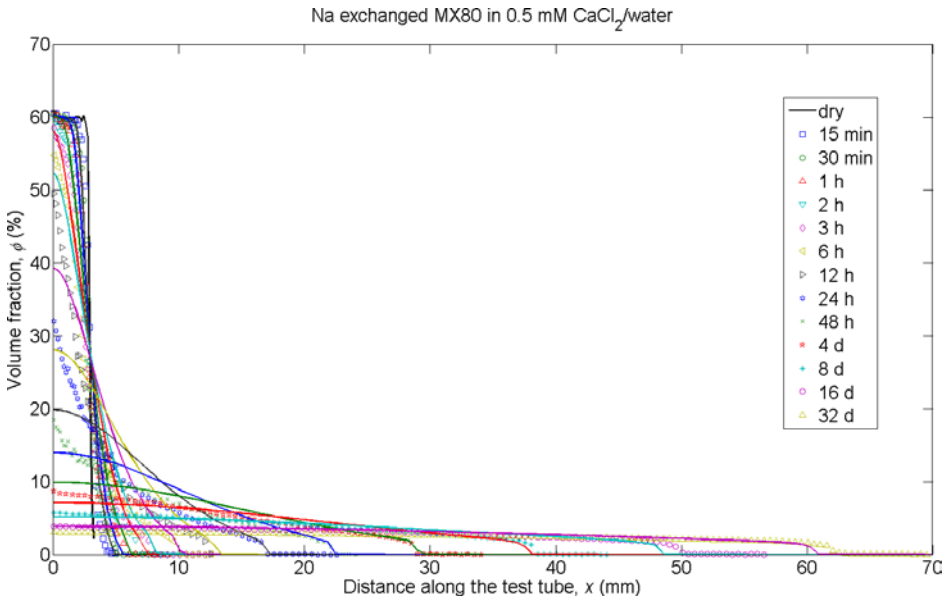

Figure 6-21. *Sodium exchanged bentonite in 0.5 mM $CaCl_2$. Kozeny-Carman equation is used with k_o=13 and particle thickness is 1 nm.*

The predicted early rate of expansion is somewhat faster and the long term expansion extends slower than the experiments. Still it is surprising that the general trend is captured so well because the expansion forces decrease by six orders of magnitude from the compact gel to the dilute gel. Similarly, the friction forces in the gel also span a number of orders of magnitude.

Using the new pressure drop model for sodium exchanged bentonite, i.e. Equation (6-22) with k_0=182, the simulation results are shown in Figure 6-22.

No changes in the basic parameter values in the model are made to do the simulation shown except that instead of a particle thickness of 1nm, 1.5 nm is used. This gave some improvement of the long time profile otherwise the results were indistinguishable. The clay/water ratio in these experiments is 0.027 g/cm^3. This is equal to a volume fraction of 0.0100. Accounting for ion exchange, discussed in chapter 7, practically all calcium enters the ion exchange positions in the smectite expelling sodium to a concentration of 0.9998 mM in the water. The calcium fraction in the smectite X_{Ca}=0.037.

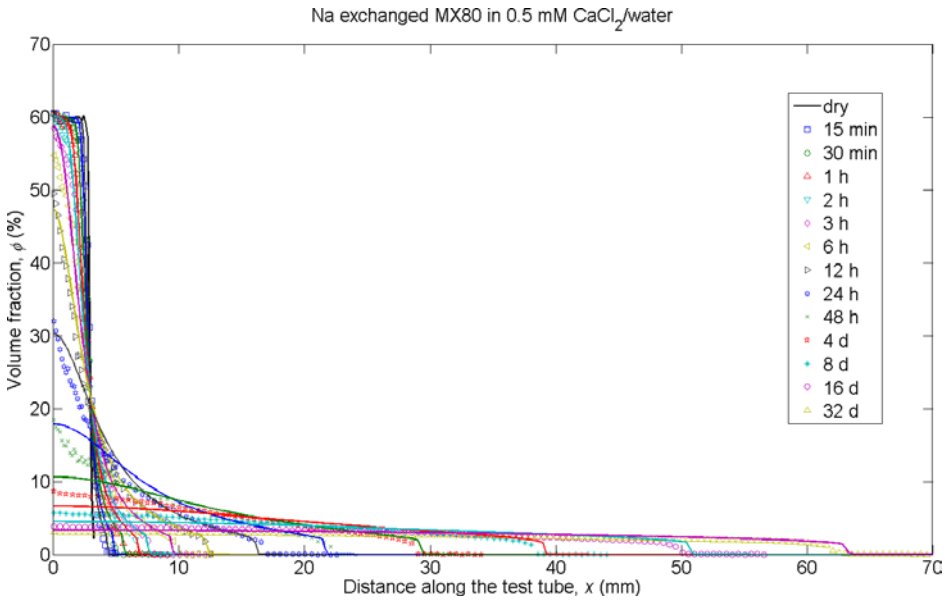

Figure 6-22. *Swelling of sodium exchanged bentonite in 0.5 mM $CaCl_2$.*

In Figure 6-23 the particle concentration is shown on a logarithmic scale. It is seen that the particle concentration at the expanding front drops very sharply. The particles attempt to diffuse downstream but are overtaken by the expanding gel compressing the front. However, for the longer times the front moves slower and slower and the diffusion makes itself felt. This is clearly seen in the figure for the longest times. The shape and width of the diffuse front deviates somewhat from that expected for a system with equally sized particles. A linear drop is then expected as shown in Equation (6-54).

It is noteworthy that the model can account for the early expansion with the sharp front as well as for the late expansion where particle diffusion starts to dominate. This is encouraging because we wish to use the model to simulate not only the expansion in a test tube but also the release of particles to seeping water.

Swelling of sodium exchanged MX-80 in 2.0 mM $CaCl_2$/water

The experiments shown in Figure 6-24 are fitted by changing the particle thickness to 1.1 nm. The new experimentally derived pressure drop equation, i.e. Equation (6-22), is used to determine the permeability. Also here the ion exchange equilibrium favours calcium in the smectite so the water concentration is taken to be 4 mM sodium.

It may be noted that in the above experiments with homo-ionic sodium smectite and 0.5 and 2 mM $CaCl_2$ solution, respectively the system contains much more sodium than calcium at final equilibrium. Practically all calcium will be in ion exchange positions in the smectite gel. The water will contain practically only sodium after an initial period. There is a continuous ion exchange occurring as more and more water intrudes the gel. The dynamics of the ion exchange process has not been accounted for in the modelling.

Swelling of sodium exchanged MX-80 in distilled water

Sodium exchanged smectite expanding in distilled water deviates considerably from what the model predicts for low ionic strength water. A reasonable fit was obtained assuming that the monovalent ion concentration is 0.5 mM instead of micro molar it should have with distilled water with essentially only protons present. A possible explanation could be that the smectite with its counterions dissolves and supplies cations to the water. Such dissolution was observed in the experiments with clay expansion in slits, /Neretnieks 2009/.

Other minor adjustments were also tested to see how sensitive the results are to changes in fitting parameters. For example using a particle thickness of 1.6 nm for the early phase of expansion and 1.7 nm for the later phase gave a better fit as is seen in Figure 6-25.

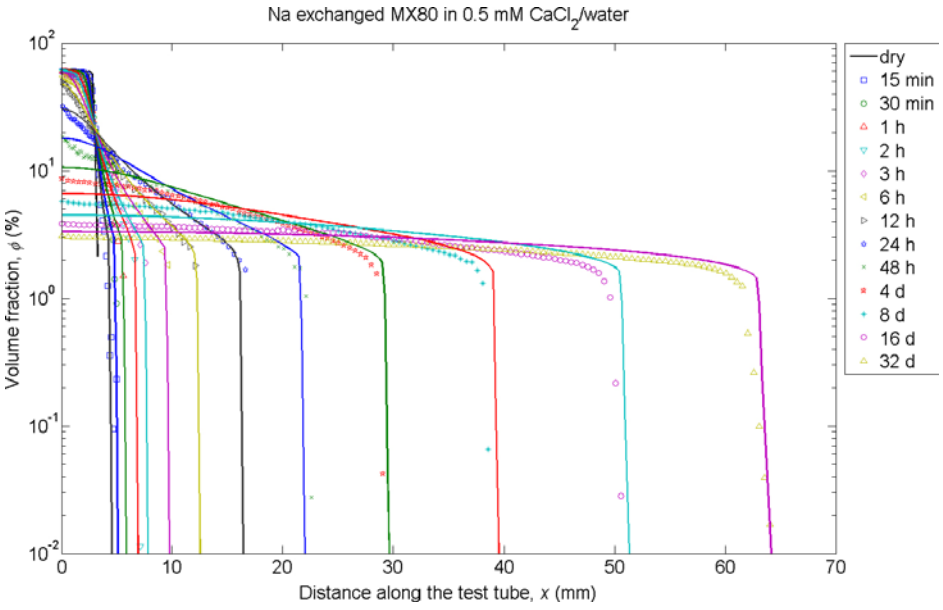

Figure 6-23. *Sodium exchanged bentonite in 0.5 mM $CaCl_2$. Logarithmic scale.*

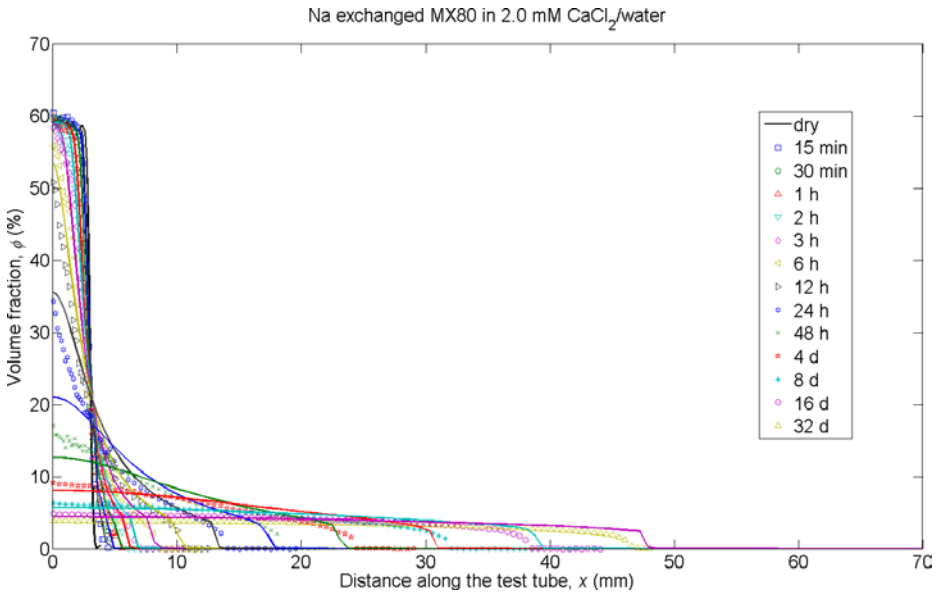

Figure 6-24. *Sodium exchanged bentonite in 2 mM $CaCl_2$.*

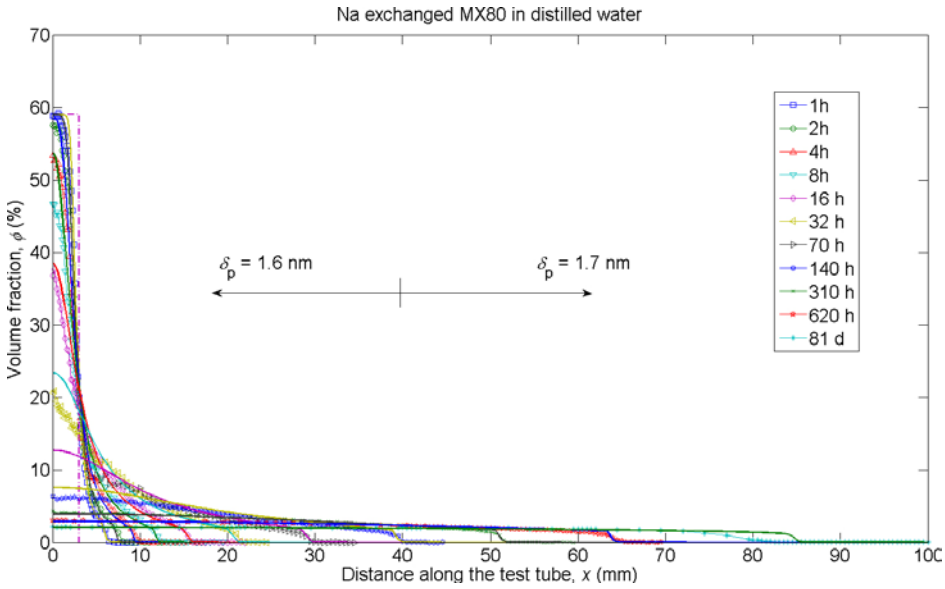

Figure 6-25. *Sodium exchanged bentonite in distilled water.*

Swelling of natural MX-80 in distilled water

Natural bentonite swelling in distilled water is more complex as the bentonite contains soluble gypsum which dissolves and supplies the water with up to 15 mM of calcium. When the gel expands by taking up more distilled water the gypsum can fully dissolve and the pore water is diluted. The dissolution rate of the gypsum is not known but the chemistry of the pore water can change considerably during the expansion. Our model accounts in a rather simple way for changing water chemistry.

In addition, the dependence of the permeability on ϕ for natural MX-80 is very different from that of sodium exchanged bentonite. Therefore, we use measured permeability data for MX-80 to obtain the relation used in the swelling model, i.e. Equation (6-23) with k_0=6.

Using this modified expression, a reasonable fit was obtained by using three different values for the monovalent ion concentration in different regions of the expansion, considering that at equilibrium the sodium concentration is about 3 mM in the case studied. This is shown in Figure 6-26. The adjustment of the porewater was needed for the dilute gel. We think that this may be due to the slow

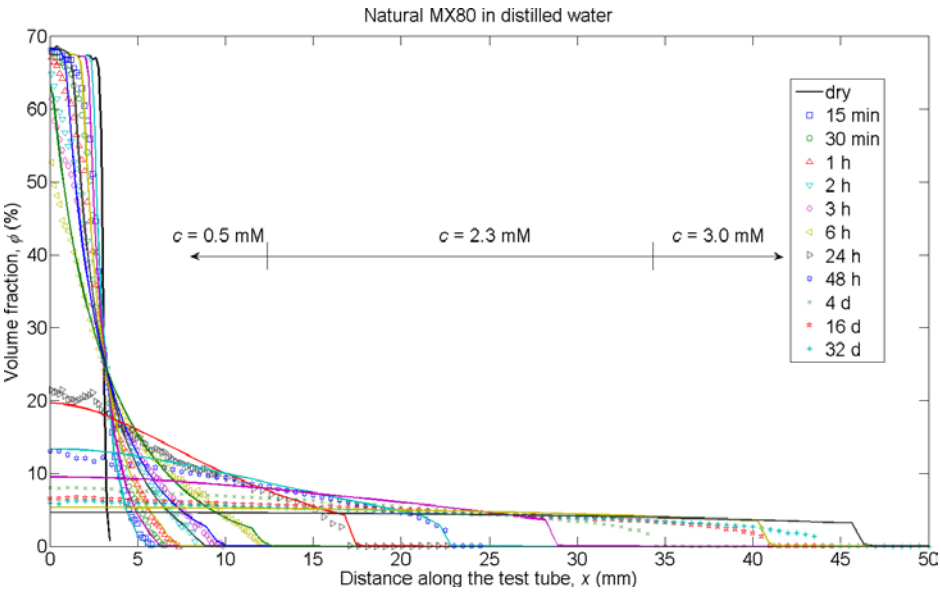

Figure 6-26. *Natural MX-80 bentonite in distilled water.*

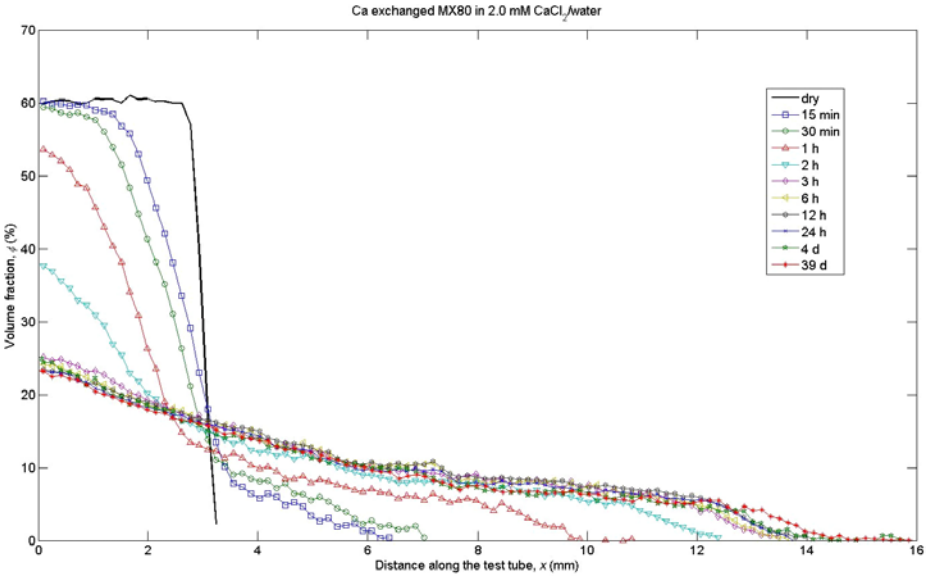

Figure 6-27. *Calcium exchanged bentonite in 2 mM $CaCl_2$ water.*

dissolution of gypsum. In the early phase with intruding water the gypsum has no time to dissolve but for longer times it has and the pore water in the long tail has days to a month to dissolve.

Swelling of calcium exchanged MX-80 in 2.0 mM $CaCl_2$/water

Figure 6-26 shows the expansion of a pure calcium exchanged smectite in calcium chloride water. Simulations were made using divalent ions in the Poisson-Boltzmann equation and adjusting the particle thickness. It was unsuccessful to obtain reasonably good agreement with these attempts, partly due to lack of measured permeability data for calcium exchanged bentonite over a wide range of volume fractions.

It is noted, however, that calcium dominated smectite expands to a solid volume fraction of ϕ=5 to 7% which clearly shows that calcium smectite does not collapse to a solid with ϕ=50%. Furthermore the gel is obviously expansive at least up to at least ϕ=5% and there is a diffuse region of particles even after that extending over a few millimetres.

The dynamics of sodium system is found to be reasonably well described by the model. The calcium system also qualitatively agrees with the model. The underlying reasons are not understood but we speculate that heterogeneities in surface charge density distributions between and on particles, particle size distributions and presence of particle fragments could cause deviations from the idealized assumptions used in the modelling of the calcium system.

6.12 Assessing the critical coagulation concentration, CCC, by the Dynamic model

In Figure 6-15 it is seen that there is an ionic concentration for which the diffusivity function becomes negative when the attractive forces begin to dominate over the repulsive diffuse layer forces and Brownian motion. By solving the equations in the Dynamic model for the ionic concentration at which this occurs one can determine the CCC and the volume fraction at which this occurs, /Liu et al. 2009b/. As expected, the surface charge density, the charge of the cation and the particle thickness and size strongly impact the results.

Figure 6-28 shows results for a sodium system. The Dynamic model can readily be solved numerically but a simplified analytical solution was also obtained. The solutions agree well in the ranges tested as can be seen in the figure.

Note also that measured smectite particle surface areas vary from about $0.2 \cdot 10^4$ to below 10^5 nm^2, and for sodium smectites the individual sheets largely form individual particles with a thickness of 1 nm, see chapter 2.

CCC values found in the literature for sodium vary between 5 and 250 mM for different clays. The results seem to depend on solid liquid ratio and on the method used to determine CCC. The predicted CCC values by the Dynamic model thus fall within the observed range. The volume fraction of the cohesive gel at the CCC will be on the order of a few %.

It may be noted that the DLVO model predicts on the order of one molar concentration, which is one to two order of magnitude larger for thin flat particles. Figure 6-29 shows results for a calcium system.

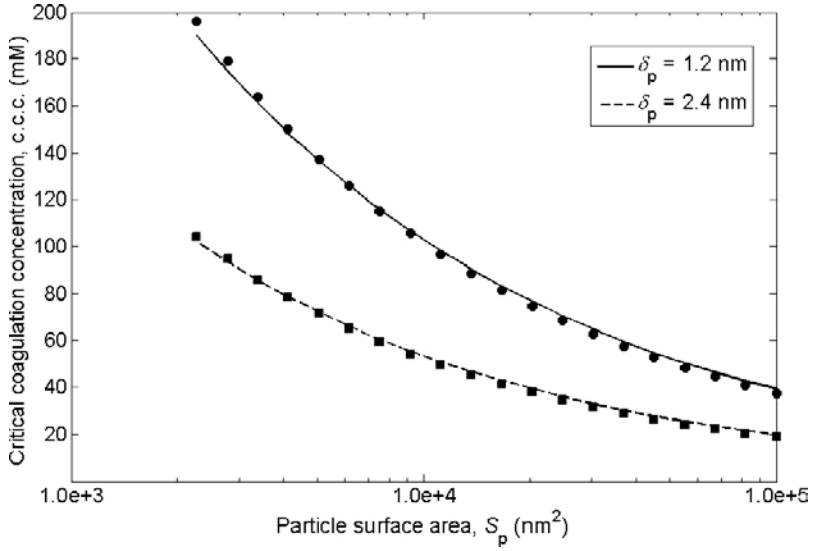

Figure 6-28. *CCC as a function of the surface area of the particles for a monovalent electrolyte, where the numerical results are represented by lines whereas the approximate results are shown by solid markers. The surface charge density is σ^0=–131 C m^{-2}.*

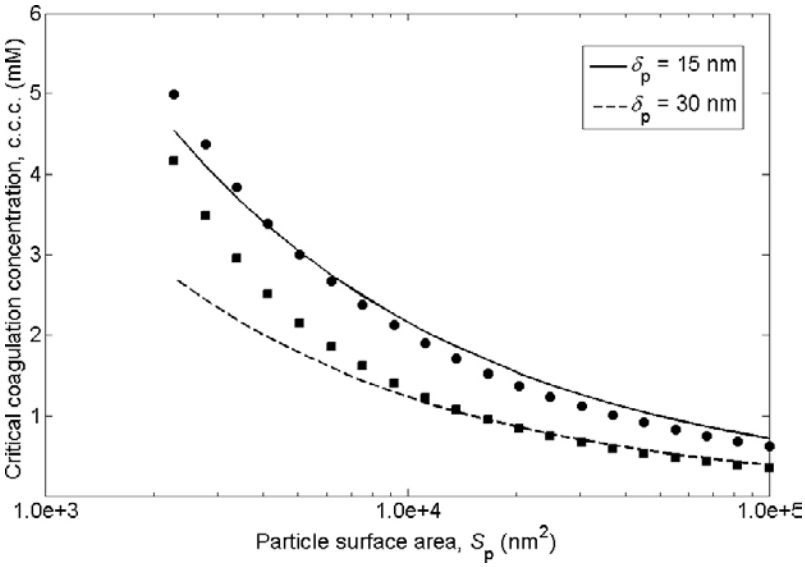

Figure 6-29. *CCC value as a function of the surface area of the particles for a divalent electrolyte, where the numerical results are represented by lines whereas the approximate results are shown by solid markers. The surface charge density is σ^0=–0.131 C m^{-2}.*

CCC values found in the literature for calcium vary between 0.36 and 3 mM for different clays, depending also on solid liquid ratio and on the method used. The predicted CCC values thus fall within the observed range. However, the approximate analytical solution is not as good for divalent ions as for monovalent. The volume fraction of the cohesive gel at the CCC will also be less than a few %.

Hence, the Dynamic model gives fairly good prediction of CCC values for the cases tested which gives addition support to the model.

6.13 Discussion and conclusions

The developed model considers a number of forces between and on the particles in a smectite gel. For sodium dominated systems below the CCC we expect the gel to be expansive over all solid volume fractions. Van der Waals forces will be negligible. At high compactions and volume fractions down to a few percent or less the double layer forces dominate the repulsion between particles forcing them to expand. In addition gravity pulling the particles downward is accounted for in the *Dynamic force model*.

Expansion is counteracted by friction between particles in the gel and the water in which the particles move. We therefore developed relations for friction in gels with sodium, calcium and for natural MX-80 bentonite to quantify the force acting against particle movement in the expanding gel. This was done using independent measurements of hydraulic conductivity found in the literature. The dynamic force model for expansion and the counteracting *friction model* make up the model used to simulate gel expansion or contraction. In the present application the influence of gravity is only felt in rather dilute gels.

In the dynamic force balance model, friction on the water and particles in the gel were modelled by the Kozeny-Carman equation originally but modifications were needed to this relation. With the modifications good agreement with measured data were obtained for homoionic as well as for untreated bentonites.

The dynamic force balance model has been tested against experiments measuring the rate of expansion of bentonite pellets in water with different ion concentrations. For monovalent ions in water below the CCC the model predicts the expansion very well qualitatively as well as quantitatively. Smectites dominated by calcium have not been as successfully modelled but behave qualitatively as

the dynamic force balance suggests down to volume fractions of 5–20%. The Dynamic force model also predicts CCC values in the ranges observed for sodium as well as calcium dominated clays.

For sodium dominated systems, the dynamic force balance model together with the viscosity model can be used to simulate the expansion of sodium dominated bentonites in fractures and to assess the loss rate of smectite particles from the gel/water interface by Brownian motion as well as by slow flow of the low viscosity gel when the ion content in the water at the gel/water interface is below the CCC. When above the CCC, the model predicts that there will be no release of colloidal particles by Brownian motion.

The behaviour of calcium dominated gels cannot be reliably simulated by these models because the size and properties of the calcium smectite stacks, which do not delaminate as the sodium stacks do, are not easily quantified. However, much experimental evidence shows that strongly calcium dominated gels do not readily release colloidal particles against gravity and that calcium dominated gels do not readily penetrate pores, as was shown in chapter 3.

Together with the model devised for the viscosity of dilute gels in Chapter 5, which accounts for the impact of ionic strength as well as of the solid volume fraction in the gel, the dynamic expansion model described in this chapter forms the core of the erosion model for smectite gels. One problem is that we have not found any data on the viscosity of dilute calcium dominated gels and therefore cannot confidently model *flow* of such gels.

7 Diffusion: Processes, experiments, interpretation and impact on conditions at gel/water interface

7.1 Short overview of Chapter 7

A simplified model for evolution of pore water chemistry by mineral dissolution and ion migration in expanding smectite gels is presented. It is used to explore expansion of gel and how the pore water chemistry changes in the expanding bed in a fracture. The model is used to describe simultaneous transport of ions through the gel in a fracture in contact with the compact buffer in a deposition hole on one side and the gel/water interface on the other.

At the gel/water interface, colloidal particles can be released if the solute concentration at the gel/water interface is below the critical coagulation concentration, CCC. It is also explored whether the smectite at the interface may contain a large fraction, X_{Ca}, of calcium in ion exchange positions. Observations suggest that if $X_{Ca} > 0.9$ colloids will not be as readily released. At equilibrium, X_{Ca} is determined by the total ion concentration and by the ratio Ca/Na in the water. The more dilute the water is the more Ca is favoured in exchange sites. Ion exchange equilibrium therefore plays an important role in determining the local conditions. Soluble calcium minerals especially gypsum, when it dissolves in water taken up by the gel, can supply calcium to pore water and to the smectite. At the same time, the calcium concentration in the water in the gel will decrease with increasing water uptake in the expanding gel by dilution as well as uptake in the smectite and thus it can drop below CCC. However X_{Ca} would increase.

Ion transport in the gel is influenced by the presence of the negatively charged smectite particles. Anions are partly excluded from the water whereas the much larger amount of cations, present to compensate the negative charges of the smectite, are mobile and can strongly influence the ion transport in the gel. Neglecting the mobility of the cations in exchange positions can lead to serious errors in transport rates and in transport direction as well as in the composition at the gel/water interface.

Furthermore, the composition of the water at the interface is not the same as that of the seeping water. It will be determined by the relative transport resistances in the gel and in the water flowing past the gel/water interface. The transport resistance in the seeping water is influenced by water velocity, contact area and diffusivity in the water. The transport resistance in the gel is influenced by the diffusivity in the gel, the solids content and the distance the gel has penetrated into the fracture.

The mathematical model has been used to calculate some simple stationary cases under limiting assumptions, with data that are deemed to span the range of data that will be encountered during an ice age with relatively high flowrates of seeping non-saline water.

The results suggest that it is unlikely that the CCC criterion will be upheld or that X_{Ca} will exceed 0.9 in many situations that can be expected.

7.2 Introduction and background

The compacted bentonite in a deposition hole swells when it takes up water and can release smectite particles into the seeping water in the fractures intersecting the deposition hole if the concentration of dissolved salts in the water is below the critical coagulation concentration, CCC. We are especially interested in situations where very non-saline waters may come in contact with smectite containing clay. Such waters can come from melting glaciers or may be fresh meteoric water that has not yet dissolved much minerals.

Divalent ions such as calcium need a much lower concentration than monovalent ions such as sodium to reach the CCC. In a previous study, the leaching of calcium from the compacted buffer through the bentonite gel to the seeping water was modelled and the rate of loss of smectite particles could be related to the loss of calcium to the non-saline water /Liu and Neretnieks 2006/. This very simple model did not account for the ion exchange capacity of the smectite in the bentonite or the possible impact of the ions in exchange positions on the willingness of the gel to release colloids.

As the ion exchange equilibrium of smectite favours calcium over sodium in non-saline waters, it is expected that the gel will have a higher proportion of calcium at the gel/water interface than nearer the deposition hole. It has been suggested by /Birgersson et al. 2009/ that when the proportion of divalent ions such as calcium is larger than about 90% in the smectite this may hinder the smectite from eroding, even if the ion concentration in the water is below what is commonly thought to be the CCC. The non-saline groundwaters expected during an ice age contain some calcium and are so non-saline that if the smectite is equilibrated with such waters the proportion of calcium would be well in excess of 90%. Smectite at the gel/water interface where the colloid release would take place is, however, not in equilibrium with the approaching water because of mass transfer and other limitations.

We explore the conditions at the gel/water interface by studying dilution and mass transport processes within the gel and the mass transfer by diffusion to and from the seeping water outside the gel/water interface. For this we model the gel as a system consisting of "free" water at low particle concentrations and of water near the particle surface, the so called electrical diffuse double layer, DDL, in which the charge compensating counterions reside, which neutralize the negative charges of the particles. These are the ions that can be exchanged e.g. sodium being substituted for calcium when conditions favour this. The ions in the DDL are also mobile and in denser gels the DDL's of the particles overlap and form a continuous concentrated water phase through which the cations can move. Anions are largely excluded in dense gels. Such gels behave similarly to ion selective membranes and in synthetic ion exchange polymers in which charged groups have been introduced into the polymer lattice, /Helfferich 1962/. Such materials are used extensively in industrial applications to purify water and separate different ions. We apply the same basic concept in the modelling presented in this report. The division of water in "free" water and water in the DDL is highly simplified but is illustrative. We call the counterions (charge compensations ions) in the DDL ion exchange ions or sorbed ions. This conceptual model is consistent with the dual porosity concept but also with Donnan gel model in the context of this report. Some reasons for using this idealized picture will be given later.

In one explorative study, the model describes the transport of two cations, sodium and calcium, and an unspecified anion through a gel in a fracture in contact on one side with the compacted bentonite in the deposition hole and with the seeping water at the other side, which we call the gel/water interface. In our scenario, the ion concentration in the gel at the entrance to the fracture is larger than in the water seeping in the fracture. The net transport of ions is towards the gel/water interface from which they further diffuse into the seeping water. It should be noted that the ion concentrations at the gel/water interface differ from those in the approaching water. Provided conditions permit the particles to be released, forming a sol, these particles may diffuse out into the seeping water and be carried away. In the stable sol the particles do not recombine to a gel. In addition, and more importantly, the dilute gel can flow away as a suspension somewhat more viscous than water.

We use the term gel for a cohesive gel as well as for an expansive gel. In an expansive gel repulsive forces act to expand the gel. The expansion could continue indefinitely if gravity does not stop the expansion. The more the gel expands the smaller the repulsive forces become and finally only Brownian motion makes the system become further diluted. It becomes a stable sol.

A cohesive gel can develop when the ion concentration is above the CCC. Then the repulsive forces can just be balanced by and be overcome by attractive forces between particles at some distance. In other words, a cohesive gel expands due to the repulsive forces until a distance is reached between the particles where the attractive forces just balance the repulsive forces and then expansion stops. The gel will not expand further or release particles spontaneously. For a cohesive gel this applies irrespective of if there is gravity or not. Until this point is reached an expansive gel and a cohesive gel can be expected to behave in a similar way because in both cases the repulsive forces caused by the diffuse layer overlap force the particles apart. This was described in chapter 6.

It may be noted that most clay expansion and sedimentation experiments are made under the influence of gravity. Unless the clay/water ratio is very low, a gel is always seen to form at the bottom of a test tube. This is, however, not an indication that the gel is cohesive as gravity will generate such a gel profile, see e.g. Figures 6-17. In a cohesive gel, the water above the gel interface must be essentially free of colloids already extremely near the gel water interface, see Figure 6-18.

Therefore, much of the present work aims to determine the concentrations of the ions in the water at the gel/water interface and the fractions of cations in the smectite gel under different conditions. We explore simple mixing of smectite with water of known composition as well as a scenario where in addition diffusion can cause transport of various ions in the gel. To achieve this, we use conventional transport modelling based on Fick's first law and include the equilibrium coupling between the concentrations in water and in the smectite. At the gel/water interface, the mass transfer resistance due to diffusion in the seeping water is assessed by the equivalent flowrate model, the so called Q_{eq} concept. This makes it possible to simplify a two dimensional flow and transport situation to a one-dimensional problem. By doing this, some limiting cases can be studied and analytical solutions can be obtained for a pseudo-steady state situation. This gives important insights into the migration processes and allows a series of scoping calculations to be made.

The porewater composition and the composition in exchange position in the smectite as it evolves with increasing ingress of water during swelling is studied. We also simulate the expansion of a gel in a fracture where the gel can form a sol at the gel/water interface but also where the gel can simultaneously flow when it is so dilute that its viscosity allows this. This is coupled to diffusion of ions in the expanding gel because the ionic strength also influences the viscosity. In all these simulations, we have had to make various simplifications to our conceptual model in order to emphasize one mechanism or another and to be able to obtain solutions.

7.3 Pore water chemistry

7.3.1 Initial water composition after water saturation

The bentonite is essentially dry when emplaced although it contains some moisture about 10% by weight. The ion exchange capacity of pure bentonites (smectite) is of the order 0.7 to 0.8 meq per gram, Table 7-1. Thus there are exchangeable cations in this amount. Natural bentonites contain tens of percent of accessory minerals. These often contain more or less soluble calcium minerals such as calcite, ($CaCO_3$) and gypsum ($CaSO_4$). These minerals can make up several percent of the natural bentonite.

Table 7-1 shows the mineralogical composition of two candidate bentonites /Arcos et al. 2006/. These data are somewhat different from those presented in /Karnland et al. 2006/.

Calcium and magnesium are favoured over sodium and potassium in the ion exchange equilibrium. When water invades the dry bentonite buffer, the pore water will equilibrate with the soluble minerals and the ions in ion exchange positions. In addition, the edge sites of the smectites can participate in the equilibration by protonation, de-protonation reactions and ion exchange with the de-protonated sites. Such equilibration modelling has been studied and is discussed below. However, first some general observations are made.

Table 7-1. Mineralogical composition of two candidate bentonites.

Mineral (wt %) and other specified units	MX-80	Deponit CA-N
Montmorillonite	87	81
Quartz	5	2
Feldspar + mica	7	2
Dolomite	0	3
Calcite + siderite	0	10
Calcite + siderite mmol/g	0	1
Pyrite	0.07	0.5
Gypsum	0.7	1.8
Gypsum meq/g	0.1	0.26
CEC (meq/g)	0.75	0.70
NaX (%)	72	24
KX (%)	2	2
CaX_2(%)	18	46
MgX_2(%)	8	29

Gypsum is much more soluble than calcite, dolomite and siderite. Gypsum contains 0.1 and 0.26 meq Ca per gram of MX-80 and Deponit CA-bentonites respectively. This is considerably less than sodium bound in the NaX sites. If only dissolution and equilibration were involved, there might be some exchange of NaX for CaX_2 sites, provided the equilibrium was favourable enough. This may well be the case in low ionic strength waters where divalent ions are strongly favoured over monovalent ions. In such cases the gypsum could dissolve entirely and the pore waters become essentially sodium dominated with calcium content less than CCC for Ca, which is about 1 mM. The sodium concentration in the pore water will increase as sodium is expelled from the ion exchange sites but as the CCC of sodium is about 50 to 100 mM this may not be sufficient to be above the CCC. The smectite gel would then expand into the fresh water in the factures, turn to a sol and be carried away The release rate would be considerably faster than if there still was gypsum dissolving to replenish the pore water with calcium or if there was dissolved calcium in the pore water in concentrations above the CCC. We therefore explore the gypsum dissolution during the wetting phase.

The reader is cautioned that the notion of CCC is considerably oversimplified. However, it conveys the important fact that with ion concentrations above the CCC the gel does not spontaneously release colloidal particles and has a cohesion that hinders gel to be dislodged by the shear force of water flowing at the gel/water boundary.

Several groups have modelled the pore water chemistry during the wetting phase. /Bradbury and Baeyens 2003/ calculated porewater compositions in compacted bentonites considering such factors as montmorillonite swelling, semi-permeable membrane effects, very low ‘‘free water’’ volumes, and the highly effective buffering characteristics of the exchangeable cations and the amphoteric edge sites. The exchangeable ions buffer the cation concentrations and the edge sites strongly influence the pH in the porewater bentonite. The MX-80 bentonite has about 87% monovalent sodium and 13% divalent ions, magnesium plus calcium, in the exchange sites prior to wetting. For the MX-80 the porewaters calculated for initial dry densities between 1,200 and 1,600 kg m^{-3} had relatively high ionic strengths around 0.3 M, similar cation concentrations and a pH equal to 8.0. The porewaters contained 220–260 mM sodium and 15–18 mM of the divalent ions. This would be considerably above the CCC.

/Ochs et al. 2004/ made a sensitivity analysis on the influence of important parameters on pore-water chemistry in compacted bentonite. The principal parameters varied were the fractions of calcite, gypsum, and NaCl dissolving from bentonite, and p_{CO2}. In their modelling they accounted for surface chemical thermodynamics, solution/mineral equilibria as well as surface complexation and ion exchange reactions at the edges and siloxane surfaces of clay minerals. Some calculations also accounted for electric double layer effects. It was found that two powerful pH buffer systems influence the pH, namely the amphoteric edge SOH sites and the carbonate buffer system. If p_{CO2} is imposed externally, the resulting porewater pH is mainly controlled by the carbonate buffer. If the bentonite is treated as a closed system, which is the case for initial wetting without further exchange with the surrounding water, the buffering action of the SOH sites becomes more important. In both cases, the dissolution of calcite and gypsum is important. The dissolution of impurities and the ion exchange reactions have an important influence in compacted bentonite, and porewater composition is relatively independent of groundwater composition that invades the dry bentonite. This is not surprising considering that there is a considerable amount of minerals and especially a large amount of ions on the ion exchange sites. It was also found that at higher dry densities (1,200 kg/m^3) the entire pore space may be occupied by water in the diffuse layer.

The clays studied were the Japanese crude (Kunigel-V1) and a purified (Kunipia-F), The Kunigel-V1 contains 46–49% smectite, approximately 5% calcite and dolomite and 0.38% gypsum. The rest is mostly quartz and feldspar. The purified bentonite has no calcite/dolomite but 0.7% gypsum. The situation is quite complex because the p_{CO2} influences the final equilibrium and it is not fixed in an open dynamic system and several levels are conceivable. However, the pH in these simulations never was lower than 7.5 and then practically all gypsum would dissolve. At reasonable values of p_{CO2}, pH is buffered to values between 7.5 and 8.5. The results suggest that gypsum can be entirely dissolved after wetting, the calcium entering the ion exchange sites expelling some of the sodium. This work shows that situations may be encountered where the calcium concentration in the pore water after wetting is determined by calcite solubility which has solubility considerably below that needed for calcium to be above the CCC of about 1 mM.

/Wersin 2003/ studied the porewater chemistry of bentonite using a similar thermodynamic modelling approach. It includes ion exchange, surface complexation and mineral equilibrium reactions. The focus was to identify the geochemical reactions controlling the major ion chemistry and acid-base properties and to explore parameter uncertainties specifically at high compaction degrees. The main reactions controlling major ion chemistry were found to be calcite equilibrium and concurrent Na-Ca exchange reactions and deprotonation of functional surface groups. A sensitivity analysis showed a remarkable robustness of the model with regard to parameter uncertainties. Like /Bradbury and Baeyens 2003/ the uncertainty in pH was found to be mainly induced by the p_{CO2} of the surrounding host rock. Wersin used two different clay models and applied the modelling approach to the Na-rich MX-80 bentonite. The modelling results were compared with experimental results that showed that at a dry density of 1,500 kg/m^3 the concentration of the divalent calcium and magnesium were 7 mM and 52 mM when wetted with fresh water and saline water respectively. The saline water contained 100 mM Ca and 2.3 mM Mg, the fresh water 0.46 and 0.19 mM. The modelling results indicate a significant increase in ionic strength due to the dissolution of gypsum, which agrees with the experiments of /Muurinen and Lehikonen 1999/, i.e. calcite and gypsum dissolution, exchange of Ca for Na and de-protonation of surface hydroxyl groups. In the presence of gypsum and calcite the calcium concentrations in the pore waters were found to be 13–16 mM depending on the imposed partial pressure of CO_2.

/Wersin et al. 2004/ extended previous studies on compacted clays by including anion exclusion induced by swelling of the expandable clay fraction and by the formation of electrical double layers on charged edge surfaces. They evaluated such phenomena by applying a refined diffuse double layer (DDL) approach to model porewater composition in a compacted bentonite backfill surrounded by argillaceous host rock, as foreseen for the Swiss high-level waste repository. Model calculations also include the effect of water incorporation in the structural interlayers. The results indicate that the conventional model and the refined DDL model without distinction between interlayer and external water only differ slightly. As in other studies they find that the main buffering reactions include ion exchange of Ca for Na, calcite and gypsum dissolution and deprotonation of surface hydroxyl groups. On the other hand, the calculation accounting for the distinction of external and interlayer water indicates significant anion exclusion effects on the external water composition. Most notably, this leads to increased salinity and drop in pH. They conclude that from a performance assessment perspective, however, the differences induced by the inclusion of swelling and diffuse double layer effects are not very significant relative to uncertainties related to the system variables, such as the p_{CO2} of the host rock.

It may then be questioned if the system should be thought of as having some free porewater and some water adjacent to the smectite surfaces where all the ion exchange ions reside and which is depleted of anions. An alternative model which has been successfully used is one where the clay is viewed as a macromolecular gel where the smectite particles are modelled as large highly charged macromolecules and the small anions and cations together compensate the macromolecule charges. There will be more counterions, positive ions in this case, when the smectite has negative charge, than coions in the gel. All the water in the gel is assumed to have the same concentration. The concentrations are obtained from the so called Donnan equilibrium model /Hiemenz 1986/. This model has been successfully used to model clay swelling and exchange equilibria /Karnland et al. 2003, Birgersson et al. 2009/. However this approach has not been used to also account for the variably charged edge sites, nor is it readily used to model the presence of soluble minerals in the gel.

7.3.2 Water chemistry evolution in buffer

The previous studies only addressed equilibrium conditions and did not address the evolution over time when the buffer can exchange dissolved species with passing groundwater. /Arcos et al. 2006/ performed simulations to obtain the initial chemical composition of pore water in bentonite, which then was followed by a period when water flows in the fracture intersecting the deposition hole. The flowing water in the fracture has a composition that is different from that in the pore water and solutes are exchanged between the pore water and the flowing water. Concentration gradients develop in the buffer and move in the buffer over time. The buffer nearest the mouth of the fracture equilibrates rapidly with the flowing water but the larger the distance is from the fracture mouth the longer it takes for any change to occur.

These calculations have been done by first "filling" the porous space in the bentonite with Forsmark groundwater and letting the system to equilibrate. The bentonite has a porosity of 43%. The reactions considered include equilibration also with bentonite accessory minerals such as gypsum and quartz and ion exchange and surface reactions. Equilibrium with carbonate minerals has also been calculated when considering the Deponit CA-N bentonite. After equilibration with Forsmark groundwater the Ca+Mg concentrations were 15 and 48 mM for the MX-80 and Deponit CA-N bentonites respectively. Table 7-2 gives some ground water compositions relevant for these simulations.

The evolution of the porewater chemistry over time was modelled for several cases with Forsmark water as well as ice melt water seeping in the fractures intersecting the deposition hole. The Forsmark water has a higher concentration of calcium than the equilibrated MX-80 porewater and there will be an uptake of calcium in the ion exchange sites in the buffer. However, at the same time the remaining gypsum gradually dissolves.

Subsequently simulations with ice melt water, which has low ionic strength and only 0.1 mM calcium, were made starting after 10,000 years of Forsmark water interaction. Ten thousand years after start of the ice melting intrusion the pore waters in the bentonite are below 10^{-3} mM and CaX_2 has increased from 0.28 to 0.45 moles/litre of pore water near the canister surface. This makes up about two thirds of the ion exchange sites now being occupied by calcium. This implies that at the water gel interface there is a pore water that is well below CCC and a bentonite that is depleted of gypsum and a smectite that, although it now has two thirds of the ion exchange sites occupied by calcium still behaves as a sodium bentonite for its swelling and gel/sol properties. Such a smectite will very rapidly swell out even into very fine pores and fractures unless hindered by some other effects. Such effects are discussed in section 3.3 where especially filtering and straining in accessory minerals is discussed. In the study just discussed no bentonite is assumed to be lost.

The initial pore water chemistry will be mostly determined by bentonite and its soluble salts. Typical groundwaters that may intrude initially has no large impact on the composition of the pore water. pH will be circum neutral and ionic strengths on the order of 0.1 to 0.5 M will develop containing sodium as well as calcium well above the CCC. Although there are very little soluble sodium salts in the dry bentonite the pore water will contain sodium coming from the charge compensating ions in the smectite when soluble calcium minerals dissolve and calcium is exchanged for sodium in the smectite. The bentonite has a considerable pH buffering capacity.

Over time the pore water composition can change considerably by exchange of ions with the groundwater seeping in the fractures that intersect the deposition hole. The pore water in the buffer nearest the fracture mouths will tend to equilibrate much faster than the bulk of the compacted bentonite further in the deposition hole. The pore water composition at the buffer (gel)/water interface will determine if the gel can turn to a sol and will thus be much more quickly influenced by a change in seeping water composition.

Table 7-2. Chemical composition of some groundwaters, from /Arcos et al. 2006/.

Moles/l	Forsmark	Laxemar saline	Grimsel Ice-melting
pH	7.2	7.9	9.6
pe	–2.42	–5.08	–3.38
HCO_3^-	2.2×10^{-3}	1.00×10^{-4}	4.5×10^{-4}
Ca	2.33×10^{-2}	4.64×10^{-1}	1.4×10^{-4}
Cl	1.53×10^{-1}	1.28	1.6×10^{-4}
Fe tot	3.31×10^{-5}	8.00×10^{-6}	3.00×10^{-9}
K	8.75×10^{-4}	7.00×10^{-4}	5.00×10^{-6}
Mg	9.3×10^{-3}	1.00×10^{-4}	5.00×10^{-7}
Na	8.88×10^{-2}	3.49×10^{-1}	6.9×10^{-4}
SO_4^{2-}	6.8×10^{-3}	9.00×10^{-3}	6.1×10^{-5}
Si	1.85×10^{-4}	8.00×10^{-5}	2.05×10^{-4}

7.4 Ion exchange equilibria and ion diffusion in gels

It has been observed that when smectites are equilibrated with waters so that they have more than about 90% calcium in ion exchange positions they do not disengage particles even when the counterion concentration in the water is below CCC /Birgersson et al. 2009/. The ion exchange equilibrium is such that the lower the total concentration of ions in the water is the larger fraction of the exchange sites will be occupied by calcium for one and the same calcium/sodium ratio in the water.

The equilibrium relation is commonly written as

$$K = \frac{c_{Na}^2 X_{Ca}}{c_{Ca}(1 - X_{Ca})^2} \tag{7-1}$$

or

$$K = \frac{c_{tot}(1 - f_{Ca})^2 X_{Ca}}{f_{Ca}(1 - X_{Ca})^2} \tag{7-2}$$

where X_{Ca} is the equivalent charge fraction of Ca in the exchange positions. c_{Ca} and c_{Na} are the concentrations of calcium and sodium in the "free" water. $f_{Ca}c_{tot}$ is the total concentration, f_{Ca} is the mole fraction of calcium in the "free" water.

The equilibrium coefficient K is between 3,200 and 4,700 mol/m^3, varying somewhat with ionic strength. This has been valid for dilute suspension , /Birgersson et al. 2009/ and it is near the value of 2,600 mol/m^3, proposed by /Bradbury and Baeyens 2003/ and later used in the geochemical simulations in this report. Figure 7-1 shows the fraction of calcium in the smectite as a function of the fraction of calcium in the water for four total concentrations in water. It is seen that the equilibrium is very favoured for calcium for low total concentrations in water.

For an illustration, the Grimsel groundwater /Missana et al. 2003/ is used as an example. It contains 0.14 mM Ca and 0.69 mM Na, giving a total concentration of 0.83 mM. The mole fraction of calcium in exchange positions at equilibrium would thus be X_{Ca}=0.975, which is well above the value needed to obtain a stable gel without any particle release, presuming that the gel at the gel/water interface is in equilibrium with the Grimsel water. However, this may not be the case in a dynamic system because then there is a continuous transport of solutes from the pore water to the interface and there is a mass transfer resistance between the interface and the seeping water. These effects are explored below.

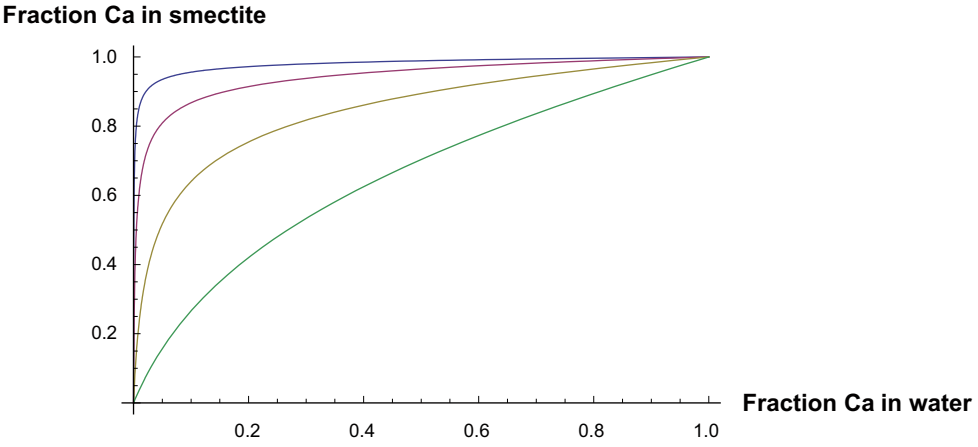

Figure 7-1. *Fraction of calcium in the smectite as a function of the fraction of calcium in the water for four total concentrations in water. 1, 10, 100 and 1,000 mM from left to right, exemplified for K=4,000 mol/m^3.*

7.5 Smectite gel stability and ion exchange equilibria

The conventional view is that the ionic strength of the water determines whether a smectite is cohesive or not. The underlying idea is that at higher ionic strengths the DDL around the smectite particles becomes thin enough for the particles to come close enough together to allow the attractive van der Waal's forces to overcome the repulsive DDL forces. The ionic concentration at which this happens is called the critical coagulation concentration denoted by CCC. This is the basis for the long used DLVO theory /See e.g. Evans and Wennerström 1999/. This theory has over the years been supplemented with additional mechanisms to make it fit observations that the DLVO theory cannot explain.

Multivalent ions are much more efficient to compress the diffuse layer and the CCC is found to be much lower than it is for monovalent ions. For water containing both mono- and divalent ions the basic simplifying approach is just to consider the impact on the diffuse layer by the ionic strength and not to account for ion specific effects.

Recent observations have shown that divalent cations such as calcium may have an additional specific effect on the gel stability that is not included in the DLVO theory, namely that when the more than about 90% of the fixed charges in the smectite are compensated by divalent ions, the gel is stabilized at an average smectite volume fraction in the range around 10–20% irrespective of the ionic strength of the water. It has been proposed by /Birgersson et al. 2009/ that this should be used as an additional criterion for smectite stability. They present a number of different experiments that point in this direction. We do not agree to the conclusions that their experiments show that the calcium gels are cohesive as we have argued in sections 3.3.3. and 6.9. Nevertheless, the idea is appealing and it is clear that strongly calcium dominated gels behave very differently than sodium dominated gels do. We therefore explore conditions when the smectite could attain a very large proportion of divalent ions in ion exchange positions.

One reason for the stabilisation is thought to be that with a large fraction of divalent ions in the inter lamellar space strong attractive forces develop between the smectite sheets by ion-ion correlation effects, which leads to the formation of agglomerates of sheets, forming larger particles. The particles are large enough not to be seriously disturbed by the thermal forces causing Brownian dispersion of colloidal particles. These attractive forces have also been theoretically predicted to stabilise calcium smectite at a solid volume fraction of 50% to an essentially solid body /Jönsson et al. 2009/. This is definitely not observed for the gel as whole and there seems to be other effects, as yet not understood, that on one hand form dense aggregates of smectite particles but allow these aggregates to repel each other. In the aggregates smectite sheets are aligned as closely as predicted, but on the other hand still retain repulsive forces between the larger aggregates to allow considerable swelling of the gel.

/Birgersson et al. 2009/ propose that two mechanisms be considered, which stabilise the gel. In a gel in which less than 90% of the fixed charge are divalent such as calcium, i.e. $X_{Ca}<0.9$, the gel may become cohesive if the ionic strength is above the CCC, i.e. the conventional DLVO idea. This is illustrated by the upper line in Figure 7-2. It starts at the CCC for a pure sodium system and extends to the right with increasing calcium content in the water. Along this line the ionic strength is the same. It thus compresses the diffuse layer equally according to the basic theory for DDL behaviour. This is an idealised assumption and it should be remembered that the situation is much more complex when a mixture of monovalent and divalent ions are present simultaneously, /Lyklema 2005/. We use the term CCC to mean that the gel becomes *cohesive* when the ion concentration compresses the diffuse electrical layer sufficiently to let van der Waal's forces hold the particle together.

The lower curve depicts the combination of sodium and calcium concentrations in the pore water where the smectite in equilibrium has $X_{Ca}=0.9$. /Birgersson et al. 2009/ argue that such gel is also cohesive. We are not convinced by their interpretation of experiments and arguments that the gel is cohesive, but agree that it is very different in structure and behaviour compared to a expansive gel and consists of considerably larger particles than the size of individual sheets. Such gels will not readily give off particles against gravity and they will also be retained by much lagers pores they try to pass. It is therefore of interest to explore under what conditions $X_{Ca}>0.9$ could be attained. We use the notation X_{Ca} for the fraction of all divalent ions for simplicity.

The two above described conditions, when combined, predict that there will be a limited region of water compositions where the gel can release colloidal particles. An example of the sol formation region is shown in Figure 7-2 suggested for the Wyoming bentonite MX-80 by /Birgersson et al. 2009/.

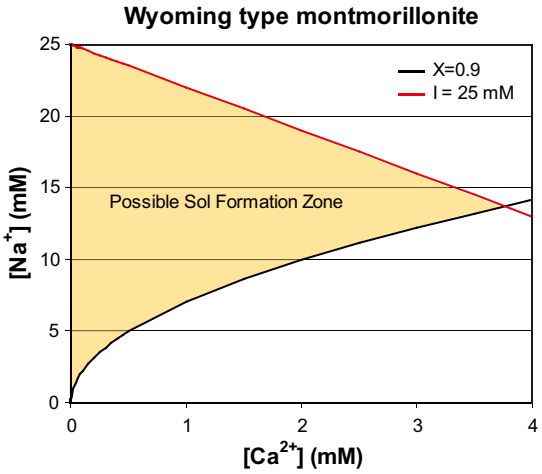

Figure 7-2. *Limitations of a possible sol formation zone for Wyoming type montmorillonite in equilibrium with an external Ca/Na-solution and monovalent anions (e.g. Cl^-). /From Birgersson et al. 2009/.*

It has been found experimentally that in mixed sodium and calcium systems the above sol formation range may be conservative and overestimate the region in which sol formation can be expected. /Birgersson et al. 2009/ find that when $0.2<X_{Ca}<0.9$ sol will not readily form if in the pore water $c_{Ca}+c_{Na}$ is larger than about 2–4 mM.

The equivalent fraction X_{Ca} of calcium at equilibrium depends on the composition of the pore water. This is described next.

7.6 Use of mass balance to assess whether $X_{Ca}>0.9$ could be reached before the gel can turn to a sol

In this section, we make a simple estimate of the volume of water that is needed to supply one gram of smectite with sufficient calcium to reach $X_{Ca}=0.9$, starting from $X_{Ca}=0.5$. Considering only calcium as the divalent ion present, this starting value is much higher than either of the two clays discussed in more detail later. The higher value is chosen because dissolving calcium minerals may supply more calcium that enters the ion exchange positions. This will also be discussed later.

For the Grimsel water, which has 0.138 mM calcium, 1.45 litres is needed to supply 1 g of smectite with the calcium needed to attain $X_{Ca}=0.9$. It is then assumed that all calcium from the water goes into the smectite. This is only slightly exaggerated and allows for any errors in the selectivity coefficient.

If one gram of smectite is dispersed in the 1.45 litres of water, the suspension would have a volume fraction of smectite $\phi=0.026\%$. As the gel turns to sol already at considerable larger volume fractions, 0.1–1%, this means that the smectite could solubilise long before it could attain the stable $X_{Ca}>0.9$ condition.

Table 7-3 shows the same calculations for a number of other glacial waters. In none of the waters in the table, the smectite would stabilize by taking up calcium from the water if just a simple mixing of the smectite with increasing volumes of water was made. The conditions would allow smectite to solubilise already in a small fraction of the water volume before it could attain $X_{Ca}=0.9$.

Another way to look at the possibility of sol formation is to assess what X_{Ca} would be in a suspension with smectite volume fraction $\phi=0.3\%$. This is about when the smectite particle can start to rotate freely and where it has been found that the gel/sol viscosity is low enough for the gel/sol to flow downstream /Moreno et al. 2009/. For 1 g smectite dispersed to this volume fraction in water, the water volume needed is 0.123 litres. It is seen in the rightmost column in Table 7-3 that only few X_{Ca} values exceed 0.6 but none are as large as 0.7 if dispersed in 0.123 litres of water. In all cases, the gel would be unstable and could form a sol that could potentially be carried away by the seeping water.

Table 7-3. Data from /Brown 2002/. The Eq X_{Ca} column show what the equilibrium fraction of divalent ions should be in ion exchange positions calculated using the sum of monovalent and sum of divalent ions in solution. The V_w column shows how many litres water is needed to change 1 gram of smectite from XCa=0.5 to 0.9 and the ϕ column shows the smectite volume fraction for one gram of smectite when dispersed in Vw litres water. The right hand column shows XCa if one gram of smectite is dispersed in 0.123 litres of water, resulting in ϕ=0.3%.

	Ca mM	Mg mM	Na mM	K mM	Divalent	Monovalent	Eq X_{Ca}	V_w,l	ϕ %	X_{Ca}
	0.275	0.018	0.025	0.061	0.293	0.086	0.997	0.68	0.054	0.572
	0.158	0.016	0.0205	0.0117	0.1735	0.0322	0.999	1.15	0.032	0.543
	0.012	0.0023	0.0166	0.0027	0.0140	0.0193	0.997	14.2	0.0026	0.503
	0.116	0.0515	0.0258	0.0178	0.1675	0.0436	0.998	1.19	0.031	0.541
	0.380	0.051	0.057	0.0176	0.4305	0.0746	0.998	0.46	0.080	0.606
	0.041	0.0031	0.0225	0.0038	0.0441	0.0263	0.998	4.54	0.008	0.511
	0.604	0.079	0.487	0.056	0.682	0.543	0.990	0.29	0.126	0.668
	0.388	0.156	1.1575	0.0995	0.544	1.257	0.973	0.37	0.101	0.634
	0.213	0.0051	0.0043	0.0027	0.218	0.0071	0.9998	0.92	0.040	0.554
	0.319	0.046	0.0049	0.0063	0.365	0.0112	0.9997	0.55	0.068	0.590
	0.084	0.012	0.045	0.0365	0.0956	0.0815	0.966	2.09	0.018	0.524
	0.105	0.097	0.425	0.0120	0.202	0.437	0.985	0.99	0.037	0.550
	0.121	0.023	0.075	0.005	0.144	0.08	0.997	1.39	0.027	0.535
	0.095	0.033	0.0065	0.0026	0.127	0.0091	0.9996	1.57	0.024	0.531
	0.176	0.017	0.112	0.0135	0.193	0.125	0.996	1.03	0.036	0.548
	0.180	0.058	0.482	0.012	0.237	0.494	0.984	0.84	0.044	0.558
	0.173	0.012	0.076	0.0166	0.185	0.0926	0.997	1.08	0.034	0.546
	0.125	0.018	0.050	0.0056	0.143	0.0551	0.998	1.40	0.026	0.535
minimum	0.012	0.002	0.004	0.003	0.014	0.007				
average	0.198	0.039	0.172	0.021	0.237	0.193				
maximum	0.604	0.156	1.158	0.100	0.683	1.257				
Grimsel meltwater /Missana et al. 2003/										
	0.137	0.0007	0.685	0.0004	0.138	0.685	0.971	1.45	0.026	0.534
Preliminary data proposed for Laxemar 2020 in SR-Can										
	0.38	0.26	2.42	0.06	0.64	2.48	0.952	0.31	0.119	0.657

7.7 Other sources of calcium

The mass balance and mixing examples neglect other possible sources of calcium. There are, however, other sources that may supply the smectite with calcium and other divalent ions.

The compacted bentonite in the deposition hole contains dissolved calcium. This may diffuse in the pore water in the gel in the fracture towards the gel/water interface and add to the calcium that may enter the ion exchange positions, provided the calcium concentration gradient is directed towards the seeping water. In addition, simultaneously there is a possibility that calcium in the seeping water diffuses towards the gel/water interface. The latter situation may seem strange at first but can occur if the ion exchange equilibrium at the gel/water interface strongly favours calcium. As will be shown later, this can occur if the water at the gel/water interface is dilute.

It will be shown below that, to account for this migration, we need to understand the ion migration processes in the smectite gel. It will be seen that in addition to migration of the ions in the pore water in the gel, the charge compensating cations present in the DDL can migrate. In fact, because by far most of the cations reside in the diffuse layer this migration can dominate over the diffusion in the "free" water, especially when the gel has not expanded to near sol consistency.

We describe the migration processes and the data that will be used in subsequent simulations in the sections below.

7.8 Diffusion: Processes, experiments and interpretation

To study the rate of transport of ions by diffusion in the gel and over the gel/water interface, we need first to describe and quantify the diffusion mechanisms and the mass transfer resistance in the seeping water in the fracture. As the diffusion in the gel is strongly influenced by the presence of the charged smectite particles, which leads to anion exclusion as well as "surface diffusion" of cations, we describe these processes and the experiments used to obtain the necessary data. We develop a simple model that can account for diffusion of anions as well as cations in a smectite gel with strongly varying density from one side to the other side. This model is coupled to a model that accounts for the mass transfer resistance in the seeping water in the fracture.

It will be seen that there are several uncertainties that cannot be readily surmounted and that several assumption need to be made, which further adds to the uncertainties. Nevertheless, we feel that the effort needs to be made to explore if these processes may add to stabilize the gel.

7.8.1 Diffusion: Experiments and interpretation

Two main types of experiments are used to determine diffusion coefficients in porous media: The pulse spreading experiment and the through diffusion experiment.

Pulse spreading experiment

In the pulse spreading experiment a small amount of tracer is placed between two pieces of the porous medium, in this case saturated compacted bentonite. After some time when the tracer has diffused the tracer concentration profile is measured. The apparent diffusivity D_a is determined by fitting the profile to the solution of the diffusion equation for the appropriate boundary conditions.

$$\frac{\partial C}{\partial t} = D_a \frac{\partial^2 C}{\partial z^2} \tag{7-3}$$

where C is the total concentration of the species in the porous medium including what is in the water and what may be bound to the solid in some way.

The apparent diffusivity D_a thus summarizes the effects of diffusion in the water and in or on the solid in the porous medium. For ion diffusion D_a varies with porosity as well as with ionic strength and is usually different for anions and cations and is also different for different cations. It also contains effects of constrictivity and tortuosity of the pores.

Through diffusion experiment

The sample is placed between two containers with different concentrations of the tracer. The tracer migrates from the high concentration side to the low concentration side. The flux of the tracer is proportional to the effective diffusion coefficient D_e.

$$J = D_e \frac{c_{high} - c_{low}}{\Delta z} \tag{7-4}$$

In this equation c is the concentration in the water at the sample surface. The apparent and the effective diffusivities are related to each other via the capacity factor α,

$$D_a = \frac{D_e}{\alpha} \tag{7-5}$$

For a medium where the water can be seen to be a distinct homogeneous phase and the solid another homogeneous phase, the capacity factor can be written as

$$C = \alpha c = \left[\varepsilon + K_V (1-\varepsilon)\right] c \tag{7-6}$$

where ε is the porosity (water volumetric fraction) and K_V the volumetric partition coefficient. It can be obtained from the ion exchange equilibrium relation, Equation (7-1), and varies with concentration. In the smectite water system of interest here, the conditions are not as simple as Equation (7-6)

suggests. Anions may not have the same concentration in the pore water when in equilibrium with bulk water due to ion exclusion effects. Water may be present in different compartments with distinctly different properties because of electrical diffuse layer influence. The diffusivity may be different in water at different distances from the surfaces. There are probably more effects that are poorly understood.

A difficulty with through diffusion experiments is that the filters that are needed to contain the swelling clay sample have a diffusion resistance in series with the sample. When the capacity factor and the apparent diffusion are both high, the filters can make up a considerable resistance to the tracer flux. When the relative resistance in the filters is large and this is not accounted for in the evaluations, the errors in the effective diffusivity can be considerable.

It has therefore been found to be a complex matter to evaluate and describe diffusion in water saturated smectite. Below some model concepts used for diffusion in smectite systems are described.

7.8.2 Experimental data on diffusion coefficients

Figure 7-3 shows the effective diffusivity of chloride for three different solid volume fractions as a function of NaCl concentration in the equilibrated water /van Loon et al. 2007/. It is seen that it is strongly influenced by the ion concentration as well as the solid volume fraction in the gel ϕ. The diffusion accessible porosity ε_{free} increased from 0.017 to 0.112 for ϕ= 0.481 (1,300 kg/m^3 dry density), from 0.004 to 0.063 for ϕ=0.593 (1,600 kg/m^3 dry density) and from 0.001 to 0.024 for ϕ=0.704 (1,900 kg/m^3 dry density). This suggests that anion exclusion is very strong and that cation diffusion will be dominated by diffusion in the sorbed (ion exchange) state at these high dry densities. Under these conditions practically all cations are present to compensate the fixed charges. The amount of additional cations is equal to the amount of anions, which was very small as stated before.

The effective diffusivity varies over more than three orders of magnitude. The Donnan model predicts the same qualitative dependence but quantitatively deviates by up to an order of magnitude for ϕ=0.481 and low ionic concentration in water /Birgersson et al. 2009/. This is still a very good agreement considering that a homogeneous system is modelled and that ion activity effects are neglected.

Additionally, /Kozaki et al. 2005/ measured sodium diffusion in Kunipia-F montmorillonite by observing a trace of radioactive sodium spreading between the pieces of compacted clay samples. The trace sodium ions move in the diffuse layer by surface diffusion exchanging for other sodium ions there. No anions need to accompany this movement. From such experiments D_s values can be obtained. Their experiments show the rate of diffusion of the cation. They found different diffusion behaviour for different compactions and conclude that three mechanisms are involved. At dry clay densities <1,000 kg/m^3 pore water diffusion is dominant. External (on surfaces outside the interlayers) surface diffusion dominates at dry densities between 1,000 and 1,400 kg/m^{3}and interlayer diffusion dominates above about 1,400 kg/m^3.

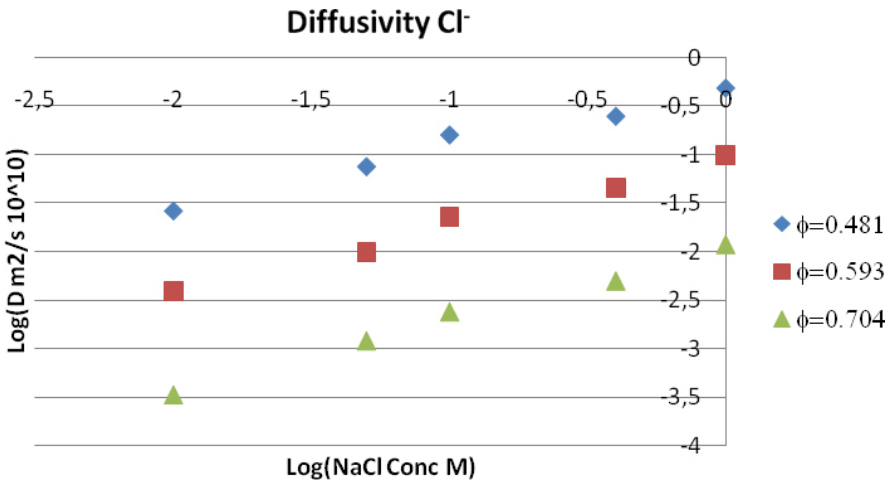

Figure 7-3. *Effective diffusivity of chloride for three different solid volume fractions as a function of NaCl concentration in equilibrated water. /van Loon et al. 2007/.*

At a temperature of 298 K, /Kozaki et al. 2005/ found apparent (D_a or D_s) Na^+ diffusivities in the gel of about $3 \cdot 10^{-11}$ m^2/s for a Na dominated clay with dry density around 1,600 kg/m^3. For a dry density around 700 kg/m^3 the diffusivity was $1.3 \cdot 10^{-10}$ m^2/s and for a dry density around 1,800 kg/m^3 it was about $2.3 \cdot 10^{-11}$ m^2/s. Mixtures of Ca/Na bentonite in the range 0.25 to 1 made little difference to the Na diffusivity. These results show that the charge compensating cations are mobile but D_s is far smaller than the diffusivity in unconfined water. It can be caused by tortuosity and constrictivity effects as well as by the possibly lower mobility of the water molecules adjacent to the surface.

Figure 7-4 shows sodium diffusivity D_a and the product of $D_a\phi$ versus volume fraction ϕ. Data from /Kozaki et al. 2005/. It is seen that the product $D_a\phi$ varies less with changing volume fraction of solids than does D_a.

/Sato et al. 1992/ present data for strontium diffusion in sodium bentonite. These data are shown in Figure 7-5. Strontium apparent diffusivities are a factor of 5 to 10 lower than those for sodium at the same volume fraction.

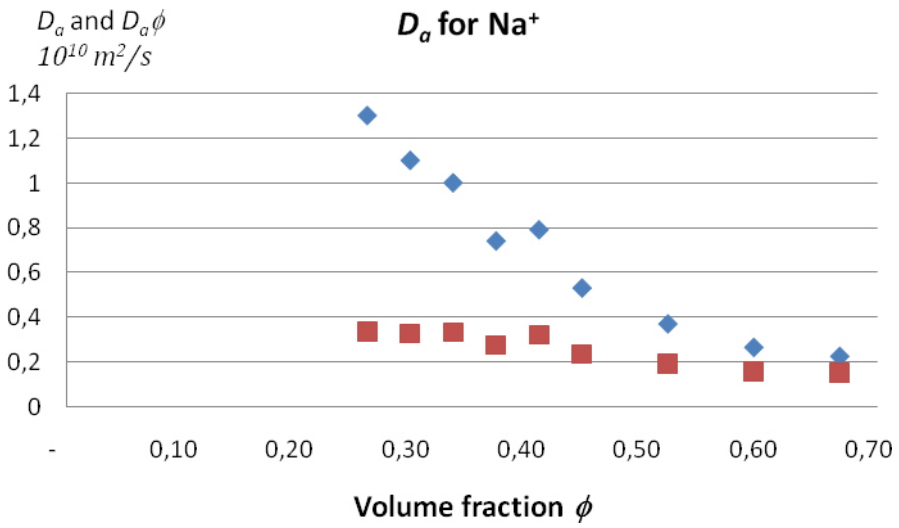

Figure 7-4. *Sodium diffusivity, diamonds and product of sodium diffusivity and solid volume fraction squares versus volume fraction, Data from /Kozaki et al. 2005/. Temperature 298 K.*

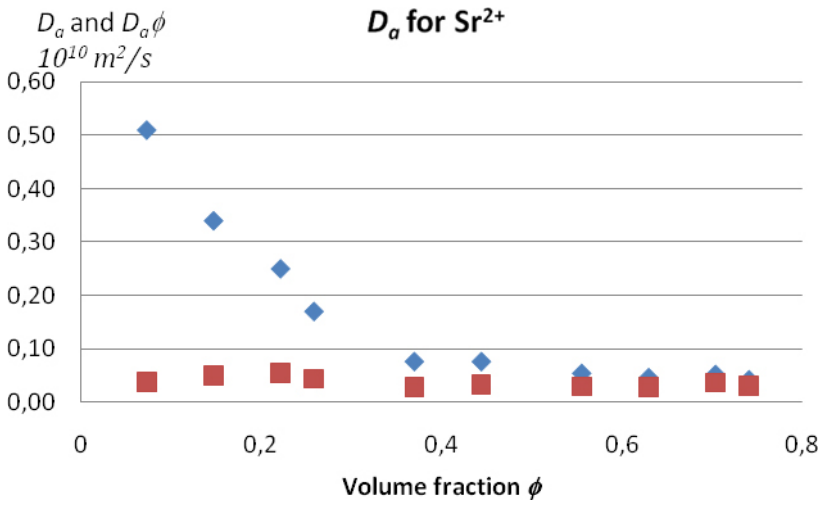

Figure 7-5. *Strontium diffusivity diamonds, and product of strontium diffusivity and solid volume fraction squares, versus volume fraction, Data from /Sato et al. 1992/.*

/Bourg et al. 2007/ analysed and interpreted several experimental studies of sodium and strontium diffusion using their model including the data presented in Figures 7-4 and 7-5. They found that strontium apparent diffusion coefficients were about 3 to 10 times lower than those for sodium over a wide range of dry densities. The sodium diffusion coefficients in turn were lower than those for water molecules especially at lower compactions.

/Birgersson et al. 2009/ measured diffusion rates through pure montmorillonite systems contacted with crystalline gypsum in a controlled geometry as well as with gypsum saturated solution in order to gain understanding of the dissolution process of accessory minerals in water saturated bentonite. By comparing the diffusion behaviour of Ca^{2+}- Na^{+}- and SO_4^{2-} ions in montmorillonite either by gypsum dissolution surrounded by water saturated clay or by through diffusion they found that the mass transport cannot be described by single diffusion coefficients. For calcium clays with dry density around 1,600 kg/m^3 they obtained effective $CaSO_4$ diffusivities D_e around $1.7 \cdot 10^{-12}$ m^2/s. In an experiment when Na is expelled from a Na-bentonite from one side by in-diffusing Ca the SO_4^{2-} diffusivity was about 4 times larger. It should be noted that in these through diffusion experiment in dense clay the ion flux is essentially determined by the anion due to ion exclusion effects. The results are thus indicative of anion diffusivities. The results agree reasonably well with those of /van Loon et al. 2007, Figure 7-3/, who found chloride effective diffusivities around 10^{-12} m^2/s for a dry density of 1,600 kg/m^3 at an ion concentration around 15 mM, the solubility of gypsum.

7.8.3 Diffusion model concepts for porous media

Three different concepts of ion movement in water saturated bentonites are discussed below. They are not necessarily mutually exclusive alternatives.

The surface diffusion model

The medium is conceived as a porosity system with water with dissolved species and solids with the tracer attached to the surfaces by sorption or ion exchange due to the fixed negative charges on the surfaces. The dissolved species in the water are mobile as are the species attached to the surfaces. The migration in both phases is in parallel and equilibrium between the phases is assumed. Diffusion in the water is slowed down by tortuosity and constrictivity effects. Such effects are built into the surface diffusion coefficient, which may also vary with the porosity of the medium.

Dual porosity system with nano- and macropores

This system is conceived as a system with nanopores and macropores where the surfaces of the nanopores have fixed negative charges. Mobile counterions reside in the nanopores compensating all surface charges. The counterions are mobile. Anions are excluded from the nanopores. The macropores exist between the particles but only in the region where anions are mobile. The water fraction in the macropores can approach zero in highly compacted systems. The diffusivities in nano- and macropores can be different. The migration in both phases is in parallel and there is equilibrium between the phases.

Homogeneous system called a Donnan gel

Another concept is what we call a Donnan gel. It is conceived as a homogeneous material with fixed evenly distributed negative charges compensated by mobile counter ions. Anions are also present but in lower concentrations than the cations. This is called anion exclusion. The sum of the fixed negative charges and the anions equal the amount of cations.

Properties of the models

In compact water saturated bentonite, the individual thin smectite sheets are aligned closely together forming stacks with distances between sheets as small as 0.6–0.7 nm. The individual sheets are about 1 nm thick. At dry densities of over 1,900 kg/m^3, the water exists practically only between the sheets. This is sometimes called nanopore water. At lower dry densities, the stacks expand and may also break up. /Bourg et al. 2006, Glaus et al. 2007, van Loon et al. 2007/. Some water exists in connected macropores between the stacks of sheets. Increasingly lower dry densities increases the fraction of the water in macropores. In many investigations, the interest has been on dry densities above 1,000 kg/m^3 and this concept has been the basis for modelling and experimental interpretations. /Bourg et al. 2006, 2007, 2008/

analysed a number of diffusion experiments and showed that such a concept could be used for water self diffusion as well for anion and cation migration. Ion exclusion effects and the influence of ionic strength could also be successfully modelled. Their model is based on the concept that macropore and nanopore diffusions act in parallel, both pores have the same tortuosity but the nanopores in addition have constrictions slowing the diffusion in the nanopores compared to that in macropores.

Their model states that the apparent diffusivity of a species can be written as follows

$$D_{a,i} = D_0 \frac{1}{G_i}(\alpha_{macropore} + \alpha_{nanopore}\delta_{inanopore}) \quad (7\text{-}7)$$

where D_0 is the diffusion coefficient in unconfined water, $D_{a,i}$ is the apparent diffusivity for species "i", G_i is a factor accounting for the effects of the tortuous paths, $\alpha_{macropore}$ and $\alpha_{nanopore}$ are the fractions of the diffusing species residing in the macropores and in the nanopores, respectively. $\delta_{inanopore}$ is a fitting parameter and it accounts for the lower mobility of the ions in the nanopores.

This way of writing the relation allows the expression to be used for uncharged species such as water molecules, which have equal access to both pores, for anions that are entirely excluded from the nanopores and for cations that may reside entirely in nanopores at high compactions. Note that the fractions α can be obtained from ion exchange capacity information for the cations. Anions are, however, not allowed to enter into the narrow nanopores.

The model has been successfully applied to water /Bourg et al. 2006/, to the cations Na and Sr /Bourg et al. 2007/ and to account for ionic strength effects in the dry density range 980 to 1,950 kg/m^3. In this range G_i is about 4 and $\delta_{inanopore}$ was found to be between 0.08 and 0.32 for water molecule tracers /Bourg et al. 2006/. Water tracer data down to dry densities between 0 and 0.2 kg/m^3 reveal that the tortuosity function G rapidly decreases to 1.

/Bourg et al. 2007/ also compared this model to the traditional surface diffusion model for cation diffusion. The influence of ionic strength was also studied. They found that their model performed better in the density range studied, although the differences for the ionic strength were not very large. They write the surface diffusion relation as follows.

$$D_a = \frac{1}{G_i}\frac{D_0\varepsilon + K_d\rho_s D_s}{\varepsilon + K_d\rho_s} \quad (7\text{-}8)$$

where ε is the porosity, $K_d\rho_s$ the volumetric partition coefficient and D_s the surface diffusion coefficient. As before the diffusion coefficient is species dependent but we for brevity omit the index "i" in the equation.

The main cause of difference between the models can be traced to the use of all water in the system, ε, to be accessible to the anions and surplus cations. It may be noted that when the transport in the sorbed phase dominates over that in the "free" water $K_d\rho_s >> \varepsilon$ Equation (7-8) reduces to $D_a = \frac{D_s}{G_i}$.

The model may also be adapted for anion exclusion effects by accounting for the fraction of water in which the anions can reside /van Loon et al. 2007/. The ion exclusion will depend strongly on the ionic strength and the dry density of the material. It may be noted that if there is anion exclusion there is also cation exclusion to ensure charge balance in the water where the anions are conceived to reside. For porosities larger than about 90% in both models, if defined as above, the decrease of G_i must be accounted for.

The Donnan model concept of diffusion in gels was explored by /Birgersson et al. 2009/. In gels with stationary charges such as smectite gels, cations will be present in the gel to compensate negative charges of the smectite, in addition to the cations present to charge balance the anions that also have access to the water in the gel. There will thus be more cations than anions in the gel. The average ion concentrations in such gels, when in equilibrium with water outside the gel, can be described by the Donnan equilibrium. The Donnan model assumes a homogeneous gel and does not account for the possibility that the particles carrying the fixed charges may form heterogeneous structures with macropores. The properties describing a Donnan gel are averaged over the entire gel volume. This is convenient and has been successfully used to describe swelling, ion exchange and transport properties in many cases.

Using the concept of ion exclusion, which is inherent in the Donnan model, the surface diffusion model can be modified by introducing the "free" water concept.

$$D_a = \frac{1}{G_i}\frac{D_0\varepsilon_{free} + K_d\rho_s D_s}{\varepsilon_{free} + K_d\rho_s} \quad (7\text{-}9)$$

This puts even more emphasises on the domination of diffusion by the sorbed or ion exchange ions. It is a minor modification of the surface diffusion model, but it is important because it shows that the anions will have increasingly smaller effective diffusivity D_e. Note, in addition, that the use of a constant volumetric partition coefficient is not correct when the relation between the concentration in the solid and concentration in liquid is not linear, which is the case for ion exchange. However, by using the equilibrium relation, Equation (7-1), a relation between X_i and c_i can be obtained and a concentration dependent partition coefficient can be defined as

$$K_d = \frac{X_i}{z_i c_i}\phi CEC \quad (7\text{-}10)$$

where z_i is the charge of the counterion.

From Equations (7-9) and (7-10), it can be deduced that D_a will be dominated by surface diffusion for large volume fractions of smectite as ε_{free} approaches zero, due to anion exclusion. For low volume fractions, however, it will be determined essentially by the diffusion in unconfined water as ε_{free} approaches 1 and tortuosity effects become small.

Regarding the Donnan exclusion effects, these can be accounted for by exchanging ε for $\varepsilon_{free} = \varepsilon\psi$ in Equation (7-8) where ψ is the ratio of anion concentration in the water in the gel to that in external water, c_w. It can also be seen as the fraction of water in the gel that would have the same concentration as that in the external water. Derivation of Equation (7-11) can be found in /Birgersson et al. 2009/.

$$\psi = \frac{c_{gelwater}}{c_w} = -\frac{E}{2c_w} + \sqrt{\left(\frac{E}{2c_w}\right)^2 + \Gamma_w^2} \quad (7\text{-}11)$$

with the ion exclusion ratio E given by

$$E = \frac{\phi}{1-\phi}\frac{CEC \cdot \rho_s}{z} \quad (7\text{-}12)$$

For large $\frac{E}{2c_w}$ Equation (7-11) reduces to $\psi \cong \frac{c_w}{E}$ assuming $\Gamma_w^2 = 1$.

Note that Γ is the ratio of activity coefficient products in the outside water and in the gel respectively. It is usually assumed to equal to unity, mostly because data are not available for the conditions in the gel. This introduces a non-negligible uncertainty which must be kept in mind. The results are thus quantitatively uncertain but are usually considered to be qualitatively correct. Figure 7-6 show the ion exclusion ratio for CEC=1eq/kg, ρ_s=2,700 kg/m^3 and z=2.

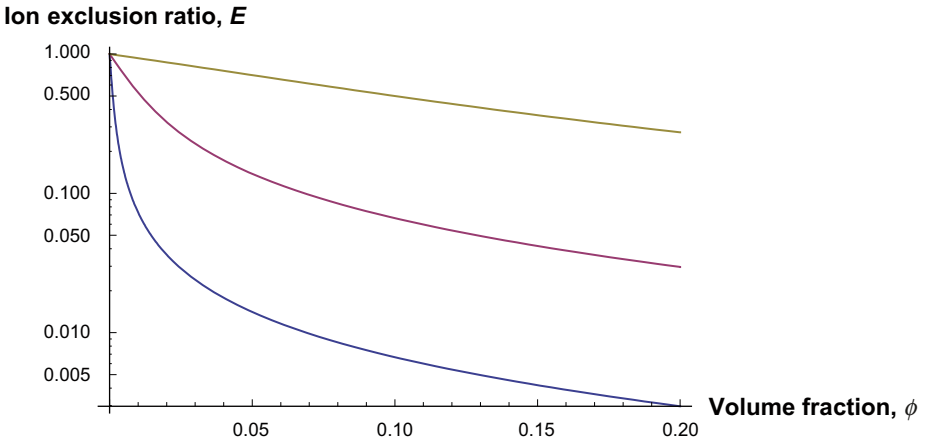

Figure 7-6. *Ion exclusion ratio as a function of volume fraction of smectite. Curves for c_w 1,10 and 100 mol/m^3 from bottom and up.*

7.9 Structure of water saturated bentonite and diffusion

None of the models described above are well suited to cover the whole range of volume fractions, down to nearly free particles, we wish to model. In the present report, we use the modification of surface diffusion model by introducing the concept of "free" water, Equation (7-9). It in essence applies the Donnan equilibrium concept to assess the water available for transport of anions due to ion exclusion effects.

7.9.1 Concepts of smectite-water system related to diffusion

In our model concept, the cations present to compensate the permanent negative charges of the smectite are mobile as in the surface diffusion model. However, the medium we call a gel consists of water in which the charge compensating cations reside and of "free" water containing the additional anions and cations. In the "free" water the anions and the equal amount of cations (charge wise) are mobile. The fraction of water called "free" water depends on the ionic strength as well as the volume fraction of smectite and can be estimated by the Donnan model.

/Van Loon et al. 2007/ present an illustrative conceptual model of how smectite sheets are arranged in compact gels and how water behaves in such gels. At high solid volume fractions, the thin flat particles are arranged in stacks with many sheets in one stack. The water between the sheets is called interlayer water. The water between the stacks is called interparticle water. This is essential the same as nanopore and macropore water in the /Bourg et al. 2006/ description. At high compaction, the interlayer water can be only 2 to 3 water molecules thick and the electrical double layers of the adjacent particles overlap considerably. As the smectite particles have a permanent negative charge, anions will be essentially excluded from the interlayer water at high compaction. At lower compaction, the double layers overlap less and permit some anions to enter. At higher ionic strengths, the double layer is thinner and there will be less overlap at a given particle distance allowing more anions to enter. The distance between the particles is larger than that between sheets and interparticle water is conceived to consist of not only the diffuse layer water but also of "free" water. /Van Loon et al. 2007/ present the following conceptual model of a smectite gel. It is shown in Figure 7-7. TOT is the smectite sheet with an octahedral layer sandwiched between two tetrahedral layers.

This model concept is conceptually attractive for moderately to highly compacted clays.

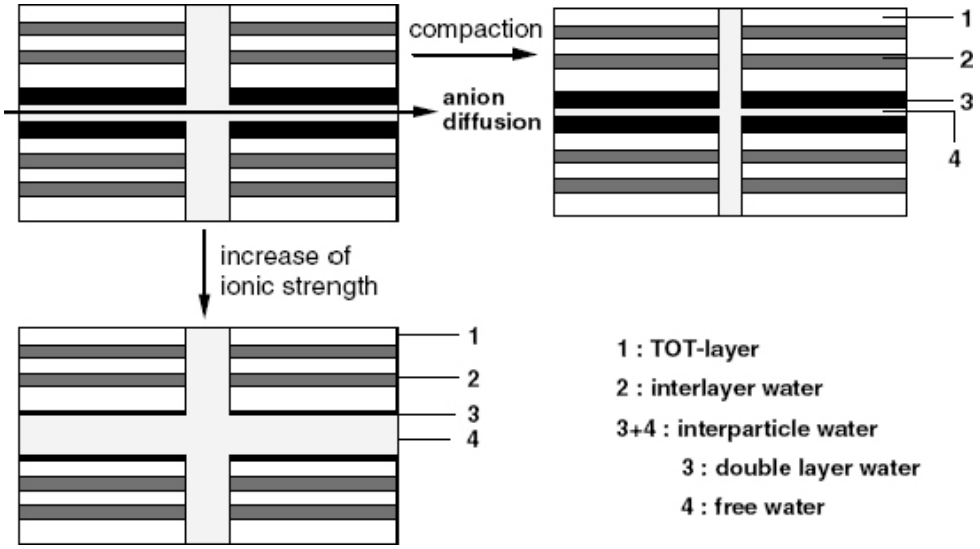

Figure 7-7. *Schematic picture of the pore space of compacted bentonite and the effect of mechanical compaction and changes of ionic strength on the pore space. The total pore space equals the interlayer and the interparticle pore space. The interparticle pore space equals the double layer pore space (3) and the "free" pore space (4). Anion diffusion takes place in the "free" pore space.*

In our model concept, the individual sheets of the smectite are also closely packed in stacks at high dry densities. For decreasing dry densities, the stacks may break up to form stacks with increasingly fewer sheets. At the same time, the stacks themselves expand and the distance between the sheets increases. The sheets in sodium dominated bentonites can delaminate to form individual particles at low ionic strengths. This will happen at solid volume fraction below or well below 1%, depending on the ionic strength in the water. The notion of nanopore water therefore becomes increasingly less viable in dilute gels.

Figures 7-8a to 7-8c show how we conceive the system for the present paper. In the dense system, the diffuse layers overlap and the cations can move in the connected diffuse layers. In a more dilute system, there is weaker connection between the diffuse layers and the ions move in the "free" water, Figure 7-8b. Figure 7-8c shows that in dilute gels the smectite particles can rotate freely at high ionic strengths where the diffuse layer is thin, but at low ionic strengths the particles will interact when rotating as their diffuse layers may touch during rotation. Thus, the surface diffusion contribution could be expected even at low gel densities.

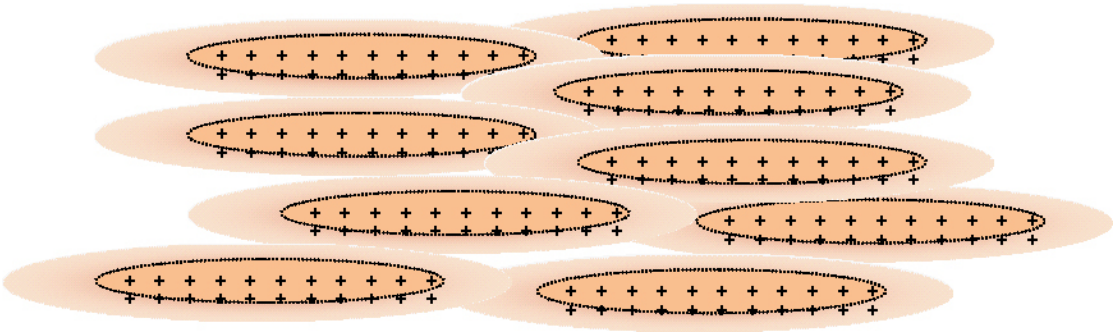

Figure 7-8a. *The particles are so close that the diffuse layers "overlap" allowing the cations to diffuse in the connected diffuse layer. There is very little "free" water.*

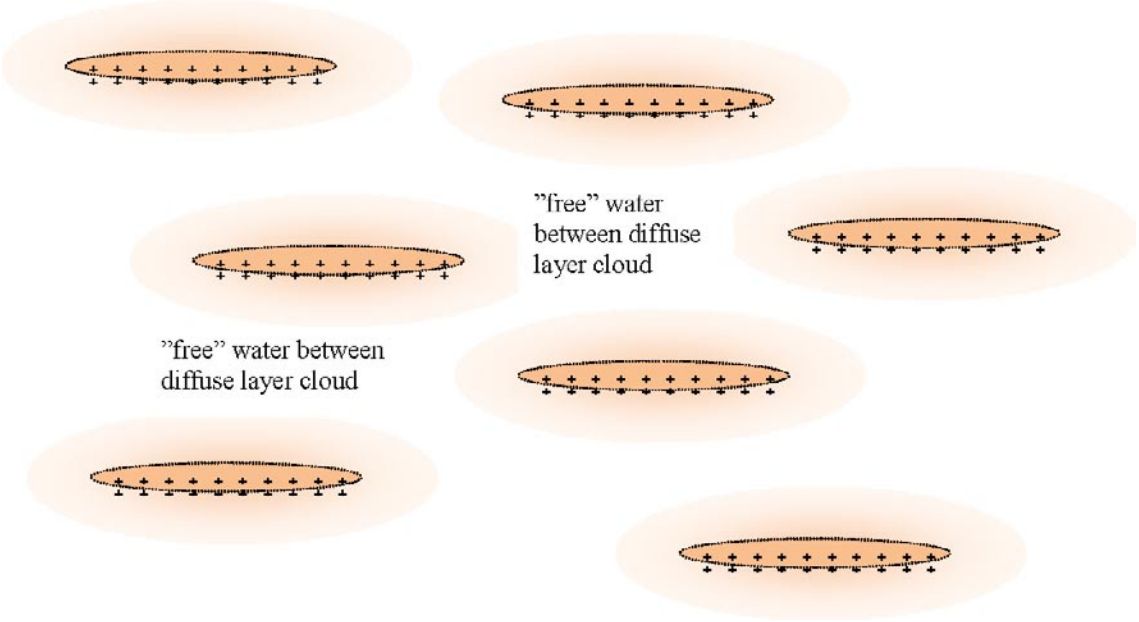

Figure 7-8b. *The particles are far from each other and the diffuse layers are only partly in contact. Ions move also in the "free" water. Sheets still cannot rotate freely due to geometric reasons.*

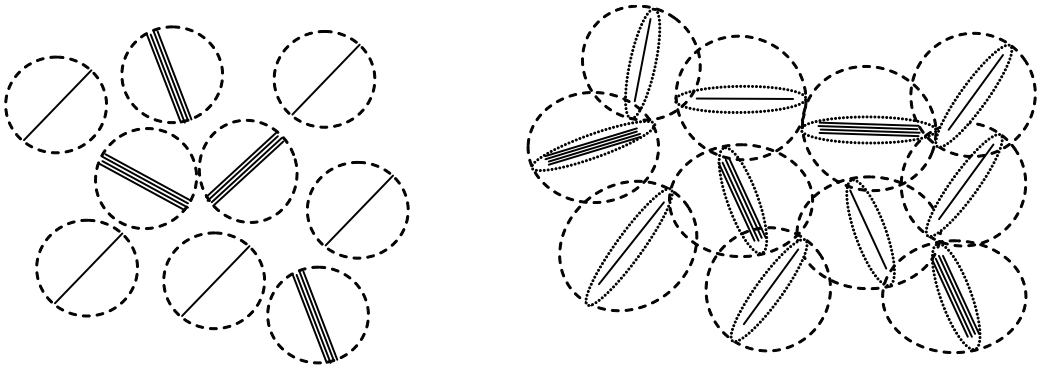

Figure 7-8c. *The particles are far from each other and the diffuse layers are not in contact, left figure. Sheets/stacks can rotate freely. In low ionic strength water double layers may overlap and ions may move both in free water and in overlapping double layers.*

The picture is based on observations that, in sodium dominated clays, the smectite sheets tend to separate and form individual colloidal particles due to double layer repulsion forces /Liu et al. 2009a/. This is of course a much idealized picture but serves our purpose for the present modelling, because our concern is for clays that behave as sodium dominated clays. Strongly calcium dominated clays swell less than sodium dominated clays and do not separate into individual sheets. Stacks with many sheets in close contact remain /Bergaya et al. 2006/.

/Birgersson et al. 2009/ use the term *Donnan contribution* to describe the additional ion concentration in the gel. We use the more illustrative term *"free" water* as we also want to describe very dilute gel/sol systems. This picture is useful when considering the ion exchange and transport processes in both dilute gels and in dense gels. In a dilute gel, the amount of fixed charges and charge compensating ions per unit volume can be small compared to the concentration in the "free" water.

There are further complications. The ion transport in gels is not well described by the conventional Fick's law approach as the movement of one ion will influence the movement of the other ions to maintain charge neutrality. A lower anion flux will hinder the movement of a potentially faster cation and may determine the total ion flux. In a system with more than two mobile ions, a correct modelling becomes complex because of mutual interactions between the different ions. Models exist and are used to achieve this. The Maxwell-Stefan equations are convenient for such situations /Bird et al. 2002, Wesselingh and Krishna 2000/. However, the Maxwell-Stefan equations are not as transparent as Fick's law equations and need diffusion coefficients that are not readily available. The Fick's law formulations can be used in limiting cases when the Maxwell-Stefan and Fick's equations can be transformed in each other. We will use equations which are based on Fick's law and apply them to some limiting cases where they are essentially correct, or at least are not deemed to give large errors compared to other uncertainties present.

7.10 Model used for the calculations

The smectite gel expands into the fracture. In the fracture, the gel can be exposed to water with a different composition at the gel/water interface than what was originally present in the gel. Ions will then start to diffuse between the gel and the water. In very dilute gels, the transport is dominated by diffusion in the "free" water in the gel and not by surface diffusion. This may be essentially correct at low particle concentrations when the electrical diffuse layers of the particles are not very close and practically not in contact with each other. In denser gels, however, this is not correct. There also the ions in the diffuse layer can form continuous paths through the overlapping diffuse layers for the ions to move in. At very low gel densities when the diffuse layers only slightly touch as shown in Figure 7-8c it can also be expected that gel viscosity decreases so as to approach that of water, and that sol formation and gel flow may commence. This is the region where smectite loss can be expected.

For this scenario, we specifically wish to explore if in a situation where the composition of the water in the compacted buffer is different from that in the non-saline seeping water, the calcium/sodium ratio in the smectite could increase to above a limit where the gel becomes so calcium dominated that it will not release colloids at the gel/water interface. We also wish to explore whether the ion concentration at the interface could be above the CCC.

To this end, we may use our dynamic force-balance model to describe the gel expansion in the fracture /Liu et al. 2009a/, giving the following continuity equation, which was described in more detail in chapter 6,

$$\frac{\partial \phi}{\partial t} = \frac{\partial}{\partial z}\left(\frac{\chi}{f} \frac{\partial \phi}{\partial z} \right) \tag{7-13}$$

This together with Darcy equation for flow, the model for gel viscosity as a function of ionic strength and gel volume fraction, as well as the equation for diffusion of ions in the gel is used to calculate the steady state gel concentration profile in the fracture /Moreno et al. 2009/. The present chapter discusses the ion transport in somewhat more detail.

To describe the ion transport in the gel, we base our modelling on the surface diffusion concept, with diffusion coefficients modified as outlined in Equation (7-8). The ion flux is then obtained from

$$J_i = -D_{p,i} \varepsilon_{free} \frac{dc_i}{dz} - D^*_{a,i} \phi \frac{dq_i}{dz} \tag{7-14}$$

where q is concentration of ions in smectite phase and

$$D_{p,i} = \frac{D_{0,i}}{G(\phi)} \tag{7-15a}$$

and

$$D^*_{s,i} = \frac{D_{s,i}}{G(\phi)} \tag{7-15b}$$

where we write D^*_s with the star to indicate that the apparent diffusivity now only includes the surface diffusion part and not the diffusion in the "free" water. For medium to high gel densities these are numerically indistinguishable. The tortuosity function $G(\phi)$ depends on the volume fraction of smectite. /Bourg et al. 2007/ found that it decreased from about 4 to 1 when the dry density decreases from 200 to 0 kg/m^3 and that $D^*_s\phi$ is fairly constant for $0.25 < \phi < 0.7$ for sodium and for $0.07 < \phi < 0.75$ for strontium, as shown in Figures 7-4 and 7-5, respectively.

In Equation (7-14), q_i is the concentration of species "i" in ion exchange positions and it is given by

$$q_i = X_i \cdot CEC \cdot \rho_s / z_i \tag{7-16}$$

where X_i is the equivalent charge fraction of ion "i" in the smectite, $CEC \cdot \rho_s$ is the ion exchange capacity in equivalents per volume of smectite, and z_i is the charge of the ion.

We wish to apply the model to a situation where there is a decreasing smectite fraction in the gel ranging from about ϕ=0.5 to 0.01 or less. At the gel/water interface, smectite gel with its water is continuously lost and carried away by the seeping water in the fracture. At present, we deem that the loose gel flows away as a gel/sol with a viscosity larger but not very much larger than that of water. The gel thus carries with it the water and the smectite particles. New gel enters the fracture from the large reservoir in the deposition hole. The gel expands by the internal repulsive forces between the smectite sheets soaking up water as it expands /Liu et al. 2009a/.

The seeping water has, however, very low ion strength. We will use the two criteria described earlier to assess when the release of colloids could happen. It will take place if the water composition in the water in the gel is below the critical coagulation concentration CCC and if the calcium fraction, X_{Ca}, in the smectite is less than about 0.9. The CCC is around 50 mM when there is only sodium in the water and is about 1 mM if there is calcium in the water but X_{Ca}<0.9. No CCC is defined for water with both calcium and sodium present, but we assume the upper line shown in Figure 7-2 to be a reasonable measure of CCC. If one of these conditions is fulfilled, no colloids are released and

the gel expands further and further out in the fracture, although at a decreasing rate. This we do not conceive as erosion, because the smectite loss will be very slow once the gel has expanded some tens of meters into the fracture.

We have the option to actually model the water flowing in the fracture, how the concentration develops in it as it passes and how it sweeps away the gel/sol by flow of the low viscosity gel or alternatively to use the approximation that at certain $\phi=\phi_{front}$ the gel turns to a dilute sol which flows away. The first option was used in the calculations presented in /Moreno et al. 2009/. As these calculations are very time consuming and sometimes cause numerical instabilities, we choose a simpler approach, based on a pseudo steady state approximation in the present report. The approximate value of the distance to the gel/water interface is where the smectite volume fraction ϕ_{front} is such that the thermal deviation function $\xi=\chi/k_BT$ (explained in /Liu et al. 2009a/) deviates from unity by a small amount. This essentially means that this is the point where the particles disperse into the water mainly by Brownian motion. Then the Q_{eq} concept can be used both for the ions and for the smectite particles. It could include the particle diffusion into the flowing water as well as the advective flow of the dilute gel itself.

Solving the Darcy equation in two dimensions with a ϕ and ion concentration dependent gel sol viscosity is feasible but time consuming. We have derived such a relation for small volume fractions from experimental data but have not been able to do it for higher volume fractions due to lack of experimental data /Liu and Liu 2009/. The simulations with solutions of the Darcy equation coupled to the gel expansion equation and one component (sodium) diffusion suggests that gel/sol advection occurs in a narrow range of ϕ, on the order of 0.01 and less /Moreno et al. 2009/. A steady state penetration of gel into the fracture can be expected to range from a few cm to a metre or more depending on the flowrate of water.

To simplify the modelling of mass transfer to and from the seeping water, we use the Q_{eq} approach for the scoping calculations in this report. This approximates the two dimensional flow and transport in the fracture to a one-dimensional problem, which considerably simplifies the solution. A further important gain with this approach is that it facilitates understanding of how different factors influence the results.

The flux of a species that diffuses into the seeping water and is carried away by it as it leaves the vicinity of the deposition hole can be described by /Neretnieks 1979, Neretnieks et al. 2009b/,

$$J_i = \frac{Q_{eq,i}}{A_{slit}}(c_i^{front} - c_i^w) \tag{7-17}$$

where $Q_{eq,i}$ is the equivalent flowrate for mass transfer between the gel/water interface and the seeping water, A_{slit} is the contact area between the seeping water and gel/water interface, c_i^{front} is the concentration at the interface and c_i^w that in the approaching water.

Combining Equation (7-14) with (7-17) gives, for each ion,

$$-D_{p,i}\,\varepsilon_{free}\frac{dc_i}{dz}(z=z_{front}) - D_{s,i}^{*}\phi\frac{dq_i}{dz}(z=z_{front}) = \frac{Q_{eq,i}}{A_{slit}}(c_i^{front} - c_i^w) \tag{7-18}$$

This seemingly simple expression must be solved simultaneously for all ions, by accounting for charge balance in the "free" water as well as of the different cations in the sorbed state. Furthermore, the variation of tortuosity function G and the variation of D_s^* with ϕ and ionic strength must be known. Much of this information is, however, not known, and therefore we are forced to make some bounding calculations using reasonable assumptions.

Two bounding cases are obvious. One is when diffusion in free water would dominate the transport. The other is when surface diffusion dominates the transport. The first would be expected for dilute gels whereas the second for dense gels. However, the gel through which the transport takes place is dense at one boundary and very dilute at the other, so the transport modes and resistances will vary with the location in the gel. We attempt to solve the equations for cases where the coupling can be disregarded or at least can be expected not to give unreasonable errors. We discuss the deliberations made for the simplifications.

7.11 Steady state solutions

We wish to explore the calcium and sodium concentrations at the gel/water interface with the specific aim to see if the calcium fraction in the ion exchange ions in the smectite is large enough to prevent particle release, according to the hypothesis that when the calcium fraction is larger than about 90% particles are not released. Steady state solutions may give some indications when this may be possible and especially when it would not be expected.

From Equation (7-18) and the equilibrium relation, Equation (7-1) the fluxes of anion and cations can be derived. A more detailed discussion of these conditions is given in /Neretnieks et al. 2009a/.

The flux for the single anion is less dependent of the cation transport in the "free" water, because the cation transport will be dominated by surface diffusion. Also because the anion and cation diffusion coefficients in the "free" water" are similar, the transport can be treated as a single component migration. The anion just carries along whatever cation composition is present at each location, and from Equation (7-18), the flux can be written as,

$$J_{An} = -D_p \varepsilon_{free} \frac{dc_{An}}{dz} = -D_{eAn} \frac{dc_{An}}{dz} \tag{7-19}$$

where D_{eAn} is the effective diffusion coefficient for anions and thus incorporates the effect of tortuosity and anion exclusion.

Equation (7-19) can be solved independently from the other equations and the variation of $D_p\varepsilon_{free}$ with ionic strength and ϕ can be accounted for to obtain the flux and the anion concentration profile. We actually do not do this but choose to solve for a constant value of $D_p\varepsilon_{free}$, which leads to a linear profile.

Different values of $D_p\varepsilon_{free}$ over a wide range are used to assess the sensitivity of this entity.

For the two cation system studied here, sodium and calcium, the fluxes are

$$J_{Na} = -D_p \varepsilon_{free} \frac{dc_{Na}}{dz} - D_s^* \cdot CEC \cdot \rho_s \phi \frac{dX_{Na}}{dz} \tag{7-20}$$

and

$$J_{Ca} = -D_p \varepsilon_{free} \frac{dc_{Ca}}{dz} - D_s^* \cdot CEC \cdot \rho_s \phi \frac{1}{2} \frac{dX_{Ca}}{dz} = J_{An} - J_{Na} \tag{7-21}$$

Charge equilibrium has to be maintained in the "free" water as well as in the ion exchange phase. Thus only one of the Equations (7-20) and (7-21) are needed. A further useful simplification is that $D_s^*\phi$ is constant, see Figures 7-4 and 7-5.

The mass flow rate N is also given by the transport in the seeping water via the Qeq relations for each ion.

$$N_i = Q_{eq,i}(c_i^{front} - c_i^w) \tag{7-22}$$

The boundary conditions at z=0 at the deposition hole are

$$c_i(z = 0) = c_{i,z=0} \tag{7-23}$$

Some exploratory results for a simple case where at the inlet end of the fracture conditions are known as well as those in the approaching seeping water are presented. Two limiting cases are modelled. In the first, it is assumed that transport only takes place in the "free" water and then D_s^*=0. In the other case, the transport of cations is only due to diffusion of the ions in ion exchange position and D_p is neglected for the cations. Both cases are idealized, because in reality both processes are active and their relative magnitude depends strongly on the fraction of solids in the gel and on the ion concentration.

7.11.1 A simple solution when $D_s^*=0$

When transport only takes place in the "free" water in the gel, steady state linear concentration profiles are established provided that $D_p\varepsilon_{free}$ is constant. Figure 7-9 shows the concentration profile of ions in the "free" water in the gel and in the seeping water outside the gel/water interface. It is seen that the concentration at the interface is higher than that in the seeping water. Note, however, that $D_p\varepsilon_{free}$ actually varies over several orders of magnitude when ϕ and c_{An} change and this assumption is over-simplified. Nevertheless, the flux will be mostly influenced by the region where $D_p\varepsilon_{free}$ is smallest and therefore we will use low values for the base case calculations.

In addition, for these steady state solutions, it is assumed that the expansion of the gel has stabilized so that z_{front} is constant and is known.

In this case, only ions in the "free" water are mobile. The boundary conditions are: high concentration at z=0 and low in the approaching seeping water. The anion and the two cations diffuse outward, uninfluenced by the presence of the ion exchange at steady state. The concentration of the anions and the cations at the gel/water interface are then determined by the relative transport resistances in the gel and in the seeping water. This can be directly obtained from the flux equations shown previously.

This case could possibly be a fair approximation for a very dilute gel. However, even if such a gel exists near the gel/water interface, it will be preceded in the ion transport path by a much denser gel where other transport processes dominate. Especially the diffusion of anions compared to the diffusion of cations in the "free" water will be less in the denser gel because there is less "free" water and therefore much less anions. The resulting X_{Ca} values will therefore be larger than they will be when a denser gel is present nearer the deposition hole. Nevertheless we want to present this case for illustration purposes and to give an upper bound for X_{Ca} values. For the anion, Equation (7-18) gives

$$-D_p\,\varepsilon_{free}A_{slit}\frac{dc_{An}}{dz}(z=z_{front})=Q_{eq}(c_{An}^{front}-c_{An}^{w}) \tag{7-24}$$

As the right hand side is constant, the gradient will depend on how $D_p\varepsilon_{free}$ varies with c_{An} and z. For the simplified discussions that follow, we chose constant values of this entity and obtain a linear concentration profile. This simplified case is reasonable when anion exclusion is important. Thus, we have

$$N_{An}=D_p\,\varepsilon_{free}A_{slit}\frac{c_{An,z=0}-c_{An}^{front}}{z_{front}}=Q_{eq}(c_{An}^{front}-c_{An}^{w}) \tag{7-25}$$

so that

$$c_i^{front}=\frac{c_{i,z=0}+B_i\,c_i^{w}}{1+B_i} \tag{7-26}$$

with

$$B_i=\frac{Q_{eq}z_{front}}{D_w\varepsilon_i A_{slit}} \tag{7-27}$$

It may be noted that, in this case when the ions move only in the free water, the above two equations are valid also for the cations in the "free" water. Hence, if the composition of the "free" water in the gel at the entrance of the fracture $c_{i,z=0}$ and in the seeping water c_i^w is known, c_i^{front} can be obtained, as given in Equation (7-26,) and then be used to calculate $X_{Ca,front}$.

In Equations (7-25) and (7-27), the contact area between the seeping water and gel/water interface can be explicitly written as

$$A_{slit}=(2r_h+2z_{front})\cdot\pi\cdot\delta_{fr} \tag{7-28}$$

where r_h is the radius of the deposition hole and δ_{fr} the fracture aperture.

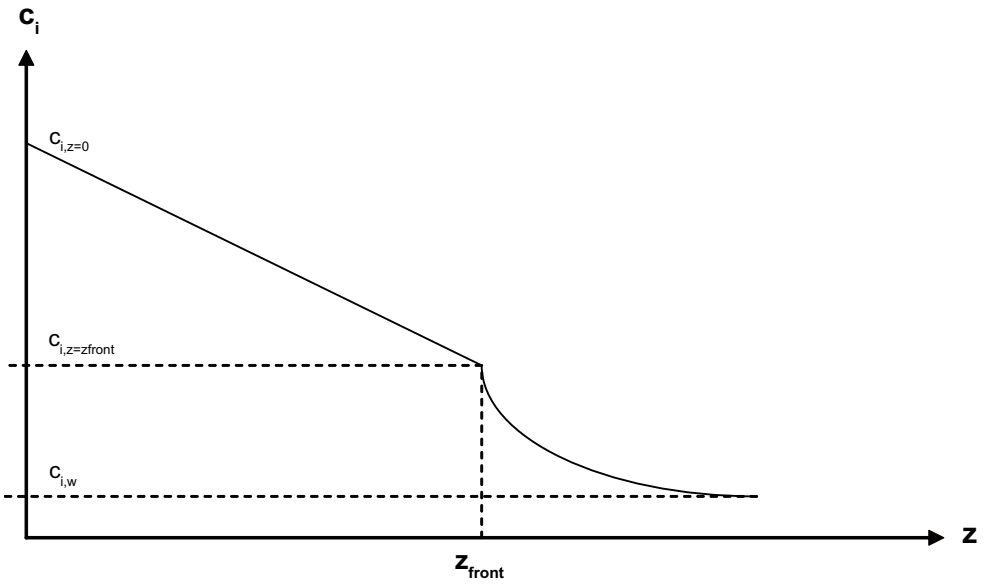

Figure 7-9. *Concentration of ions in "free" water in gel and in seeping water at steady state.*

The equivalent flowrate for mass transfer between the gel/water interface and the seeping water Q_{eq} can, on the other hand, be obtained from /Chambré et al. 1982/.

$$Q_{eq} = 4.5135\sqrt{TiD_{wseep}\,\delta_{fr}\,(r_h + z_{front})} \qquad (7\text{-}29)$$

where T is transmissivity, i hydraulic gradient and D_{wseep} is the diffusivity in the seeping water, which is like in unconfined water but deemed to be larger than the diffusivity in the "free" water as conceptualised in Figure 7-7.

General data used for the simulations are: Diffusivity D_{wseep}= $2\cdot10^{-9}$ m²/s, and $D_p\varepsilon_{free}=D_{wseep}/10$ in the central case. The radius of deposition hole r_h=0.875 m, and hydraulic gradient, i= 0.1. Other data are chosen such that they are reasonably representative for the expected conditions. For example the seeping water is assumed to be the Grimsel water /Missana et al. 2003/. The thickness z_{front} of the gel in the fracture is chosen from simulations of its rates of expansion and loss due to colloid release by /Moreno et al. 2009/. It is 0.5 m in the base case.

The total ion concentration in the seeping water c_w is taken to be 1 mM in the base case, which are taken from /Bradbury and Baeyens 2003/ but increased to round figures. Of this Ca makes up 0.14 mM. It should be noted that the concentrations in the buffer in the deposition are assumed to kept constant. In reality, however, they will drop over time as the dissolved species are depleted and especially the calcium concentration will drop much when gypsum is exhausted. Some results are presented in Table 7-4 below.

Table 7-4. Some calculated cases for diffusion in "free" water. First line is taken as a central case. In the other lines only deviations from the central case are shown.

$c_{tot,z=0}$ mM	$c_{Ca,z=0}$ mM	z_{Front} m	T m²/s	δ_{fr} mm	$D_p\varepsilon_{free}/D_{wseep}$	c_w mM	$c_{w,front}$ mM	$c_{Ca,front}$ mM	$X_{Ca,front}$	Q_{eq} l/yr
300	**30**	**0.5**	**10^{-7}**	**1**	**0.1**	**1**	**1.69**	**0.208**	**0.950**	**23.5**
1,000							3.30	0.209	**0.899**	23.5
	150						1.69	0.485	**0.973**	23.5
		0.1					3.88	0.427	**0.920**	19.9
			10^{-6}				1.22	0.162	**0.959**	74.6
				0.1			1.22	0.162	**0.959**	7.46
					0.001		1.007	0.141	**0.964**	23.5
						10	10.67	0.209	**0.700**	23.5

It is seen that for the calculated cases $X_{Ca,front}$ range from 0.700 to 0.972. It may also be noted that in all cases $c_{Ca,front}$ is below 1 mM, which is the expected CCC for calcium. This implies that for the case when $X_{Ca,front}$ <0.9 erosion could occur. All the calcium that goes into the ion exchange potions and increases $X_{Ca,front}$ comes from the buffer in the deposition hole. The source of calcium will eventually be exhausted. This effect will be explored in a later section when mineral dissolution effects are explored.

The above example shows that there are conditions that could give $X_{Ca,front} > 0.9$ at the gel/water interface and thus hinder loss of smectite considering only equilibrium conditions. We now consider how much smectite could attain $X_{Ca,front} > 0.9$ starting from $X_{Ca,front} = 0.5$ by the supply of diffusion. This can be directly obtained using Equation (7-25) by considering a limit case that the calcium enters the smectite instead of migrating further into the seeping water. The sodium expelled from the smectite will continue to migrate to the water accompanied by the sulphate. Using the same data for the base case, we have

$$N_{Ca} = D_p \varepsilon_{free} A_{slit} \frac{c_{Ca,z=0} - c_{Ca}^{front}}{z_{front}} = 2 \cdot 10^{-10} (1.75+1)\pi\, 0.001 \frac{30 - 0.208}{0.5} =$$

$$= 1.036 \cdot 10^{-10} \ mmol/s \ or \ 3.26 \cdot 10^{-3} \ mmol/y.$$

This amount of calcium is sufficient to increase $X_{Ca,front}$ from 0.5 to 0.9 in 16.3 mg/yr of smectite, which would then be hindered from dispersing into the seeping water. This amount of smectite is, however, entirely negligible compared to the release expected by particle diffusion and gel flow. Therefore, the smectite erosion will not be impeded in this case.

Note that we have in the calculations neglected the mobility of the ion exchange ions. This is unrealistic in denser gels, and the influence is explored below.

7.11.2 Solution when migration of ion-exchange ions dominates transport

A more realistic situation is presented below. The diffusion of the sorbed ions can be considerably larger than in the "free" water as is shown below.

The fluxes in the "free" water and in the gel can be compared by inspecting Equations (7-14) and (7-16). Equation (7-14) is slightly re-written using the mole fraction gradient $\frac{dx_{Ca}}{dz}$ in the water instead of concentration gradient to facilitate comparison of ion fluxes in water and on solid. This gives

$$J_{Ca} = -D_p \varepsilon_{free} c_{tot} \frac{dx_{Ca}}{dz} - D_s^* \cdot CEC \cdot \rho_s \phi \frac{1}{2} \frac{dX_{Ca}}{dz} = J_w + J_s \qquad (7\text{-}30)$$

where x_{Ca} is the mole fraction of calcium in the water.

An estimate of the relative fluxes in "free" water J_w and by surface diffusion J_s can be made from Equation (7-30). For the same relative gradients $\frac{dx_{Ca}}{dz}$ and $\frac{dX_{Ca}}{dz}$ the ratio $\frac{J_s}{J_w} = \frac{D_s^* \cdot CEC \cdot \rho_s \phi}{D_p \varepsilon_{free} 2 c_{tot}}$ can be assessed under different conditions.

Note that *CEC* is about 1 eq/kg, and ρ_s is ~ 2,700 kg/m^3. The total ion concentration in "free" water is expected to range from some 100 down to 1 mol/m^3 or lower. The gel volume fraction ranges from ϕ=0.5 to 0.01 in the expanding gel. The free water diffusion term varies, however, over a wide range as was shown in Figure 7-3. In dilute gels the anion exclusion will be marginal and the diffusion coefficient will approach that in water. Thus, for several credible conditions, as listed in Table 7-5, the flux in the gel phase can be considerably larger than in the "free" water.

Table 7-5. Relative flux of calcium in gel water and in "free" water for $D_s\phi = 2 \cdot 10^{-11}$ m^2/s.

$D_p\varepsilon_{free}$ c_{tot} mol/m^3/	$D_p\varepsilon_{free} = 10^{-9}$ m^2/s (would represent low ϕ)	$D_p\varepsilon_{free} = 10^{-12}$ m^2/s (would represent high ϕ)
1	27	27,000
100	0.27	270

Consequently, we now assume that the diffusion in the gel phase for the cations is much larger than in the "free" water and neglect the latter. This leads to a formulation identical to that used for a Donnan gel if we define the entity

$$D_X = D_s^* \cdot CEC \cdot \rho_s \phi \tag{7-31}$$

The transport equations become as before for the anions

$$J_{An} = -D_p \varepsilon_{free} \frac{dc_{An}}{dz}(z = z_{front}) = \frac{Q_{eq}}{A_{slit}}(c_{An}^{front} - c_{An}^{w}) \tag{7-32}$$

But for the cations that diffuse only in the ion exchange positions, the equation becomes for sodium

$$J_{Na} = -D_X \frac{dX_{Na}}{dz}(z = z_{front}) = \frac{Q_{eq}}{A_{slit}}(c_{Na}^{front} - c_{Na}^{w}) \tag{7-33}$$

and because

$$X_{Ca} + X_{Na} = 1 \tag{7-34}$$

for calcium, we have

$$J_{Ca} = -\frac{1}{2} J_{Na} = \frac{1}{2} D_X \frac{dX_{Na}}{dz}(z = z_{front}) = \frac{Q_{eq}}{A_{slit}}(c_{Ca}^{front} - c_{Ca}^{w}) \tag{7-35}$$

This implies that if Na diffuses from the entrance of the fracture towards the seeping water, Ca must diffuse from the water into the gel. This further implies that if sodium migrates from the gel to the seeping water $c_{Ca}^{front} < c_{Ca}^{w}$. Because X_{Ca} increases strongly with decreasing total ion concentration for a given Ca/Na ratio it can be expected that X_{Ca} will increase with z.

Using the observation that $D_a^* \phi$ varies little, $\frac{dX_{Ca}}{dz}$ can be approximated to be constant at steady state, and the problem is simplified to finding the c_{Ca}^{front} for which

$$-D_X A_{slit} \frac{X_{Ca,front} - X_{Ca,z=0}}{z_{front}} = Q_{eq}(c_{Ca}^{front} - c_{Ca}^{w}) \tag{7-36}$$

This is readily done with the help of the equilibrium relation after having solved the anion concentration profile as before, Equation (7-26) which gives the total anion as well as cation concentration at the front. Equation (7-36) contains the two unknowns $X_{Ca,front}$ and c_{Ca}^{front} which are related by the equilibrium relation Equation (7-1).

Figure 7-10 shows an illustration of the concentration profiles for this case. It may seem surprising that the concentration gradients in the pore water and the seeping water have different signs at the front but it should be remembered that the diffusion in the "free" water for the cations is assumed to be negligible compared to that on the smectite. The X_{Ca} gradient in the gel is in the same direction as in the seeping water so the transport is into and through the gel.

The same base-case data as the previous section are used here. In addition, the diffusion coefficients for the cations are taken as an average of the $D_a^* \phi$ data in Figure 7-4. This gives, with $D_s^* \phi = 0.2 \cdot 10^{-10}$ m^2/s, CEC=1 eq/kg and ρ_s=2,700 kg/m^3, the value of $D_X = 5.4 \cdot 10^{-8}$ eq/s/m. The results of the sensitivity analysis are tabulated in Table 7-6.

It is seen that the results are quite sensitive to the parameter values. It cannot be ruled out that $X_{Ca,front}$ can be considerably less than 0.9 at the same time as $c_{Ca,front}$ is well below the CCC.

From the quite different results shown in Tables 7-4 and 7-6, it may be concluded that neglecting the mobility of the ion exchange ions can lead to major errors qualitatively as well as quantitatively. Note that many commonly used geochemical codes that also can handle transport assume that ions in exchange positions are immobilised so results from such calculations should be used with caution.

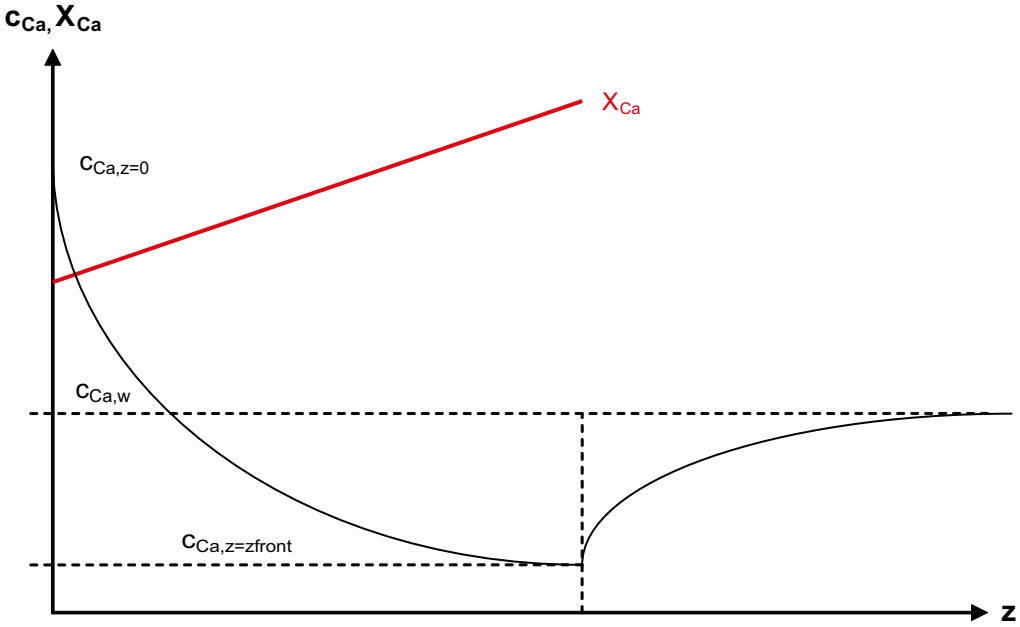

Figure 7-10. Concentration profiles of calcium on smectite, calcium in "free" water and in smectite and in seeping water.

Table 7-6. Some calculated cases for diffusion in gel. First line is taken as a central case. In the other lines only deviations from the central case are shown.

$C_{tot,z=0}$ mM	$c_{Ca,w}$, mM	$X_{Ca,z=0}$	z_{Front} m	$D_X\,10^8$ eq/s/m	$D_p\varepsilon_{free}/D_{wseep}$	T m^2/s	δ_{fr} mm	c_w mM	$c_{Ca,front}$ mM	$X_{Ca,front}$	Q_{eq} l/yr
300	0.14	0.3	0.5	5.4	0.001	10^{-7}	1	1	0.00058	0.524	23.6
	0.25								0.0019	0.698	23.6
		0.7							0.0191	0.894	23.6
			0.1						0.00021	0.353	19.9
				0.54					0.0991	0.956	23.6
					1				0.0016	0.522	23.57
						10^{-6}			0.0217	0.900	74.5
							0.1		0.0217	0.900	7.45
								10	0.0395	0.461	23.6
1,000									0.00060	0.524	23.6

7.12 CEC and distance to front and presence of gypsum in gel

7.12.1 Rapid release of colloids at front

In the previous sections, it was assumed that a steady state thickness of the gel is established and that the thickness, or distance to gel/water interface, was on the order of 0.1 to 0.5 m. This was based on scoping calculations, in which the not very viscous gel/sol itself flows downstream allowing new gel to expand into the fracture so that eventually a steady state is reached where the same amount of gel enters the fracture as the amount that flows away /Moreno et al. 2009/.

No unusual gravity effects were accounted for in these calculations. However, there are observations that a gel/sol, below CCC rapidly disengages particles from the gel that can sediment downward from the gel/water interface /Jansson 2009/. This release and sedimentation is much faster than can be explained by the sedimentation of individual colloid particles. The mechanisms of this process are not understood. Under such circumstances an extensive continuous gel may not form, which otherwise could act as a thick diffusion barrier and it was found to be important in the previous calculations.

If we assume that the particles disengage themselves at a location where concentration in the gel drops to CCC, and rapidly escape, we can calculate the gel thickness where this happens using the relations obtained in section 5.3. If we say that the calcium in the gel is calcium sulphate (gypsum), which has a much higher solubility than the CCC, there will be a net transport of calcium towards the seeping water. The rate of transport is determined by the concentration difference between the entrance to the fracture and the seeping water. The overall transport resistance for the diffusing species is the sum of that in the gel and in the seeping water. That is what Equation (7-36) describes. Equation (7-36) can be solved for the distance z_{front} where the calcium concentration is equal to CCC instead of solving for the calcium concentration for a given gel thickness.

With the same values as in the base case in Table 7-6 (first line) it is found that the CCC is reached just a fraction of mm from the entrance to the fracture, z_{front} <1 mm, where the gel can turn to sol. At this location X_{Ca} is only slightly less than the value at the fracture entrance. The calcium transport is thus in the same direction in the "free" water as in the DDL water. . The rate of loss of smectite is then proportional to the rate of loss of calcium in the gel. This was the basis for the 0th order model /Liu and Neretnieks 2006/.

One question to address is whether even faster release could take place. This could occur if there is much less dissolved or soluble calcium in the clay so that CCC could not be exceeded.

Several investigations have been made to assess the pore water composition in the compacted buffer. /Bradbury and Baeyens 2003, Wersin 2003, Ochs et al. 2004, Wersin et al. 2004, Arcos et al. 2006/ modelled porewater compositions in compacted bentonites after initial intrusion of different groundwaters. In general, they found that, after water saturation, the pore water in the compacted gel would contain several mM calcium and that initially present calcium could to some extent remain undissolved.

In the next section, we explore the fate of gypsum (calcium sulphate), as the compacted gel expands into the fracture acquiring more and more water into which the gypsum can dissolve and at the same time ion exchange Na in the smectite for Ca, eventually decreasing the calcium concentration in the water in the gel to below CCC. This can happen even when there is no loss of calcium to the seeping water.

7.12.2 Calcium concentration profile in gel

Some bentonites contain gypsum in percent amounts. When the bentonite is wetted initially, some gypsum dissolves and some of the calcium is ion exchanged for sodium in the smectite releasing sodium to the water in the gel. In the highly compacted gel. not all gypsum may dissolve in this way. However, when the gel expands into the fracture taking up more water, more gypsum dissolves, ion exchanges calcium with the smectite whereby the smectite turns increasingly more calcium rich, i.e. X_{Ca} increases. We explore this process here by calculating the concentration of calcium in the water at different volume fractions ϕ in the gel. Note that no transport of ions is assumed to take place. The system described only depicts mixing bentonite with water in increasing proportions. If loss of gel or transport of solutes are to be considered these effect must be accounted for.

This is done by solving the mass balance equation for calcium, and sodium in a system where a mass of smectite with initial X^0_{Ca} and a mass of gypsum, m^0_{gy}, are equilibrated in a given water volume. The equilibrium relation, Equation (7-1), combined with the mass balances of Ca and Na are solved.

The mass balance for Ca is

$$V_w c_{Ca} + \frac{1}{2} m_{smec} CEC \cdot X_{Ca} + \frac{m_{gy}}{M_{gy}} = \frac{1}{2} m_{smec} CEC \cdot X^0_{Ca} + \frac{m^0_{gy}}{M_{gy}} \quad (7\text{-}37)$$

and for Na

$$V_w c_{Na} + m_{smec} CEC \cdot X_{Na} = m_{smec} CEC \cdot X^0_{Na} \quad (7\text{-}38)$$

where m_{smec} and m_{gy} stand for masses of smectite and gypsum, M_{gy} for gypsum mole mass and superscript 0 stands for what was originally in the system before adding a volume V_w of fresh water.

The water volume is related to the volume fraction in the following way,

$$V_w = \frac{m_{smec}}{\rho_s}\frac{(1-\phi)}{\phi} \tag{7-39}$$

The solubility constant for gypsum was estimated to be K_{gy}=240 (mol/m³)² /CRC 1980/ and it sets up a relation between calcium and sodium concentrations, i.e.

$$K_{gy} = c_{Ca} \cdot c_{SO_4} = c_{Ca}(c_{Ca} + \frac{1}{2}c_{Na}) \tag{7-40}$$

Equations (7-37) to (7-40) together with the ion exchange equilibrium relation, Equation (7-1), are solved to obtain c_{Ca} as a function of ϕ. We only consider the case when all gypsum has been dissolved and determine at what ϕ this occurs. The system is further diluted as ϕ decreases. Before all gypsum has dissolved the ion concentration is set by the solubility equilibrium. We do not discuss the latter case.

Figures 7-11 and 7-12 show results for a case where there is 10 g and 20 g gypsum in 1 kg smectite, respectively. The starting X_{Ca}=0.3. This would be representative of Deponit CA-N, which also has nearly 20 g gypsum/kg /Arcos et al. 2006/.

In the ranges shown all gypsum has dissolved, the calcium being taken up by the smectite. At higher volume fractions ϕ than those shown in the figure, some gypsum remains and calcium and sulphate concentrations are equal to the maximum values shown in the figures.

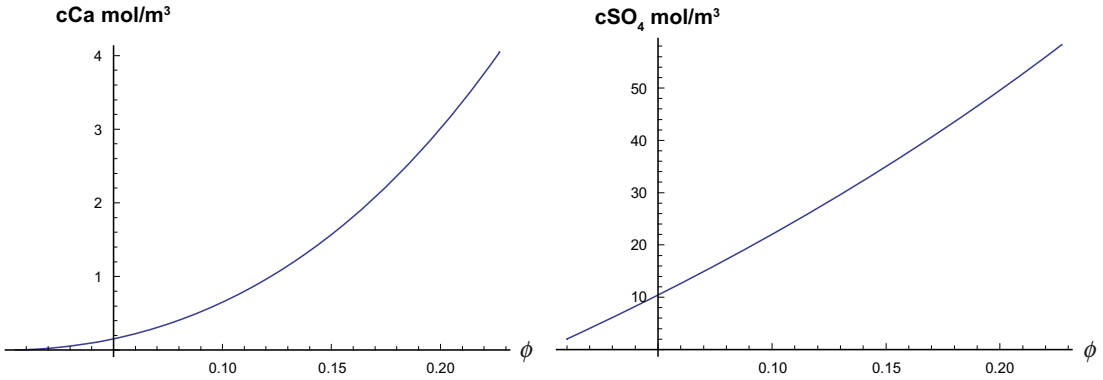

Figure 7-11. *Calcium and sulphate concentrations with different volume fractions smectite, assuming that gypsum has been fully dissolved. 10 g gypsum/kg smectite. The starting X_{Ca}=0.3.*

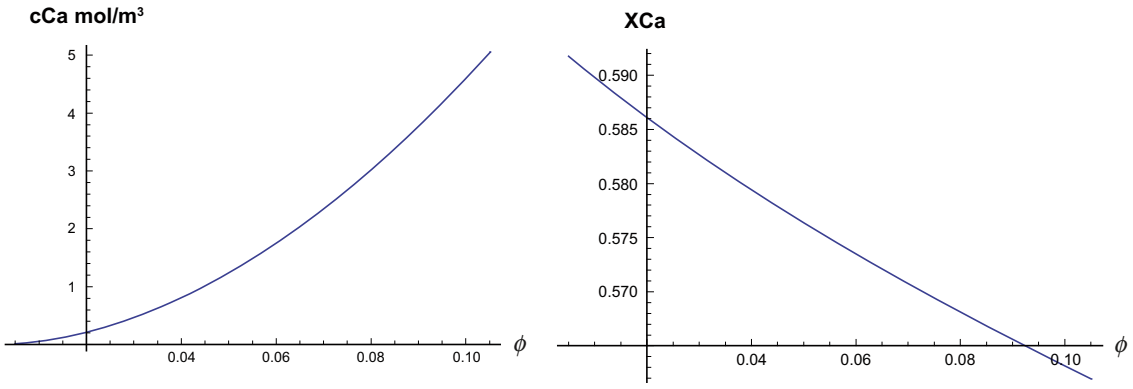

Figure 7-12. *Calcium concentration and calcium fraction in smectite with different volume fractions smectite, assuming that gypsum has been fully dissolved. 20 g gypsum/kg smectite. The starting X_{Ca}=0.3*

It is seen that X_{Ca} is well below 0.9 in all cases. Gypsum remains undissolved at $\phi > 0.23$ and $\phi > 0.12$ for 10 and 20 g gypsum, respectively. c_{Ca} is about 5 mol/m^{3}at this point. At a volume fraction of about 0.13 and 0.04 the calcium concentration is 1 mol/m^3 (mM) for the two cases which we take as a typical CCC value for calcium. When the gel expands further, c_{Ca} decreases below CCC.

In these calculations, the calcium in the water in the gel has not been washed away by diffusion into the seeping water. It has been internally depleted by ion exchange with the smectite. The results thus imply that gel can turn to sol and enter the seeping water as colloids at some distance where the repulsion forces are dominated by Brownian motion. This will occur when ϕ is on the order of 0.01. Release of gel/sol by advective flow is also expected at the lower volume fractions under these conditions.

In sodium dominated clays containing even a few percent gypsum, however, neither the CCC criterion nor the X_{Ca} criterion will hinder smectite loss.

An example with very large initial X_{Ca}=0.5 and 20 g gypsum is presented in Figures 7-13 and 7-14. X_{Ca} is still less than 0.9 but c_{Ca} is above CCC still at around ϕ=0.01. Thus, one would have to go even higher initial X_{Ca} to ensure that one or both of the criteria could be upheld. On the other hand, it is noted that increasing the gypsum content to 40 g results in X_{Ca} fraction larger than 0.9 for ϕ less than some percent.

Below we explore how diffusional exchange would further influence the conditions at the gel/water interface. We again emphasize that the above calculations show the gypsum dissolution and ion exchange when the smectite is just equilibrated with increasing amounts of water. No loss of smectite or ions to the seeping water is accounted for. It is found that an expansive gel can result under such circumstances implying that conditions would favour the gel to expand further and further into the fracture.

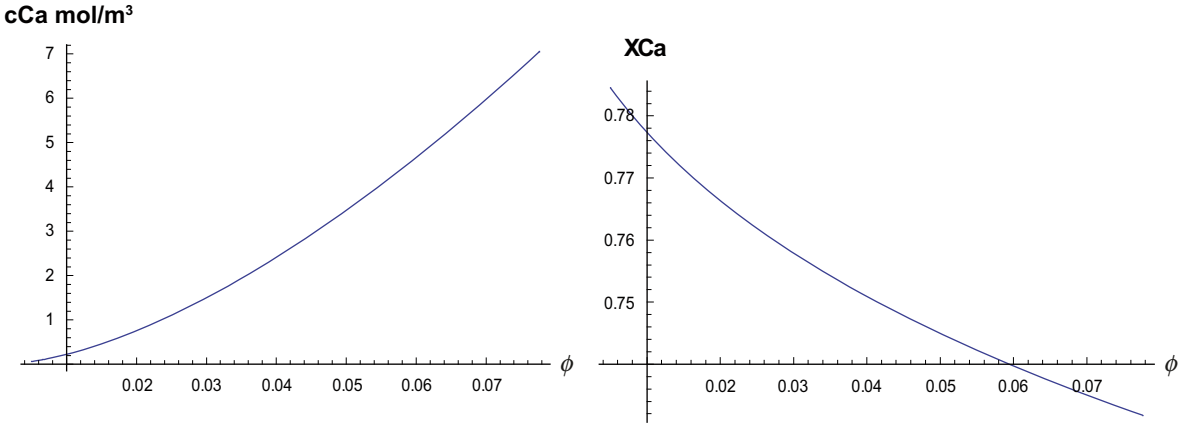

Figure 7-13. *Calcium concentration and calcium fraction in smectite with different volume fractions smectite. 20 g gypsum/kg smectite. The starting X_{Ca}=0.5.*

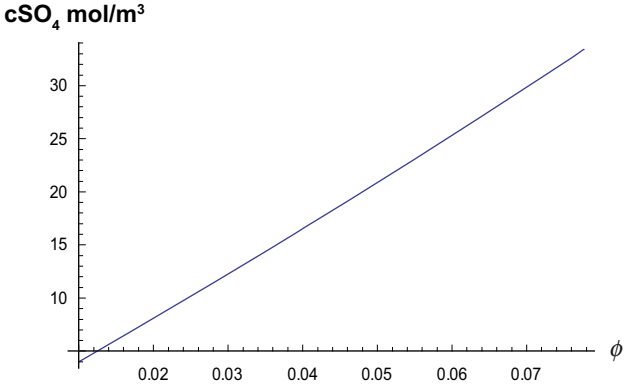

Figure 7-14. *Sulphate concentration for different volume fractions smectite. 20 g gypsum/kg smectite. The starting X_{Ca}=0.5.*

Should there be loss of smectite at some location, eventually a steady state would be reached with new smectite entering from the deposition hole and smectite being lost at the gel/water interface. However, the mode of loss will influence if the dilution, the gypsum dissolution and ion exchange will occur as described above. If the loss is due solely to smectite particle release from the interface, the water in the gel in the fracture is stagnant and will be saturated with gypsum as more smectite and gypsum move into one end of the fracture and smectite is lost the other end. The simple dilution model is not valid then and the full model including ion migration must be used.

If, on the other hand, the dilute gel with its water is swept away by flow due to a decrease of the viscosity of the gel, new water will also be brought in to the gel entering from the deposition hole. The dissolution (at least partly the effects of dilution) and ion exchange will remain.

7.12.3 Exploration of influence of dissolution of soluble minerals by geochemical modelling

In the previous section, some simplified calculations were presented where dissolution of gypsum and ion exchange equilibrium was used to explore how the pore water composition and the cation fractions in the exchange positions change when the clay expands and takes up more and more water. In this section, we continue this exploration by more elaborate geochemical modelling. We include the presence of other minerals, primarily calcite but also allow a calcium-montmorillonite to dissolve, potentially freeing calcium to the pore water and also influencing the pH. It is further attempted to assess which of other minerals could possibly participate in the reaction by e.g. precipitating new minerals such as amorphous silica, silicates and aluminium-silicates.

In the modelling, clay is taken to contain smectite with known CEC and equilibrium relation for sodium, potassium, calcium and magnesium. The minerals gypsum, calcite, dolomite, amorphous silica and surplus of kaolinite or calcium montmorillonite are present initially. The latter three minerals are present in large quantities. The former minerals are present in the amounts that have been experimentally found in the clays and they may be exhausted by dissolution. Kaolinite is used as a proxy for sodium-montmorillonite for which we have found no reliable thermodynamic data. In some simulations calcium-montmorillonite is used instead of kaolinite, which may be a better choice in calcium dominated systems. This is done to explore if and how much smectite could dissolve and potentially supply the pore water with additional cations and also influence pH. Thermodynamic data for the mineral reactions are taken from the database supplied with the geochemical program PhreeqC, /Parkhurst and Appelo 1999/, which is used in the simulations. Surface complexation and ion exchange data are taken from /Bradbury and Baeyens 1999, 2003, 2009/.

Two different clays were used in the modelling, Wyoming MX-80 and Deponit CA-N. Data for the clays are found in /Karnland et al. 2006/. The data are summarized in Table 7-7, where MX denotes the equivalent fraction of the ion exchange capacity taken up by metal M, and S=OH sites denotes the moles of sites per kg of the clay that can be de-protonated or protonated. Note that the CA-N clay has dolomite as well as gypsum and calcite. Dolomite contains magnesium in addition to calcium, and one can expect that magnesium stabilizes the gel similarly to calcium.

Table 7-7. Data for the two bentonite clays used in simulations.

	MX-80	CA-N
Montmorillonite kg/kg	0.835	0.81
Calcite kg/kg	0.002	0.053
Gypsum kg/kg	0.009	0.004
Dolomite kg/kg	0	0.013
CEC eq/kg	0.75	0.70
NaX % eq	72	24
KX % eq	2	2
CaX_2 % eq	18	45
MgX_2 % eq	8	29
Total S=0H sites	0.08	0.08

In the calculations, 1 kg clay is mixed with M_W kg deionised water. M_W is taken to be 10, 37 and 100 kg. This will give volume fractions of smectite in water equal to about 0.029, 0.008 and 0.003 for both clays. Within the range 0.001 to 0.01, the smectite particles can start to be released as colloids if the pore water composition is below CCC and when the fraction of X_{Ca} is less than 0.9.

We are thus looking for the pore water composition and the value of X_{Ca} for different water masses added to 1 kg of clay. The results are tabulated in Table 7-8, where only the case M_W = 37 kg is presented for MX-80 as all minerals already have dissolved then and further dilution gives small changes in X_{Ca}.

It is seen that for MX-80 the Na concentration is well below the CCC for Na, which is in the range 25 to 100 mM. The calcium concentration is 0.03 mM, which is well below the CCC for calcium, about 1–2 mM. X_{Ca} is 0.42, which is well below 0.9.

For CA-N clay, the Na concentration in the water is below CCC as is the sum of Ca and Mg. However, with M_W 37 kg $X_{Ca} + X_{Mg} = 0.864$ and with M_W = 100 kg, $X_{Ca} + X_{Mg} = 0.916$. Thus if smectite with $X_{Ca} + X_{Mg} > 0.9$ stabilizes the clay, the CA-N might reach this value. It can be seen from the table that it is the initial high content of calcium and magnesium in the smectite and the presence of calcite and dolomite that gives the favourable conditions, as the dolomite supplies the water with Mg in addition to Ca. Calcite alone would not have dissolved sufficient Ca to attain $X_{Ca} > 0.9$ but comes near. The presence of small amounts of gypsum contributes but does not seem to be crucial as long as there is sufficient calcite and dolomite.

An additional observation of interest is that the surface charge and surface potential of the edge sites is clearly negative and about –0.13 V and thus will hinder edge to face agglomeration of the smectite sheets.

The kaolinite has dissolved in negligible quantities but the amorphous silica dissolves to equilibrium concentration. Aluminium hydroxide is strongly under-saturated. About 10% of Ca and Mg in solution are found as sulphate complexes. Other values of M_W give similar results. Changing kaolinite to calcium-montmorillonite makes negligible difference in the results. Some silicates and aluminosilicates for which thermodynamic data are available in the database are oversaturated. These are albite (slightly), chlorite, illite (slightly), K-feldspar and K-mica, sepiolite and talc. They are not likely to form under experimental conditions in the laboratory, but it cannot be ruled out that over long times they may influence the pore water chemistry by precipitating, especially the magnesium minerals.

/Wersin 2003/ made similar modelling using essentially the same thermodynamic data and also compared the results with the experiments by /Muurinen and Lehikonen 1999/. Their results are very similar to those presented here. Wersin also used alternative thermodynamic data in some simulations but found no major differences in the results.

Note that these simulation results with PhreeqC give similar calcium and sulphate concentrations as the model in the last section.

Table 7-8. Resulting compositions after equilibration at a temperature of 25°C.

M_W kg water/kg clay	37 MX-80	10 CA-N	37 CA-N	100 CA-N
NaX Equivalent %	48.3	16.6	12	7.3
KX Equivalent %	1.8	1.9	1.6	1.1
CaX_2 Equivalent %	42	50.2	53	56.2
MgX_2 Equivalent %	8	31.6	33.4	35.4
Undissolved Calcite mol	0	0.55	0.55	0.55
Undissolved Dolomite mol	0	0.059	0.052	0.0365
Undissolved Gypsum mol	0	0	0	0
pH	9.17	8.93	9.17	9.14
Na in solution mM	5.5	6.03	2.95	1.85
K in solution mM	0.05	0.18	0.1	0.071
Ca in solution mM	0.03	0.399	0.16	0.169
Mg in solution mM	0.007	0.303	0.118	0.124
Si in solution mM	2.4	2.24	2.39	2.36

7.13 Discussion and conclusions

For pure clay, i.e. with no soluble calcium minerals, in most cases studied neither the CCC criterion nor the $X_{Ca} > 0.9$ criterion can be upheld. This is because the relative transport resistances in the gel and in the seeping water do not allow the gel at the gel/water interface to equilibrate with the water seeping in the fractures. Such gel is expansive and will penetrate far out in the fracture and can be carried away as flowing dilute gel and as colloids by the water.

Clay containing soluble calcium minerals e.g. calcium sulphate (gypsum) will dissolve and supply the water intruding in the gel with calcium. When there is no loss of calcium to the seeping water the dissolved gypsum would give rise to calcium concentrations above the CCC at high compaction. However, when more low salinity water intrudes and dilutes the gel, the gypsum dissolves, the calcium is diluted and is ion exchanged for sodium in the smectite because this is favoured at low salinities. When the gel has expanded to lower volume fractions of smectite, the calcium concentration in the water in the gel falls below CCC. In addition, X_{Ca} will not exceed 0.9 for original gypsum content as high as 2% unless a very calcium rich smectite was present to begin with.

The Deponit CA-N clay, in addition to gypsum and calcite also contains dolomite, a calcium-magnesium mineral. This clay also has a much higher fraction of divalent ions in ion exchange positions initially. When this clay is ingressed by non-saline waters, it can reach $X_{Ca}+X_{Mg}$ about 0.9 when it has expanded to 0.3 volume percent smectite. This is about when clay may disperse and gel may start to flow away. These results are based on simple clay/water mixing modelling.

Diffusion of ions from the gel towards the seeping water can lead to loss of calcium under some conditions. However, the rate of diffusion of calcium from the deposition hole is too small to have any impact on the pore water composition at the gel/water interface or on X_{Ca}. Under other conditions calcium can diffuse into the gel even from very non-saline seeping water and contribute with divalent cations in ion exchange positions, increasing the equivalent charge fraction of calcium in the smectite at the gel/water interface.

Indeed, there are a number of complex ion transport processes which influence the pore water composition in the expanding clay in the fracture, including diffusion in the “free” water in the gel, surface diffusion, anion exclusion and mass transfer in the seeping water in the fracture. We have tried to assess their relative importance and to see if they can have an impact on the results. We find the dilution of the clay by the seeping water ingress is the most important factor together with the dissolution of the calcium and magnesium containing minerals in the clay.

However, it is warranted to point out a number of assumptions and uncertainties that underlie the presented result. Some of the more important are mentioned below.

- The diffusion model used is based on the notion that one can distinguish between diffusion in “free” water and in the DDL water. This is a simplification but gives similar qualitative and quantitative results as the Donnan concept.
- The model is simplified using an idealized concept of diffusion in “free” water and in gel water. The anion and cation diffusion date support the model used. Viewing the system as a purely Donnan gel leads to similar results and to the same conclusions.
- The transport in the seeping water, which is two-dimensional, has been simplified to one dimension. The transport resistance in the water that first contacts the gel/water interface is considerably different from that at the point when water leaves the interface. It is entirely possible that X_{Ca} can be larger than 0.9 in the beginning and smaller at the end of the path causing erosion on the downstream side.
- The results are very sensitive to the total concentration as well as to the fraction of calcium in the seeping water.
- The transmissivity and the fracture aperture strongly influence X_{Ca}.
- The initial pore water composition and fraction of calcium in ion exchange positions has a strong influence on X_{Ca}.
- The presence of gypsum can have a strong impact on the conditions at the gel/water interface.

In summary, we conclude that it is not likely that X_{Ca} will exceed 90%, nor that the ion concentration in the pore water will be larger than the CCC under many conceivable and likely situations. Further modelling is needed to elucidate the transport processes as there are considerable uncertainties in data and model assumptions. For this the fragments of the models described and used above must be developed and integrated so that all processes can be handled simultaneously

We wish also to state here that the $X_{Ca} > 0.9$ criterion still is a hypothesis although it is supported by some experiments. Other experiments show, however, that pure calcium clays expand to a solid volume fraction of 0.05 and that the clay is not cohesive. See section 3.3.3 and 6.9. Nevertheless, it is certain that at $X_{Ca} > 0.9$ the clay forms larger particles that do not readily penetrate through narrow pores, which may lead to filtering and straining much more efficiently than for sodium dominated clays.

8 Filtering and straining

8.1 Introduction

Filtering as a general term is used to describe separation of solid particles from a gas or a liquid. Sometimes also separation of small droplets from gas or another liquid is called filtering. A common filtering method is to use a net or cloth with pore size less than the particles to separate the particles when the suspension is passed through the filter cloth or sieve. This is also called sieving, mechanical filtration or straining.

We will use the term *straining* to describe the phenomenon where particles larger than the pore size of the medium are hindered from passing.

Deep bed filtering is a process in which a bed of particles much larger than those to be filtered is used to separate the small particles from the fluid, may it be a gas or a liquid. A deep bed of the filter cake particles is formed in some way. The fluid with the particles is passed through the bed. The fluid with small particles can readily flow in the larger pores in the bed. The small particles can by sedimentation, impingement, or by Brownian motion hit the wall of the bed forming particles and be attached there by sorption due to electrical or other mechanisms. The bed will be increasingly filled with the small particles. Depending on a number of reasons the bed can either be so filled with the small particles that flow drops to negligible values or some state can be reached when the small particles always find the open paths through which they can penetrate the bed.

The ratio between the filtered particle diameter and the bed forming particles have a great influence on the separation as well as how the particles stick on or are repulsed from the bed forming particles.

Usually the particles in the fluid are poly disperse with some particle size distribution. This is also true for the bed forming particles. The mean size of the bed forming particles as well the form and magnitude of the size distributions will impact on the filtering and the straining.

We will explore especially the possibility of straining of the smectite particles in beds of small bed forming particles, which may emanate from the bentonite itself or that may be added to the bentonite from which the buffer material is fabricated. The underlying idea is that the mixture of smectite and bed forming particles will leave behind the latter, should the small mobile smectite particles be released to the seeping water. The bed forming particles should have a particle size distribution such that they on the one hand cannot penetrate far into the rock fractures but stay there. On the other hand the particles should be sufficiently small to be strained in the spaces between the larger particles that were stopped in the fracture so that the remaining pores eventually become smaller than the smectite particles. If this is successful further loss of smectite would decrease to low values allowing only a fraction of the smallest smectite fragments to penetrate.

/Richards 2009/ summarises filtration theory related to smectite filtration and straining. Below we outline the processes that influence the colloidal particle movement in a porous bed formed by the coarser material left behind as some smectite is lost. Forced fluid flow through the porous bed is also included. It will be negligible during the expansion of the bed but the term is included because we will use the equation also to illustrate filtration processes when colloid laden water flows in the rock fractures. The colloid expansion/contraction model described in chapter 6, Equation (6-51) can be extended with an advection term $\frac{\partial u_s \phi}{\partial x}$ and a term $R(\phi)$ that accounts for deposition or release of particles from the porous medium in which the gel expands or contracts (which can occur during sedimentation for example). u_s is the velocity of the suspension. The resulted equation then reads,

$$\frac{\partial \phi}{\partial t} = -\frac{\partial u_s \phi}{\partial x} + F_s \frac{\partial}{\partial x}\left(\frac{\phi}{f_{fr}}\right) + \frac{\partial}{\partial x}\left(\frac{\chi}{f_{fr}}\frac{\partial \phi}{\partial x}\right) - R(\phi) \qquad (8\text{-}1)$$

where $R(\phi)$ accounts for how the colloidal particles are withdrawn from the gel/sol and stick to the surfaces of the coarse particles or alternatively are released. It depends on a variety of factors and no general expression is available for predictive purposes. For colloid filtering in fractures in granite we believe that gravity will play an important role because of the short sedimentation distances in narrow fractures.

It should also be noted that in dilute colloidal sols, when only particle diffusion by Brownian motion needs to be accounted for, Equation (8-1) reduces to the Advection-Diffusion (Dispersion) Equation. The above equation can be supplemented by the equations governing the water velocity if clogging is deemed to reduce the hydraulic conductivity of the bed. Hydraulic conductivity changes due to clogging can be very important but is not further developed here. Simulation of clogging of porous sandstone has been studied theoretically and experimentally by /Rege and Fogler 1987/.

In addition, interaction of the charged smectite particle can be both repulsive and attractive. Repulsion will occur between the negatively charged smectite and negatively charged or neutral minerals on the fracture surface or on infill materials. Attraction will occur between the smectite and positively charged minerals. The latter are deemed to make up a (very) small fraction of the fracture minerals. Those sites will eventually be filled with colloidal particles and will thereafter not influence the colloidal transport. In essence we deem that smectite colloids in granite fractures will move readily with the water if it is below the CCC.

Coarser non-smectic material will be able penetrate into fractures but may be subject to straining. If the particle size distribution is such that this will lead to clogging of passages by the larger particles, smaller particles may also be strained in the passages first filled with large particles. The overlap of pore size distribution and the fracture aperture distribution will determine if and how fast a fracture becomes clogged by particles. The pore size distribution of the porous bed formed in the fracture may in turn strain the smectite particles if the size distributions overlap favourably.

Description of many factors that influence straining of colloids can be found in /Bradford et al. 2002, 2006, Gao and Saier 2006, Xu et al. 2006/.

In chapter 3 several experiments were described where non-smectite particles were found to considerably decrease smectite migration through thin filters and filter beds. The results suggest that coarse grained material such as is present in the MX-80 bentonite can form very effective filter beds for colloids if such beds can be retained in the fractures or at the fracture mouths.

As discussed in section 3.3.5 this material when forming a porous bed has so low hydraulic conductivity that the average pore size is on the order of 0.1 μm. This material may therefore be able to form an efficient filter or straining bed for smectite particles which range in size from tens of nm to hundreds of nm.

8.2 Size of fracture apertures in granite and straining of particles

Apertures of open fractures in granite at repository depths are very narrow, much below 1 mm. Fracture apertures vary between fractures and between different locations on the fracture. No reliable data on mechanical apertures of the fractures in situ have been found. However, there are indications that the aperture would give rise to residence time of flowing water one order of magnitude or more in excess of what an ideal flat wall slit would have to generate the hydraulic transmissivities observed in in-situ measurements. Below we discuss the implication for retention of particles in variable aperture fractures.

/Liu and Neretnieks 2005/ made a numerical study of flow and solute transport in variable aperture fractures intersecting a deposition hole. They based the simulation on transmissivity data reported in the SICADA data base. The aperture field in the fracture was taken to be log-normally distributed in all realizations with the same mean 0.35 mm. Six values of standard deviation of apertures were used ranging from 0.059 to 0.26 mm, corresponding to the range of transmissivities observed in the field. Fracture roughness was also accounted for in the simulations. An example of an aperture field is shown in Figure 8-1

Figure 8-2 shows the fracture aperture as a function of the transmissivity according to the “cubic law”, the so called hydraulic aperture, δ_h, Equation (8-2). The upper curve shows the upper bound of the range of the values proposed by /Sawada et al. 2001/, Equation (8-3), which is an estimate of the aperture needed for the residence time, δ_{RT}, upper curve in Figure 8-2.

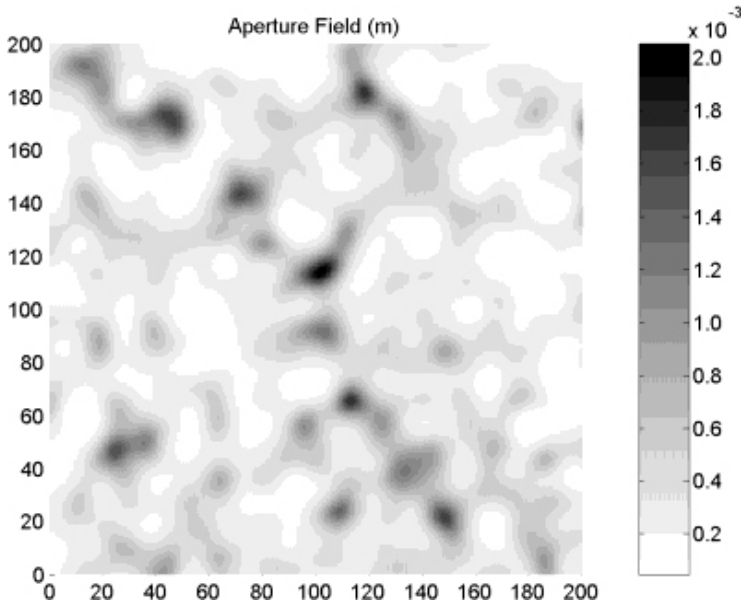

Figure 8-1. *A realization of the aperture spatial distribution in the fracture.*

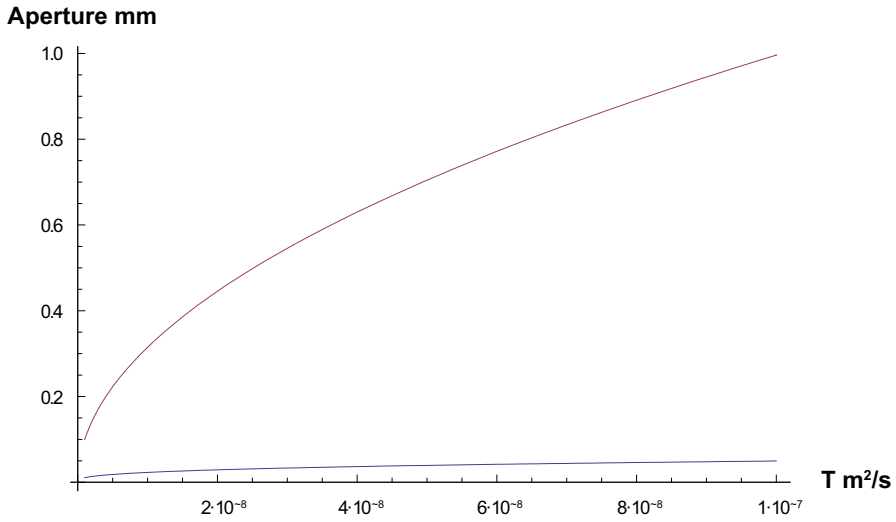

Figure 8-2. *Hydraulic, Lower curve, and residence time aperture, upper curve from /Sawada et al. 2001/ as function of transmissivity.*

$$\delta_h = \sqrt[3]{12\frac{T\eta_w}{\rho_w g_c}} \cong 10.7\sqrt[3]{T} \tag{8-2}$$

and

$$\delta_{RT} = 3\sqrt{T} \tag{8-3}$$

The latter spanned a variability of factor 3 up and down. The units are in m^2/s for the transmissivity and m for the aperture in the equations.

The hydraulic aperture for $T=10^{-7}$ m^2/s is 0.05 mm and for $T=10^{-10}$ m^2/s it is ten times smaller.

The very large difference between the hydraulic and the residence time aperture is caused by a number of different factors, many of them difficult to quantify. The roughness of the fracture walls will decrease T as well as the aperture variation for a given mean aperture because of the constrictions that are generated. Most measurement methods show transmissivity of a small local area

which needs to be connected with other connected areas that can form a continuous conduit. Another important factor that influences the transmissivity of an open fracture is the presence of infill material which can form local regions where the friction of the water is not only caused by the walls of the fracture but is due to friction in pores of infill material. We can estimate the average particle size needed to generate the pressure drop observed for a given aperture by the Kozeny-Carman equation presented in chapter 6, Equation (6-18).

The hydraulic conductivity for a porous bed K_h is

$$K_h = d_p^2 \frac{1}{150\eta_w} \frac{\rho_w g_c \varepsilon^3}{(1-\varepsilon)^2} = \delta_p^2 \frac{3}{50\eta_w} \frac{\rho_w g_c \varepsilon^3}{(1-\varepsilon)^2} \tag{8-4}$$

This directly gives the transmissivity of a fracture filled with spherical particles, second term, or shin flat sheets, rightmost term when the real aperture $\frac{\delta_{RT}}{\varepsilon}$ based on the residence time aperture δ_{RT} is introduced.

$$T = K_h \frac{\delta_{RT}}{\varepsilon} = \delta_{RT} d_p^2 \frac{1}{150\eta_w} \frac{\rho_w g_c \varepsilon^2}{(1-\varepsilon)^2} = \delta_{RT} \delta_p^2 \frac{3}{50\eta_w} \frac{\rho_w g_c \varepsilon^2}{(1-\varepsilon)^2} \tag{8-5}$$

Figure 8-3 shows the infill particle size needed to obtain a given transmissivity by solving Equation (8-5) for d_p when δ_{RT} from Equation (8-3) has been introduced.

8.3 Modelling smectite penetration through a filter

In this section, we test if our Dynamic smectite colloid diffusion model can be used to simulate smectite particle migration through filters with pores somewhat larger than the smectite particles themselves. It is first tested against experiments and then used to estimate the rate of smectite into a fracture with detritus material extending a short distance from the deposition hole. We limit the study to sodium dominated systems with ionic strengths below the critical coagulation concentration.

8.4 Dynamic model and the diffusivity function applied to expansion through filters

The diffusivity function can be thought as the diffusion coefficient for smectite particles in gel as well as in sol. The diffusivity strongly depends on the volume fraction, the ionic strength, or here expressed as the sodium concentration c_{Na} and particle diameter d_{coin} and thickness δ_p. For simplicity we model the particles as circular thin coin-like sheets.

$$D_F = D(\phi, c_{Na}, d_{coin}, \delta_p) \tag{8-6}$$

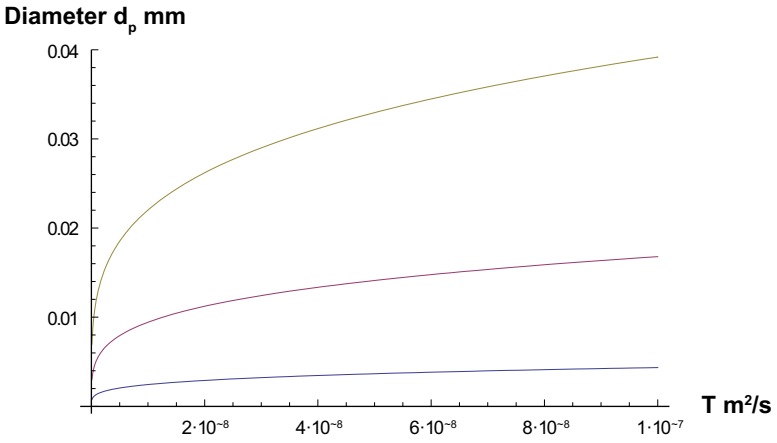

Figure 8-3. *Particle diameter d_p of the infill in the fracture to generate a given transmissivity T. Curves for porosity of infill 0.5, 0.7 and 0.9 from top and down.*

Figure 8-4 shows an example of the diffusivity function for a mean particle diameter of 175 nm, which is the average of the range 50–300 nm typically found in measurements. It may be noted that for $\phi > 0.02$ and $c_{Na} < 1$ mM, which are the conditions of interest here, the diffusivity was also found to be quite insensitive to the particle diameter. This is because in this volume fraction range the force function and the friction coefficient both depend on the particle size in a similar manner. Also the diffusivity varies weakly with ϕ for these conditions as is shown in Figure 8-4.

As we have described in Chapter 6, the rate of change of concentration of smectite particles in a concentration gradient field, neglecting gravity, is described by

$$\frac{\partial \phi}{\partial t} = \frac{\partial}{\partial x}\left(D_{\mathrm{F}}(\phi) \frac{\partial \phi}{\partial x} \right) \tag{8-7}$$

This equation has successfully been used to predict the expansion of compacted smectite pellets in water as followed by magnetic resonance imaging, /Liu et al. 2009c/ in test tubes. The dynamic model suggests that the smectite particles behave as other small diffusing species although there are additional and very strong forces acting between the particles. This implies that one would expect a gel to expand in the same way in narrow pores as in larger water volumes. This projected property has led us to test the model also on experiments where smectite diffuses through very narrow pores, as will be descried later in this paper. The rate of change term $\frac{\partial \phi}{\partial t}$ will be set to zero as we treat slowly changing conditions in the present application and apply the pseudo-steady state approximation.

8.4.1 Diffusion in and through a porous medium

In the model the smectite flowrate, N, through a filter can be described by Fick's first law in analogy to diffusion of solute molecules or ions in a fluid.

$$N = -D_e A \frac{d\phi}{dz} \tag{8-8}$$

where D_e is the effective diffusivity and A is the cross section area of the filter.

Because the filter has solid matter allowing the solute to move only in the pores of the filter, the porosity ε must be accounted for. The pores are not straight and may have constrictions so the constrictivity δ_c and the tortuosity τ^2 are also accounted for. The effective diffusivity for the filter D_e should be written as,

$$D_e = D_F \frac{\varepsilon \delta_c}{\tau^2} \tag{8-9}$$

The effective diffusivity of a filter can be measured or it may be estimated by Archie's law, /Archie 1942/.

$$D_e = D_F \varepsilon^m \tag{8-10}$$

The exponent m can take on values between 1.3 and 4 in different materials but is often taken to be 1.6, /Ruffet et al. 1995/. We will use m=1.6, recognising that the relation is very uncertain.

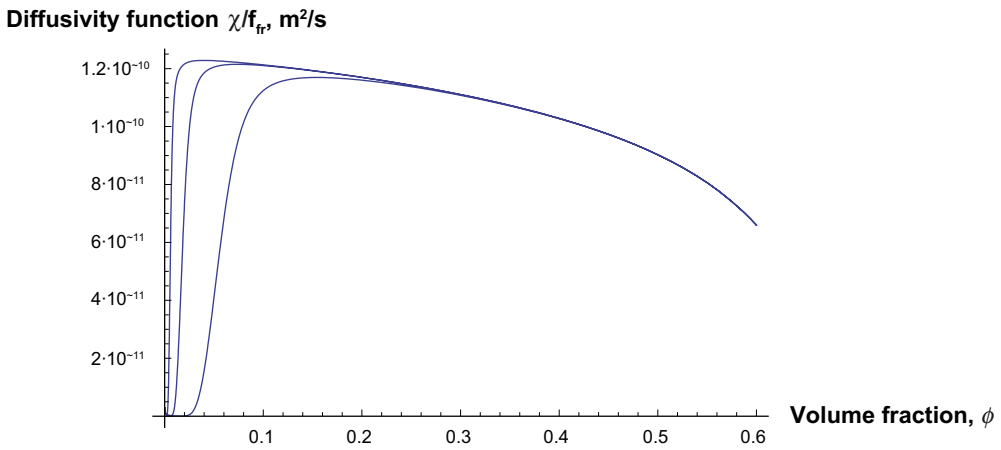

Figure 8-4. *Example of diffusivity function D_F for coin diameter 175 nm and thickness 1 nm. Curves from right to left 10, 1 and 0.1 mM sodium. Linear plot.*

8.5 Solving diffusion equation through filter for nonlinear diffusivity

8.5.1 Basic equations and solutions

For diffusion through a flat filter the boundary conditions for steady state conditions are

$$\phi(z = z_1) = \phi_1 \tag{8-11}$$

$$\phi(z = z_2) = \phi_2 \tag{8-12}$$

The diffusivity depends on the volume fraction and the relation between ϕ and z is obtained by integrating (8-8) between the boundaries. This is done by first introducing

$$F(\phi) = \int_0^{\phi} D_e(\phi)\, d\phi \tag{8-13}$$

where for simplicity we have set z_1=0.

Thus, integration of Equation (8-8) yields,

$$\frac{N}{A}\int_0^z dz = \frac{N}{A} z = -\int_{\phi_1}^{\phi} D_e(\phi')d\phi' = -F(\phi) + F(\phi_1) \tag{8-14}$$

The concentration profile is then obtained from

$$\frac{z}{\Delta z} = \frac{F(\phi_1) - F(\phi)}{F(\phi_1) - F(\phi_2)} \tag{8-15}$$

where Δz is the thickness of the filter.

Correspondingly, the flowrate is given by,

$$N = A\frac{F(\phi_2) - F(\phi_1)}{\Delta z} \tag{8-16}$$

Similarly, for diffusion radially in a cylinder from a radius r_1 to r_2, we have

$$\frac{\ln(r_1) - \ln(r)}{\ln(r_1) - \ln(r_2)} = \frac{F(\phi_1) - F(\phi)}{F(\phi_1) - F(\phi_2)} \tag{8-17}$$

and

$$N = 2\pi\Delta x \frac{F(\phi_2) - F(\phi_1)}{\ln(r_1) - \ln(r_2)} \tag{8-18}$$

where Δx is the length of the cylinder.

The same derivation of Equations (8-15) to (8-18) can be found in /Crank 1975/ although with the use of a different notation which makes his result somewhat more complex. Note in addition that for a constant diffusion coefficient D_0, Equations (8-16) and (8-18) reduce to,

$$N = D_0 A \frac{\phi_2 - \phi_1}{\Delta z} \tag{8-19}$$

and

$$N = 2\pi\Delta x D_0 \frac{\phi_2 - \phi_1}{\ln(r_1) - \ln(r_2)} \tag{8-20}$$

for the linear and radial geometry, respectively.

8.5.2 Pseudo-stationary case with depletion of the source

Consider a case where volume of swollen smectite is enclosed in a vessel by a filter through which the smectite can diffuse. As some smectite is lost the swelling pressure decreases. This influences the diffusivity function $D(\phi)$ so that after some decrease in the swelling pressure the rate of loss of smectite changes. ϕ_2 denotes the conditions in the vessel. There it is large so that the smectite migrates towards z_1 where the volume fraction ϕ_1 is low due to removal of the smectite for example by flushing. The rate of loss of smectite is then given approximately by,

$$V\frac{d\phi_2}{dt} = -N = -A\frac{F(\phi_2) - F(\phi_1)}{\Delta z} \tag{8-21}$$

where V is the volume in which the smectite resides with a volume fraction of ϕ_2. It includes the original smectite volume but also about half of the pores of the two filters. The latter is added because when diffusion starts a nearly linear smectite profile, dropping from that in the compartment down to essentially zero in the flushing water, is established in the pores.

This can be integrated from the initial condition at t=0 when $\phi_2 = \phi_{20}$

$$t = -\frac{\Delta z V}{A}\int_{\phi 2_0}^{\phi 2}\frac{d\phi_2'}{F(\phi_2') - F(\phi_1)} \tag{8-22}$$

Equation (8-22) is readily solved by numerical integration. For a constant diffusivity this can be integrated analytically and gives the well known decay formula

$$\phi_2 = \phi_1 + (\phi_{20} - \phi_1)e^{-\frac{D_0 A}{V\Delta z}t} \tag{8-23}$$

8.5.3 Some simple exploratory calculations

In this section we present these calculations to illustrate the use of the equations above and to prepare for the comparison with experiments presented later. The simplified approach will also be useful when simulating erosion of smectite from the buffer around the copper canister because it gives insights to the main processes without being too cumbersome. However, we will show that the simplified approach very accurately gives the same results as the "exact" solution and also explain why this is so.

Figure 8-4 shows that the diffusivity function could be approximated to be constant with an average value of $1\cdot10^{-10}$ m^2/s in the range $0.01 < \phi < 0.5$ for a sodium concentration less than 1 mM. A sample calculation is presented where a thin (5 mm) compacted tablet is contained by a 2 mm thick filter on both sides. These values are based on experiments described later. Water is flushed past the outside of the filter and the colloids that pass are carried away by it. See Figure 8-8. The smectite concentration on the water side is kept at a very low concentration, approaching zero.

The filter has a porosity of ε=0.38, which gives an Archie's law factor $\varepsilon^{1.6}$ equal to 0.21. The effective diffusivity then becomes D_0=$2.1\cdot10^{-11}$ m^2/s. We need, however, to further decrease the diffusivity by a factor of five in these calculations for reasons explained later.

Using the linearized diffusion equation, the volume fraction of smectite in the compartment over time with a starting volume fraction of 0.58 and no smectite in the flushing water is obtained by

$$\frac{\phi_2}{\phi_{20}} = e^{-\frac{D_0 A}{V\Delta z}t} \tag{8-24}$$

Figure 8-5 shows how the volume fraction in the compartment decreases over time

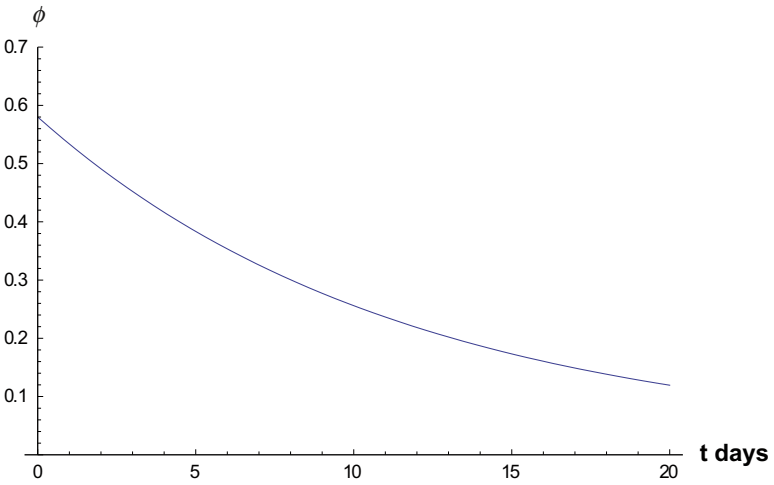

Figure 8-5. *Volume fraction versus time using the data given above.*

The relation between swelling pressure and volume fraction is obtained from the swelling pressure relation in the model discussed earlier in chapter 6.

This is used to calculate how the swelling pressure decreases with time. From Figure 8-6 it is seen that down to a volume fraction of about 0.1 the relation between swelling pressure and volume fraction is well approximated by the simple expression

$$P_{swell} = 2.5 \cdot 10^{7} \cdot \phi^{2.4} \qquad (8\text{-}25)$$

The swelling pressure decrease over time is shown in Figure 8-7 below. One of the two curves is with the "exact" solution of the swelling pressure relation and the other is for the approximate relation, Equation (8-25). Because the volume fraction does not decrease below 0.1, the results are not noticeably influenced by the sodium concentration.

8.5.4 Description of experiments and simulation results

The experiments are described in detail in /Birgersson et al. 2009/. Figure 8-8 shows the principle. Compacted purified smectite is confined between two metal filters that are swept by flushing water in channels in contact with the filters. The water carries away smectite that penetrates the filters. The swelling pressure is constantly monitored.

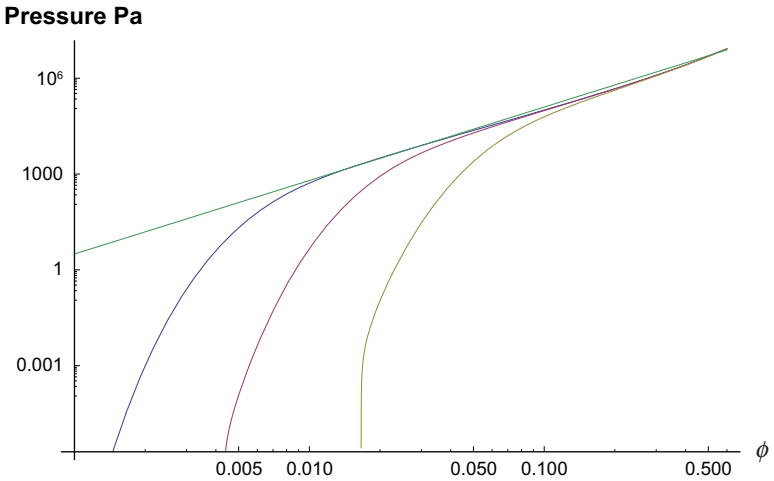

Figure 8-6. *Swelling pressure as a function of the volume fraction ϕ for different sodium ion concentrations. From left to right 0.1, 1 and 10 mM. The straight line is given by* $P_{swell} = 2.5 \cdot 10^{7} \cdot \phi^{2.4}$*. The curves are obtained from the relations described earlier.*

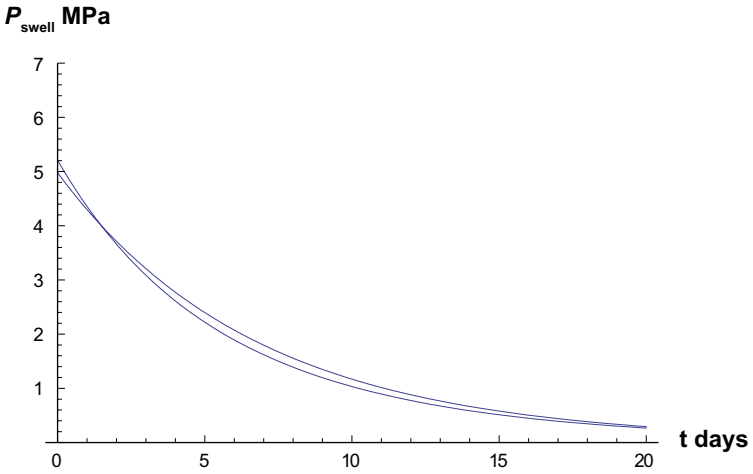

Figure 8-7. *Swelling pressure as a function of the time for both the "exact" solution, curve starting with a volume fraction 0.51, which gives a swelling pressure 5.0 MPa, as well as the approximate expression.*

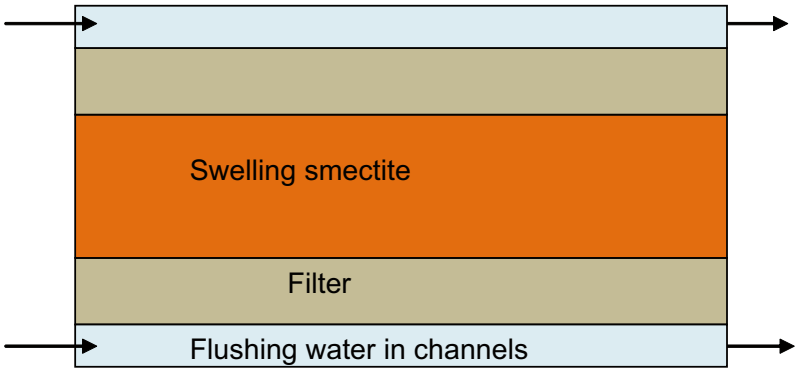

Figure 8-8. *Compacted smectite is confined between filters that on their outsides are flushed by water. Swelling pressure is monitored over time. The water in the channels only contacts about 27% of the filter surface.*

Several experiments were made with different clays, both purified and commercial. We select those where purified homo-ionic sodium smectite was used. In these experiments 2 and 10 micrometer pore filters were used. Both filters allowed the pure smectite to pass the filters with practically the same rate. In addition 0.2 and 0.5 micrometer pore sizes were tested but these did not allow smectite to pass.

The 10 micrometer filters were made of stainless steel with a porosity of 0.38 and the 2 micrometer filters were made of titanium and had a porosity of 0.314. The filters were 2 mm thick and the smectite was 5 mm thick. The smectite originally contained between the filters has access to the pore volume of the filters once the swelling has started. The volume fraction gradient in the filters is essentially straight so that on average half of the filter volume is expected to be filled with smectite giving a decrease of the effective volume fraction. This volume is included in the available volume of the smectite, V, in the calculations. The starting density of the wet smectite is 2,000 kg/m^3, which gives a volume fraction of 0.588 using a smectite mineral density of 2,700 kg/m^3. This volume fraction decrease as the gel expands into the filters. We take this as the starting point for the simulations.

Figure 8-9 shows the measured swelling pressure for the 10 and the 2 micrometer filters.

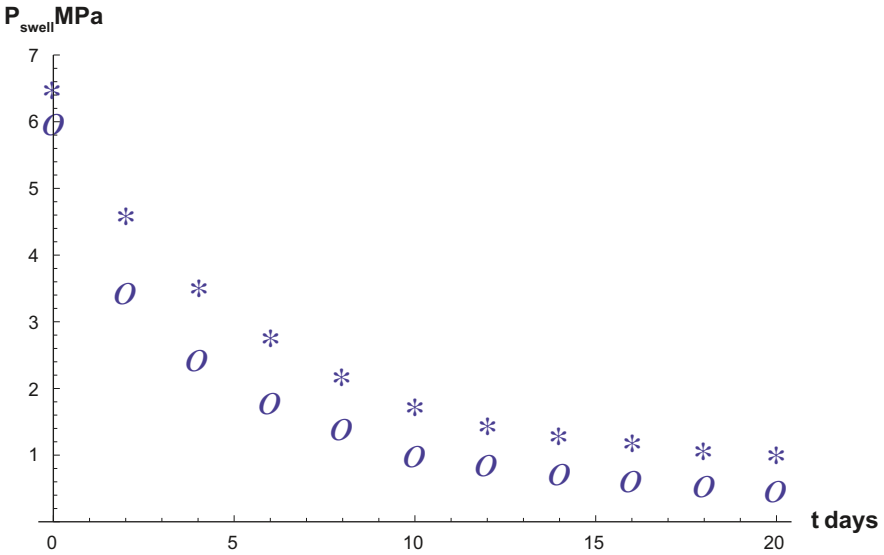

Figure 8-9. *Swelling pressure drop for purified WyNa smectite with 2 micrometer filters marked with * and 10 micrometer filters marked with o.*

Figure 8-10 shows how the calculated swelling pressure decreased for the 10 micrometer filters. The flushing channels make up only 26.8% of the filter area that is in contact with the flushing water, which limits the area for the smectite migration to the flushing water. Furthermore the distance between the channels is more than 2 times the thickness of the filter forcing a converging diffusion path. This could decrease the rate of transport by a factor of 3.7 or more if we assume that it is the narrowest part of the path that determines the rate of migration in the filter. We call this an equipment factor. Accounting for this by decreasing the cross section area for diffusion gives the lower curve in Figure 8-10. The initial swelling pressure is predicted to be about 5% too low and the pressure drop is too rapid. No adjustment has been made to the initial swelling pressure, which was determined based on the assumption that the pore volume of the filters is accessible to the bentonite and a linear gradient in the filters. This seems to be too much extra volume as the early pressure is underestimated.

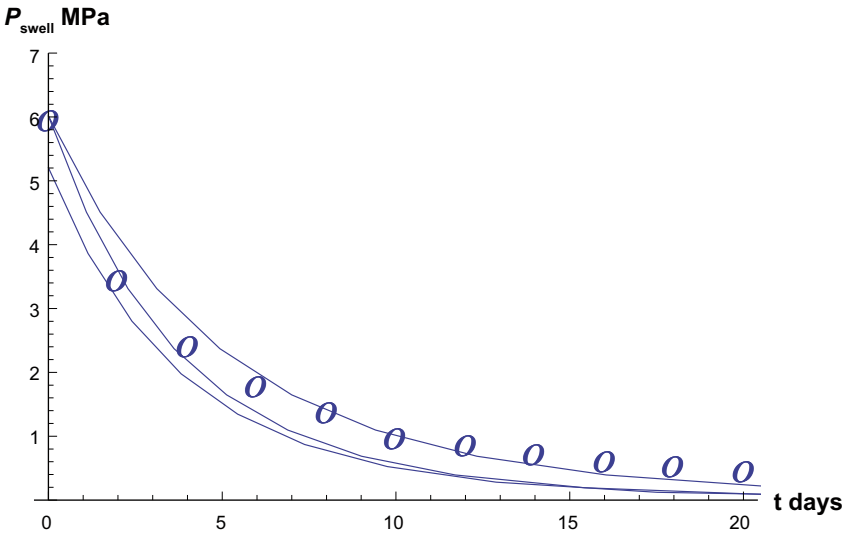

Figure 8-10. *Swelling pressure for purified WyNa smectite with 10 micrometer filters. Lower curve with equipment factor=3.7 and no adjustment of starting volume fraction. Middle curve with equipment factor=3.7 and 5% increase in starting volume fraction. Upper curve with equipment factor=5 and 5% increase in starting volume fraction.*

Adjusting the initial pressure to that observed gives the middle curve. This still predicts too rapid drop in pressure for later times. An increase of the equipment factor to 5 gives a better agreement. This is shown in the upper curve.

The model over predicts the drop in swelling pressure. One reason for this can be that the smectite concentration in the flushing water is assumed to be zero. Gravity effects were neglected. This is deemed to be permissible in this case because gravity will only come into play when the gel is very dilute.

Figure 8-11 shows the simulations for the pressure drop through 2 micrometer pore filters. We use only an equipment factor of 5 not to clutter the figure too much.

Figures 8-10 and 8-11 above show that it was not possible to obtain the correct initial swelling pressure if no corrections were made. In both cases about 5% increase is needed to obtain a good agreement between simulated and measured values at start. This suggests that not all the pore volume of the filters is accessible to the gel. However, also the use of a pseudo stationary approach, neglecting $\frac{\partial \phi}{\partial t}$ may also contribute the discrepancy.

It is seen that the 2 and the 10 micrometer filters behave very similarly. This shows that there is negligible friction between the smectite gel/sol and the pore walls. The smectite particles behave like molecules diffusing in pores and not like a gel that is forced through pores by an overpressure at the pore inlet. Should wall friction determine the rate of smectite penetration, the rate should be $(10/2)^2$=25 times smaller in the 2 micrometer pores than in the 10 micrometer pores if the pores can be considered to be tube like.

The smectite particle size ranges from 0.05 to 0.3 micrometers. These particles can obviously migrate through pores with a pore size of 2 micrometers. However, they are stopped by straining in the experiments with 0.2 and 0.5 micrometer pore size filters. No swelling pressure loss was ever observed when such filters were used.

In another experiment the smectite was confined between one 2 mm thick filter on one side and three 2 mm thick filters on the other side. The pore size was 2 micrometers in all filters. After ten days of flushing on both sides, only the side with three filters was continued to be flushed.

Figure 8-12 shows the simulation. The reason for the poor prediction of the conditions when three filters are used is not understood. The experiments not only show a slower change in swelling pressure but also show an unexpected curvature of the swelling pressure versus time.

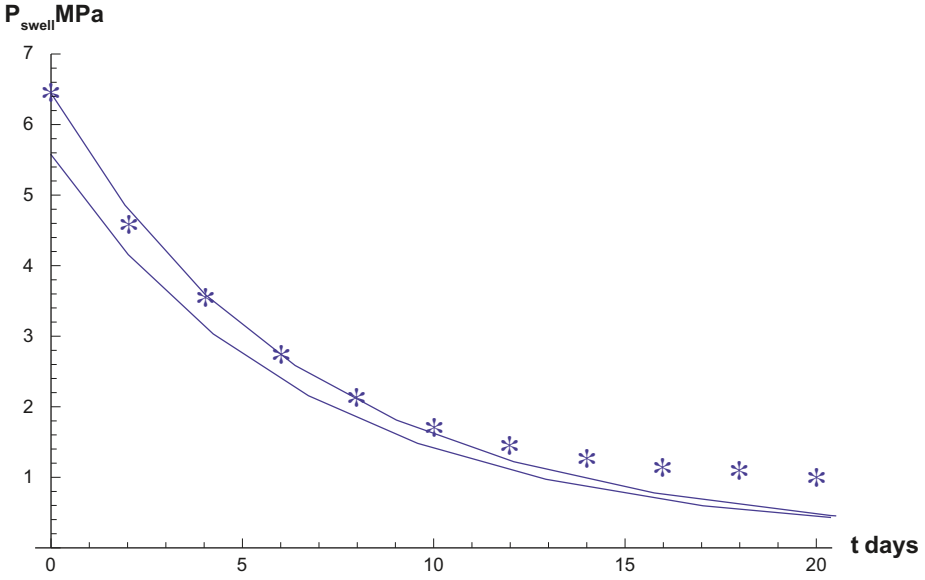

Figure 8-11. *Swelling pressure for purified WyNa smectite with 2 micrometer filters. Equipment factor=5. Lower curve, no adjustment of starting volume fraction, upper with 5% increase.*

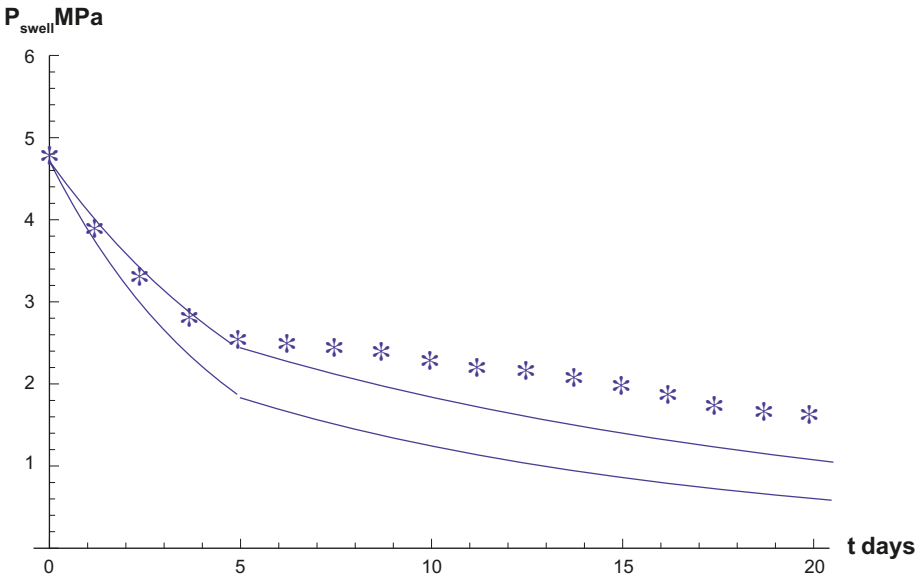

Figure 8-12. *Swelling pressure for purified WyNa smectite with 2 micrometer filters. First ten days 3+1 filters were used. Thereafter only the side with 3 filters was flushed. Equipment factor=5 lower curve and 7 upper curve. Initial volume fraction adjusted upward by 5%.*

8.6 Discussion of the simulations

The simulations show a fair agreement during the early period but predict too large loss of swelling pressure during later times. This may be caused by the assumption that the smectite concentration on the flushing side is zero. There is no information on the actual concentration at the filter surface. Mass transfer resistance for the particles to move from the filter pore surface into the flushing water channels may not be negligible but it has not been possible to estimate this with the data available. Further, the assumption that the smectite also has access to all the pore space in the filters, with on average half the volume fraction of that in the smectite compartment is also a rough estimate. The pore space in the filter makes up 20 to 23% of the compartment volume, so with a linear smectite concentration profile in the filters about 10 to 12% of the gel at any moment resides in the filters. Another possible cause may be a slow build up of particles plugging the small pores. Although the smectite used is purified some of the smallest detritus particles remain.

Notwithstanding these uncertainties and differences between experiments and simulations it is concluded that the Dynamic model reasonably well predicts the migration of smectite particles through narrow pores.

We refrain from modelling the experiments with non-purified bentonite that also were performed by /Birgersson et al. 2009/. These experiments showed a much slower decrease in swelling pressure than when purified sodium exchanged smectite was used. The modelling and interpretation of those experiments is complicated by the presence of gypsum which dissolves and supplies the pore water with divalent calcium ions which radically changes the swelling behaviour of the smectite. The untreated bentonite contains about 20% accessory minerals with much larger average particle size. Such particles may clog the pores in the filters and also may build up an addition filter when they are left behind as the smectite is depleted.

8.7 Smectite erosion from deposition hole through a bed of particles

Two simple cases are modelled. In the first it is assumed that, the left behind, accessory mineral particles have penetrated a small distance into the fracture that intersects the deposition hole. Smectite diffuses through this filter and is swept away by the seeping water in the fracture outside the filter.

Only stationary conditions are considered, assuming that there is an unlimited source of smectite in the deposition hole and that further accessory minerals accumulate at the mouth of the fracture and do not add to the material in the fracture.

In the second case it is assumed that no accessory minerals have penetrated into the fracture but only build up at the fracture entrance forming a half cylinder at the mouth of the fracture.

In both cases the diffusion function described earlier is used. The deposition hole has a diameter of d_{hole}=1.75 m. Ten % of the circumference is open and there the fracture aperture δ_{fr} is 1 mm. The penetration depth is arbitrarily chosen to be Δz=0.1 m. The results scale nearly linearly so the results for other depths are readily obtained. The cross section area A for smectite diffusion accounting for 10% opening to a fracture around the rim is

$$A = 0.1\pi d_{hole}\delta_{fr} \tag{8-26}$$

The release of smectite is

$$N = D_0 A \frac{\phi - 0}{\Delta z} \tag{8-27}$$

The smectite volume fraction in the deposition hole is taken to be ϕ=0.6. The diffusivity is considered to be D_0=2·10^{-11} m^2/s, which is the value obtained previously for a filter with a porosity of 0.38. This is in the range of values one finds in sand beds.

Using these data, we found that the smectite loss N=6.6·10^{-14} m^3 smectite mineral per s. This is 5.6 g per year or 5.6 kg per 1,000 years. If penetration depth of detritus material in the fracture is only 1 cm, the smectite loss increases to 56 kg in 1,000 years. With 0.1 mm aperture the erosion rate decreases to one tenth of the previous figures.

In the case when there is no penetration in the fracture but the accessory minerals build up a half cylinder around the open part of the fracture, like a part of a doughnut, the smectite loss is obtained from Equation (8-20) for a half cylinder, giving

$$N_{cyl} = \pi \Delta x D_0 \frac{\phi - 0}{\ln(r_1) - \ln(r_2)} \tag{8-28}$$

where Δx is the length of the cylinder (doughnut) along the fracture, i.e. 10% of the circumference Δx=0.1πd_{hole}· r_1=0.1 m is the radius of the cylinder (doughnut) and r_2=0.5 mm is half the aperture of the fracture.

With these data, we obtained that N_{cyl}=3.9·10^{-12} m^3/s, which is nearly 60 times larger than for the filled fracture case. Decreasing the aperture to 0.1 mm for the cylindrical case only decreases N_{cyl} to 2.7·10^{-12} m^3/s. The diffusion resistance in the accessory minerals covering the mouth of the fracture is thus negligible in comparison to the resistance in the in-filled fracture.

In fact, even a 10 mm depth of in-fill in the fracture would give a considerable resistance to erosion in the case that there is no advective flow in the infill. As described in /Liu and Neretnieks 2006, Richards 2009/ the particle size distribution of the accessory minerals will lead to very low hydraulic conductivity for a bed formed of such material even at low compaction. As long as there is no advective flow, even a much higher porosity of the in-fill will only increase the erosion rate by a maximum of a factor of 5 as obtained by the tortuosity effect by Archie's law.

8.8 Discussion and conclusion

Experiments show that smectite particles in an expansive sodium dominated gel readily migrate through porous media with pore sized only somewhat larger than the smectite particles. The rate of penetration by smectite particle diffusion is negligibly influenced by the pore size. The Dynamic model describes the rate of penetration well. A few cm deep penetration of detritus or other material forming a filter in the fracture intersecting the deposition hole strongly reduces the possible rate of loss of smectite considerably. The bed need not to be very compact. It is sufficient that the hydraulic transmissivity is low enough not to allow water flowing through it to attain this effect.

Detritus material left behind in the deposition hole at the mouth of the fracture adds somewhat to the resistance to smectite diffusion. However, such material will be compressed by the swelling pressure of the bentonite in the deposition hole and it will have small pores. Then, in addition, straining of smectite particles in the small pores may efficiently stop further loss of smectite after the initial period during which the detritus bed formed. There is strong experimental support for the straining of smectite in beds formed of detritus and other materials.

The low transmissivity in fractures with large aperture must be caused by either very rough surfaces, narrow constrictions, by infill in the fractures or by combinations of these factors. The apertures or pores must be on the order of tens of micrometers.

The size distribution of the detritus particle also ranges from about 10 to hundred micrometers. It is very likely that the detritus particles will be strained by the narrow passages in the fractures and by infill material in the fractures already after very short distances in the narrow passages. In the more open pores the particle may penetrate until they encounter restrictions.

We envisage that the movement of detritus particle in the fractures to take place in the following way. The expanding gel in the fracture carries with it the detritus particles until the particles encounter a small enough restriction to be stuck. We follow a "packet" of gel. The gel then moves around this location in the more open parts of the fracture. The packet expands more and more until it very nearly forms a sol and its smectite is carried away by the seeping water. The detritus material in it is left behind and settles on the fracture surface. The following "packets" of gel repeat the procedure in the fracture that is increasingly filled with detritus material also in the most open locations. The fracture is filled further and further out and the ingress of new "packets" of slows down as the smectite has increasing difficulties to diffuse through the filter already formed.

In downward slanting fractures, the detritus material can drop or roll downward ahead of the gel as soon as it is released from the gel. The particles will penetrate downward until they encounter a small enough restriction to be stuck. They cannot move sideways to avoid the restriction because there is no force to move the particle in any other direction than downwards. We believe that only very small amounts of bentonite can be lost before the fracture has efficiently closed escape routes for the smectite or at least built up a filter that strongly decreases further smectite penetration.

Should it not be possible to rely on the presence of detritus material, addition of inert particles with a suitable particle size distribution can be made.

Our bottom line conclusion is that we deem it to be highly likely that straining of accessory mineral particles from the bentonite and/or specifically added material will clog fractures with a bed of fine material. This bed will in turn filter and strain smectite particles trying to escape from the swelling bentonite gel.

9 Various aspects on quantifying erosion rates

9.1 Conceptual picture

In the previous chapters we have presented our understanding of the various mechanisms that influence the behaviour of smectite clays, which we deem will affect the possible erosion of the gel. Three main modes of erosion have been identified. In all three modes the expansion of the smectite gel into the fracture, similar to a gas expansion, allows the gel to move out into the fracture to eventually reach the gel/water interface from which smectite can be carried away. We have also identified mechanisms that will counteract the three erosion modes. The boundaries between these modes are not sharp in practice but they help to illustrate some important processes.

Advective loss of gel. In a cohesive as well as in an expansive gel erosion can be caused by the gel itself flowing away as a viscous liquid, the gel constantly being replenished by gel expanding out into the fracture.

Diffusive loss of gel. In an expansive gel, i.e. below the CCC, erosion can also be caused by the gel turning into a sol and the sol particles diffusing by Brownian motion into the seeping water, which carries them away

Shearing of particles from gel by seeping water. For the physical shearing the cohesiveness of the gel will have to be overcome by the friction force on the gel. The yield stress of the gel and the shear stress of the water will determine when this mechanism is active. The non-Newtonian properties, especially the Bingham yield stress must be quantified.

The advective and diffusive mode will be possible when the gel is expansive over all gel volume fractions i.e. when the ion concentration is below the CCC and possibly also when the calcium content in the smectite allows the particles to separate to form more or less individual sheets. In the shearing mode we assume that the gel is cohesive and does not spontaneously release particles in appreciable numbers.

Straining and filtering. Small "sand" particles naturally present or specifically added to the bentonite will, as smectite is lost, form an increasingly thicker filter through which the smectite particles have to negotiate to reach the seeping water. This will slow down the loss of smectite.

In the advective erosion mode the viscosity of the non-Newtonian gel/sol will influence the flowrate of the dilute gel/sol in the fracture. A balance between the rate of which the gel/sol flows away and the replenishing of the gel by expansion of more gel from the deposition hole will be established over time. For this erosion mode the non-Newtonian properties of the gel/sol must be quantified as influenced by chemical composition of the pore and double layer water and of the volume fraction of smectite.

For all three mechanisms the expansion of the gel from the deposition hole into and in the fracture must be understood and quantified. The gel properties are different in different locations in the fracture as they depend on the volume fraction as well as on the local ion composition in the gel. The gel properties at the gel/water interface can therefore be different from those further into the gel. The gel may e.g. be below the CCC at the gel/water interface but above CCC some distance further in. Leaching of ions from the pore water into water seeping in the fracture can then maintain a concentration below CCC at the gel/water interface and let the smectite particles disengage and be carried away. In this model it was just assumed that the particles could be carried away by the water without specifying the underlying mechanisms. This was the basis for a previous model we call the 0^{th} order model /Liu and Neretnieks 2006/.

In the present modelling we specifically study how the smectite particles can be carried away, namely by particle diffusion into the seeping water and by additionally accounting for the advection of gel itself.

For the diffusion mode our model for gel/sol expansion is coupled to the equivalent flowrate model, Q_{eq}, which previously only has been used for solute transport, now also accounting for smectite particle diffusion.

For the advection model we have developed a model for the non-Newtonian viscosity as a function of solid volume and water composition. Both entities will change with time and location in the expanding gel. We limit the model to monovalent ions, notably sodium, and to concentrations below CCC for sodium dominated clays where the smectite particles can separate into one or few sheets. There are several reasons for this. Sodium clays are considerably more studied and more data are available. Calcium dominated clays form larger particles that are less mobile by Brownian forces. Calcium dominated clays do not swell as much and do not release sol particles as readily as sodium dominated clays. Practically no information is available for the rheological properties of calcium dominated clays at lower volume fractions.

For gels that behave as sodium dominated gels the gel our Dynamic model has been verified by comparison with different types of experiments. The model contains two main parts, the forces on and between particle and the pressure drop in gel. Both have been individually verified against independent experiments. The viscosity model has also been verified.

In the erosion mode the release of colloidal particles from bentonites with pore water concentrations above the CCC has been modelled previously by assuming that the shear forces caused by the seeping water shear off individual particles, modelled as spheres, loosely attached to other particles at the gel/water interface /Pusch 1983, 1999, Grindrod et al. 1999/. We take a different approach /Liu and Neretnieks 2006/ in which the Bingham yield stress of the gel is balanced by the shear stress on the gel/water interface. This avoids the need to make any assumptions on the size of the coagulated particles that are sheared off and on the forces between coagulated particles.

Smectite penetration through fine pore filters have been found to be predictable by the Dynamic model. Using the model for smectite diffusion through even thin beds of loose detritus material in a fracture shows that this will considerably slow down smectite loss by diffusion. Physical straining of smectite particles in narrow pores is likely to further restrict smectite loss.

The conditions for when the gel is expansive depends on the CCC. The CCC is assessed by experiments but it also agrees well with our new CCC model, which in turn is based on our model for the force balance on the smectite particles /Liu et al. 2009a, b/.

9.2 Diffusive mode-Loss of smectite by the diffusion of the smectite particles themselves

In the model proposed by /Liu and Neretnieks 2006/, the so called 0^{th} order model, it is assumed that the loss of smectite is proportional to the loss of CCC determining ions. The loss of such ions is due to diffusion from the gel/water interface to the seeping water in the fracture. It is modelled by the concept of the equivalent flowrate, Q_{eq} described in chapter 8. The rate of loss of CCC ions N_{Ca}, here exemplified by calcium, is shown in Equation (9-1).

$$N_{Ca} = Q_{eq} c_{CCC} \tag{9-1}$$

Should the approaching water contain calcium the concentration should instead be (c_{ccc}–$c_{approach}$).

Q_{eq} for ionic species ranges from very low values up to tens of litres per year under high gradients and large apertures /Neretnieks et al. 2009c/.

The loss of smectite is proportional to the inverse of the content of CCC ion (exemplified by calcium) content of the clay.

$$N_{smec}^{Ca} = Q_{eq} c_{CCC} \frac{1}{x_{Ca}} \tag{9-2}$$

We remind the reader that in the 0^{th} order model it is assumed that the released smectite particles immediately are transferred to the seeping water and carried away. The transfer of smectite particles to the seeping water may, however, not be sufficiently rapid so the rate is overestimated. Below the smectite transfer rate is assessed using the same mass transfer concept for diffusing particles as for ions. It is then necessary to define a value for the smectite concentration at the gel/sol interface when the particles become free to diffuse in the water.

In previous chapters it was described that at particle volume fractions between 0.1 to a few % the gel may start to behave like a sol, releasing free particles by Brownian motion. The lower value applies to waters with very low ionic strength, the higher to waters with more salt. At lower concentrations, the particles move freely and are very little influenced by the presence of the other particles. We call this particle concentration ϕ_{min}. The Q_{eq} concept can then also be used for particle diffusion but the magnitude of Q_{eq} is proportional to the square root diffusivity of the diffusing species which is orders of magnitude lower for the particles than for the ions.

For smecite particles

$$N_{smec} = Q_{eq}^{smec} \frac{\phi_{\min}}{1-\phi_{\min}} \rho_{smec} \tag{9-3}$$

The ratio of the loss of particles due to calcium loss and due to particle diffusion is

$$\frac{N_{smec}}{N_{clay}^{Ca}} = \sqrt{\frac{D_{smec}}{D_w}} \frac{\phi_{\min}}{1-\phi_{\min}} \rho_{smec} \frac{x_{Ca}}{c_{CCC}} \tag{9-4}$$

A first approximation for the diffusivity of ions and particles is that it is proportional to the size of the species. For the example below we use the following data: Ratio of diffusivities is 300 between calcium and smectite. The CCC for calcium is 40 g/m^3. Calcium content of bentonite is 1g/100g and smectite gel/sol concentration limit is 40,000 g/m^3, (ϕ_{min}=0.015). Smectite density ρ_{smec}=2.7·10^6 g/m^3. The bentonite has crept out to zfront=0.5 m in the fracture. Table 9-1 shows the equivalent flowrates Q_{eq} as well as the smectite loss by the two mechanisms. The smallest value will determine the loss.

The ratio of the smectite loss models is 1.7, suggesting that the smectite particle diffusion will barely limit the loss of smectite. If ϕ_{min} is ten times lower the smectite loss by particle diffusion will decrease by about an order of magnitude and will clearly limit the loss.

This will not apply to a downward sloping fracture because then also gravity will pull smectite downward. The reader is also reminded that the gel is not allowed to flow in this case. However, the viscosity of the gel decreases rapidly with decreasing particle concentration and it is conceivable that particles will be lost by the gel flowing away. This is discussed below.

9.3 Advective mode-Loss of smectite by downstream flow of the gel itself

9.3.1 Model structure

The viscosity of the gel/sol increases rapidly with increasing volume fraction ϕ. The viscosity is also strongly influenced by the ion concentration because the electrical double layer extend farther from the particles at low ionic strengths and they interfere with each other at lower solid volumes. The viscosity will increase with decreasing ionic strength. This was discussed in Chapter 5.

On the other hand the repulsion forces will increase with decreasing ionic strength and force the particles apart expanding the gel. A balance will eventually be reached between the rate of expansion of the gel into the fracture and the advective transport of the increasingly dilute gel downstream. We have modelled the simultaneous expansion of the gel out into the fracture and how it is swept away

Table 9-1. Smectite loss by calcium loss and by smectite diffusion.

T m^2/s	Q_{eq} l/yr	Q_{eq}^{smec} l/yr	N_{smec}^{Ca} g/yr	N_{smec} g/yr
10^{-10}	0.74	0.043	3.0	1.8
10^{-9}	2.36	0.14	9.4	5.6
10^{-8}	7.46	0.43	29.8	17.7
10^{-7}	23.7	1.36	94.3	56.0

by flow of the increasingly dilute gel further from the deposition hole. The Darcy equation is set up for two-dimensional flow in a fracture intersecting the deposition hole. The water flows around the gel that has expanded out into the fracture. Now, however, we treat the gel/sol as a fluid with a viscosity that depends on the smectite as well as the ion concentration. The gel/sol will flow slowly where its viscosity is high and faster the more dilute it becomes further from the deposition hole.

To quantify this we simultaneously solve the Darcy flow equation, the solute diffusion equation for the ion(s) and the equations governing the expansion of the gel. The latter are described in Chapter 6. This is described in more detail in the report by /Moreno et al. 2009/.

Figure 9-1 shows an example of viscosity for a sodium smectite gel at three different ion concentrations in water. It is seen that up to ϕ=0.1% the viscosity is not much larger than for water. At 1% it is 10 to 50 times larger and rises rapidly with increasing solid content.

Figure 9-2 shows the flow vectors around the deposition hole for a fracture transmissivity T=10^{-7} m^2/s, fracture aperture 1 mm and a hydraulic gradient of 0.1. Bentonite concentration is also shown as colour. The water flow is negligible for bentonite volume fraction greater than 1–2%.

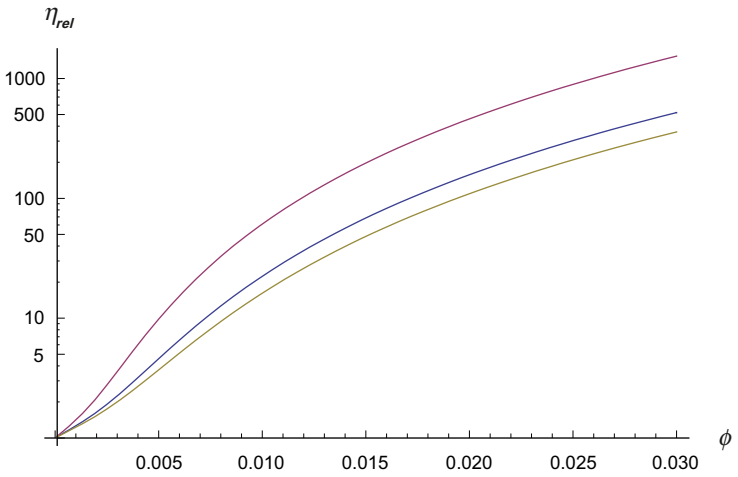

Figure 9-1. *Relative viscosity for the base case as a function of bentonite volume fraction. Curves from bottom and up for 10, 1 and 0.1 mM monovalent ion.*

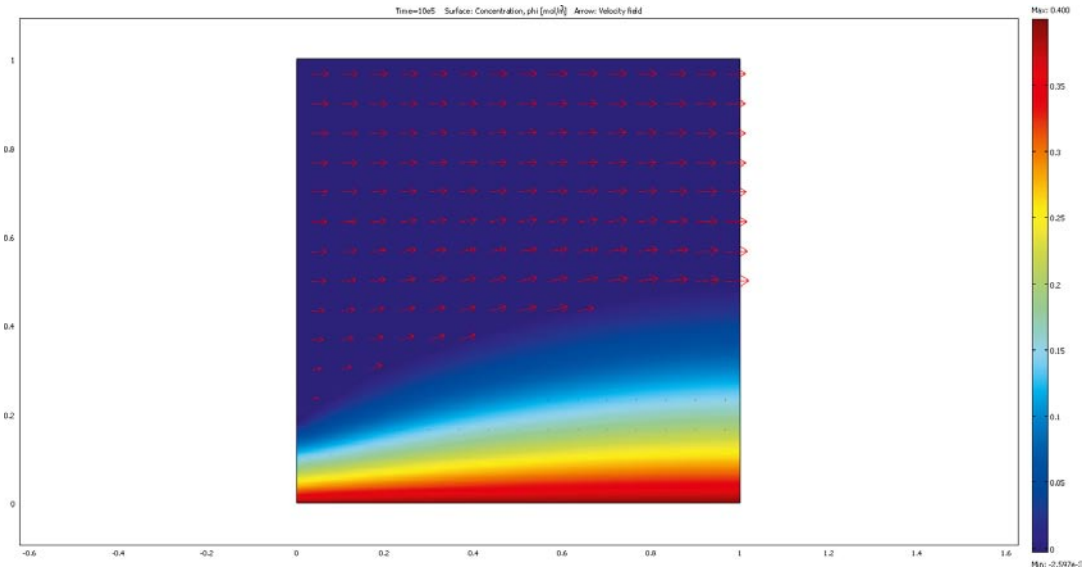

Figure 9-2. *Smectite volume fraction distribution and water velocity field in the fracture.*

The release of bentonite takes place in locations close to the gel/sol interface. Figure 9-3 shows the release of bentonite along this interface. The figure presents the product of water velocity times bentonite volume fraction. It is seen that the transport is concentrated to a very narrow region. The figure also shows also shows that the smectite flux will be concentrated to a thin region as anticipated from the results in Figure 9-2.

The flowrate of smectite with the viscous gel will be approximately proportional to the smectite volume fraction and inversely proportional to the viscosity. The ratio $\phi(\eta_w/\eta)$ will indicate the flux of smectite for a given hydraulic gradient. This is shown in Figure 9-4

It is seen that there is a thin region at the gel/water interface where smectite gel flows. Near the deposition hole the volume fraction of gel is high but the viscosity is so large that gel flow velocity is very small. Further from the deposition hole the water velocity is large but the volume fraction smectite is small. Gel/sol transport thus is limited to the thin rim shown in the figure.

Flow vectors and smectite concentrations in the gel and water in the fracture intersecting a deposition hole are shown in Figure 9-5.

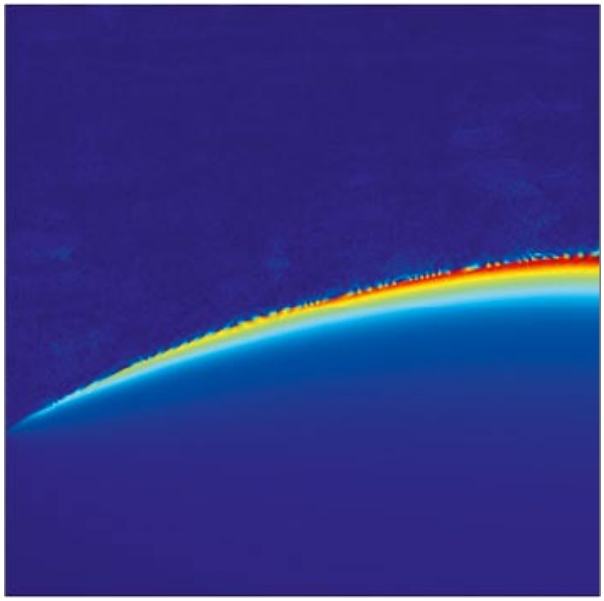

Figure 9-3. *Release of bentonite along the gel/water interface. The figure shows a region of 1 times 1 metre.*

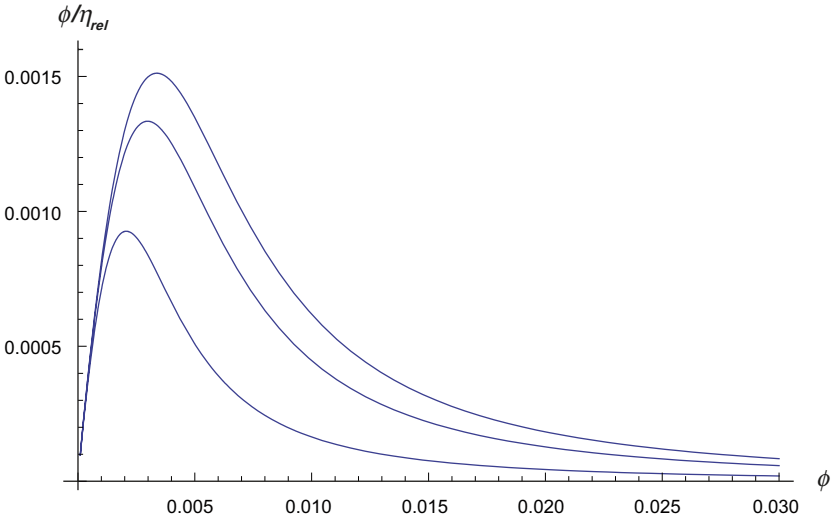

Figure 9-4. *The ratio $\phi(\eta_w/\eta)$ as a function of bentonite volume fraction. Curves from bottom and up for 0.1, 1 and 10 mM monovalent ion.*

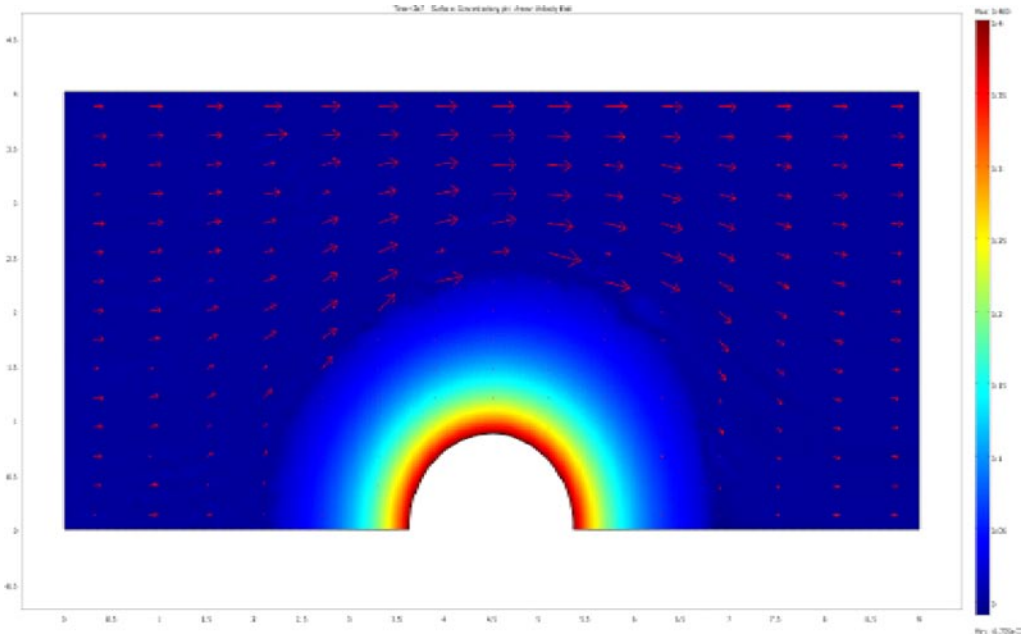

Figure 9-5. *Flow vectors around a section of the deposition hole for a fracture transmissivity $T=10^{-7}$ m^2/s, fracture aperture 1 mm and a gradient of 0.1.*

Table 9-2 shows the smectite loss for different water velocities in a 1 mm aperture fracture. The loss is proportional to the aperture which means that for an 0.1 mm aperture the loss will be ten times smaller.

The numerical method used to solve the equations /Comsol Multiphysics 2009/ converged very slowly and become unstable for the two lowest water velocities. The smectite release and the penetration depth into the fracture for the two lowest water velocities (0.1 and 0.32 m/yr) were determined by extrapolation from data for the larger velocities. The smectite release is proportional to the water velocity to the power 0.41. It may be noted that the penetration depth of the gel front increases strongly with decreasing water velocities and extends to a radius of tens of meters already for a water velocity of 1 m/s. This is a larger distance than the size of many of the fractures in the fracture network. The model is thus not appropriate to use for the lowest velocities.

Figure 9-6 shows the release rate for different diameters of the cylindrical hole containing the bentonite. A 5 m diameter hole, which could represent a deposition tunnel has a release rate less than two times larger than a canister deposition hole. More information on these simulation can be found in /Moreno et al. 2009/.

Both the diffusive model and the advective model predict an increase of smectite loss with water flowrate. The smectite loss in Table 9-2 is much larger than in Table 9-1. The former results are entirely dependent on the choice of ϕ_{min}. This has been an arbitrary choice based on the observations that around ϕ=0.01 there is a sharp rise in viscosity. The advective model also includes the effects of particle diffusion so it is not surprising that higher values will be obtained when advection is also accounted for.

Table 9-2. Loss of smectite by advective flow.

Water Velocity, m/yr	Smectite release for 1 mm fracture aperture, g/yr	Penetration into the fracture at the centre, m
0.10	11	34.6
0.32	16	18.5
0.95	26	11.5
3.15	43	7.0
31.50	117	2.1
315.00	292	0.5

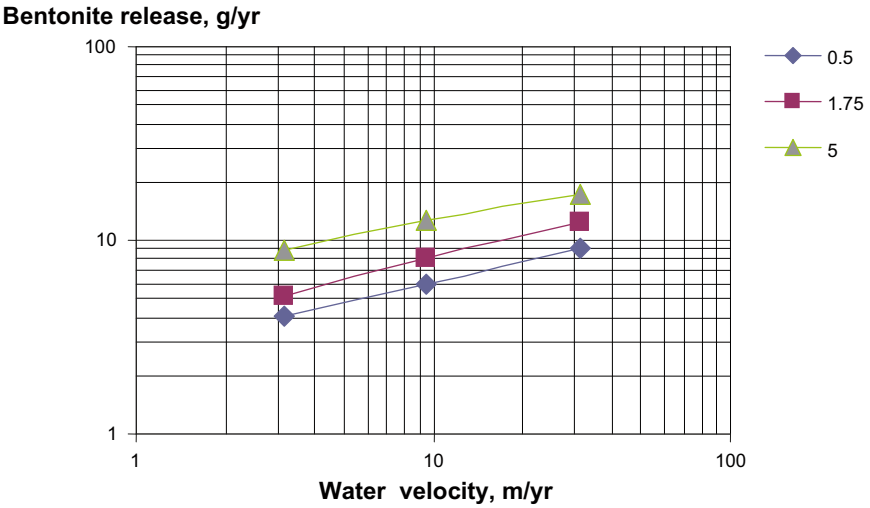

Figure 9-6. *Smectite release as a function of the water velocity for different hole diameters.*

Simulations were also performed using different values of volume fraction at the fracture mouth. Figure 9-7 shows the release of bentonite. The simulations were made with the full 2-dimensional model including also counter ion (sodium) migration. These results are expected because the release of bentonite into the flowing water is controlled by the bentonite concentration profile near the gel/water interface where the volume fraction is less than a few %. Near the deposition hole the volume fraction is so large that the large gel viscosity effectively hinders the gel to flow. The gel/sol flows only at volume fractions below a few percent.

It is therefore expected that the rate of loss of smectite will not be much influenced by the smectite volume fraction at the mouth of the fracture. The latter will mainly only influence how far out from the mouth of the fracture the gel/sol front stabilises at steady state. This is for the case when the gel expansion only takes place in one dimension. For the two dimensional expansion, as is the case for the cylindrical source around the deposition hole, this is not quite the case because the gel expands radially and the contact surface circumference of the gel/sol/water interface increases. Nevertheless, the impact of the volume fraction at the source is not very large as is seen in the figure.

From the results shown in Figure 9-7, it is seen that for high concentrations at the boundary the release is constant. When the volume fraction at the fracture mouth is 0.20 a small decrease is observed. For a volume fraction of 0.10 more than 80% of the smectite originally in the deposition hole has been lost.

More information on these simulation can be found in /Moreno et al. 2009/.

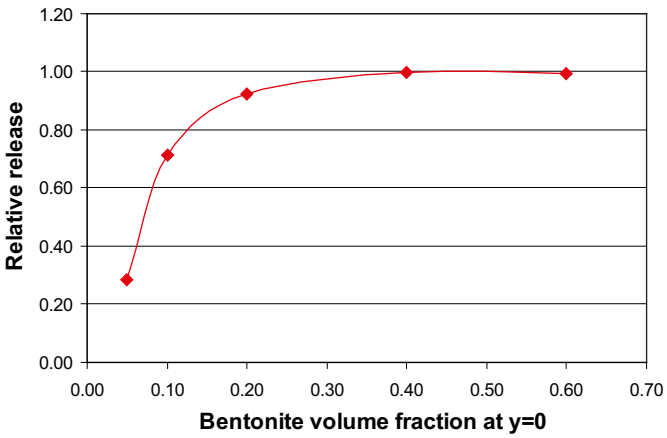

Figure 9-7. *Smectite release as a function of the bentonite volume fraction at the mouth of the fracture.*

There are several uncertainties in the results for the advective mode. In these exploratory simulations we have not fully accounted for the influence of the ion transport on the viscosity. We think that there may be an increase or decrease in smectite loss when a full account is taken of the diffusion of calcium and sodium in the gel phase of the smectite. We have not been able to find viscosity data on calcium dominated gels.

In these models the expansion has been taken to be horizontal, thus neglecting gravity. Scoping calculations suggest that gravity will give small effects as in our model the smectite sheets have separated into essentially individual colloid particles. For gravity to have an effect the particles must be considerably larger. See also Section 3.3. However, there are several observations that by reasons we do not yet understand gravity rapidly pulls smectite downwards from a gel/water interface. The models underlying the results in Tables 9-1 and 9-2 do not account for this.

An alternative model is presented by /Birgersson et al. 2009/ who modelled the rate of expansion of bentonite into a fracture restrained by friction against the walls of the fracture. In a sample calculation they arrived at a loss of 12 g/yr. The model and underlying data are very uncertain, however, as shown in the discussions of the rheologic properties presented in that report. It may also be noted that the authors of the present report consider the wall friction model proposed by /Birgersson et al. 2009/ to be unrealistic. See Appendix 1 where we discuss wall friction and its role in expanding gel into a fracture.

9.4 Shearing of cohesive gel

9.4.1 Shear forces of flowing water in a fracture

The shear stress τ on the walls of a fracture is obtained from a force balance. The force F on a slit due to the pressure drop ΔP in a slit with aperture δ, length L and width W is

$$F = \Delta P W \delta_{fr} = \Delta h \rho_w g W \delta_{fr} \tag{9-5}$$

This force is balanced by the friction force on the surfaces of the slit

$$F = 2WL\tau \tag{9-6}$$

Combining Equations 9-5 and 9-6 gives the shear stress as a function of the hydraulic gradient and fracture aperture.

$$\tau = \frac{1}{2}\delta_{fr}\rho_w g \frac{\Delta h}{L} \tag{9-7}$$

In the thin slit that makes up the narrow fracture the same shear stress will also act on the gel as long as the gel does not move. This is a fair approximation as the velocity gradient across the aperture rises from zero at the wall to maximum in the middle of the fracture. Similarly the velocity at a distance of about one aperture from the gel/water interface will have risen from zero to the maximum velocity in the middle of the fracture because at larger distances the profile will be set by the nearness of the fracture walls and will be marginally influenced by the presence of the gel/water interface. It is possible to derive exact numerical numbers for simple geometries if necessary but considering that the fracture in reality has variable aperture and the gel/water interface is poorly defined the above relation is sufficient for our purposes.

Figure 9-8 shows the shear stress for apertures 0.1 and 1mm for hydraulic gradients from 0.001 to 0.1.

It is seen that even for so high a gradient as 10% and a large fracture aperture as 1 mm, the shear stress is no more than 0.5 N/m^2. This is a very low shear stress and is less than the yield stress of cohesive gels as found by /Birgersson et al. 2009/. They found that the shear strength of MX-80 at a water ratio of 100 (ϕ=0.0037) for sodium concentration of 10 and 100 mM is larger than 5 Pa. This is the concentration range where the gel is expected to be cohesive. Even in distilled water the shear strength is larger than 1 Pa for water ratios below 40, Figures 4-47 to 4-49 in /Birgersson et al. 2009/.

The mean aperture is expected be much less than 1 mm.

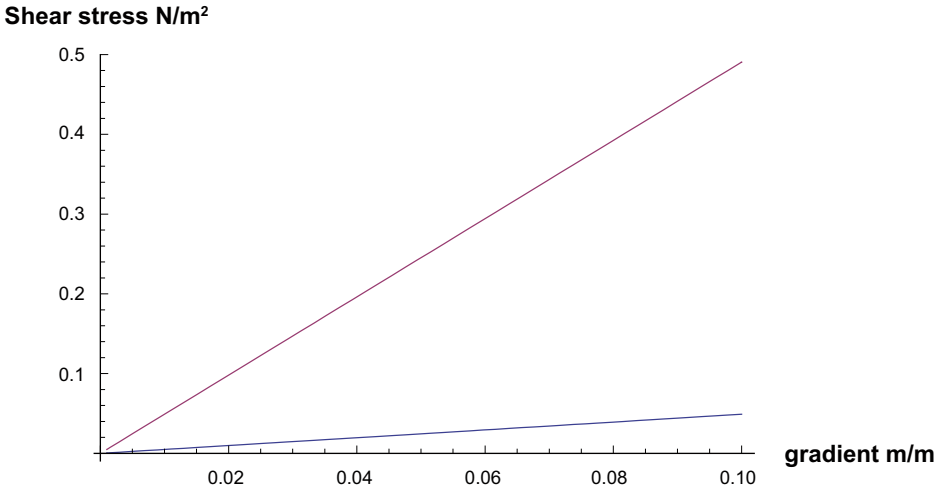

Figure 9-8. *Shear stress at gel/water interface as a function of hydraulic gradient and aperture, Lower curve 0.1 mm, upper curve 1 mm aperture.*

9.5 Gravity effects

In Appendix H in /Moreno et al. 2009/ some experiments that show sedimentation of bentonite gel in downward facing fractures are described. In the experiments reported by /Jansson 2009/ the test tube has a diameter of about 2.5 cm, which gives a cross section area of 5 cm^2. A mass of 0.2 g of homoionic smectite sedimented through the 17 µm mesh size net in about 10 minutes. The specific release rate, flux, of smectite is 0.24 g cm^{-2} $hour^{-1}$. In this experiment the smectite "blobs" were smaller than the diameter of the tube and they were probably not much influenced by wall friction. On the other hand they had no difficulty in rapidly wriggling through 17 µm openings.

This rapid release differs from what was observed in the experiments in slits. In the experiment with untreated bentonite MX-80 in distilled water it took 0.106 g bentonite in a slit with 1.32 mm aperture and 13 cm long about 48 hours to be released and sediment, /Neretnieks 2009/. This gives 0.0013 g cm^{-2} $hour^{-1}$. This is more than 100 times less than in the previous case. However, the "blobs" were several mm to a centimetre large and visibly could be seen to slowly change shape as they moved downward. This was interpreted as being caused by friction against the walls of the slit.

In another experiment dry clay particles that stuck between the glass plates were about 1 mm diameter before the slit was filled with water. It is roughly estimated that they are 1 mm^3 and have a mass of 1 mg. After filling the slit with water the particles rapidly swelled out in 2 dimensions to become about one cm across. The swollen "blobs" slowly disintegrated into much smaller particles, which sedimented. The release took place from a cm length in a 1.3 mm wide slit. The "blobs" had essentially disappeared in 48 hours so the flux is about $1.6 \cdot 10^{-4}$ g cm^{-2} $hour^{-1}$. In this case wall friction is not deemed to have influenced the rate of disintegration of the blobs.

Should these release rates be representative of conditions around the canister deposition hole an estimate of the rate of loss of bentonite can be made. The diameter of the deposition hole is 1.75 m and its mean aperture is taken to be 0.1 mm. This gives an area for release of 1.75 cm^2.

With a release rate of 0.24 g cm^{-2} $hour^{-1}$ this gives a loss rate of 0.42 g $hour^{-1}$. This is equivalent to 3,700 g $year^{-1}$ or 3,700 kg per 1,000 years.

With a release rate of $1.3 \cdot 10^{-3}$ g cm^{-2} $hour^{-1}$ this gives a loss rate of 0.0023 g $hour^{-1}$. This is equivalent to 19.9 g $year^{-1}$ or 19.9 kg per 1,000 years.

With a release rate of $1.6 \cdot 10^{-4}$ g cm^{-2} $hour^{-1}$ this gives a loss rate of 0.00028 g $hour^{-1}$. This is equivalent to 2.5 g $year^{-1}$ or 2.5 kg per 1,000 years.

9.6 Discussion and conclusions

9.6.1 The critical coagulation concentration CCC and conditions at gel/water interface

Although the CCC is not well defined, and the notion is somewhat controversial, it is a practically observable entity. When the pore waters contain more than about 50 mM monovalent cations, give or take a factor of 2, the smectite gel is cohesive and does not release individual particles by Brownian motion. For calcium only about 1 mM is needed to generate a cohesive gel. If above CCC conditions can be maintained at the gel/water interface, no erosion by release of smectite particles to the seeping water is expected. The shear strength of the cohesive gel is well above the shear force that the seeping water can generate so no mechanical sharing of gel is expected either.

If the seeping groundwater is below the CCC, ions can be leached from the gel at the gel water interface and the pore water concentration can fall below the CCC making the gel expansive. This leads to release of particles to the water by Brownian motion. The dilute gel can also flow away because viscosity can decrease to values approaching that of water.

Smectite gels with practically only divalent charge compensating ions (calcium) behave differently from gels with monovalent ions. Calcium gels will not separate the smectite into individual sheets as sodium gels do. The sheets are held together in larger particles, such as stacks or more complex structures. These larger particles are not seen to separate from the gel by Brownian motion in an upward gravity field. It is not known if the gel formed of these larger particles is cohesive in the sense that particles would not be released in a downward facing gravity field. Magnetic resonance imaging show a 2 mm diffuse layer above the denser gels which suggests that the gel is not cohesive, Figure 3-18.

However, more than about 90% of the charge compensating ions must be calcium in calcium/sodium clays for these conditions to prevail. With less than this amount of calcium the smectite behaves more like a pure sodium clay.

The chemical conditions at the gel/water interface are influenced by the original conditions in the smectite, by the composition and flowrate of the seeping water, and by the diffusion properties in pore water and in the gel-phase. There is a considerable uncertainty in the data needed to quantitatively modelling these processes. Furthermore the models themselves are not mature enough to convincingly simulate these processes.

9.6.2 Models

We have presented a number of conceptual and mathematical models that describe the smectite behaviour as well the broader picture where all mechanisms are combined to simulate smectite erosion. The *Dynamic force balance model* is the most important because it describes the forces that drive the dispersion of the smectite particles. This model has been successfully tested against experiments. The gel *viscosity* model is needed to assess the advective flow of the gel. This model is based on a limited set of experiment and does not account for thixotropy and is probably conservative. The *gel hydraulic conductivity model(s)* are based on experiments and well known model structures, which however have been modified to better agree with experimental data on viscosity.

Ion diffusion modelling in the gel is based on experimental data on diffusivities and established principles of diffusion in ion exchange membranes but is considerably simplified. *Mass transfer between seeping* water and gel is based on established mass transfer principles.

9.6.3 Filtering and straining

The previous discussion has been based on the assumption that the smectite behaviour only depends on the smectite particles themselves and that there are no physical barriers that impede their movement. Smectite particles readily wriggle through pores in filter by the repulsive forces between them and by Brownian motion. However, even thin filters will slow down the smectite penetration rate which is inversely proportional to the thickness of the filter. The presence of some cm of detritus material in the fracture has a strong retarding effect.

We have not presented a quantitative model for the effects of straining. There is, however, strong experimental and theoretical evidence that the smectite particles will be strained by accessory material in the bentonite that will be left behind when some smectite is lost. We believe that very small amounts of the accessory minerals are needed to form a straining filter bed at the entrance of the fracture or in the fracture itself. The accessory minerals will not be able to penetrate far into the fractures because the particles will be retained and clog the fractures. Experiments in real fractures should be made to support this projection.

9.6.4 Uncertainties

The models have been used to simulate smectite loss under some idealised conditions and with simplifying assumptions. The uncertainties in the conceptual as well as in the mathematical models are considerable. The combination of the individual models into a coherent model is not straightforward because it has to combine chemistry, surface chemistry, basic physics, rheology, hydrology, transport phenomena and more into one consistent overall model. In addition the uncertainties in data are considerable. A reliable and credible overall model will need considerable development work.

Nevertheless, we believe that the exploratory modelling described in section 9.3 is basically sound. It cannot, however, be used to obtain quantitatively reliable simulation result at present.

9.6.5 Overall erosion rate simulations

The rate of smectite loss under different conditions presented in chapter 9 lead us to the conclusion that the advective mode is reasonably well founded based on our present understanding of the system. In low salinity waters with ion charge concentrations less than 2–4 meq/l the gel is expansive and can be carried away by the seeping water in the fracture. In these circumstances the smectite particles separate into individual sheets and diffuse and flow away from the source. Gravity should not influence the transport because the individual sheets are so small that other forces dominate. We are, however, aware of the experiments where gravity aided the release of colloids, which are not fully understood, section 3.3.2.

For given water velocity in the fracture the rate of loss is proportional to the fracture aperture. In a situation where all the circumference of the fracture that intersects the hole is open and the seeping water is in contact with the buffer all along the fracture intersection, our estimate of erosion rate is presented in Table 9-2.

It should be noted that the data in the table exemplify a case with a 1 mm aperture and that the entire fracture is open and exposed to seeping water. This is conservative for two reasons. At repository depth the fracture aperture is probably much smaller than 1 mm in most fractures. The other conservatism is that the fracture is open everywhere. This is contrary to observations, which show that fractures have variable apertures and actually are open only on approximately 10% of the entire surface. This leads to channelling effects and that only about 10% of the fracture intersection with the deposition hole would have flowing water in contact with the buffer. As a first approximation this would reduce the rate of erosion by a factor 3.

A more realistic erosion rate would then be about 10 times smaller than the figures in Table 9-2 if the fracture is 0.3 mm and the channelling effects are accounted for. For a water velocity of 3 m/yr the erosion rate would be about 4 g/yr.

9.7 Suggestion for future work

The behaviour of calcium dominated smectite is not well understood and should be further studied.

We believe that the intrusion of detritus material in the fractures will form an efficient barrier against smectite loss. Experiments study this phenomenon should be performed.

10 Overall discussion and conclusions

Clay colloid chemistry and the properties of bentonites and smectites have been studied intensively during a long time. There is a sound theoretical basis for the forces acting on and between smectite particles in gels and suspensions and how these are influenced by water chemistry. Much experience has been gathered on practical use of bentonite suspensions used as drilling muds and as additives to various products including paints to give them thixotropic properties.

Nevertheless, there are areas where the behaviour of smectite gels and sols, which have important impact on the possible erosion of the bentonite buffer, that are not sufficiently understood. The thixotropic behaviour of the gel/sol, although much studied, has not resulted in a coherent model that can be used to quantitatively predict the non-Newtonian viscous behaviour and especially not how resting time influences the stress-strain behaviour of the gel. The possible shearing of a gel therefore has been approached in a simplified way neglecting thixotropy. This is deemed to be a conservative approach and shearing is not expected to cause erosion of cohesive gels under reasonably credible scenarios.

The viscosity of dilute gel/sols is described based on a new model that accounts for the co-volume of the rotating coin-like smectite particles, including also the seeming increase of the particle size caused by the extent of the electrical double layer. The model is based on a limited amount of experiments but we deem it to be reasonably well suited for the purpose of modelling smectite gel/sol flow. Such flow has been found to potentially be an important mechanism for smectite erosion.

Expansion of a smectite gel is caused by strong repulsion forces between the negatively charged smectite particles. The rate of expansion is mediated by the friction of the particles against the water that enters the gel. Expansive forces have been modelled using the Poisson-Boltzmann equations which are known to give a good description of sodium smectite behaviour. The friction forces in the gel have been modelled by modified Kozeny-Carman expressions. These forces together with the attractive van der Waals forces, buoyancy forces and forces generated by the chemical potential gradient have formed the core of the Dynamic force balance model that quantifies the expansion rate of the gel and release of colloids to the seeping water. The model has been qualitatively and quantitatively verified by comparison with different experiments for sodium dominated systems. We deem it to be reliable for the purpose at hand although there is a lack of fundamental understanding of the behaviour of calcium dominated gels.

The pore water chemistry at the gel/water interface determines whether smectite particles can be released from the gel or not. The conditions at the gel/water interface are influenced by the presence of soluble minerals in the bentonite, by the ion exchange properties of the smectite and by type and amount of counterions in the ion exchange positions in the smectite. Furthermore the diffusion properties of the ions in the gel as well as the mass transfer resistance and the composition of the approaching non-saline groundwater influence the condition at the gel/water interface. The possible variations in these properties, taken together, makes it impossible to firmly state that the conditions will not favour colloid release and smectite erosion, should there be no other restraining mechanisms.

Experiments in downward facing slits (fractures) have been found to release swelling bentonite much faster than expected. The bentonite is released and sediments as gel agglomerates also under conditions where it is expected that the smectite particles should have separated into individual smectite sheets. Such colloidal particles would not noticeably be influenced by gravity. The reasons for this behaviour are not understood.

One restraining effect we deem is very important is the formation of a porous region of accessory minerals naturally present in the bentonites and left behind when smectite is lost. The accessory minerals have negligible surface charge and are order to orders of magnitude larger than the smectite particles. A filter will form at the mouth of the fracture and also some distance into the fracture. The rate of smectite migration through the filter is inversely proportional to its thickness.

The filter that forms at the mouth of the fracture inside the compacted buffer is compressed by the buffer swelling pressure. Even a few mm thick filters of non-smectite minerals have been found to efficiently stop smectite penetration *by straining*. The accessory minerals are at the same time large enough not to be able to penetrate very far into the narrow fractures in deep lying rock and so be lost because they will be caught in the narrow passages in the fractures.

The formation of filters and their filtering properties have been studied in a series of laboratory experiments with very encouraging results. However, it would be prudent to make experiments in fractures to firmly validate the process. Our final conclusions are that we believe that chemical conditions at the gel/water interface cannot be proved to generate a cohesive gel in low salinity waters. However, the detritus material left behind when smectite is lost from the bentonite will form filters in the fracture and at the fracture mouth and decrease the smectite loss to very low values.

11 Notation

Units used are according to SI system unless otherwise stated in the text

$a_{R,}$	Specific area of particles, area/particle volume
a_v	Specific area of particles, area/liquid volume
A_{bed}	Cross section area of a porous bed (perpendicular to flow)
A_H	Hamaker constant
c	Concentration of ions
CCC	Critical coagulation concentration
c_{FW}	Concentration of ions in fresh water
c_{PW}	Concentration of ions in pore water
C	Total concentration in medium
CEC	Cation exchange capacity
d_{coin}	Coin-like particle diameter
d_p	Particle diameter
d_s	Sheet diameter
d_{tube}	Diameter of tube
D_a	Apparent diffusivity
D_e	Effective diffusivity
D_F	Diffusivity function for particles
D_0	Diffusivity unconfined water
D_p	Diffusivity of particles
D_s	Surface diffusivity of ions, Diffusivity in gel water
D_w	Diffusivity of ions
f_{Ca}	Fraction of calcium in water
f_{fr}	Friction factor based on velocity difference between water and particles
F	Faraday constant
F_{bed}	Force on a porous bed
F_{DDL}	Diffuse layer force between particles
F_g	Buoyancy force on particle
F_s	Body force in general
F_{vdW}	van der Waal's force between particles
F_η	Friction force on particle
F_μ	Force on particle due to chemical potential
g_c	Gravitation constant
G	Tortuosity function
h	Distance between sheets
h_{stack}	Distance between stacks
h	Hydraulic head
h_1	Distance between sheets

h_2	Distance between stacks
I	Ionic strength
J	Flux (flowrate/cross section area)
k	Permeability
k_0	Kozeny's constant
k_B	Boltzmann constant
K	Ion exchange equilibrium constant
K_d	Sorption coefficient (mass based)
K_{gy}	Solubility constant for gypsum
K_h	Hydraulic conductivity
K_H	Huggins coefficient
K_V	Sorption coefficient (volume based)
l_p	Lateral extent of stack/particle/quasi-crystal
l_s	Lateral extent of sheet
L_o	Length of tablet
L_T	Length of test tube
m	Mass
M	Molecular mass
n	Number of sheets in a stack
n_{part}	Number of particles
N	Flowrate of ions or particles
P	Pressure
P_{DDL}	Pressure due to double layer forces
P_{swell}	Swelling pressure
P_{vdW}	Pressure due to van der Waal's forces
q	Concentration of ions in smectite phase
Q_{eq}	Equivalent flowrate
r_{eqv}	Equivalent radius of particles
r_h	Radius of deposition hole
R	Gas constant
S_p	Particle surface area one side
T	Absolute temperature
T	Hydraulic transmissivity
u	Velocity in pores
u_o	Superficial velocity/flux
u_p	Particle velocity
V_{bed}	Volume of porous bed
V_{cov}	Co-volume for particle
V_p	Volume of particle
V_s	Volume of solids
V_{sheet}	Volume of sheet

V_w	Volume of water
W	Fracture width
x_{Ca}	Mass of calcium per mass of bentonite
X_{Ca}	Fraction of calcium in ion exchange positions
yd	Dimensionless surface potential
z	Valence of ions
α	Capacity factor
$\alpha_{macropore}$	fraction of ions in macropores
$\alpha_{nanaopores}$	fraction of ions in nanopores
δ_{fr}	Fracture aperture
δ_h	Hydraulic aperture of fracture
δ_p	Particle thickness
δ_{RT}	Residence time aperture of fracture
δ_s	Sheet thickness
ε	Porosity
ε_{An}	Volume fraction of gel accessible for anions
ε_o	Permittivity in vacuum
ε_r	Relative dielectric permittivity
η	Viscosity
η_i	Intrinsic viscosity
η_w	Viscosity of water
κ	Reciprocal Debye length
μ	Chemical potential
ξ	Thermal deviation factor
ρ	Density
ρ_p	Density of particle
ρ_s	Density of smectite
ρ_w	Density of water
σ_o	Surface charge density
τ	Shear stress
ϕ	Volume fraction of solids (1-ε) in gel/sol
ϕ_{cov}	Co-volume fraction
ϕ^{κ}_{cov}	Co-volume fraction including effects of electrical double layer extension
ϕ_p	Volume fraction of solids in Stack/particle/quasi-crystal thickness
ϕ_s	Volume fraction of stacks inscribed in spherical shell
$\phi_{spheres}$	Volume fraction of spheres
Φ_0	Surface electrical potential
χ	Term in generalized diffusion coefficient
Ψ	Anion exclusion factor
θ	Angle from direction the particle moves

12 List of reports from erosion project participants

Birgersson M, Börgesson L, Hedström M, Karnland O, Nilsson U, 2009. Bentonite erosion, Final Report from Clay Technology, Clay Technology AB, IDEON Research Center S-223 70 Lund, Sweden.

Dvinskikh S, Furó I, 2009. Magnetic resonance imaging and nuclear magnetic resonance investigations of bentonite systems, Report, Physical Chemistry, Royal Institute of Technology, KTH.

Jansson M, 2009. Laboratory studies of Bentonite Erosion, Report, Nuclear Chemistry, Royal Institute of Technology, KTH.

Jönsson B, Åkesson T, Jönsson B, Meehdi M S, Janiak J, Wallenberg R, 2009. Structure and Forces in Bentonite MX-80, Report, Theoretical Chemistry, Chemical Center, POB 124, S-221 00 Lund, Sweden.

Liu L, Neretnieks I, 2007. Bentonite erosion Literature review, Report, Chemical Engineering and Technology, Royal Institute of Technology, KTH, Stockholm.

Liu L, Neretnieks I, 2008. Homo-interaction between Parallel Plates at Constant Charge, Colloids Surf. A: Physicochem. Eng. Aspects 2008, 317, 636.

Liu L, Moreno L, Neretnieks I, 2008. Interaction between colloidal particles, Literature Review, Report Chemical Engineering and Technology, Royal Institute of Technology, KTH, Stockholm.

Liu L, Moreno L, Neretnieks I, 2008. A Dynamic Force Balance Model for Colloidal Expansion, Report Chemical Engineering and Technology, Royal Institute of Technology, KTH.

Liu L, Moreno L, Neretnieks I, 2009a. A Dynamic Force Balance Model for Colloidal Expansion and Its DLVO-based Application, Langmuir, 2009, 25(2), 679–687.

Liu L, Moreno L, Neretnieks I, 2009b. A Novel Approach to Determine the Critical Coagulation Concentration of a Colloidal Dispersion with Plate-like Particles, Langmuir, 2009, 25(2), 688–697.

Liu D, Liu L, 2009. The viscosity of sodium montmorillonite suspensions, Report Chemical Engineering and Technology, Royal Institute of Technology, KTH, Stockholm, In preparation.

Moreno L, Liu L, Neretnieks I, 2009. Modelling of erosion of bentonite gel by gel/sol flow, Report, Chemical Engineering and Technology, Royal Institute of Technology, Stockholm, Sweden.

Neretnieks I, 2009. Some scoping erosion experiments in thin slits between glass plates, Report, Chemical Engineering, Royal Institute of Technology, KTH.

Neretnieks I, Liu L, Moreno L, 2009. Ion exchange and transport and in smectite clays, Report, Chemical Engineering and Technology, Royal Institute of Technology, KTH.

Neretnieks I, Liu L, Moreno L, 2009. Mechanisms and Models for bentonite erosion, Main report, Chemical Engineering and Technology, Royal Institute of Technology, KTH. (This is the present report).

Pettersson, T, Thormann E, Claesson P, 2008. AFM study of Montmorillonite, Report, Department of Chemistry, Surface Chemistry, Royal Institute of Technology, SE-100 44, Stockholm, Sweden.

Puura E, Kirismäe K, 2008. Impact of the changes in the chemical composition of pore water on chemical and physical stability of natural clays: – a review of natural cases and related laboratory experiments and the ideas on natural analogues for bentonite erosion/non-erosion, Report, Institute of Ecology and Earth Sciences, University of Tartu, Tartu, Estonia.

Richards T, 2009. Particle clogging in porous media – Filtration of a smectite solution, Report, Chalmers University of Technology, Göteborg.

13 References

Abend S, Lagaly G, 2000. Sol–gel transitions of sodium montmorillonite dispersions, Applied Clay Science, 16, 201–227.

Adachi Y, Nakaishi K, Tamaki M, 1998. Viscosity of a dilute suspension of sodium montmorillonite in a electrostatically stable condition, Journal of Colloid and Interface Science 198, 100–105.

Archie, G E, 1942. The Electrical Resistivity Log as an Aid in Determining Some Reservoir Characteristics', Trans. AIME 146, 56–62.

Arcos D, Grandia F, Domènech C, 2006. Geochemical evolution of the near field of a KBS-3 repository SKB TR-06-16, Svensk Kärnbränslehantering AB.

Baik M-H, Cho W-J, Hahn P-S, 2007. Erosion of bentonite particles at the interface of a compacted bentonite and a fractured granite, Engineering Geology 91 229–239

Barnes H A, 1997. Thixotropy – a review, J. Non-Newtonian Fluid Mech, 70, 1–33.

Batchelor G K, 1970. Slender body theory for particles of arbitrary cross-section in Stokes flow. J. Fluid Mech, 44, 419–440.

Bekkour K, Leyama M, Benchabane A l, Scrivener O, 2005. Time-dependent rheological behaviour of bentonite suspensions: An experimental study, J. Rheol. 49(6), 1329–1345.

Benna M, Kbir-Ariguib N, Magnin A, Bergaya F, 1999. Effect of pH on rheological properties of purified sodium bentonite suspensions. J. Colloid Interface Sci. 218, 442–455.

Bergaya F, Theng B K G, Lagaly G, 2006. Elsevier. Handbook of Clay Science.

Bird R B, Stewart W E, Lightfoot, 2002. Transport Phenomena, Wiley.

Birgersson M, Börgesson L, Hedström M, Karnland O, Nilsson U, 2009. Bentonite erosion, Final Report from Clay Technology, Clay Technology AB, IDEON Research Center S-223 70 Lund, Sweden.

Boisson J Y, 1989. Study on the Possibilities by Flowing Ground Waters on Bentonite Plugs Expanded from Borehole into Fractures, Proc. NEA/CEC Workshop Sealing of Radioactive Waste Repositories.

Bourg I C, Sposito G, Bourg A C M, 2006. Tracer diffusion in compacted, water saturated bentonite, Clays and Clay Minerals, Vol. 54, No. 3, 363–374.

Bourg I C, Sposito G, Bourg, A C M, 2007. Modeling cation diffusion in compacted water-saturated sodium bentonite at low ionic strength, Environ. Sci. Technol, 41, 8118–8122.

Bourg I C, Sposito G, Bourg A C M, 2008. Modelling the diffusion of Na+ in compacted water-saturated Na-bentonite as a function of pore water ionic strength, Applied Geochemistry 23, 3635–3641.

Bradbury M H, Baeyens B, 1999. Modelling the sorption of Zn and Ni on Ca-montmorillonite, Geochimica et Cosmochimica Acta, 63(3-4), 325–336.

Bradbury M H, Baeyens B, 2003. Porewater chemistry in compacted re-saturated MX-80 bentonite, Journal of Contaminant Hydrology, 61, 329–338.

Bradbury M H, Baeyens B, 2009. Sorption modelling on illite Part I: Titration measurements and the sorption of Ni, Co, Eu and Sn, Geochimica et Cosmochimica Acta, 73(4), 990–1003.

Bradford S A, Simunek J, Bettahar M, Tadassa Y F, van Genuchten M T, Yates S R, 2002. Physical factors affecting the transport and fate of colloids in saturated porous media. Water Resour. Res, 38(12), 63 1–12.

Bradford S A, Simunek J, Walker S L, 2006. Significance of straining in colloid deposition: Evidence and implications. Water Resour. Res, 42, W12S15, 2006.

Brandenburg U, Lagaly G, 1988. Rheological Properties of sodium montmorillonite dispersions, Applied Clay Science, 3 263–279 263.

Brown G H, 2002. Glacier meltwater hydrogeochemistry. Applied geochemistry, 17, 855–883.

Brown A B D, Clarke S M, Rennie A R, 1998. Ordered Phase of Platelike Particles in Concentrated Dispersions, Langmuir, 14, 3129–3132.

Brown A D B, Ferrero C, Narayanan T, Rennie A R, 1999. Phase separation and structure in a concentrated colloidal dispersion of uniform plates, Eur. Phys. J. B., 11, 481.

Börgesson L, Nilsson U, 2008. Bentonite penetrating into rock fractures, Laboratory results from rheological measurements and theoretical considerations, Clay Technology AB, IDEON Research Center S-223 70 Lund, Sweden.

Cadene A, Durand-Vidal S, Turq P, Brendle J, 2005. Study of individual Na-montmorillonite particles size, morphology and apparent charge, Journal of Colloid and Interface Science 285 719–730.

Chambré P L, Pigford T H, Sato Y, Fujita A, Lung H, Zavoshy S J, Kobayashi R, 1982. Analytical Performance Models, LBL-14842, Lawrence Berkeley Laboratory.

Chapuis R P, Aubertin M, 2003. On the use of the Kozeny-Carman equation to predict the hydraulic conductivity of soils, Can. Geotech. J. 40, 616–628.

Chen J S, Cushman J H, Low P F, 1990. Rheological behavior of Na-montmorillonite suspensions at low electrolyte concentration. Clays Clay Miner. 38, 57–62.

Christidis G E, 1998. Physical and chemical properties of some bentonite deposits of Kimolos Island, Greece, Applied Clay Science 13, 79–98.

Christidis G E, Eberl D D, 2003. Determination of layer-charge characteristics of smectites, Clays and Clay Minerals, 51(6), 644–655.

Christidis G E, Blum A E, Eberl D D, 2006. Influence of layer charge and charge distribution of smectites on the flow behaviour and swelling of bentonites, Applied Clay Science 34, 125–138.

Christidis G E, 2008. Validity of the structural formula method for layer charge determination of smectites, A re-evaluation of published data, Applied Clay Science.

Comsol Multiphysics, 1998–2009. COMSOL AB.

Crank J, 1975. The Mathematics of Diffusion, Clarendon Press.

CRC, 1981. Handbook of Chemsitry and Physics 61st, Ed. 1980–1981, CRC-Press.

Duran J D G, Ramos-Tejeda M M, Arroyo F J, Gonzáles-Caballero F, 2000. Rheological and electrokinetic properties of sodium montmorillonite suspensions: I. Rheological properties and interparticle energy of interaction. J. Colloid Interface Sci. 229, 107–117.

Dvinskikh S, Furó I, 2009. Magnetic resonance imaging and nuclear magnetic resonance investigations of bentonite systems, Report, Physical Chemistry, Royal Institute of Technology, KTH.

Evans D F, Wennerström H, 1999. The colloidal domain, Wiley.

Frey E, Lagaly G, 1979. Selective coagulation in mixed colloidal suspensions, Journal of Colloid and Interface Science, 70.

Galindo-Rosales F J, Rubio-Hernández F J, 2006. Structural breakdown and build-up in bentonite dispersions, Applied Clay Science, 33, 109–115.

Gao B, Saier J E, 2006. Pore–scale mechanisms of colloid deposition and mobilization during steady and transient flow through unsaturated granular media. Water Resour. Res, 42, W0l4l0.

Glaus M A, Baeyens B, Bradbury M H, Jakob A, Van Loon L R, Yaroshchuk A, 2007. Diffusion of ^{22}Na and ^{85}Sr in montmorillonite, Evidence of interlayer diffusion being the dominant pathway at high compaction, Environ. Sci. Technol, 41 (2), 478–485. DOI: 10.1021/es061908d.

Grindrod P, Peletier M, Takase H, 1999. Mechanical interaction between swelling compacted clay and fractured rock, and the leaching of clay colloids, Engineering Geology, 54, 159–165.

Helfferich, 1962. Ion Exchange, McGraw Hill NY.

Hiemenz P C, 1986. Principles of Colloid and Surface Chemistry, Marcel Dekker NY.

Hubbard J B, Douglas J F, 1993. Hydrodynamic friction of arbitrarily shaped Brownian particles, Phys. Rev. E 47, 2983–2986.

Ichikawa Y, Kawamura K, Nakano M, Kitayama K, Kawamura H, 1999. Unified molecular dynamics and homogenization analysis for bentonite behavior: current results and future possibilities. Eng. Geol. 54, 21–32.

Jansson M, 2009. Laboratory studies of Bentonite Erosion, Report, Nuclear Chemistry, Royal Institute of Technology, KTH.

Jönsson B, Åkesson T, Jönsson B, Meehdi M S, Janiak J, Wallenberg R, 2009. Structure and Forces in Bentonite MX-80, Report Theoretical Chemistry, Chemical Center, Lund, Sweden.

Kanno T, Wakamatsu H, 1991. Experimental Study on Bentonite Gel Migration from a Deposition Hole, Proc. 3rd Int. Conf. Nuclear Fuel Reprocessing and Waste Management (RECOD ’91).

Kanno T, Matsumoto K, Sugino H, 1999. Evaluation of extrusion and erosion of bentonite buffer, Proc. 7th Int. Conf. on Radioactive Waste Management and Environmental Remediation (ICEM ’99).

Karnland O, Muurinen A, Karlsson F, 2003. Bentonite swelling pressure in NaCl solutions, Experimentally determined data and model calculations. In Advances in understanding engineered clay barriers. Proceedings of the international symposium on large scale field tests in granite, Barcelona, Spain, 12–14 th November 2003, p 241–256.

Karnland O, Olsson S, Nilsson U, 2006. Mineralogy and sealing properties of various bentonites and smectite-rich clay materials. SKB TR-06-30, Svensk Kärnbränslehantering AB.

Kelessidis V C, Tsamantaki C, Dalamarinis P, 2007. Effect of pH and electrolyte on the rheology of aqueous Wyoming bentonite dispersions, Applied Clay Science, 38, 86–96.

Kjellander R, Marcelja S, Quirk, JP, 1988. Attractive double-layer interactions between calcium clay particles, Journal of Colloid and Interface Science, 126 (1).

Kjellander R, Åkesson T, Jönsson B, Marcelja S, 1992. Double layer interactions in mono- and divalent electrolytes: A comparison of the anisotropic hypernetted chain theory and Monte Carlo simulations, J. Chem. Phys, 97 (2).

Kozaki T, Fujishima A, Saito N, Sato S, Ohashi H, 2005. Effects of dry density and exchangeable cations on the diffusion process of sodium ions in compacted montmorillonite, Engineering Geology 81, 246–254.

Kosakowski G, 2004. Anomalous transport of colloids and solutes in a shear zone, Journal of Contaminant Hydrology 72 23–46.

Kurosawa S, Kato H, Ueta S, Yokoyama K, Fujihara H, 1999. Erosion properties and dispersion-flocculation behavior of bentonite particles. Mater. Res. Soc. Symp. Proc. 556, 679–686.

Kurosawa S, James S C, Yui M, Ibaraki M, 2006. Model analysis of the colloid and radionuclide retardation experiment at the Grimsel Test Site, Journal of Colloid and Interface Science 298 467–475.

Liu D, Liu L, 2009. The viscosity of sodium montmorillonite suspensions, Report Chemical Engineering and Technology, Royal Institute of Technology, KTH, Stockholm, In preparation.

Liu J, Neretnieks I, 2006. Physical and chemical stability of the bentonite buffer. SKB R-06-103, Svensk Kärnbränslehantering AB.

Liu L, Neretnieks I, 2005. Analysis of fluid flow and solute transport in a fracture intersecting a canister with variable aperture fractures and arbitrary intersection angles, Nuclear Technology, 150, 132–144.

Liu L, Neretnieks I, 2008. Homo-interaction between parallel plates at constant charge, Colloids and Surfaces, A: Physiochem. Eng. Aspects, 317, 636–642.

Liu L, Moreno L, Neretnieks I, 2009a. A Dynamic Force Balance Model for Colloidal Expansion and Its DLVO-based Application, Langmuir, 2009, 25(2), 679–687.

Liu L, Moreno L, Neretnieks I, 2009b. A Novel Approach to Determine the Critical Coagulation Concentration of a Colloidal Dispersion with Plate-like Particles, Langmuir, 2009, 25(2), 688–697.

Liu L, Moreno L, Neretnieks I, 2009c. A Dynamic Force Balance Model for Colloidal Expansion and Its DLVO-Based Application, Langmuir, 25(2), 679–687. DOI: 10.1021/la8026573.

Liu L, 2010. Permeability and expansibility of sodium bentonite in dilute solutions, accepted for publication in Colloids Surf. A: Physicochem. Eng. Aspects, 358, 68–78.

Luckham P F, Rossi S, 1999. The colloidal and rheological properties of bentonite suspensions, Advances in Colloid and Interface Science, 82, 43–92.

Lyklema, J, 2005. Fundamentals of Interface and Colloid Science, Vol. IV: Particulate Colloids, Elsevier.

Malfoy C, Fontaine C, Pantet A, Monnet P, 2007. The effect of mineralogical and cationic heterogeneities on rheological properties of suspensions with Li-smectites, extracted from Volclay MX-80, C. R. Geoscience, 339, 960–969.

McBride M B, Baveye P, 2002. DivisionS-2-Particle interactions in colloidal systems, Soil Sci. Am J. 66, 1207–1217).

Michot L J, Bihannic I, Porsch K, Maddi S, Baravian C, Mougel J, Levitz P, 2004. Phase diagrams of Wyoming Na-montmorillonite clay. Influence of particle anisotropy, Langmuir, 20, 10829–10837.

Missana T, Alonso U, Turrero M J, 2003. Generation and stability of bentonite colloids at the bentonite/granite interface of a deep geological radioactive waste repository, Journal of Contaminant Hydrology, 61, 17– 31.

Missana T, Geckeis H (Eds.), 2008. GTS Phase V: CRR Experiment: Supporting laboratory experiments with radionuclides and bentonite colloids. July 2006. Nagra Technical Report Series, NTB 03-02, Nagra, Wettingen Switzerland.

Moreno L, Liu L, Neretnieks I, 2009. Modelling of erosion of bentonite gel by gel/sol flow, Report, Chemical Engineering and Technology, Royal Institute of Technology, Stockholm, Sweden.

Muurinen A, Lehikonen J, 1999. Pore water chemistry in compacted bentonite, Posiva Technical Report, 99–20.

Möller P C F, Mewis J, Bonn D, 2006. Yield stress and thixotropy: on the difficulty of measuring yield stresses in practice, Soft Matter, 2, 274–283.

Möri A (Ed.), 2004. GTS Phase V: The CRR project final report series I: Description of the field phase – Methodologies and raw data, Dec. 2004. Nagra Technical Report Series, NTB 03-01, Nagra, Wettingen Switzerland.

Neretnieks I, 1979. Transport mechanisms and rates of transport of radionuclides in the geosphere as related to the Swedish KBS concept. Proceedings, International Atomic Energy Agency IAEA – SM – 243/108, p 315–339, July 2–6, 1979.

Neretnieks I, 2009. Some scoping erosion experiments in thin slits between glass plates, Report, Chemical Engineering, Royal Institute of Technology, KTH.

Neretnieks I, Liu L, Moreno L, 2009a. Diffusion of sodium and calcium in smectite gel – Impact on concentration at gel/water interface by ion exchange processes, Report, Chemical Engineering and Technology, Royal Institute of Technology, Stockholm, Sweden.

Neretnieks I, Moreno L, Liu L, 2009b. Revisiting the Qeq concept and expression, Chemical Engineering and Technology, Royal Institute of Technology, Stockholm, Sweden.

Neretnieks I, Moreno L, Liu L, 2009c. Revisiting the Qeq concept and expression, Chemical Engineering and Technology, Royal Institute of Technology, Stockholm, Sweden, in preparation.

Ochs M, Lothenbach B, Shibata M, Yui M, 2004. Thermodynamic modelling and sensitivity analysis of porewater chemistry in compacted bentonite, Physics and Chemistry of the Earth, 29, 129–136.

Onsager L, 1949. The effect of shape on the interaction of colloidal particles. Ann. N.Y. Acad. Sci. 51: 627–659.

Parkhurst D L, Appelo C A J, 1999. User's guide to PHREEQC (Version2)—A computer program for speciation, batch-reaction, one-dimensional transport, and inverse geochemical calculations: U.S. Geological Survey Water-Resources Investigations Report 99-4259, 310 p.

Penner D, Lagaly G, 2001. Influence of anions on the rheological properties of clay mineral dispersions, Applied Clay Science, 131–142.

Pettersson, T, Thormann E, Claesson P, 2008. AFM study of Montmorillonite, Report, Department of Chemistry, Surface Chemistry, Royal Institute of Technology, SE-100 44, Stockholm, Sweden.

Petsev D N, Starov I B, Ivanov, 1993. Concentrated dispersions of charged colloidal particles: sedimentation, ultrafiltration V.M. and diffusion, Colloids and Surfaces A: Physicochemical and Engineering Aspect 81, 65–81.

Plaschke M, Schäfer T, Bundschuh T, Ngo Manh T, Knopp R, Geckeis H, Kim J I, 2001. Size characterization of bentonite colloids by different methods, Anal. Chem. 73, 4338–4347.

Puura E, Kirismäe K, 2008. Impact of the changes in the chemical composition of pore water on chemical and physical stability of natural clays: – a review of natural cases and related laboratory experiments and the ideas on natural analogues for bentonite erosion/non-erosion, Report, Institute of Ecology and Earth Sciences, University of Tartu, Tartu, Estonia.

Pusch R, 1983. Stability of Bentonite Gels in Crystalline Rock – Physical Aspects. SKBF/KBS SKB TR-83-04, Svensk Kärnbränslehantering AB.

Pusch R, 1999. Clay Colloid Formation and Release from MX-80 Buffer. SKB TR-99-31, Svensk Kärnbränslehantering AB.

Pusch R, Young R N, 2006. Microstructure of smectite clays and engineering performance, Taylor and Francis.

Pusch R, 2007. Colloids formed from buffer clay – nature and physical stability, Report. Geodevelopment international AB, Ideon Science park. SE-22370 LUND, SWEDEN, 2007-03-22.

Rege S D, Fogler H S, 1987. Network model for straining dominated particle entrapment in porous media, Chemical Engineering Science, 42 (7), 1553–1564.

Richards T, 2009. Particle clogging in porous media – Filtration of a smectite solution Report Chalmers University of Technology, Göteborg.

Rubio-Hernández F J, Carrique F, Ruiz-Reina E, 2004. The primary electroviscous effect in colloidal suspensions, Advances in Colloidal and Interface Science, 107, 51–60.

Ruffet C, Dardot M, Gueguen Y, 1995. Surface conductivity in rocks: a review, Surveys in geophysics, Vol 16, No 1, 83–105.

Sato H, Ashida T, Kohara Y, Yui M, Sasaki N, 1992. Effect of density on diffusion of some radionuclides in compacted sodium bentonite, J. Nuclear Science and Technology, 29, 873–882.

Sawada A, Uchida M, Shimo M, Yamamoto H, Takahara H, Doe T W, 2001. Anisotropy, reversibility and scale dependence of transport properties in single fracture and fractured zone – Non-sorbing tracer experiment at the Kamaishi mine, SKB, TR-01-24, Svensk Kärnbränslehantering AB.

Sjöblom R, Kalbantner P, Bjurström H, Pusch R, 1999. Application of the general microstructural model to erosion phenomena – Mechanisms for the chemical-hydrodynamic conversion of bentonite to a pumpable slurry in conjunction with retrieval. Eng. Geol. 54, 109–116.

Smith P A, Guimerà J, Kosakowski G, Pudewills A, Ibaraki M (Eds.), 2008. GTS Phase V: CRR final project report series III: Results of the supporting modelling programme. June 2006. Nagra Technical Report Series, NTB 03-03, Nagra, Wettingen Switzerland.

Tanai K, Matsumoto K, 2007. A study on extrusion behavior of buffer material into fractures using X-ray CT method, Proc. 3rd International Meeting on Clays in Natural & Engineered Barriers for Radioactive Waste Confinement.

Tombácz E, Szekeres M, 2004. Colloidal behavior of aqueous montmorillonite suspensions: the specific role of pH in the presence of indifferent electrolytes. Appl. Clay Sci. 27, 75–94.

Tombacz E, Nyilas T, Libor Z, Csanaki C, 2004. Surface charge heterogeneity and aggregation of clay lamellae in aqueous suspensions, Progr Colloid Polym Sci (2004) 125: 206–215.

van de Ven T G M, 2001. Electroviscous phenomena in colloidal dispersions, Chemical Engineering Science, 56, 2947–2955.

van der Kooij F M, Lekkerkerker H N W, 1998. Formation of Nematic Liquid Crystals in Suspensions of Hard Colloidal Platelets J. Phys. Chem. B 102, 7829–7832.

van der Kooij F M, Kassapidou K, Lekkerkerker H N W, 2000. Liquid crystal phase transitions in suspensions of polydisperse plate-like particles, Nature, Vol. 406, August 2000.

Van Loon L R, Glaus M A, Muller W, 2007. Anion exclusion effects in compacted bentonites: Towards a better understanding of anion diffusion, Applied Geochemistry 22, 2536 – 2552.

van Olphen H, 1977. An Introduction to Clay Colloid Chemistry: For Clay Technologists, Geologists, and Soil Scientists, John Wiley and Sons: New York.

Verbeke J, Ahn J, Chambré P L, 1997. Long-Term Behaviour of Buffer Materials in Geologic Repositories for High-Level Wastes, Report University of California at Berkeley UCB-NE-4220 (1997).

Wersin P, 2003. Geochemical modelling of bentonite porewater in high-level waste repositories, Journal of Contaminant Hydrology, 61, 405–422.

Wersin P, Curti E, Appelo C A J, 2004. Modelling bentonite–water interactions at high solid/liquid ratios: swelling and diffuse double layer effect, Applied Clay Science, 26, 249– 257.

Wesselingh J A, Krishna R, 2000. Mass transfer in multicomponent mixtures, VSSD, The Netherlands.

Xu S, Gao B, Saiers J E, 2006. Straining of colloidal particles in saturated porous media, Water Resour. Res, 42, W12S16, 1–10.

Appendix 1

On wall friction

The question of wall friction of gel expanding into fractures has been found to raise some questions among the reviewers of our report and has also led to discussions between the group a Clay Technology and our group. It therefore is appropriate to try to clarify our understanding of the phenomena involved.

The group at Clay Technology has proposed an erosion model where the rate of expansion of the buffer/gel into the fracture is governed by balance of the swelling pressure of the buffer and the friction force of the buffer/gel as it moves out into the fracture.

We, at department of Chemical Engineering on the other hand have modelled the rate of expansion into the fracture mainly determined by a balance of the repulsion force between the clay colloidal particles (swelling pressure) and the friction between the particles and the water as the particles move outward against the water that intrudes into the gel in the fracture in the other direction.

Below we discuss under what conditions the wall friction may be important and under which conditions the particle/water friction is important and may be the dominating effect. For this purpose we use three idealized situations.

Figure A1-1 shows an idealized situation where the water is supplied not through the fracture but through the walls of the container and the swelling pressure has developed. The fracture is devoid of water. We intentionally do not include water here to highlight the case for wall friction. Later in connection with Figure A1-3 the presence of water in the fracture is specifically addressed.

It is assumed that the compacted clay gel can flow if there is a pressure difference between the gel in the container and the fracture.

In the case depicted in Figure A1-1 the gel can expand and its increasing volume will be pressed out through the fracture. If the intrusion of water through the walls is not rate limiting the rate of expansion will be determined by the friction in the fracture.

The rheologic properties of the gel could be used to assess the rate of expansion of the gel into the slit the pressure difference and the rheologic properties of the highly compacted gel are known. The rheologic properties are quite complex, the compacted clay is highly non-Newtonian, probably Bingham like and possibly thixotropic. This makes it difficult to make well founded estimates of expansion into the fracture in this idealized situation.

The other extreme situation is where the walls are impervious to water and the fracture contains no water but the buffer is fully water saturated and has a swelling pressure in the container. This is illustrated in Figure A1-2

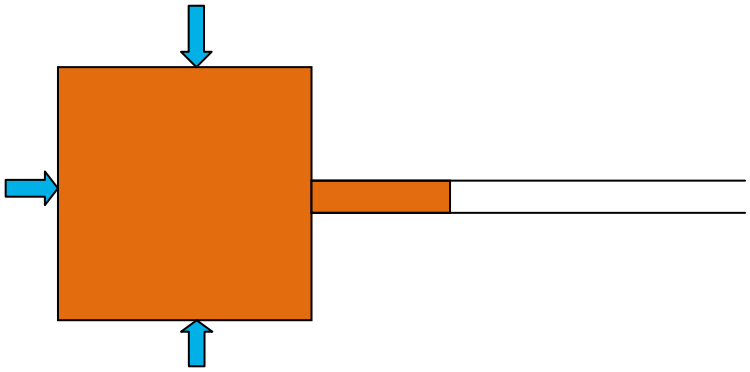

Figure A1-1. *Water intrudes through the walls of the container that is impervious to colloids, for example from the rock matrix. The expanding gel is pressed out through the fracture.*

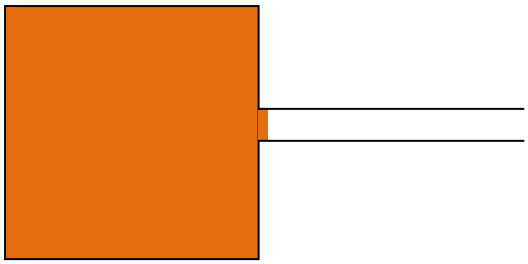

Figure A1-2. *The walls of the container are impervious to water and to colloids. There is no water in the fracture.*

In this case we assume that the compacted buffer is contained in the vessel and exerts the same strong swelling pressure against its walls as in the previous example. If the wall at one location is ruptured there will be no net transport of gel into the fracture except possibly that due to the expansion by gel compressibility effects. The swelling pressure can drop to zero if the rheology permits internal movement in the gel. There will be a minimal expansion of the gel volume. This is what happens when a fully wetted compressed sample is released of external stress by removing the "lid" of the compartment without allowing water to enter.

If however the rupture is small there may be negligible loss of swelling pressure as the highly viscous gel may not be able to penetrate the small rupture. This would be expected for a gel with Bingham body/fluid properties.

Finally in the third case we let a water filled fracture intersect the wall of the container with the impervious walls. This is illustrated in Figure A1-3.

In this case there is no net transport of gel (particle+water volume) in the fracture. When a particle moves to the right the same volume of water moves to the left in the fracture in the figure. The gel thus does not flow and therefore need to no involve friction between gel and wall. The rate of transport of the particles in the fracture is set by the balance of repulsion forces between particles and water as they move relative to each other.

This is what the dynamic model describes. Both the MRI experiments in section 6.11 and the swelling pressure drop experiments of Clay Technology modelled in section 8.3 give strong support to the dynamic model. The latter clearly demonstrate that wall friction has not played an important role in these cases.

In a deposition hole the walls are not impervious because the granite matrix is porous and allows water intrusion to the buffer through the matrix porosity. Thus in the real situation there will be both the effect shown in Figure A1-1 and in Figure A1-3. However, so far we have not invoked the Figure A1-1 mechanism because we have not found reliable rheological data of highly compacted bentonite that we can use to assess transport in thin fractures. Also scoping calculations and observations of water intrusion rates through the rock matrix suggest that the colloid transport mechanisms depicted in Figure A1-3 dominate over those in Figure A1-1.

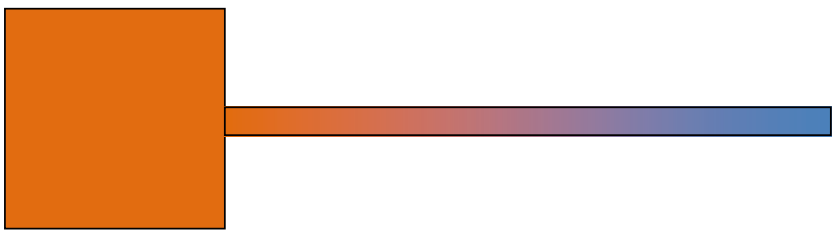

Figure A1-3. *The walls of the container are impervious to water and to colloids. The clay in the container is fully water saturated and the fracture is filled with water.*

ISSN 1404-0344
CM Gruppen AB, Bromma, 2010